Annex B – ADVANCED TOPICS AND RECENT PROGRESS

INTRODUCTORY COMMENTS

This Annex provides an overall view of the recent progress made on the prediction and simulation of aspects of gas turbine engine component performance. These components are inlet, compressor, combustor, turbine, afterburner, nozzle, splitters, mixers, and secondary flow systems. It also includes a section on control systems modeling. The Annex is arranged as follows. We begin with the rotating components (compressor and turbines); this is then followed by the non-rotating components.

B.1 COMPRESSOR SYSTEMS PERFORMANCE

Engine compressor performance is represented by the basic compressor map, as illustrated in **Figure B.1**. Total Pressure Ratio versus Corrected Airflow characteristics are shown for various percent corrected (referred) speeds. Efficiency islands and the surge line complete the performance definition of the compression system.

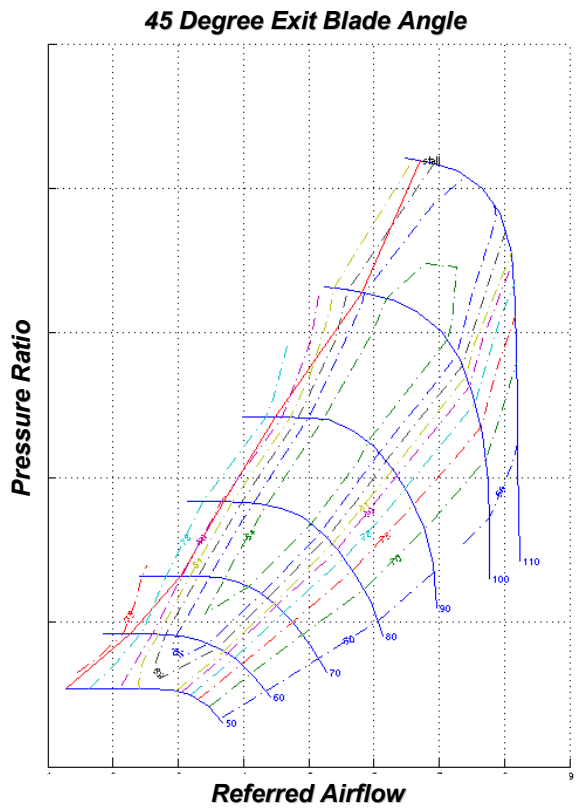

Figure B.1: Basic Compressor Map.

The Performance level of a compression system is dependent on a number of variables; air flow and pressure ratio requirements, speed compatibility with the turbine, the type of application, and cost considerations. The type of compression system is determined by the same parameters. The primary configurations consist of multi-stage axial, multi-stage axial + centrifugal, and single or multi-stage centrifugal compressors. A Mixed-flow compressor configuration has been applied in a few applications. **Figure B.2** depicts these various compression systems.

Performance comparisons of these configurations are shown in **Figure B.3**. Overall compressor efficiency is plotted versus overall compressor exit corrected flow. Exit corrected flow was selected as the abscissa as it collapses the data into the 3 curves shown and removes Pressure Ratio as a parameter. It is well established that for large size compression systems, axial type compressors have a significant efficiency advantage over centrifugal configurations. As airflow requirements decrease, the performance of the axial compressor starts to decrease due to the reduction in physical size. Clearance and secondary flow losses begin to dominate and better performance can be obtained with a centrifugal stage.

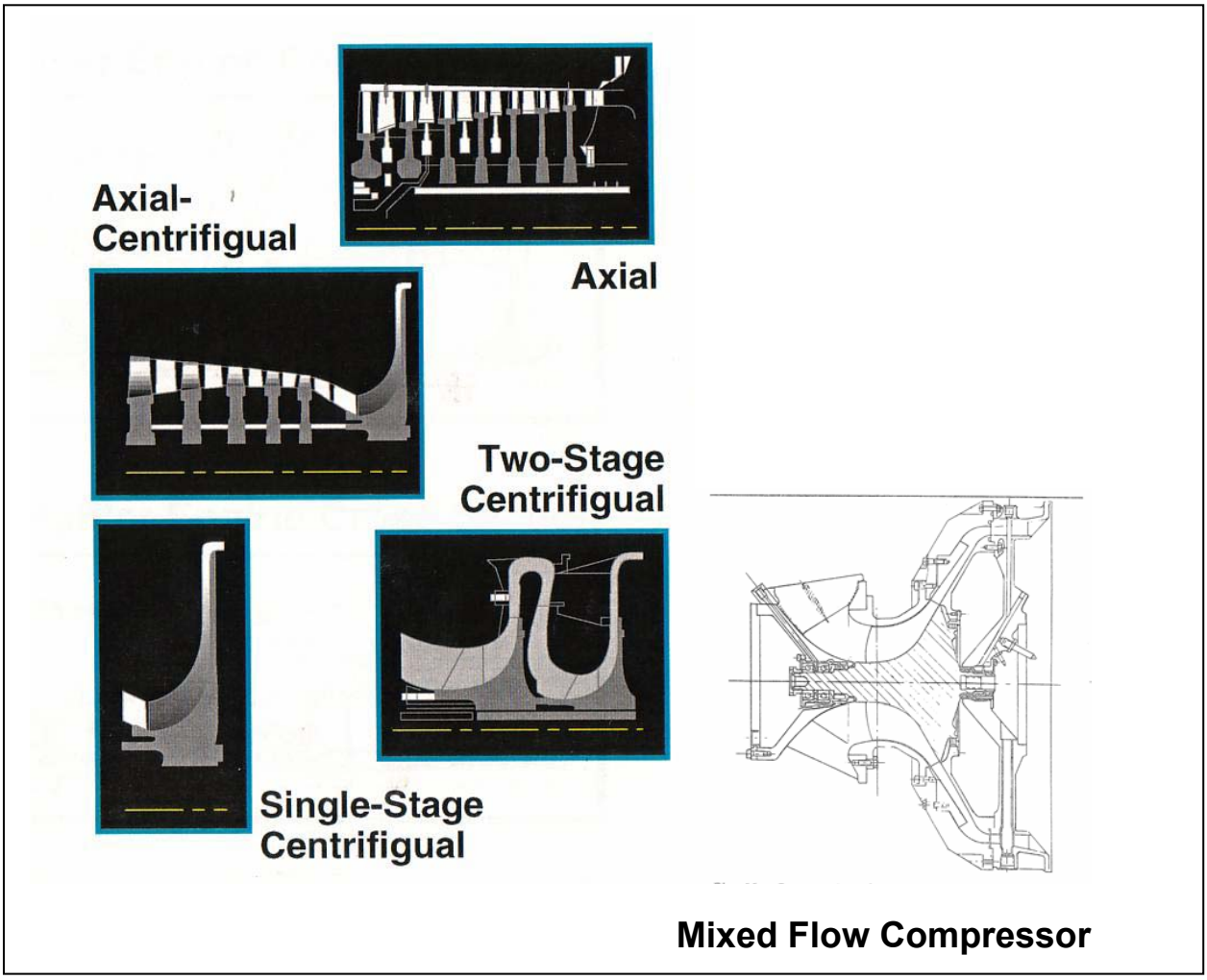

Figure B.2: Types of Compressors.

Another method used to select the type of compressor configuration is shown in **Figure B.4** where Compressor Exit Corrected Flow is plotted versus Pressure Ratio. Curves are generated for constant compressor Inlet Corrected Flow. Indicated at the top of the figure is the area where axial compressors should be used, and the area at the bottom of the figure where centrifugal compressors will have better performance. In the middle of the figure is a "gray" area where either type of compressor may be used from an efficiency point of view. This figure may also be used to determine in a multi-stage axial + centrifugal configuration the point at which a designer should consider changing from an axial stage to a centrifugal stage. As the overall pressure ratio increases and axial stages are added, the exit corrected flow decreases. At the combination of lower inlet corrected flow and higher pressure ratio, performance of centrifugal compressors will be better than that of axial compressors. Based on the selection of the axial

pressure ratio per stage, this figure can be used in determining the appropriate number of axial stages in a multi-stage axial + centrifugal configuration.

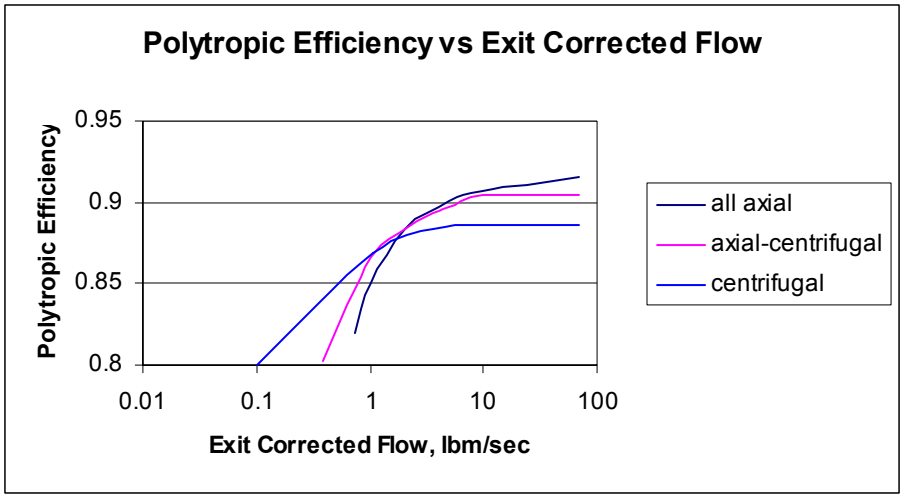

Figure B.3: Polytropic Efficiency for Various Types of Compression Systems.

Up to this point, considerations have been given to primarily aerodynamic parameters as far as determining the type of compressor configuration. As mentioned in the initial paragraphs, application and cost considerations can be of equal importance. For prime commercial and large military applications which require extremely large thrust and therefore very large inlet airflow, all axial configurations are preferred, as evident from **Figure B.3**. For these types of applications, the following section describes the performance and simulation of axial compressors.

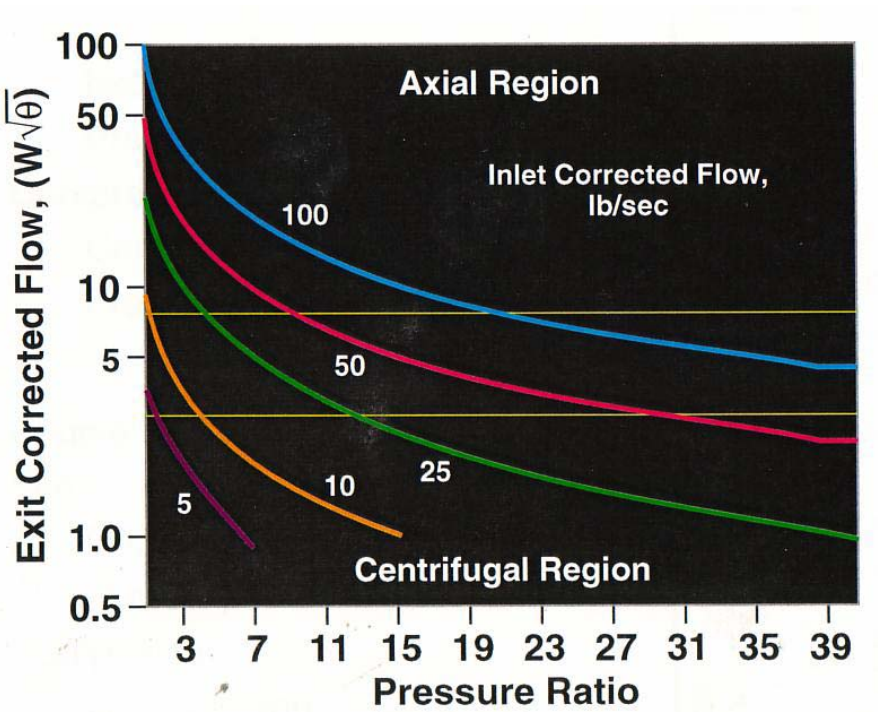

Figure B.4: Compressor Configuration as a Function of Flow and Pressure Ratio.

For military helicopters, turboprops, and auxiliary power unit (APU) applications, the inclusion of axial-centrifugal and centrifugal compressor stages is preferred as inlet flow requirements are much smaller for these types of applications. In addition, cost has become a significant consideration during engine selection. Minimizing the number of parts and variable geometry components translates into increased compressor reliability and maintainability and thus have become major factors in the selection of new engine configurations. Centrifugal stages have inherent advantages in these applications. ***Section B.2.2*** describes examples and attributes of centrifugal compressor configurations.

Engine performance is computed by utilizing the basic component maps for each of the turbomachinery components. Depending on the type of compressor and the amount of variable geometry and interstage bleed configurations, numerous maps may have to be included in the cycle deck. Alternatively, map scalars are supplied to represent various effects. These scalars may also vary with corrected speed. The remaining sections discuss in detail the most critical parameters that can change the performance of compressors and provide information on how to include these effects in the overall engine simulation model.

B.1.1 Simulation of Axial Compressor Performance

The performance map for a specific compressor configuration can be obtained through both systematic experimental measurements and computations. With the recent advances made in numerical techniques **[B.1** and **B.2]**, and the availability of computational resources, it is now possible to evaluate the performance and the design changes in multi-stage compressor, on a three-dimensional flow basis using a computational flow solver. It is intended to provide a concise delineation of those factors that can potentially modify baseline compressor performance-characteristics, rather than to discuss the details of the measurement and computation techniques for compressor performance maps. These factors are commonly referred to as characteristic modifiers.

There are thus two items of interest in this chapter, shown in **Figure B.5**:

- The generation of a baseline compressor map for a specific configuration; and
- The change in the pressure rise characteristic, the efficiency, and the operability limit (the surge line and the flutter boundary).

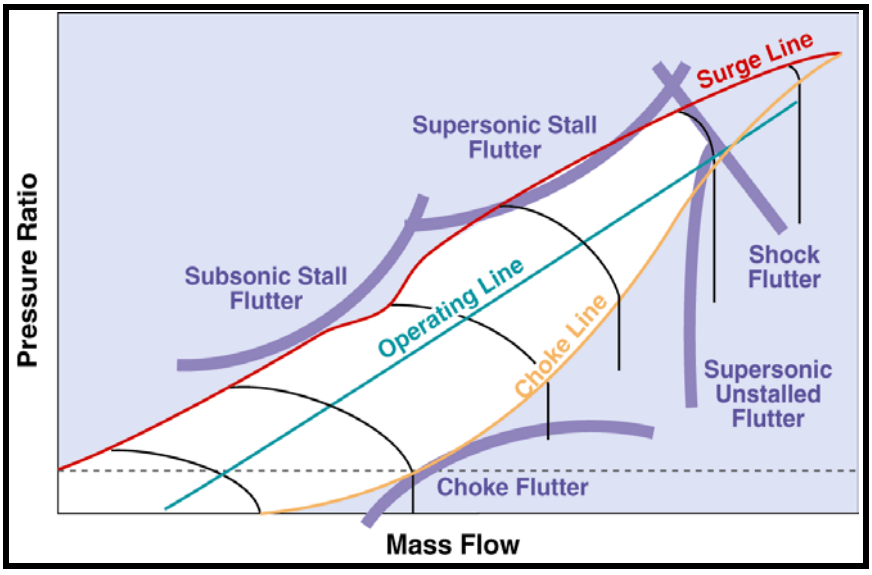

Figure B.5: Representative Compressor-Map, with Surge-Line, Speed-Line, Efficiency Contours, and Flutter Boundary.

In particular the specific focus will be on compressor performance changes associated with:

- Changes in compressor tip clearance;
- Stationary and rotating distortion, either self-induced (due to asymmetric compressor tip clearance) or externally imposed (due inlet distortion);
- Changes in intra-blade row gap;
- Blade surface roughness and Reynolds number effect;
- Changes in bleeds;
- Changes in stator schedule and position;
- Blade untwist associated centrifugal effect (this is of particular significance in fan rotor); and
- Heat transfer to compressor.

In this, it is assumed that the baseline compressor-performance characteristics are known and that one would like to determine the change in compressor characteristics and operability range, for instance, due to changes in compressor tip clearance. As such, the material present here is not meant to be exhaustive and extensive; it is aimed at providing the readers with an adequate knowledge base (in line with the objective of the monograph) to aid the readers in:

- Interpreting data from gas turbine engine; and
- Implementing gas turbine engine system simulation.

The readers are strongly advised to refer to the wealth of information on compressor aerodynamics, in the excellent book by Cumpsty **[B.3]** and ASME Journal of Turbomachinery **[B.4]**.

This section is organized as follows, based on work reported in journal publications up to 1999, of which the authors are aware:

- Generation of the baseline compressor map;
- Effects of changes in (axisymmetric) compressor tip clearance on compressor pressure rise characteristics, efficiency and stall inception point;
- Response of compressors to stationary and rotating distortion, induced by inlet distortion and asymmetric compressor tip clearance;
- How changes in blade row gap can alter the performance characteristics of compressor (Experimental data is first presented to elucidate the consequence of changing the axial spacing between compressor blade rows. Unsteady computational results are then used to establish the causes for the observed changes in compressor performance);
- The impact of blade surface roughness and Reynolds number on compressor performance;
- Changes associated with bleeds, stator schedule and position and heat transfer effects;
- Because the fan and the bypass duct system are distinct from the core compressor, we devote a separate section to the fan and factors that modify its performance characteristics. An example is the blade structural deformation associated with high-speed rotation of the fan rotor;
- A concise description of the importance of aeromechanics (flutter and forced response) on the operability of high performance aircraft engines; and
- Recent progress made in the development of computational compressor flow models and computational fluid dynamics for predicting and simulating flow phenomena of interest in multi-stage compressors.

B.1.1.1 Generation of Baseline Compressor Map

A compressor map is the 0-D representation of its performance, showing the mass flow and efficiency of the compressor for a range of operating conditions. It may also include stall line operating limits and various flutter boundaries, as shown in **Figure B.5**. The requirements for the map vary with their application. For engine and control system design, maps may be required to run from near zero speed to extreme over speed conditions that are beyond shaft break limits, and from stall down to windmill pressure ratios less that unity. For special studies, post-stall maps may be required.

A map represents the performance for a nominal set of conditions that may include:

- Stator position;
- Bleed amount and location;
- Entrance temperature, pressure and gas properties (including Reynolds number, gas composition changes such as water vapor or combustion products); and
- Tip clearance.

B.1.1.2 Effect of Axisymmetric Compressor Tip Clearance on Performance

Compressor tip clearance causes a leakage of gas across the blade tip from the pressure surface to the suction surface. This tip leakage interacts with the primary gas stream and the wall boundary layer. Indeed, the tip leakage flow dominates the aerothermodynamic behavior of the end-wall flow and the blade-to-blade flow in the tip regions. As such it has a strong impact on compressor efficiency and stability. The influence of tip leakage flow manifests itself in two ways:

- Fluid dynamic blockage that effectively reduced the flow area; and
- A thermodynamic effect, in that the work done in the tip region is different from that in the free stream.

The measured impact on compressor or fan performance due to increased tip clearance is shown in **Figure B.6** and **Figure B.7 [B.4]**. As shown in **Figure B.6** when the tip clearance was increased from the baseline value of 1.38 to 2.8 per cent of span for a low speed multi-stage compressor:

- Peak efficiency reduced by 1.5 points;
- Peak pressure rise dropped by 9.7 per cent; and
- Operability range reduced from 17.5 to 9.7 per cent (a reduction in stall margin).

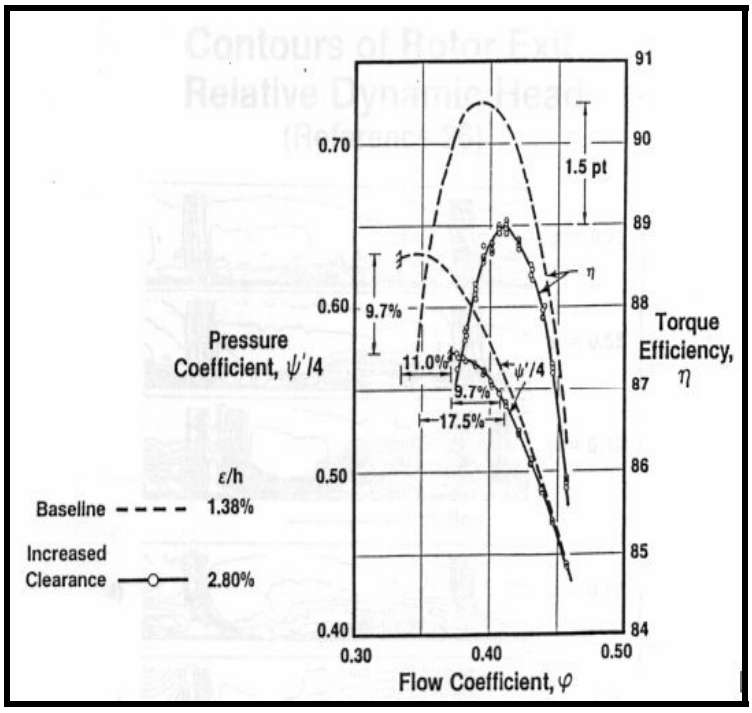

Figure B.6: Effect of Increased Tip Clearance on Overall Compressor Performance for a Low-Speed Compressor [B.4].

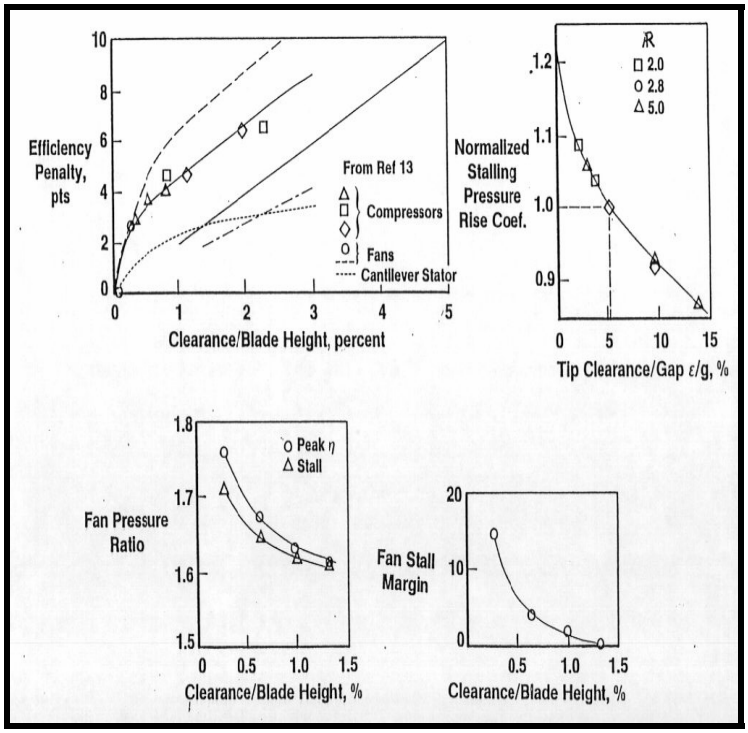

Figure B.7: Effect of Tip Clearance on Overall Compressor and Fan Performance [B.4].

The parametric trend of loss in performance (in terms of efficiency, pressure rise or pressure ratio and stalling pressure rise coefficient or stall margin) with increased tip clearance is further brought out in

Figure B.7. L. Smith **[B.5]** has developed a correlative approach for estimating the effect of end-wall flow on multi-stage compressor efficiency. This works in terms of:

- Efficiency, uncorrected for end-wall effects;
- Averaged staggered-spacing-to-blade-height ratio;
- Displacement thickness; and
- Tangential force thickness associated with end-wall flows.

The analysis that derives this correlation is based on a repeating stage assumption, and uses data from a set of multi-stage designs or builds.

While the approach does not provide information about the flow, it is apparently a useful approach as elucidated in the results shown in **Figure B.8 [B.5]**. More recently a slight more complex correlation has been developed by Khalid et al. **[B.6]** for the pressure rise capability across a rotor v blockage associated with the tip leakage flow; as the results in **Figure B.9** show it has a behavior analogous to the diffusion factor used for correlating cascade data. While these approaches appear correlative, their utility could lie in enabling the post-processing of vast amounts of computed data (e.g. from the use of CFD to simulate flow in multi-blade rows compressor). This data could then be used for simulating gas turbine engine systems.

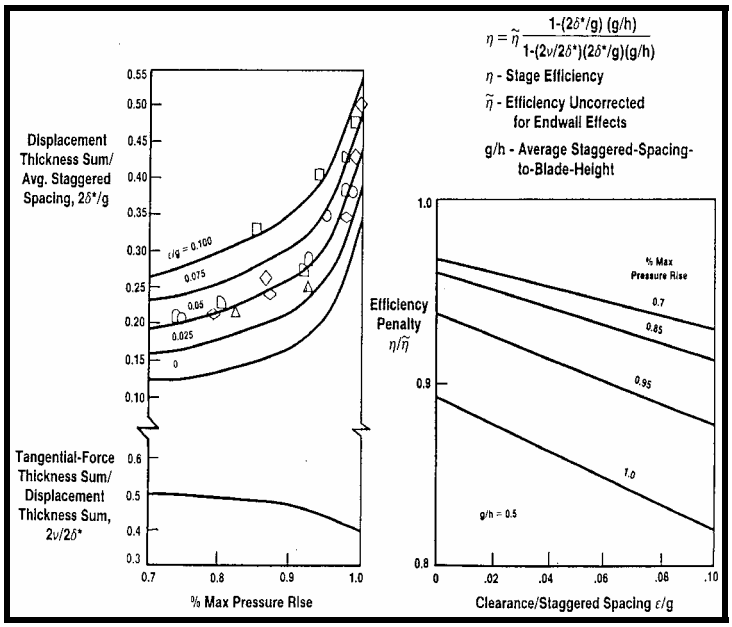

Figure B.8: Effect of Tip Clearance on Overall Compressor and Fan Performance [B.5].

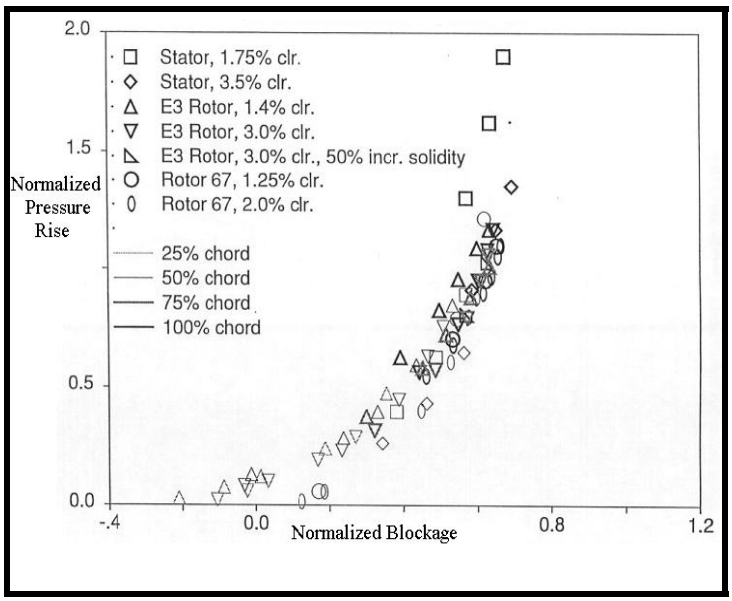

Figure B.9: Correlation of Rotor Pressure Rise Capability Against Flow Blockage Associated with Tip Leakage Flow [B.6].

Useful measured information on tip clearance effects in high-speed compressors was given in a paper by Freeman [B.7] and Schmucker [B.10]. **Figure B.10** (taken from a lecture at VKI by Freeman) and **Figure B.11** (taken from [B.10]) show the impact of increased tip clearance on the efficiency and pressure ratio of high-pressure compressors. Not only do the efficiency and pressure ratio deteriorate with increased tip clearance, but also the loss or gain in efficiency is not monotonic with increasing or decreasing tip clearance. Indeed, for tip clearances below a threshold value, the efficiency deteriorates and the surge line moves considerably to the right so that the compressor would surge at higher mass flows. All these measured effects are highly detrimental to the operability of a compressor.

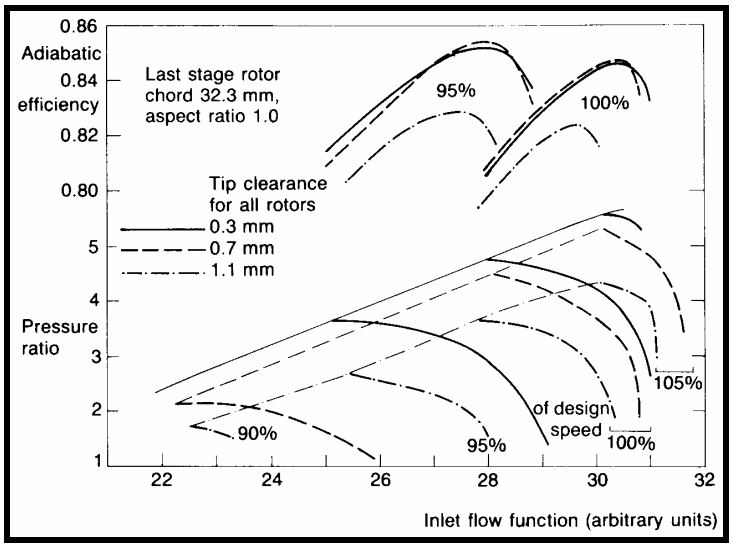

Figure B.10: Effect of Tip Clearance on Pressure Ratio, Surge Line and Efficiency of 6-Stage, High-Speed Compressor [B.7].

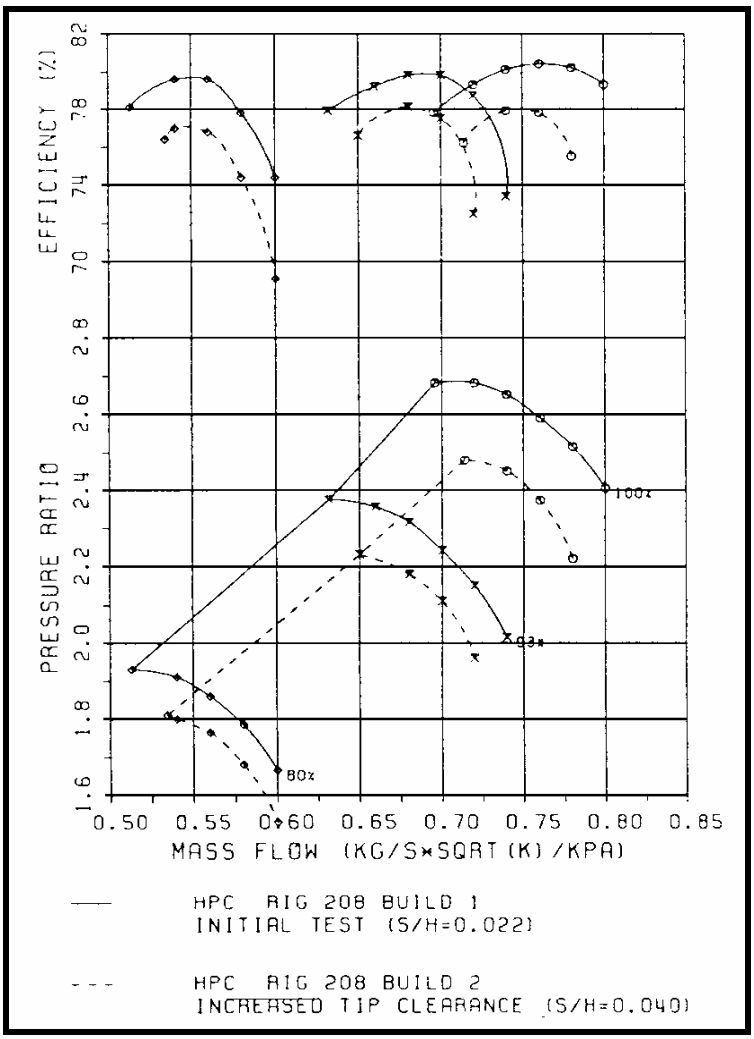

Figure B.11: Influence of Tip Clearance on Performance – Measurements from HPC-Rig [B.10].

In a multi-stage compressor environment the effect of changes in tip clearance would generate additional blockage and loss (say for instance to the front stages), altering the matching of the downstream stages. Likewise, the alteration in the performance of a specific stage, due to changes in tip clearance, could influence the aerodynamic matching with the upstream stage. These aspects of tip clearance together with the consequential impact on stage matching have yet to be defined on a quantitative basis. This is required if they are to be incorporated into a simulation procedure for gas turbine engine performance changes associated with changes in tip clearance.

Measurement of detailed flow in the rotor tip region has always been difficult. The advances in computational fluid dynamics and computer technology have enabled the simulation of unsteady three-dimensional flow for rotors with tip clearance, both in isolation and in multi-stage environments. This opens up an entirely new way of probing the physics of tip leakage flow, with the objective of establishing its role on compressor performance on a non-correlative basis.

To summarize, we have reviewed physical measurements to show compressor performance deterioration with increased compressor tip clearance. This may be attributed to the response of the flow behavior in the tip region, which is essentially dominated by the tip leakage vortices. While the overall performance of compressor is set by the pressure rise characteristics, its change is determined by the fluid dynamic event

local to the compressor blade passage and the flow conditions set by the preceding and succeeding blade row.

B.1.1.3 Stationary and Rotating Distortion

An operating compressor or fan may be subjected to various types of flow distortion. In general, the distortion is of the combined radial-circumferential type. Purely radial distortion can be assessed or analyzed using standard streamline-curvature methods for computing steady-state axisymmetric flows. Circumferential distortion introduces additional fluid dynamic effects that are associated with flow unsteadiness. Thus, a different class of methods is needed to assess the response of compressors to circumferential distortions.

In this section, we shall consider the impact of following types of distortion on compressor performance:

- Stationary inlet distortion, such as that due to flow separation in an inlet (e.g. due to cross-winds or aircraft maneuver) upstream of the fan or compressor;
- Rotating distortion, which can occur in a multi-spool compressors when rotating stall occurs in an upstream compressor, thus imposing a rotating distortion on the downstream compressor;
- Self-induced stationary distortion, associated with tip clearance asymmetry due to an off-centered rotor or oval casing, **Figure B.12**; and
- Self-induced rotating distortion associated with rotating tip clearance asymmetry due to non-uniform blade height or whirling rotor, **Figure B.12**. Whenever a compressor is subjected to an externally imposed distortion or self-induced distortion, its stall margin and performance are degraded and that there could be aeromechanical consequences as well.

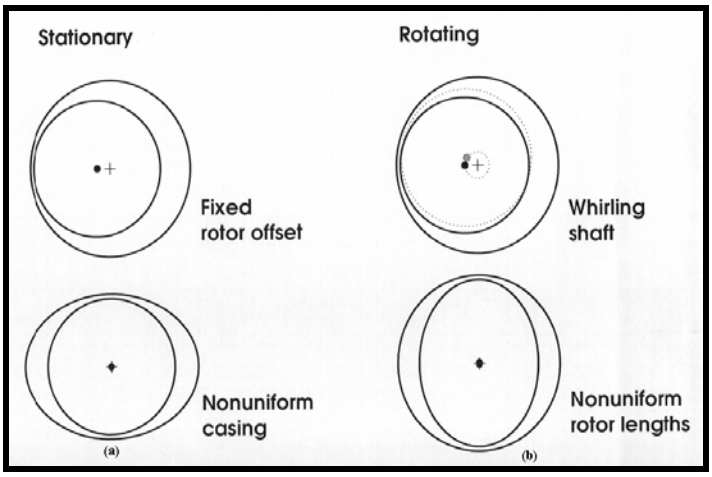

Figure B.12: Non-Axisymmetric Tip Clearance: (a) Stationary Caused by Off-Centered Rotor and Oval Casing; (b) Rotating Caused by Whirling Shaft and Non-Uniform Rotor Heights.

Because of the significant impact circumferential-flow distortion has on compressor performance, empirical and correlative approaches (SAE AIR 1419 [B.8], SAE ARP 1420 [B.9]), based on laborious compressor testing, have been developed for estimating the aerodynamic consequence. The parallel or multi-segments compressor model [B.11] provides useful results in certain class of problems and gives an overall view of the associated fluid dynamics. For instance, for a compressor subjected to circumferential distortion it yields a loss in stability margin and stalling pressure ratio. It also gives the result that for effective attenuation of distortion; a given compressor should have a steeper slope in the unstalled pressure rise characteristics. However, the method does not provide an adequate stall point prediction. Advances in

analytical and computational techniques for assessing compressor response to flow distortion will be described in the section on methodologies.

B.1.1.3.1 Stationary and Rotating Inlet Distortion

The measured effects of inlet distortion on the performance of a 9-stage axial compressor are shown in **Figure B.13**. The measurements showed that the stall line with circumferential inlet distortion moved considerably to the right, a degradation in compressor stall margin. The general trends of compressor performance with different inlet distortions are elucidated through a series of experiments undertaken by Reid **[B.12]**. A representative set of these results is shown in **Figure B.14**, which shows the compressor delivery pressure at the surge line for different types of distortions. Two key aspects may be deduced from these data:

- As the angular extent of the spoiled sector (low inlet total pressure) is increased, there is an angle above which the exit static pressure changes little (**Figure B.14**). This angular extent is often referred to as the critical sector angle.
- Fixing the total angular extent of the distortion, the effect of sub-dividing it into different number of equal sections is shown in **Figure B.15**. The greatest effect on the loss of peak pressure rise is observed when there is only one region. This suggests that inlet distortion patterns, which have a longer length scale and a lower circumferential harmonic content, are the most important.

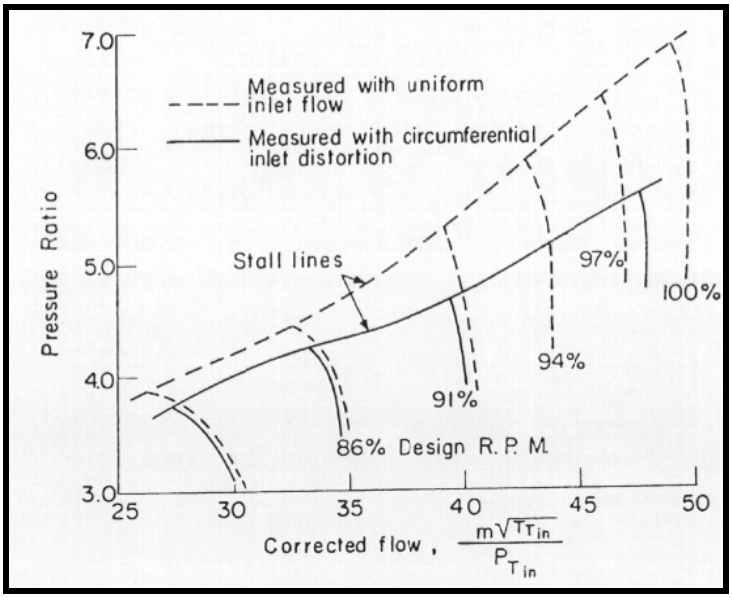

Figure B.13: Effects of Circumferential Inlet Distortion on Multi-Stage Axial Compressor Performance.

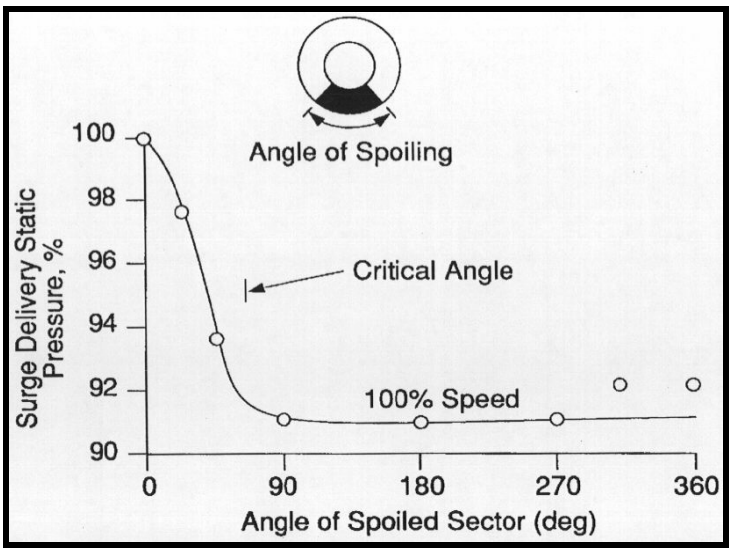

Figure B.14: Effect of Circumferential Distortion Sector Angle on Surge Pressure Ratio.

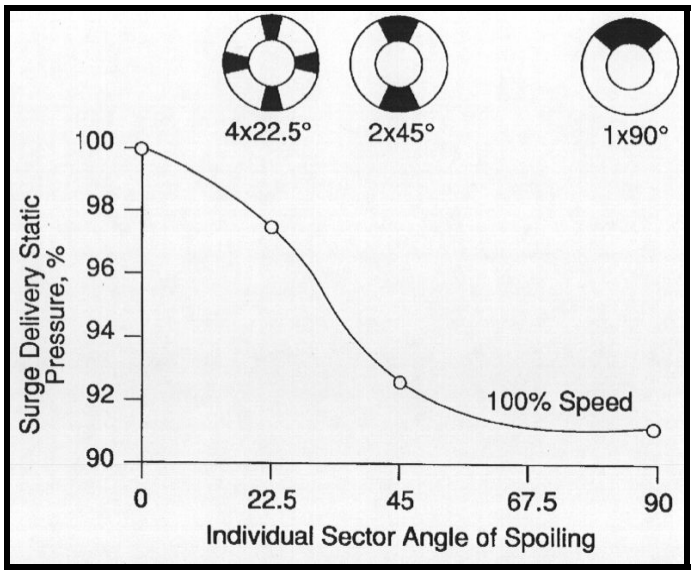

Figure B.15: Effect of Number of Sectors, on Surge Pressure Ratio.

While there is a considerable database on the response of compressor to stationary inlet distortion, only limited physical measurements are available on the degradation in performance (particularly in stall margin) when compressors are subjected to a rotating inlet distortion. Experiments by Ludwig et al. [B.13] for an isolated rotor show clearly that the stall margin is strongly affected by the speed at which distortion rotates. Co-rotating distortions have a larger impact than counter-rotating distortions, with the maximum loss in stability when speed of rotating distortion is near that at which a rotating stall cell would propagate if the compressor were throttled to stall. Kozarev et al. (1983) [B.14] has obtained similar results for a two-stage compressor.

A more thorough investigation on the effects of rotating inlet distortion on (low speed) multi-stage compressor stability was undertaken by Longley et al. [B.15]. A representative set of measurements from Longley et al. in **Figure B.16** showed measured mean flow coefficients at stall inception against inlet

distortion speed (normalized by rotor rotation speed) for two types of compressors with respectively different characteristic responses. The two types of compressors are distinguished by the two different routes to rotating stall inception known to occur in compressors:

- 'Modal Stall Inception' with a length scale of the order of compressor diameter; and
- Short length scale (spike) inception of the order of few blade pitches with a marked three-dimensional structure local to the rotor tip (Silkowski [B.16], Day [B.17]). The calculations from a theoretical model (described below in a separate section) are shown as solid lines in the figures. The stalling flow coefficients with no distortion and the design flow coefficients are included in the figure as reference.

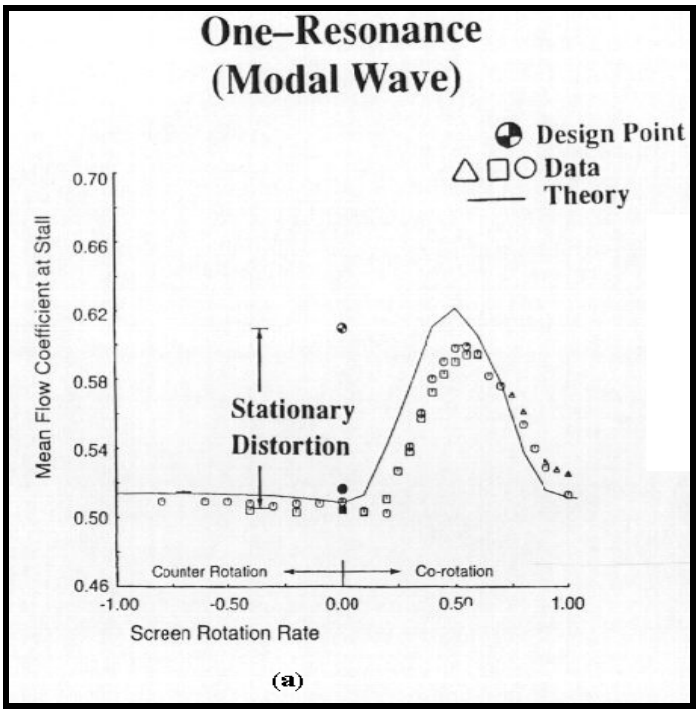

Figure B.16: Flow Coefficient at Stall versus Distortion Rate, for Single-Resonance-Peak Type of Compressor.

These measurements showed that the distortion rotational speed has a dramatic effect on the stability point, with the co-rotating one having a stronger impact. Specifically, the change in the stalling flow coefficient is a substantial fraction of the difference between that for stationary distortion and the design flow, providing a measure of the extent to which stability margin has been degraded by co-rotating distortion. For the response of the compressor shown in **Figure B.16**, the degradation of compressor stability margin is greatest when the co-rotating speed is near the measured propagating speed of modal stall inception disturbance (i.e. one resonance peak). This is approximately 40 to 50% of rotor speed, if the compressor is allowed to stall in the absence of any flow distortions. For the compressor shown in **Figure B.17**, compressor stability margin degrades considerably at two co-rotating speeds: one at 20 to 30% of rotor speed and the other at about 70% (i.e. two resonance peaks). The response of compressor to inlet distortion is an example for which the distortion-induced flow unsteadiness clearly changes the steady state compressor characteristics/performance.

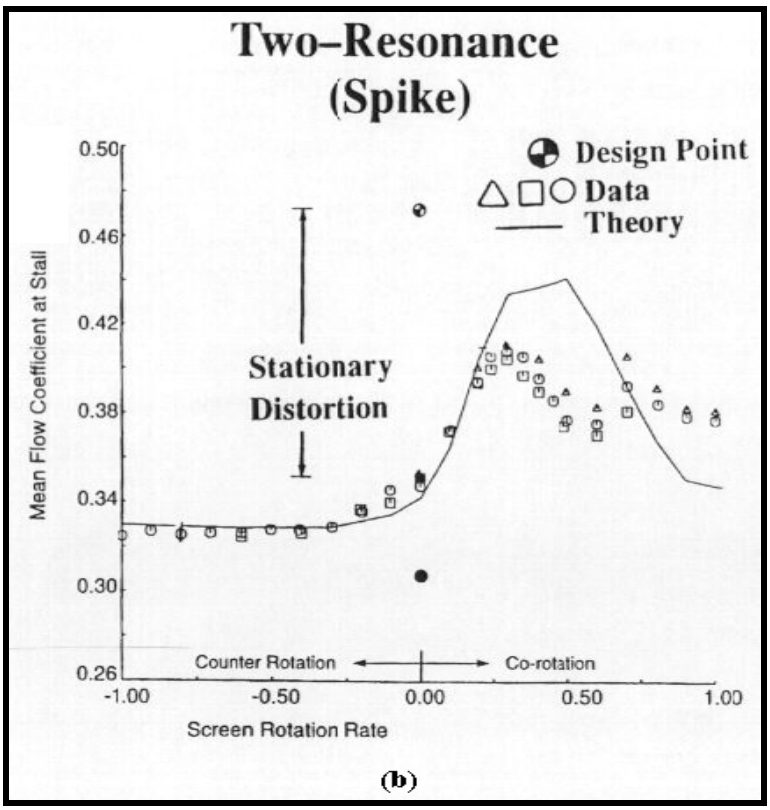

Figure B.17: Flow Coefficient at Stall versus Distortion Rate. Two Resonance Peak Type of Compressor.

In the presence of rotating distortion [B.17], the compressor performance deteriorates with a drop in pressure rise capability and a decrease in stability margin (due to a resulting increase in compressor face axial velocity non-uniformity) as the distortion co-rotating speed. For a co-rotating stall at 0.3 rotor speed, there is only a small flow regime for which the compressor is stable. A dramatic decrease in compressor stall margin can be the result when the inlet distortion is co-rotating at a speed corresponding to the propagating speed of the stall inception disturbance.

B.1.1.3.2 Aerodynamic Coupling between Inlet-Induced Distortion and Compressor

The above discussion has so far been confined to the response of compressors to a distortion pattern that was specified far upstream. However such is not often the situation encountered in practice. The development of the flow within the inlet can be substantially altered by the presence of the compressor. This aspect of the flow interaction has been clearly elucidated in the set of measurements taken by Hodder [B.18] shown in **Figure B.18**. In the absence of the compressor and with the inlet at 30-degree incidence there was a large region of low total pressure flow due to flow separation. In the presence of the compressor, and at an even larger incidence of 35-degrees, the region of low total pressure fluid was much smaller because the compressor acted to equalize the velocities. This reduced the extent of the separated flow region.

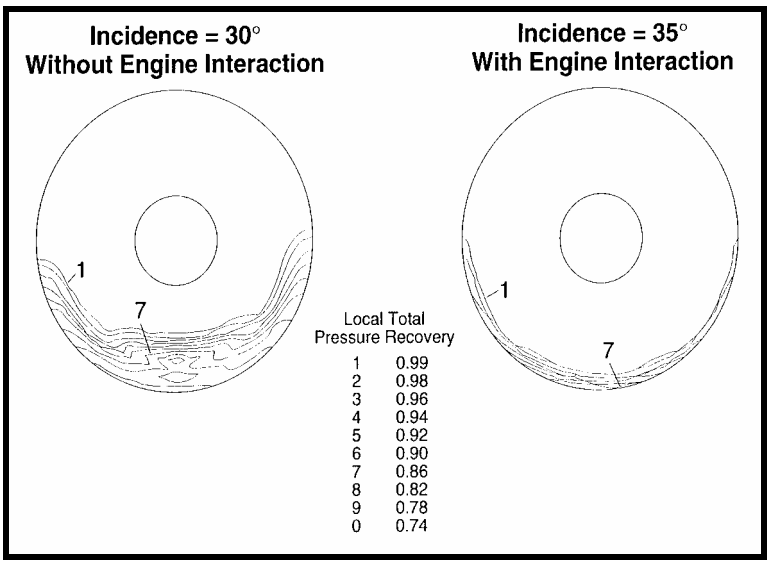

Figure B.18: Effect of Engine Presence on Total Pressure Distribution within Inlet.

One may thus infer from this that when undertaking experimental and analytical work on compressor response to inlet-induced flow distortion it is necessary to take steps to ensure correct inlet-compressor interaction. To say this differently: the assessment of engine response to flow distortion should be implemented from the global context of the airframe-inlet-engine system. Proper airframe-inlet-engine matching is needed to ensure the desired vehicle performance for the intended flight envelope. A poorly integrated inlet could result in a flight-vehicle performance penalty (see Airframe-Inlet-Engine Integration).

B.1.1.3.3 Summary on Rotating Inlet Distortion

Compressors subjected to co-rotating distortions show a significant loss in stability margin if the distortion speed matches a characteristic speed of the compressor flow-field. Measurements indicate that there are two groups of compressors:

- Those with a single peak stall margin decrement; and
- Those with a double peak stall margin decrement (a multi-stage compressor can have more than one characteristic resonance).

Compressor response to rotating inlet distortion can be linked to the disturbance structure at the onset of the stall. The results provide a clear illustration of a situation in which the unsteady flow effects directly affect the time-averaged performance of the compressor.

B.1.1.4 Stationary and Rotating Asymmetric Tip Clearance

We have examined the change in compressor performance associated with changes in compressor axisymmetric tip clearance. However, the circumferential distribution of tip clearance may become asymmetric due to engine usage and overhauls. An operational question of engineering interest is thus "Can one regard the asymmetry in tip clearance as just an effect of 'time and circumferentially averaged' clearance?"

Experimental and analytical investigations have been carried out on a low-speed multi-stage compressor [B.19] where a single and a two-lobed approximately sinusoidal variation in tip clearance had been separately introduced. The baseline configuration had an axisymmetric clearance of 4% chord. The quoted

clearances are relative to the baseline, so that +2% and –2% chord clearance corresponds to tip clearance of 6% and 2% chord respectively. The asymmetric clearance was introduced by varying the casing so that the circumferential average clearance was the same as the baseline clearance.

These results presented in **Figures B.15 to Figure B.19**, show that clearance asymmetry reduces both the compressor stability margin and efficiency. The single lobe variation has a larger impact than two and higher lobe patterns, which is a frequency effect. The reduction in stability margin is closer to the maximum than would be given by the circumferential average clearance. The sensitivity of performance to clearance asymmetry is a function of the steady state compressor response and unsteady response. The computed results from the theoretical model are in general agreement with the measurements. While no experimental data is available to depict the effect of rotating tip clearance asymmetry on compressor performance, calculations, based on the model presented in the section on methodology, show that the effect is analogous to that of rotating inlet distortion. In this case, the impact on compressor performance deterioration is greatest when tip clearance is co-rotating at a speed close to that at which the rotating stall inception would propagate.

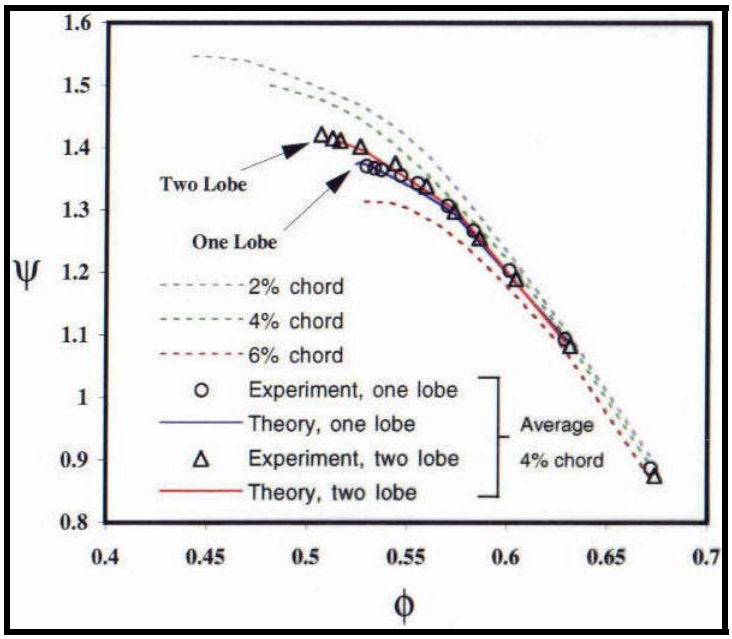

Figure B.19: Effect of Tip Clearance Distribution on Pressure Rise Characteristics and Stall Margin.

B.1.1.5 Effect of Compressor Axial Gap

The performance of axial compressors is known to depend on axial gapping between blade rows. Experimental data, published from General Electric (Smith [B.5]), Rolls Royce (Hetherington and Moritz [B.20]) and Pratt & Whitney (Mikolajczak [B.21]) and shown in **Figure B.24**, clearly show that the performance (efficiency) of axial flow compressors can be increased by optimizing the axial gap between adjacent airfoil rows. The results of **Figure B.20**, while interesting, provide neither a quantitative guideline nor an understanding of how to improve the performance of the machine. Smith's results showed a one to two per cent gain in efficiency, and a two to four per cent gain in the stage pressure rise in a low-speed research compressor, by reducing the blade row gap from 0.37 to 0.07 chords. Mikolajczak obtained similar results in a moderate speed compressor. Hetherington and Moritz, however, obtained a 2 per cent gain in efficiency by increasing the gap in front of the rotor rows in a multi-stage compressor. The experiments of Smith and Mikolajczak suggest that reduced axial gap improves performance,

while Hetherington and Moritz's investigation indicates increased axial gap can also be beneficial. A wake recovery model, developed by Smith [B.22], establishes a connection between blade row interaction and performance and is further substantiated by the computed results of Valkov and Tan [B.25] to include the tip leakage vortex flow.

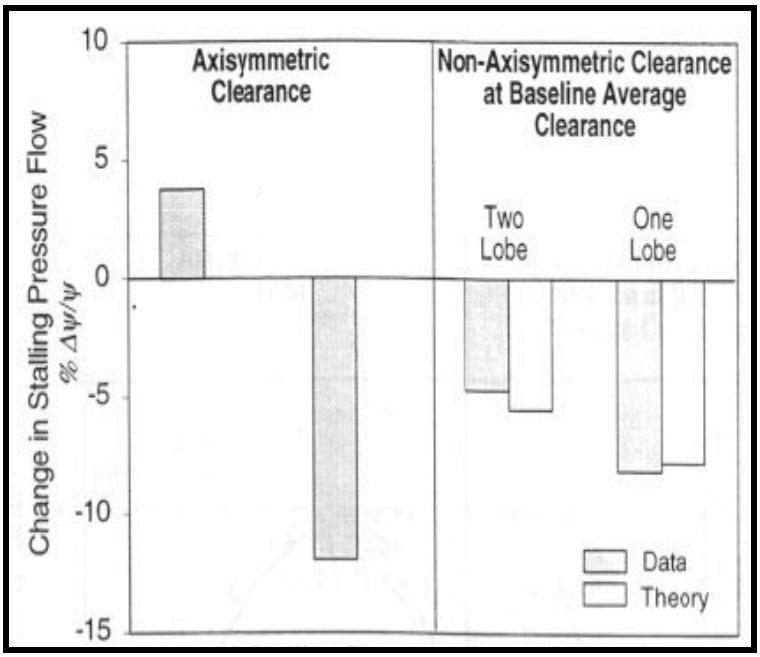

Figure B.20: Changes in Stalling Pressure Rise with Axisymmetric and Non-Axisymmetric Clearance.

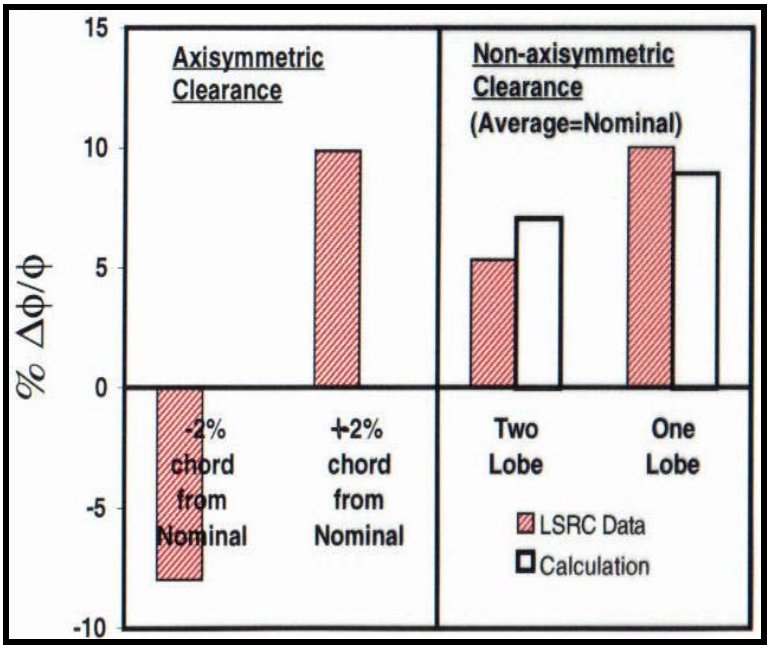

Figure B.21: Changes in Flow Coefficient with Axisymmetric and Non-Axisymmetric Clearance.

B.1.1.6 Effect of Axial Gap on Stalling Pressure Rise

Data, taken from Koch [B.24] and shown in Figure B.22, shows that the stalling pressure can increase by as much as 10% when the axial gap between the blade row is reduced by a factor of 3. The implication is that axial gap not only changes the performance at design but can also potentially change the stability margin.

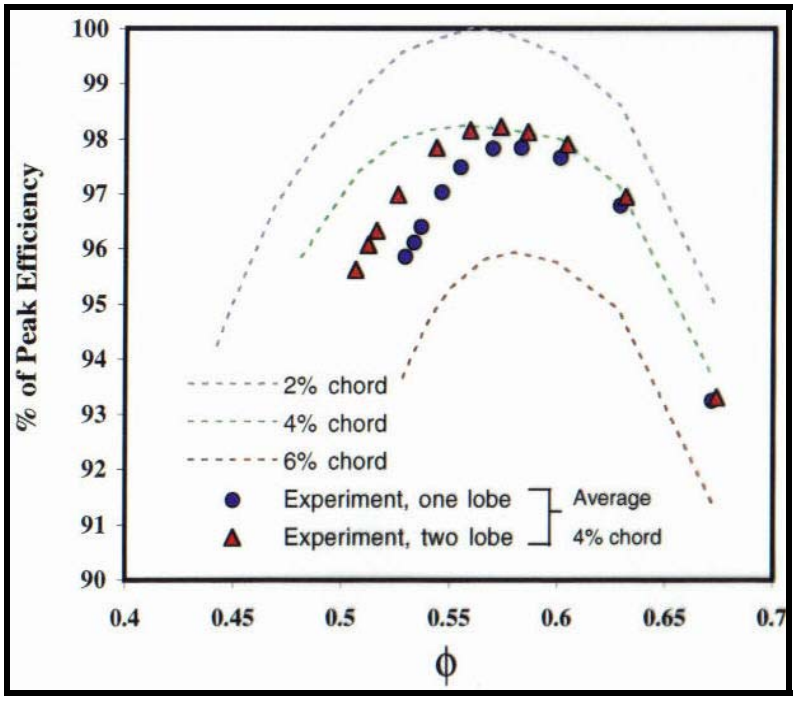

Figure B.22: Effect of Tip Clearance Distribution on Compressor Efficiency.

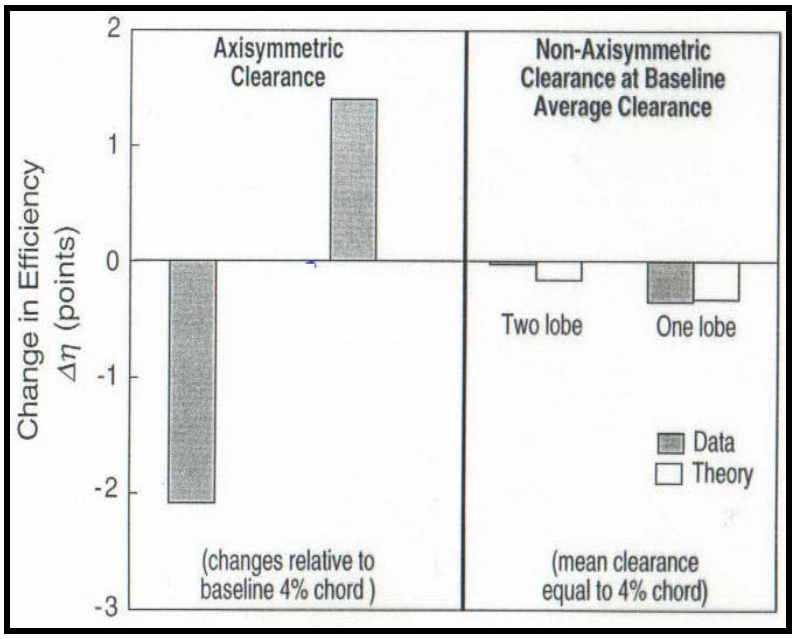

Figure B.23: Changes in Peak Efficiency with Asymmetric Clearance, with the Flow Condition Corresponding to the Peak Efficiency Points in Next Figure.

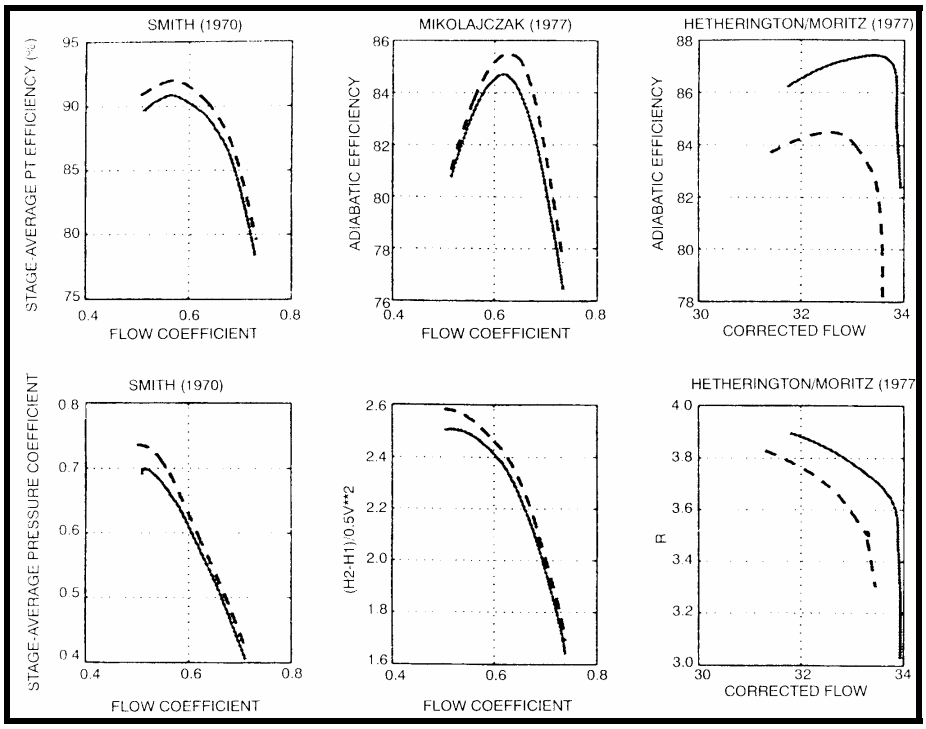

Figure B.24: Variation of Compressor Efficiency (top) and Pressure Rise (bottom) for Closely-Spaced (dashed lines) and Widely-Spaced (solid lines) Blade Rows.

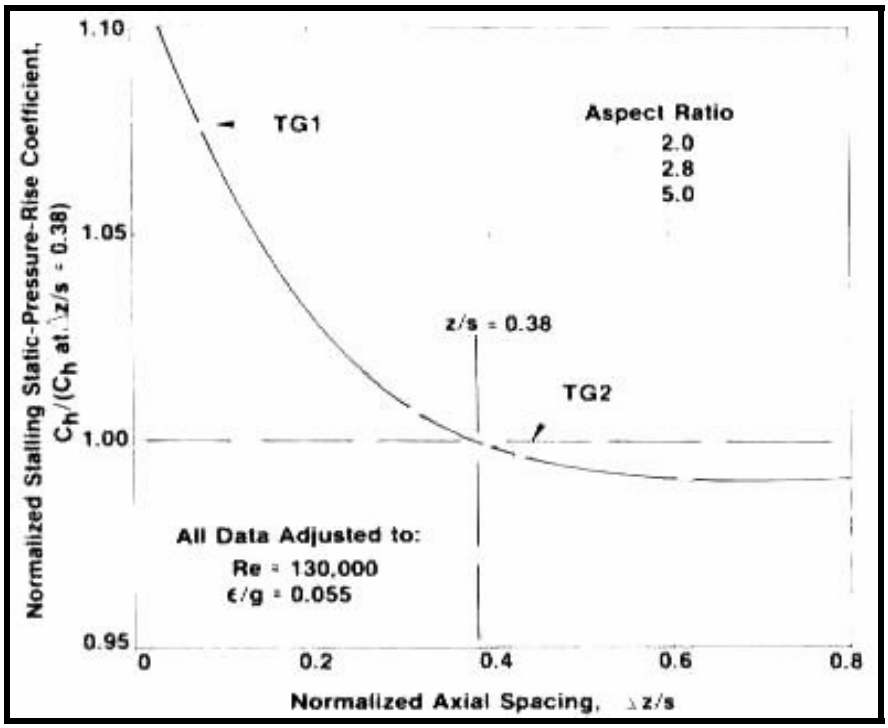

Figure B.25: Effect of Axial Spacing on Stalling Pressure Coefficient.

This section discusses how changing the axial spacing between compressor blade rows can alter the compressor performance in terms of its pressure rise capability and efficiency. Often in compressor testing

one may attempt to increase the axial spacing between blade rows to accommodate placement of instrumentation; it is to be borne in mind that this will modify the compressor performance characteristics undesirably.

B.1.1.7 Effect of Reynolds Number and Blade Surface Roughness

The performance deterioration of a high speed axial compressor rotor due to changes in Reynolds number and blade surface roughness and airfoil thickness variations has been investigated on an experimental and on an analytical and computational basis by Schaffler [B.26], Koch [B.24] and K. Suder et al. [B.27]. Within the flight envelope for a typical modern fighter aircraft indicated in **Figure B.26** [B.26], the operational Reynolds number can change by a factor of 10 (from 100,000 to 1,400,000).

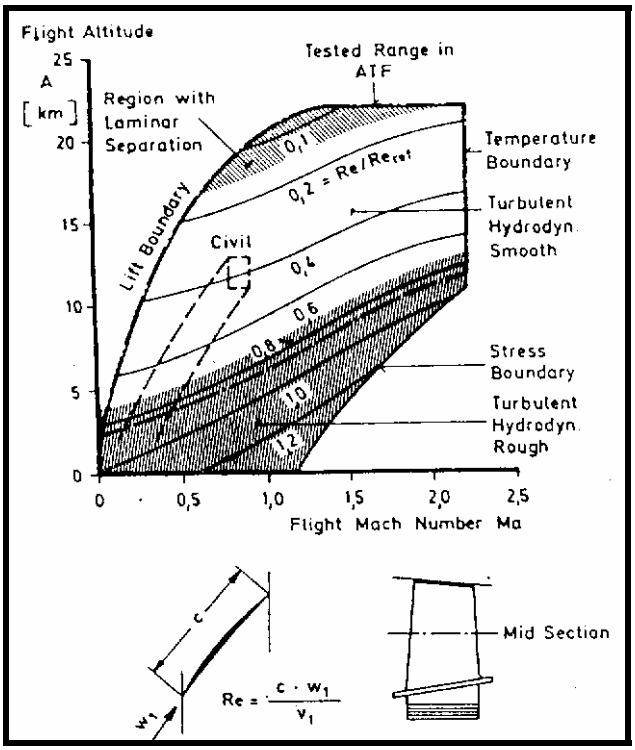

Figure B.26: Range of Operational Reynolds Number of a High-Pressure Compressor within the Flight Envelope [B.26].

Three flow regimes corresponding to this range of Reynolds number can readily be identified. These are:

- Low Reynolds number regime where laminar separation occurs at least in the front stages, resulting in reduced flow and efficiency levels and stall margin. This corresponds to operation at high altitude.
- Intermediate regime with a turbulent attached boundary layer flow and hydrodynamically smooth blade surfaces.
- High Reynolds number regime where the middle and back stages of high pressure ratio compression systems experience turbulent attached boundary layer flow with hydrodynamically rough blade surfaces. This corresponds to operation at low altitude.

A multi-stage compressor can be expected to show the following behavior over a wide Reynolds number range:

- Mass flow increases steadily with Reynolds number up to the choking condition in the blade passage;
- The surge line is essentially unaffected by Reynolds number until there is severe flow separation corresponding to operation at Reynolds number less than 100,000; and
- Polytropic efficiency varies with distinct slope changes that are dictated by specific boundary layer behavior.

The impact of boundary layer behavior on the functional dependence of efficiency on Reynolds number is shown in **Figure B.27 [B.26]** for an axial compressor at design point operation. As to be expected there are again three different regimes demarcated by a lower and an upper critical Reynolds number that define the laminar separation boundary and the surface roughness boundary. The consequence on compressor performance changes corresponding to each of the regimes is indicated in **Figure B.28**. If the Reynolds number is sufficiently high, the efficiency essentially becomes independent of the Reynolds number. Under this condition the blade surface roughness elements protrude through the laminar sub-layer of the turbulent boundary layer.

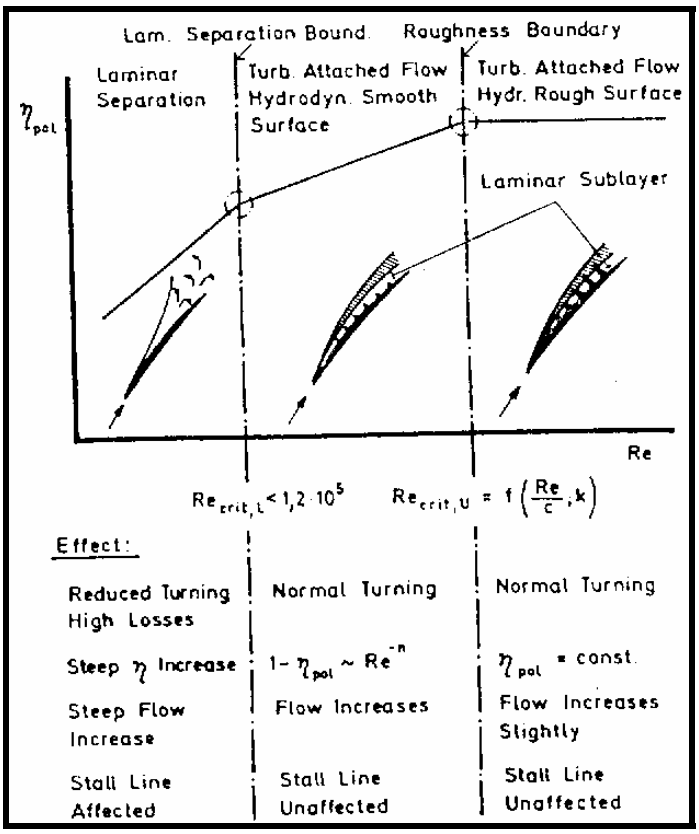

Figure B.27: Effect of Boundary Layer Condition on Compressor Behavior [B.26].

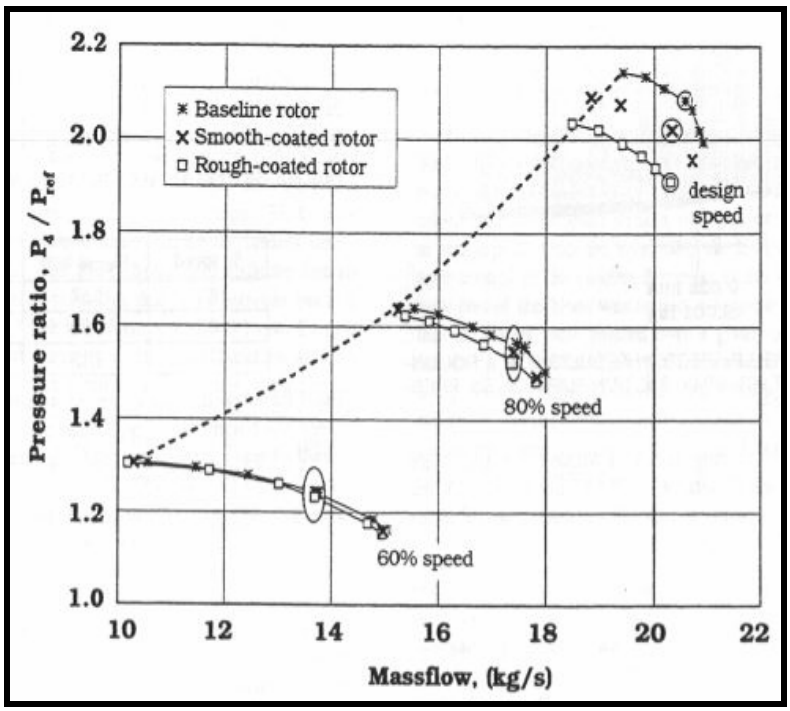

Figure B.28: Effect of Surface Roughness on Compressor Pressure Characteristics.

Results that show the effects of Reynolds number and blade surface roughness on compressor performance changes are drawn from Schaffler, Koch and Suder. The impact of blade surface roughness on the pressure ratio, efficiency, and pressure rise v mass flow characteristics of a high-speed fan stage are respectively shown in **Figure B.28** to **Figure B.30**. Likewise the influence of Reynolds number on compressor efficiency and pressure ratio of an intermediate pressure compressor and a high pressure compressor is shown in **Figure B.31**, while its influence on the stalling pressure rise coefficient (taken from Koch, 1981) is shown in **Figure B.32**.

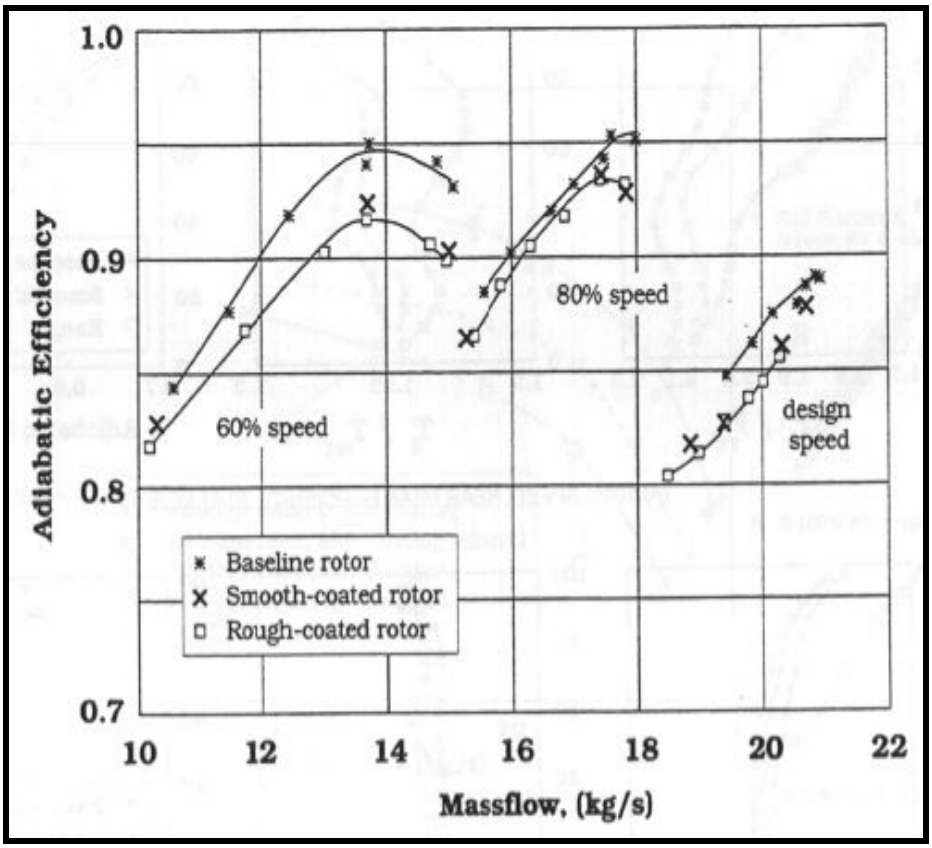

Figure B.29: Effect of Blade Surface Roughness on Compressor Efficiency.

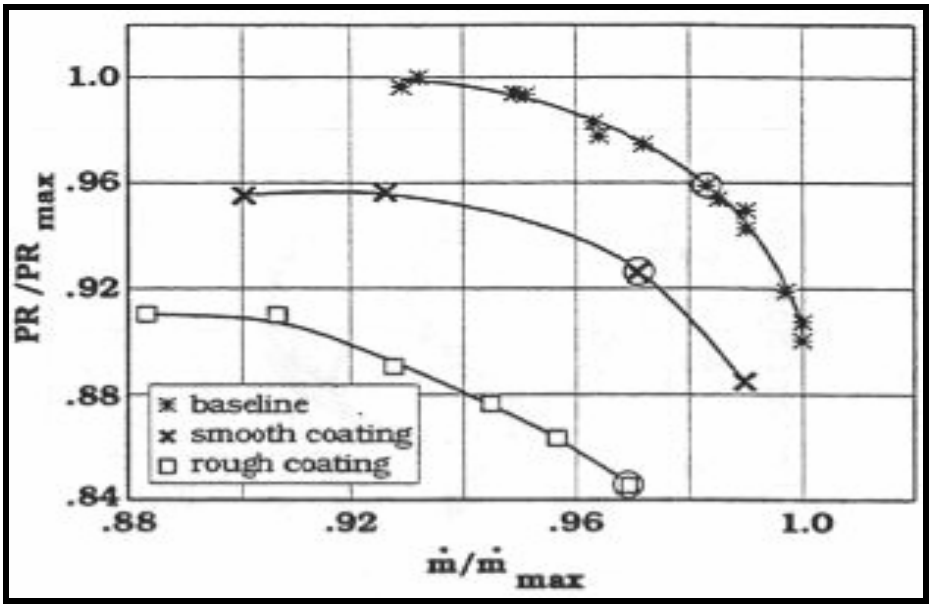

Figure B.30: Effect of Variation in Blade Surface Roughness on Pressure Ratio versus Mass Flow Characteristics at 70-Percent Span.

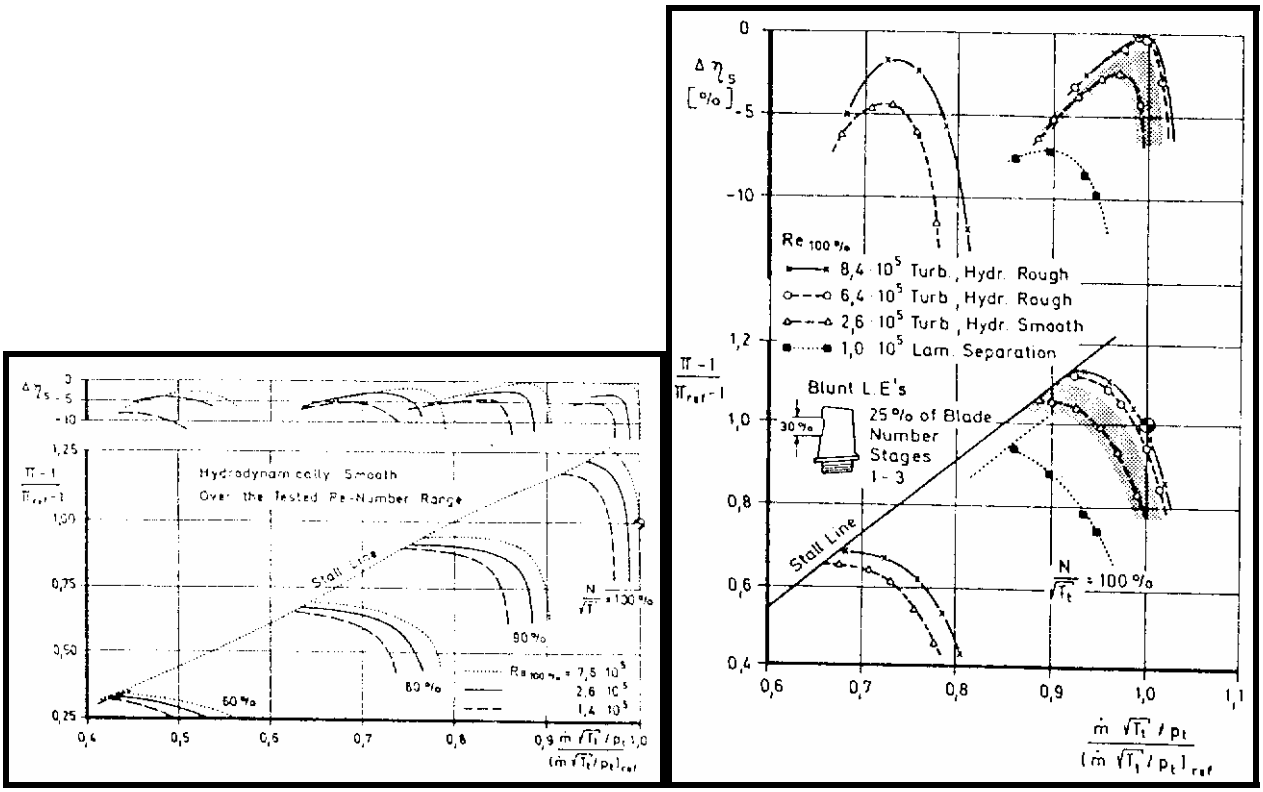

(a) (b)

Figure B.31: Effect of Reynolds Number on the Performance of: (a) A Three-Stage Intermediate Pressure Compressor; and (b) A Six-Stage High Pressure Compressor [B.26].

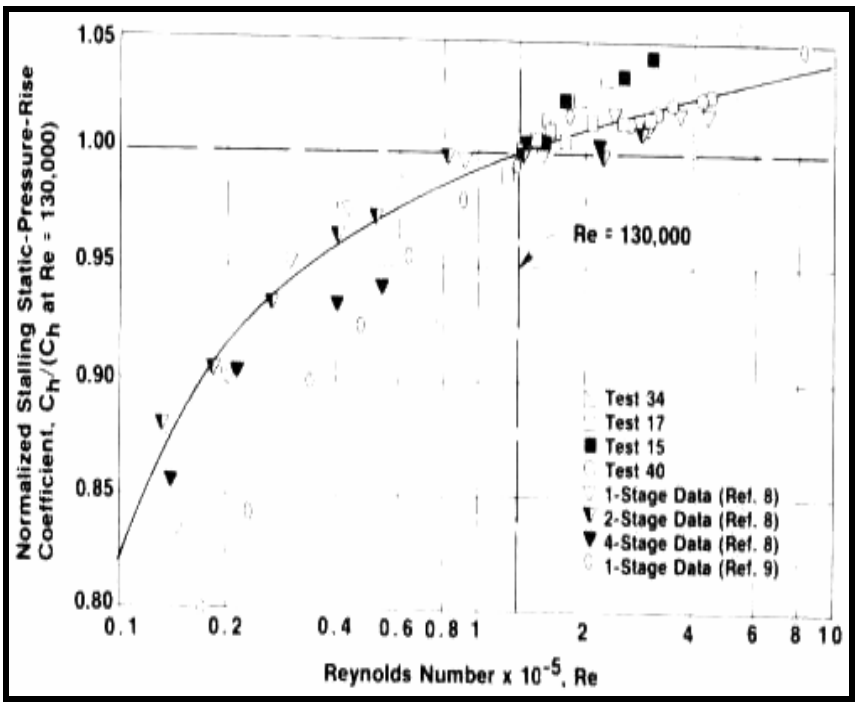

Figure B.32: Effect of Reynolds Number on Compressor Stalling Pressure Rise Coefficient.

As will be indicated in the section on methodology, present computational resources do not allow one to assess the influence of Reynolds number and blade surface roughness on compressor performance on an adequate basis. This is because one would have to resort to the use of direct numerical simulation (DNS), and presently such techniques have been applied only to very simplistic flow situations.

B.1.1.8 Variable Stator Vane Effects

Variable stator vanes (VSV) are used to optimize performance and operating stability of compression components. Compressors often operate with stator positions differing from the nominal schedule that is consistent with the map. For single stage machines, the stator angle can be used directly although an intermediate stator position indicator is often used rather than the actual airfoil angle. For multi-stage machines with multiple variable stators, the variable stators are generally ganged together and one average stator angle is used to represent the overall stator movement. Tabular 0-D compression component maps may address VSV effects by providing separate maps for different average stator positions relative to a nominal setting and interpolating between these maps for intermediate stator settings. Analytical 0-D component maps can do the same or use the implied change in the average stage characteristic and flow coefficient to indirectly model the impact of stator movement based on a simplified physical model. Stator movements change the overall performance of the component and the matching between stages, which can affect the predicted inter-stage conditions for the same overall operating conditions. This can be important for bleed and cooling flow extraction in full engine use. **Figure B.33** shows the impact of stator position on flow and efficiency as a function of speed for a particular operating line.

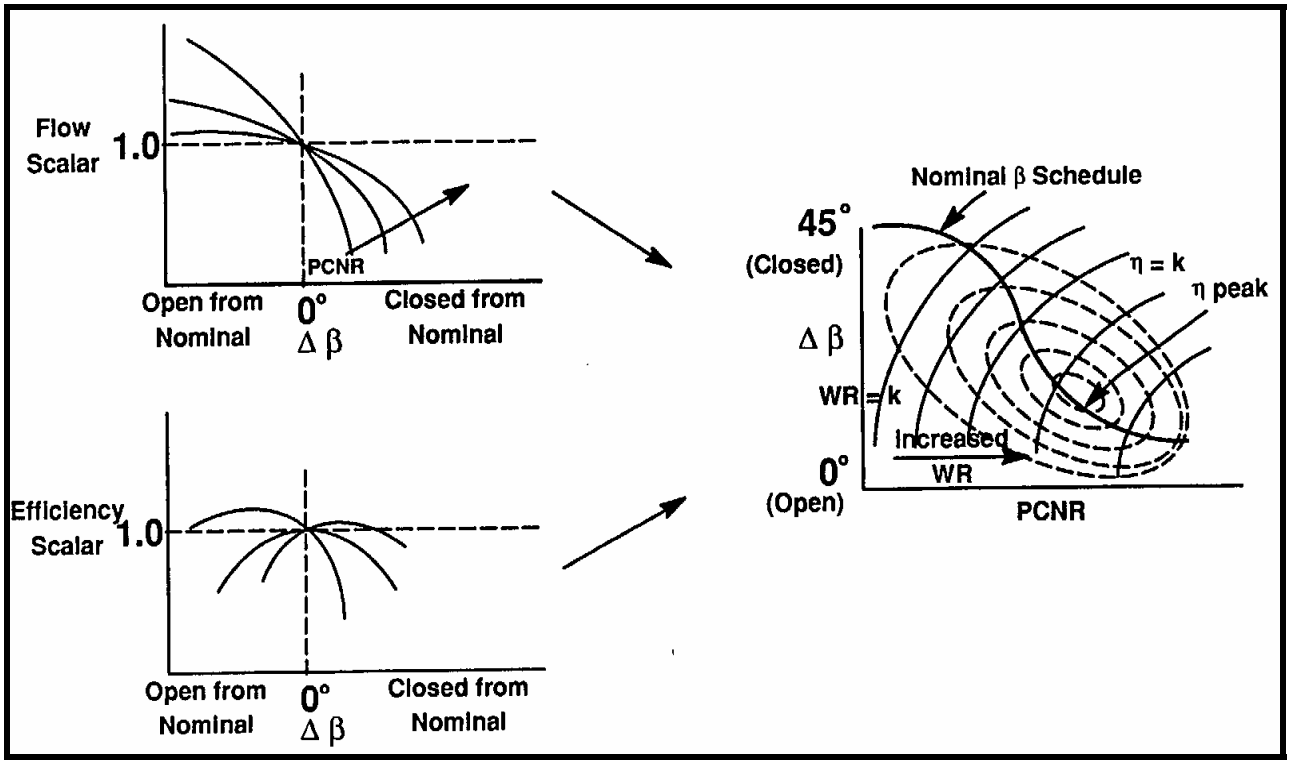

Figure B.33: Impact of Stator Position on Flow and Efficiency as a Function of Speed for a Particular Operating Line.

Higher fidelity models that require specific geometry will generally model the effect of stator position directly as part of the component representation. Stator position accuracy is critical to obtain accurate results from these high fidelity models. Stators and their position sensors are a frequent source of difficulty

in validating component models with real data due to hysteresis and variation between the indicated and actual stator position.

B.1.1.9 Effects of Thermal Origins

B.1.1.9.1 Temperature and Gas Property Effects

A compressor map generated for a specific set of entrance conditions may not be accurate at other entrance conditions due to the effects noted above. Many of these effects are compounded. Temperature changes affect clearance as the case grows. The relationship between the mechanical and corrected speed changes affects both blade untwist and blade growth. Unless the entrance pressure changes to match, entrance temperature also changes the Reynolds number. Even if all these effects are ignored, the use of temperature corrected parameters still ignores the change in the speed of sound with gas properties due to temperature and gas composition. So-called 'gamma-R' corrections are commonly used with most 0-D models to adjust base map predictions to a constant average Mach number similarity parameter. This is to allow for gas property changes. Due to lack of test data to separate these effects, it is common to select a few key effects such as clearance, Reynolds number and VSV (variable stator vane) angle to cover empirically all the effects not modeled hitherto.

B.1.1.9.2 Heat Transfer Effect

For 1-D, 2-D and 3-D models, the effect of heat transfer from the blades and static parts to the gas path flow can be modeled directly. The change in temperature will modify the stage-by-stage performance and result in an overall re-matching of the compressor. At a 0-D level, it is generally not possible to create an adjustment to the compressor performance that can be distinguished from the empirical bulk heat-transfer effects in the overall engine model. The heat transfer impact on compressor performance depends on the controlling stage in the machine and whether heat transfer at that particular operating condition moves that stage to a less or more favorable condition.

Heat-transfer effects on 0-D compressor maps are difficult to model, because performance depends on the controlling stage in the machine and whether heat transfer at that particular operating condition moves that stage to a less or more favorable conditions. However, simple approaches allow the main consequences of heat transfer to be caught.

B.1.1.10 Fan and Bypass Duct System

As shown in **Figure B.34**, the fan-bypass duct system consists of a fan followed by a splitter that subdivides the fan flow into a stream through the bypass duct and another through-the-core compressor. The core compressor may also include a row of exit guide vane and supporting struts.

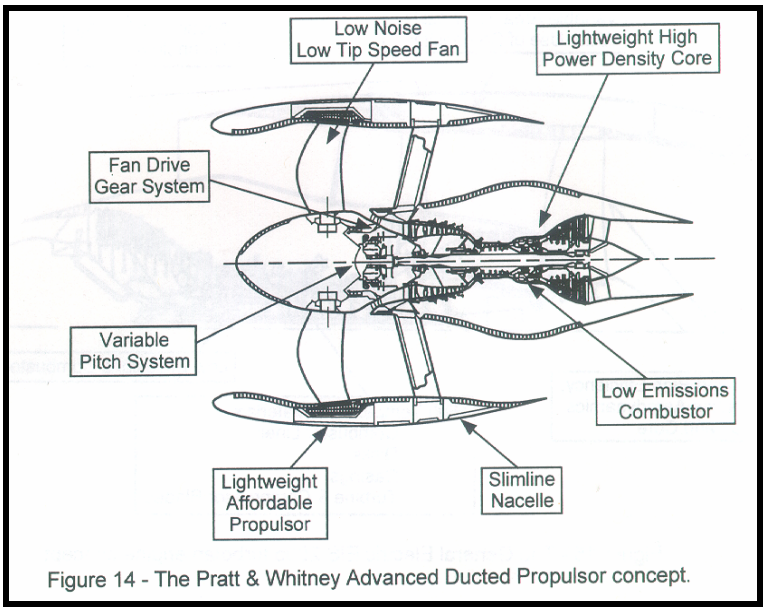

Figure B.34: Advanced Fan-By-Pass Core-Engine Duct System.

Fans have a hub-to-tip ratio ranging from 0.3 to 0.6, while core compressors have a much higher hub-to-tip ratio of 0.7 and above. Thus the outer portion of the fan generates the pressure ratio needed to maintain the required flow in the bypass duct and the inner portion of the fan generates the pressure ratio for the flow into the core compressor. The dividing streamline that demarcates the inner and outer stream of the fan is the stagnation streamline with the stagnation point located on the leading edge of the splitter.

The performance of the fan-bypass duct system can be represented through the following set of maps:

Fan OD map F($\frac{P_{t12.5}}{P_{t12}}, \frac{N}{\sqrt{\theta_{t2}}}, \frac{W_{tot}\sqrt{\theta_{t2}}}{\delta_2}, \eta_{fanOD}$, surge line, see **Figure B.35**.

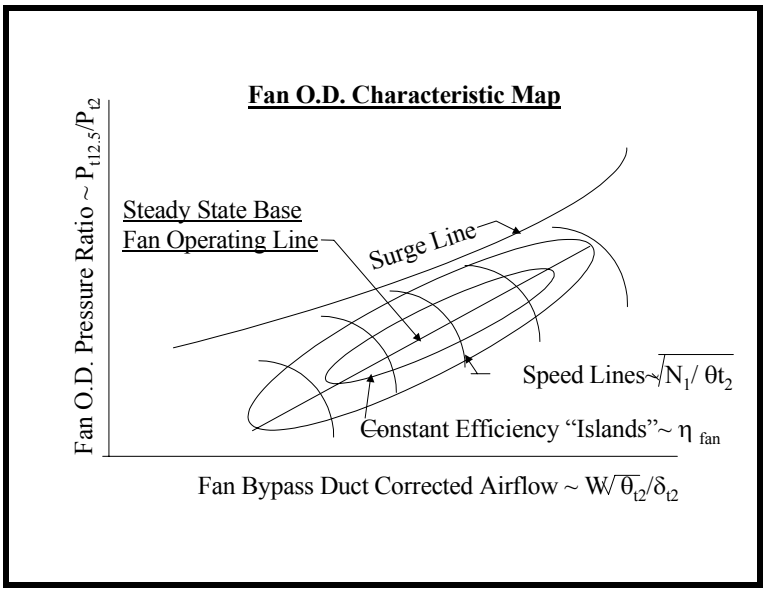

Figure B.35: Fan O. D. Map.

Fan exit guide vane (FEGV) map $F\left[\left(\frac{\Delta P}{P}\right)_{fegv}, \frac{W_{fan\,OD}\sqrt{\theta_{t12.5}}}{\delta_{t12.5}}, \frac{N}{\sqrt{\theta_{t12.5}}}\right]$, see **Figure B.36**.

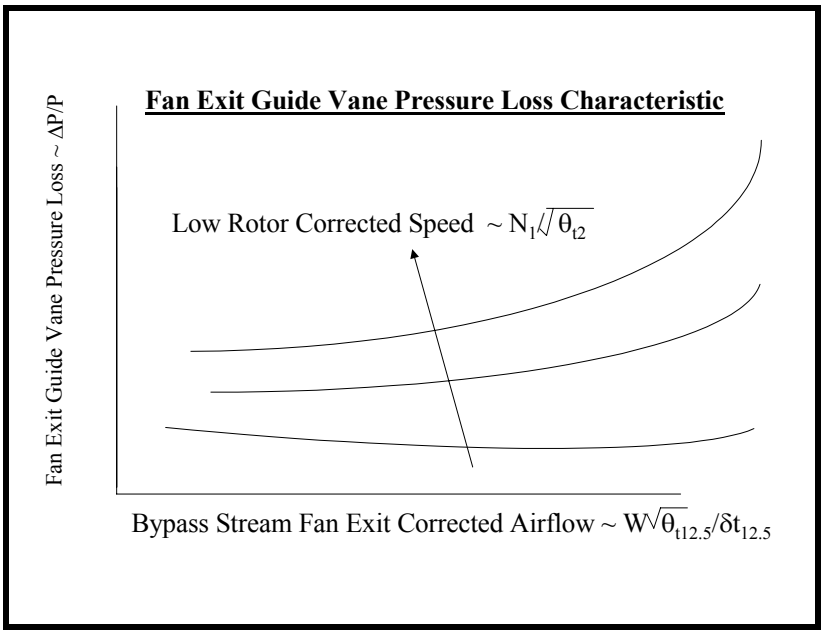

Figure B.36: Fan Exit Guide Vane (FEGV) Map.

Low pressure compressor map, including fan ID $F(\frac{P_{t2.5}}{P_{t2}}, \frac{N}{\sqrt{\theta_{t2.5}}}, \frac{W_2\sqrt{\theta_{t2.5}}}{\delta_{2.5}}, \eta_{LPC}$, surge line), see **Figure B.37**.

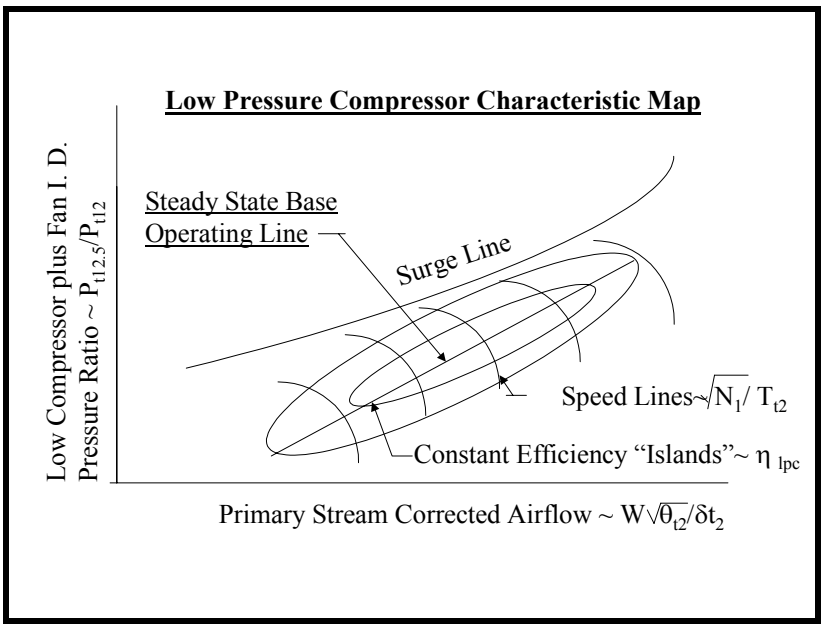

Figure B.37: Low Pressure Compressor Map, including Fan ID.

Super charging curve for primary stream $F\left[\Delta(\frac{P_{t2.5}}{P_{t2}}), \frac{N}{\sqrt{\theta_{t2}}}, BPR, \eta_{LPC}\right]$, see **Figure B.38**.

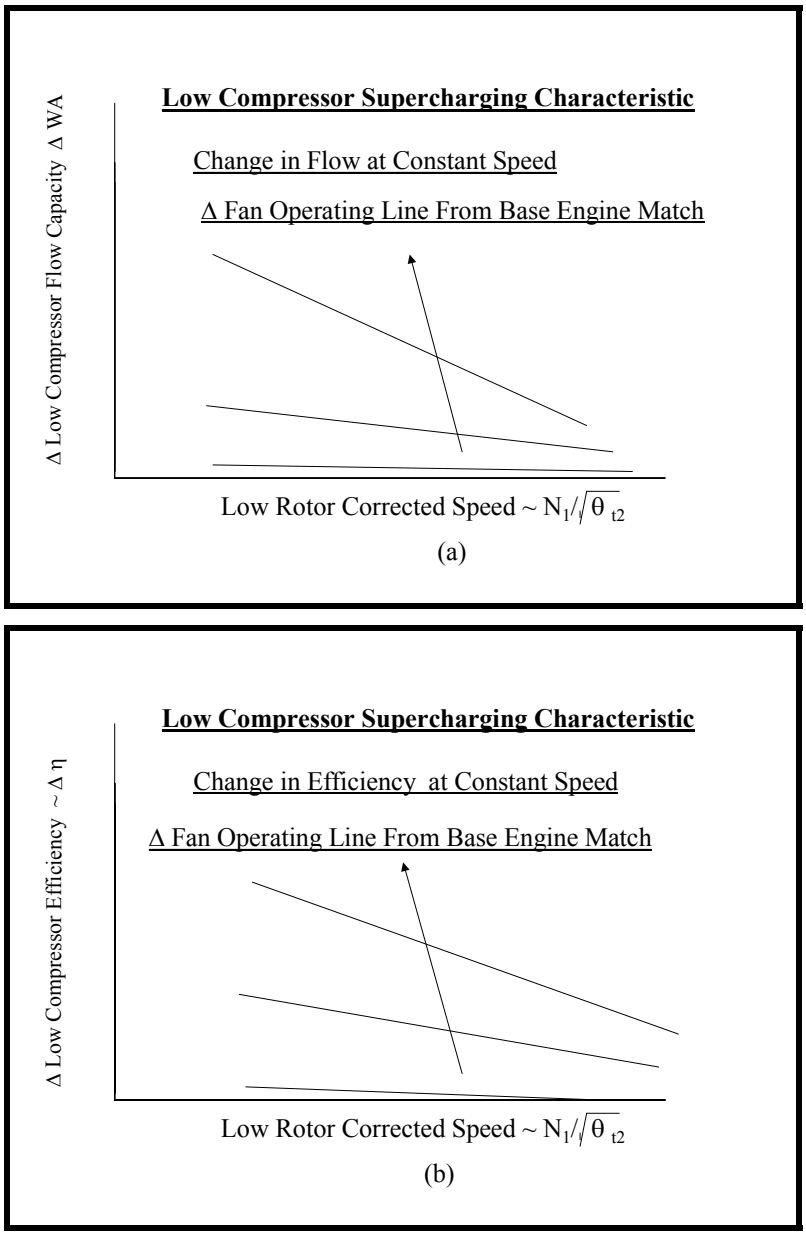

Figure B.38: Super Charging Curve for Primary Stream.

In addition to the characteristic modifiers described above there are two additional characteristic modifiers unique to the fan system. These are the fan blade untwist and stratification, which will be described below.

B.1.1.11 Blade Untwist

B.1.1.11.1 Description

Blade untwist is a mechanical phenomenon where the leading edge blade angle varies with operating condition. Typically this is due to the loads from centripetal acceleration and changing pressure forces on the

blade. It is primarily of concern for low hub/tip radius ratio blades (high bypass fans and the first stages of multi-stage medium bypass fans), but can be an issue for accurate detailed predictions of off-design behavior in highly loaded multi-stage compressors. **Figure B.39** shows an example of untwist for a high bypass fan. The change with flight condition shows the need to model more than just the centripetal accelerations. **Figure B.40** shows the impact of pressure and mechanical loading on the blade. The fan is designed with some nominal untwist which changes with both engine power setting and environmental conditions. **Figure B.41** shows the definition and conventions for untwist angle.

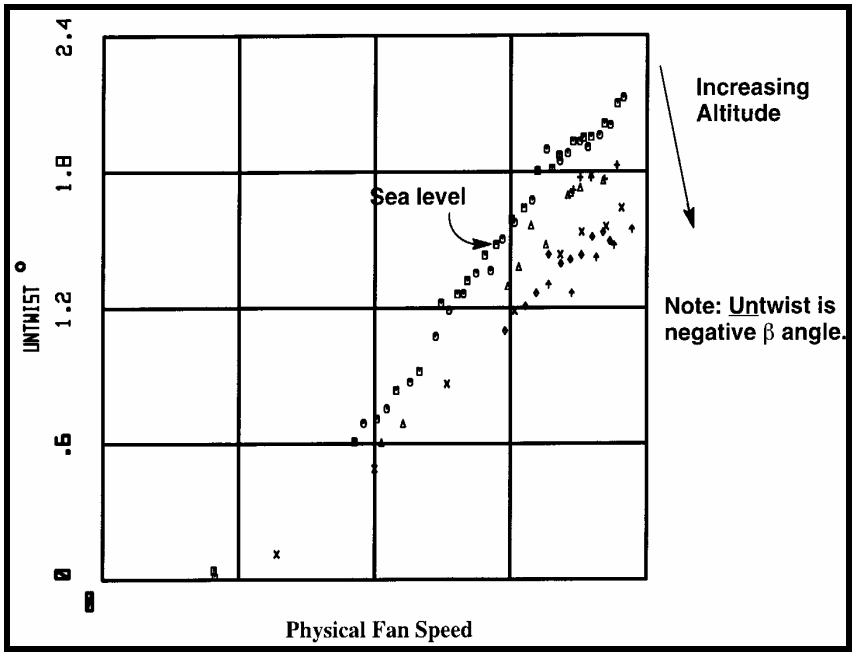

Figure B.39: Level of Untwist for a High Bypass Fan.

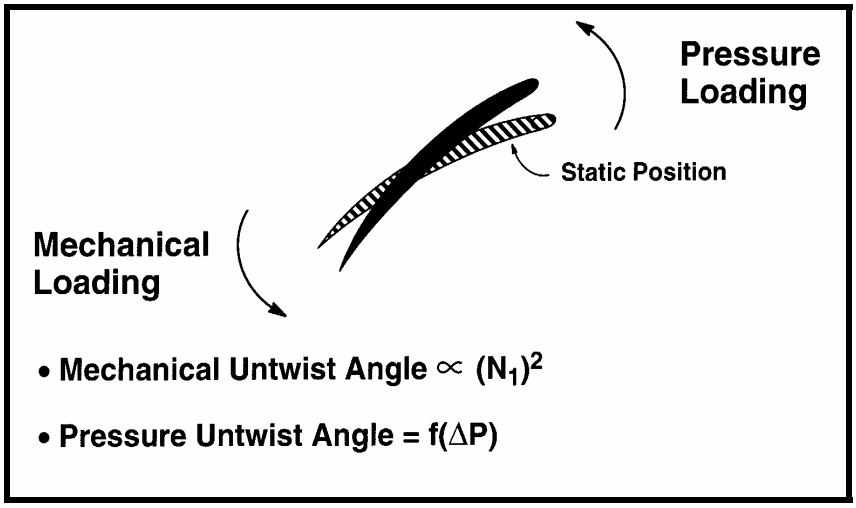

Figure B.40: Impact of Pressure and Mechanical Loading on Blade.

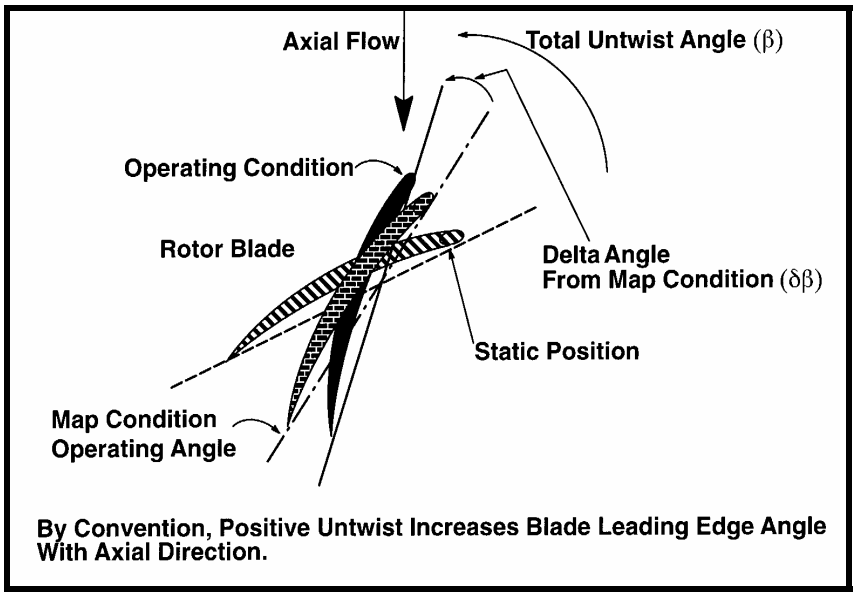

Figure B.41: Definition and Conventions for Untwist Angle.

B.1.1.11.2 Impact on Component Modeling

The primary impact of untwist is on flow capacity for high bypass fans. The same tools used to generate the basic fan model can often be used to identify the flow impact per degree of untwist. For multi-stage machines even a few tenths of a degree in blade angle can impact the stage matching and component performance, particularly with supersonic airfoils. This becomes an issue for compressor design but is rarely considered for component modeling. Blade untwist effect is typically in the order of 1% per degree at low speeds and will often double that at the maximum flow capacity of the machine as shown in **Figure B.42**.

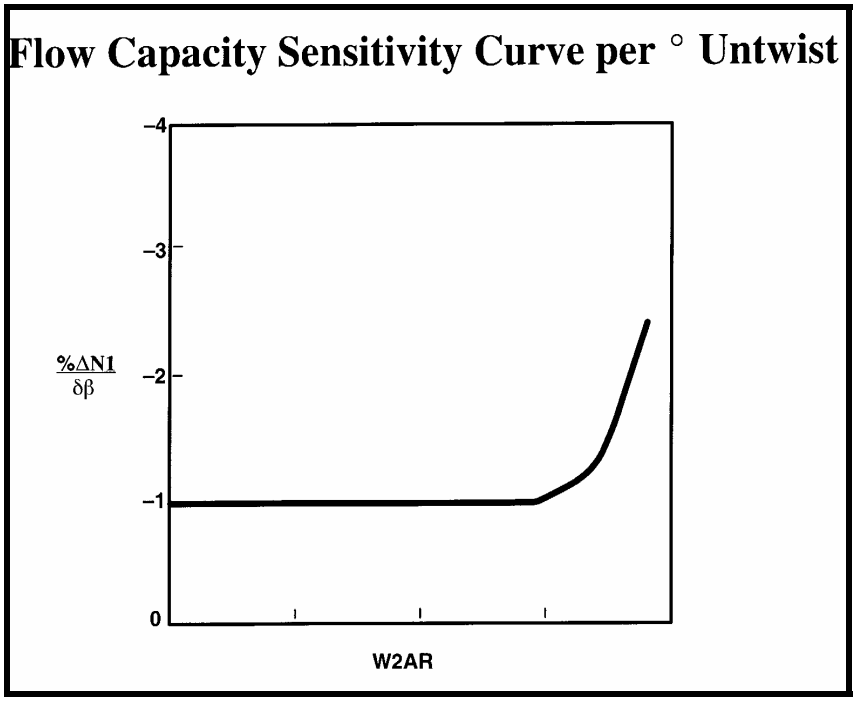

Figure B.42: Blade Untwist Effect vs. Speed.

B.1.1.11.3 Modeling Approach

Although it is possible to use a mechanical model to provide the actual change in blade angle with operating condition, a correlation is typically used for both engine design and component simulation. For engine design these correlations can be quite involved. For 0-D and 1-D models, a correlation with mechanical speed and pressure rise is usual. **Figure B.42** shows typical behavior vs. speed and flight conditions and can adequately be correlated with speed and stage pressure rise for use in a 0-D or 1-D model.

A problem with untwist modeling in multi-stage machines is the complexity of the behavior and the confounding with clearance and Reynolds number effects. Since both of these are a function of flight conditions and clearance is a function of mechanical speed, inadequacies in the models for these three effects are difficult to separate. A good model for one will be misleading when comparing the model with test data where these other effects are ignored. For high bypass fans the impact is large enough to be obvious but even there the ability to make accurate estimates may be limited by the lack of an asymmetric clearance model.

Finally for 2-D and 3-D situations, NASTRAN can be used to calculate the blade untwist effects as a function of radius.

B.1.1.12 Stratification

Stratification is the radial variation in temperature and pressure at the exit of a fan. In a mixed flow turbofan, the average conditions at the fan exit are stratified to generate the separate conditions entering the bypass duct and core. The relationship of these split conditions to the average condition varies with the operating-line, speed and engine-bypass-ratio. Although separate maps can be used for the hub portion and tip portion of the fan, as is often done on high bypass turbofans, the bypass ratio effect may still be significant. Changes in down stream geometry can also affect this behavior as shown in **Figure B.43**. If the splitter is close enough to the fan, the stream line movements to turn the flow to the splitter leading edge can change the splitting streamline position across the fan affecting both the average and stratified performance.

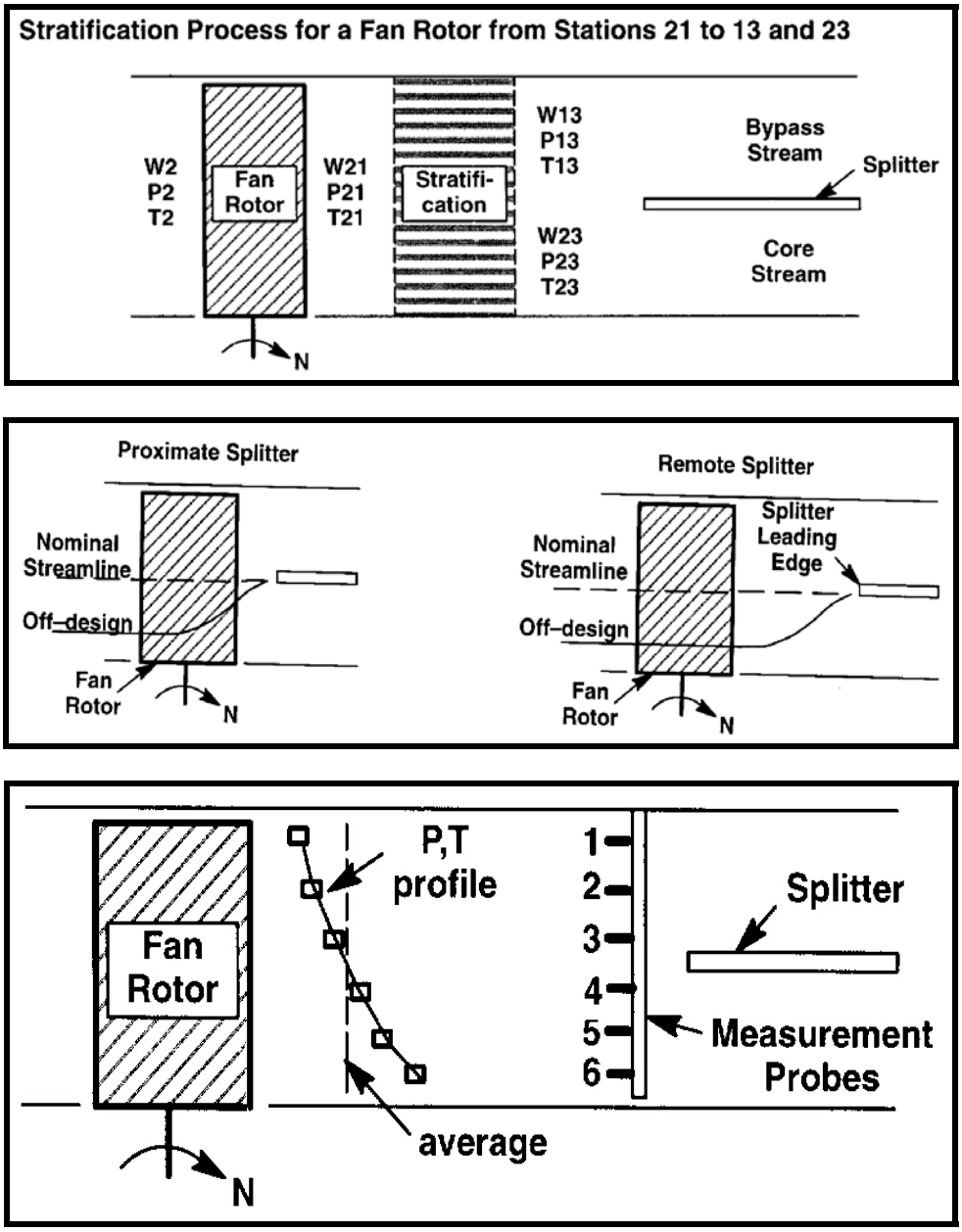

Figure B.43: Effects Associated with Stratification.

For 0-D and 1-D performance, the change in exit pressure and temperature at the tip relative to the average is usually correlated from test data or detailed model prediction. The hub values are then calculated based on conservation. For higher bypass engines the correlation basis may switch, and be based on the hub.

B.1.1.13 Parametric Analysis of Aeroengine Flutter for Flutter Clearance

So far, we have mainly focused on the aerodynamic aspects. Here we will touch on the aeromechanical aspects. Successful aeroengine designs must be free from turbomachinery flutter under all operating conditions. Flutter is a vibrational instability of the rotor blades, which can rapidly promote High Cycle Fatigue (HCF) failure. If not caught during testing and corrected before entry into service use, flutter problems can impact the readiness on a fleet-wide basis (Kandebo, 1994) [B.28].

The work of A. Khalak [B.29] addresses the problem of constructing a rational testing procedure to ensure flutter clearance throughout the operational flight regime of a turbomachine. In so doing, a new set of similarity parameters has been developed for operability assessment. This set consists of four parameters: (m_c, N_c, K_0*, g/ρ*), where the first two parameters are the corrected mass flow, m_c, and corrected rotor speed, N_c, and the latter two parameters are new. These we term the compressible reduced frequency, K_0*, and the reduced damping, g/ρ*.

$$g/\rho^* = \frac{g m_0}{c^2 \rho_0} = \frac{4}{\pi} g \mu$$

The reduced damping, g/ρ*, combines the mechanical damping, g, and the mass ratio, μ, into a single non-dimensional parameter, useful for linear stability purposes. This parameter is defined such that m_0 is the modal mass (per unit length), c is the chord, and ρ_0 is the inlet density. The g/ρ* label emphasizes the dependence upon inlet density. For cases with frictional damping (e.g. inserted blades), the reduced damping is order 1 and has a significant impact on flutter stability.

The compressible reduced frequency, K_0*, is defined as $\omega_0 c / (\gamma RT)^{1/2}$, where ω_0 is the blade natural frequency at rest, and $(\gamma RT)^{1/2}$ is the inlet speed of sound (which varies with inlet temperature, T). The K_0* parameter comes from a decoupling of corrected performance effects from purely aeroelastic effects. Roughly speaking, for a constant structure (i.e. constant $\omega_0 c$) the parameter K_0* varies with the temperature, a parameter for which the performance is "corrected".

The first two parameters of the set, m_c and N_c, account for the corrected performance, as normally measured for high speed turbomachines. For constant structural parameters, the latter two parameters, K_0* and g/ρ*, span the inlet temperature and density. These can be related to the flight conditions in terms of flight Mach number and altitude. An implication of this four-parameter viewpoint is that the flutter clearance of a machine depends on the corrected performance point, and the intended flight envelope of the aircraft.

These parameters were applied to the analysis of full-scale test data. **Figure B.44** shows the trends with K_0* and g/ρ*. Both increasing K_0* and increasing g/ρ* (at constant m_c and N_c) have stabilizing effects upon flutter stability. It is proposed that these trends hold generally. The trend with g/ρ* is analytically based in the equations of motion, and is equivalent (by similarity) to the statement that increasing the mechanical damping is stabilizing. The trend with K_0* is ultimately empirical, but it is supported by several previous studies and is equivalent (by similarity) to the widely-held design principle that increasing the natural frequency stabilizes flutter.

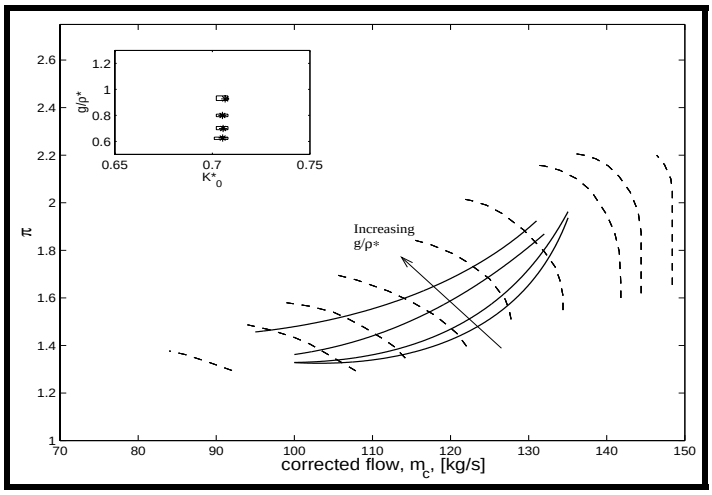

a)

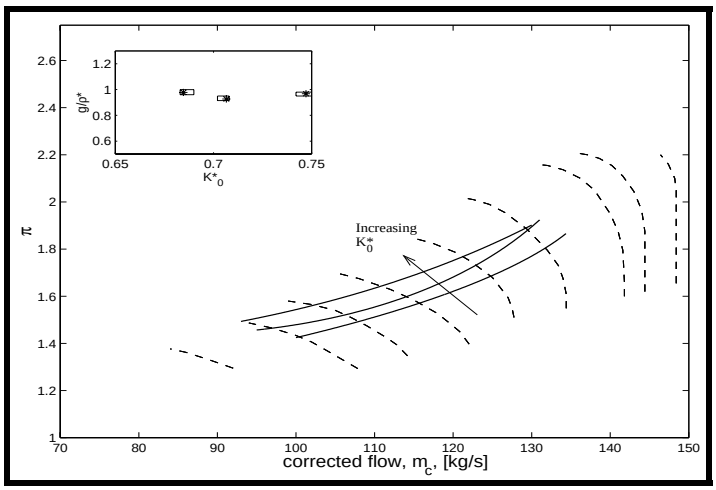

b)

Figure B.44: Trends of Performance Map Flutter Boundary with K0* and g/ρ* from Full-Scale Engine Data.

Figure (a) shows the effect of varying g/ρ*, and (b) shows the effect of varying K_0*. Increases in both K_0* and g/ρ* are stabilizing.

With the relevant similarity parameters spanning a four-dimensional space, the range of comprehensive testing is vast. The proposed trends with K_0* and g/ρ*, however, suggest a way to simplify the requirements for comprehensive testing. Since increasing K_0* and increasing g/ρ* are both stabilizing, it follows that the worst case at a particular (m_c, N_c) are the minimum values of K_0* and g/ρ*. Thus, clearance for the engine at the minimum K_0* and g/ρ* implies clearance throughout the flight regime.

B.1.2 Simulation of Centrifugal Compressor Performance

The Performance of a centrifugal compressor simulated in an engine performance model is very similar to the modeling for axial compressors. A basic compressor map is generated based either on test data or by an analytical process in the case of a new compressor. This section will discuss the primary differences

between a centrifugal stage and an axial stage and then describe the effects of various parameters on the performance of centrifugal compressors.

B.1.2.1 Key Centrifugal Compressor Characteristics

Figure B.45 shows the comparison of a typical axial stage and a centrifugal stage. An excellent description of both types of compressors is given in Cumptsy, N.A. **[B.3]**. A short summary is presented to highlight the differences that affect performance. For this discussion, centrifugal stages will be assumed to have an impeller inlet (inducer) region that is similar to an axial stage as is typical of aircraft applications. Process and industrial compressors often may not include an inducer section.

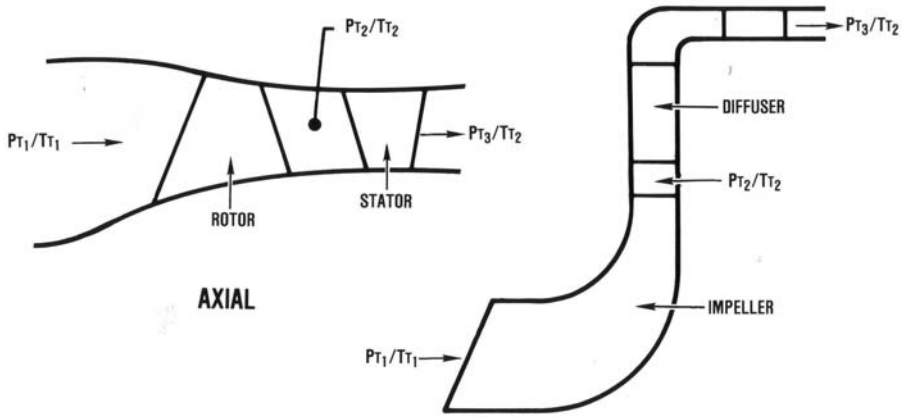

Figure B.45: Comparison of Centrifugal and Axial Stage Flowpaths.

Whereas the inlet regions of the two types of stages are similar, the exit regions are entirely different in that the impeller flowpath turns from axial at the inlet towards vertical at the exit (usually 90 degrees relative to the engine centerline). The exit radius is significantly larger than the mean inlet radius. This much larger exit radius means that the centrifugal stage can produce much higher Pressure Ratio than a single stage axial compressor. This is evident by examining the basic angular momentum equation of turbomachinery:

$$(H_{0x} - H_{0i}) \sim (U_x * V_{\theta x} - U_i * V_{\theta i}) \qquad \textbf{Eq. B-1}$$

For a centrifugal impeller, the exit tip speed, U_x can be much higher than the inlet tip speed, U_i and therefore the Work (or P/P) per stage can be much higher than for an axial stage. A typical curve of P/P versus impeller exit tip speed is shown in **Figure B.46** assuming no inlet swirl ($V_{\theta i} = 0$). Of course a multi-stage axial compressor can achieve a similar P/P by adding stages. The trade-off of axial length versus diameter and weight often determine the type of configuration selected for a given application.

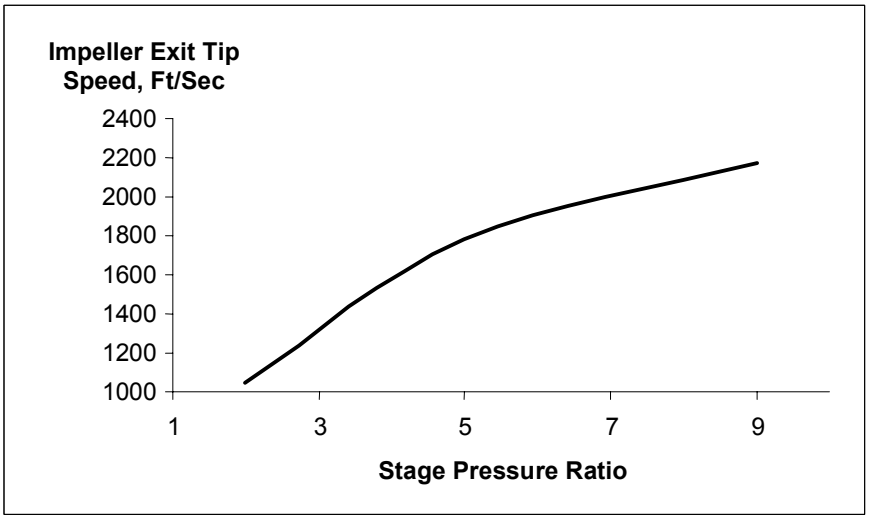

Figure B.46: Impeller Exit Tip Speed vs. Stage Pressure Ratio.

Another critical parameter for centrifugal stages is the exit blade angle of the impeller. **Eq. B-1** can be rewritten as:

$$(H_{0x} - H_{0i}) \sim (U_x{*}V_{mx}{*}\tan(\beta_x) - U_i{*}V_{mi}{*}\tan(\beta_i)) \qquad \textbf{Eq. B-2}$$

where V_m is the meridional velocity and β is the relative air angle. Correlations have been established to relate the exit air angle and blade angle. Again assuming no inlet swirl, **Figure B.47** shows the impact of exit blade angle on centrifugal stage Pressure Ratio for a fixed impeller diameter.

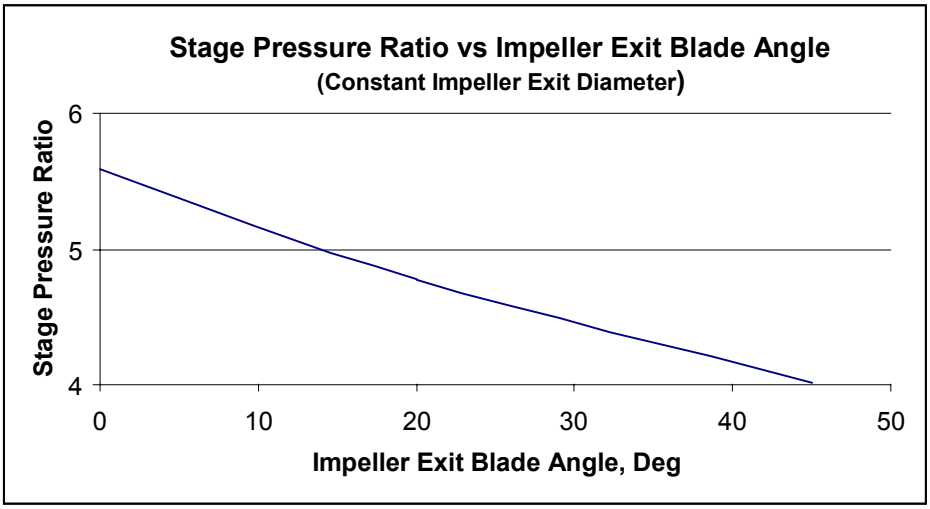

Figure B.47: Stage Pressure Ratio vs. Impeller Exit Blade Angle.

This curve clearly shows that reducing the impeller exit blade angle increases the Pressure Ratio capability of a given impeller diameter. The key missing element is the variation of stage efficiency with exit blade angle. Current technology centrifugal stages now routinely use impeller exit blade angles varying from 30 – 50 degrees. The reason for incorporating this level of exit blade angle is illustrated in **Figure B.48**, which compares the compressor maps of two stages designed for the same Pressure Ratio. The first

compressor has 0 degree exit blade angle (radial) whereas the second compressor utilizes 40+ degree of exit blade angle. Whereas the two compressors have similar Flow-Pressure Ratio characteristics and similar stall margins at design speed, the stage with the higher exit blade angle has peak efficiency at the operating line. The stage with 0 degree exit blade angle has the same level of peak efficiency but it occurs at the stall line. Efficiency at the operating line is 2+ points lower. It is clear that unless there are engine constraints such as axial thrust requirements or engine diameter constraints, impellers should use a reasonable level of exit blade angle.

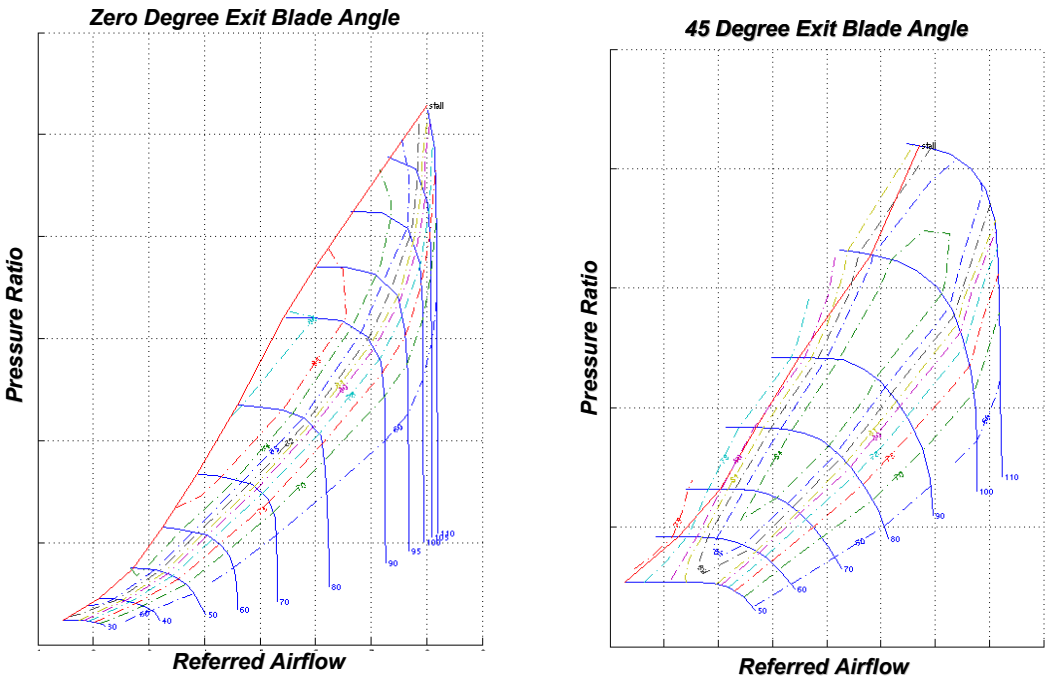

Figure B.48: Comparison of Centrifugal Compressor Maps with 0 deg and 45 deg Exit Blade Angles.

The primary materials for centrifugal impellers in aircraft applications are steel and titanium. Depending on costs, life, and environment, each material has distinct applications. Mechanically, material capability is a function of operating stress levels and temperature. This latter capability is depicted in **Figure B.49**, which shows approximate impeller tip speed versus impeller exit temperature for the two materials. The final shapes of these curves are a function of the detailed shape of the impeller disk.

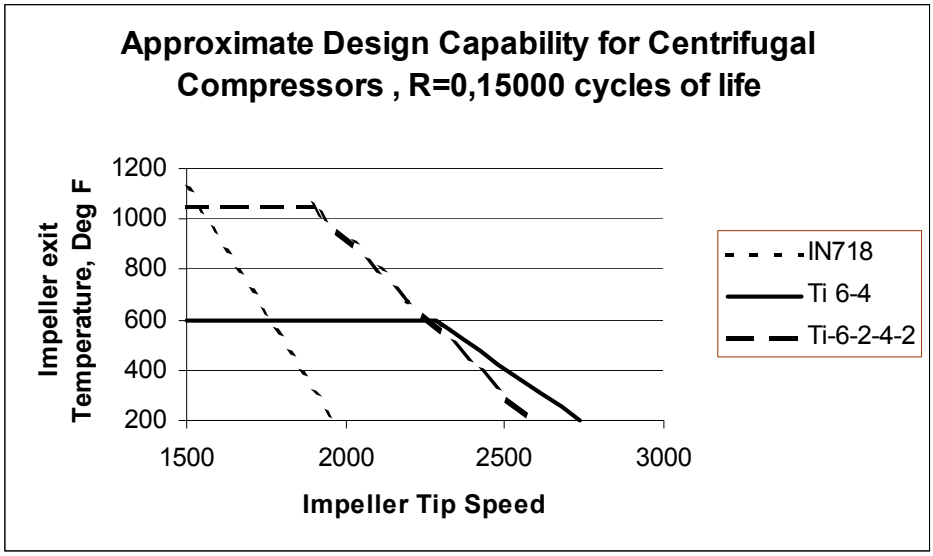

Figure B.49: Impeller Exit Temperature vs. Impeller Tip Speed Material Capability.

The diffuser is the other key component for centrifugal stages. For nearly all aircraft and APU applications, it consists of a vaneless space, radial diffuser, and either a 90 degree bend and deswirl system or a collecting scroll device. Multi-stage centrifugal compressors utilize a return duct system to return the flow back to the inducer of the following stage. All aspects of modern centrifugal stages can be seen in **Figure B.50**, which shows the engine cross-section of a modern Auxiliary Power Unit. The Power section consists of a single-stage centrifugal compressor and a Load compressor, which includes a variable inlet guide vane and collecting scroll. (**Figure B.51** added as an example of integral bleed engine, but not yet described or discussed.)

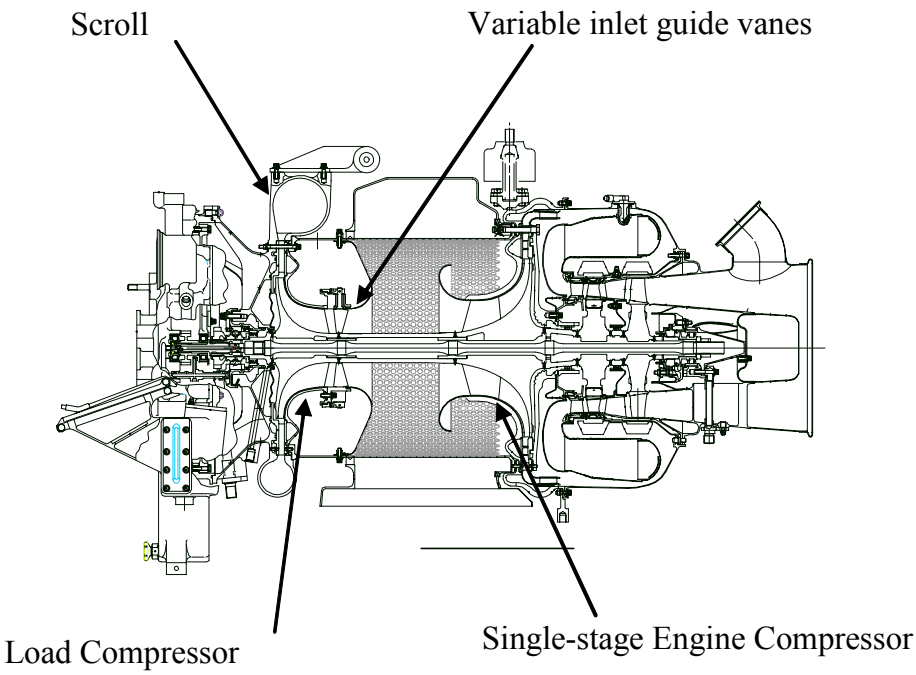

Figure B.50: Load Compressor Auxiliary Power Unit Engine Cross-Section.

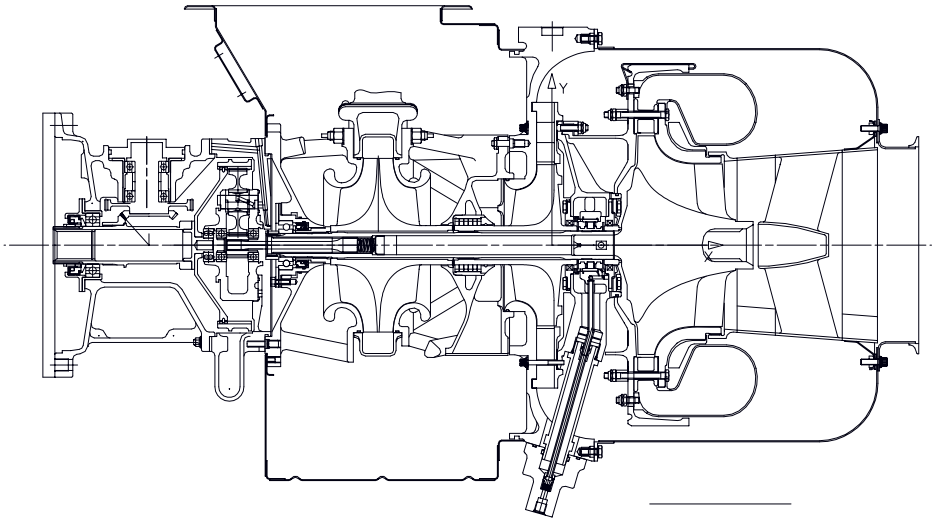

Figure B.51: Integral Bleed Auxiliary Power Unit Engine Cross-Section.

Again, Cumptsy [B.3] has an excellent description of the basic diffusion system and its performance characteristics. He points out that the static pressure rise in the diffusion system is all accomplished by decelerating the flow and converting kinetic energy into static pressure. For centrifugal compressors, this diffusion process is even more significant than for axial stages as the exit Mach number requirements are usually much lower. For two-stage centrifugal compressors, the Mach number in the return duct system can be near the second stage inlet Mach number to minimize losses. Pressure recoveries of 75 – 80% can be achieved in many diffusion systems by minimizing the flow separation in the diffusing passages.

A properly matched centrifugal stage is depicted in **Figure B.52**. The impeller usually has a much larger flow range from choke to stall than the diffusion system. When the stages are matched properly, the stall and choke flow at design speed is often set by the diffuser. At higher corrected speeds, the impeller controls flow capacity. At part speed the diffuser controls flow capacity when the stages are well matched. Peak impeller efficiency and minimum diffuser loss occur at nearly the same flow point at design speed.

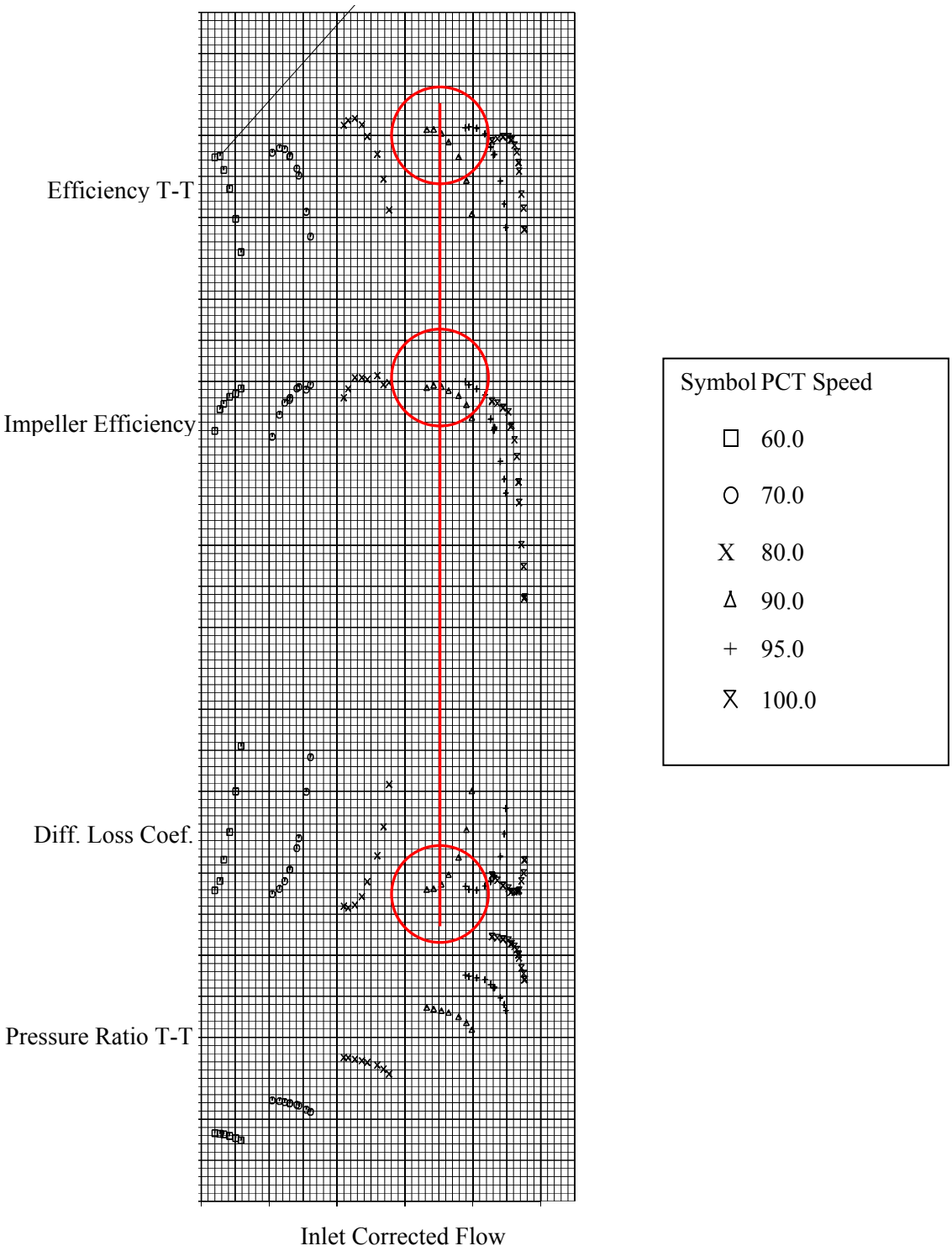

Figure B.52: Impeller-Diffuser Matching.

The Load Compressor APU is used in both military and commercial aircraft applications as a means of supplying variable air requirements for the main propulsion engine. The cross-section in **Figure B.50** illustrates the load compressor on the left side attached to the same shaft as the power section with a

common inlet. An inlet guide vane is used to essentially shut off the flow capacity of the Load Compressor during starting. An APU for aircraft applications is essentially a single speed device and runs at design physical speed for most of its operating conditions. This constant speed operation can simplify the mechanical challenges of the impeller design. Due to the significant variation in corrected speed due to ambient air changes with altitude, an APU compressor usually operates from 90% corrected (referred) speed on hot days to 115% corrected speed at high altitude, cold day. Due to the wide range of IGV positions from nearly shut-off to over open at max power, there can be significant inlet distortion patterns generated due to the unique inlet plenum configurations that are often used in APUs. These distortion patterns are very complex and are usually not symmetric circumferentially. **Figure B.53** shows a typical pattern entering an impeller from an inlet plenum.

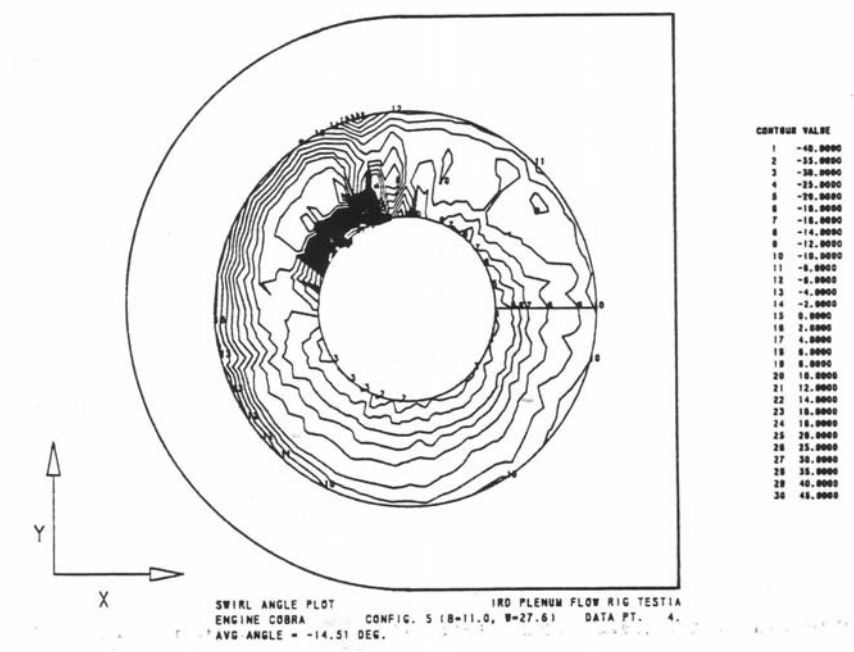

Figure B.53: Swirl Pattern Entering a Centrifugal Compressor from a Typical Plenum.

The reason for discussing the effects of these basic parameters here is for information that may useful to people who may be doing field repair work. Care must be taken in the blend repair of nicked parts both from a structural and aerodynamic viewpoint. Reworking leading and trailing edges of impellers and diffusers can significantly affected the performance of the stage. Leading edge blending can affect part speed stall margin as well as efficiency. Cutting back the trailing edge of an impeller will lower the Pressure Ratio capability of the stage and change the match with the downstream diffuser usually reducing flow capacity and potentially increasing diffuser losses. Blending a diffuser leading edge nick will change the match between the impeller and diffuser and will probably reduce the stall margin of the stage.

B.1.2.2 Effects of Tip Clearance

Due to the significant reduction in blade height as the flow passes from the inlet to the exit, tip clearance sensitivity is much larger at impeller exit than at the inlet. Correlations have been developed through significant testing to express the variation in stage efficiency as a function of impeller exit clearance to impeller exit blade height. The large scatter in the data is related to the detailed blade shapes defined in the design process. This significant variation was illustrated in Palmer and Waterman's ASME Paper **[B.30]** and is presented in **Figure B.54**.

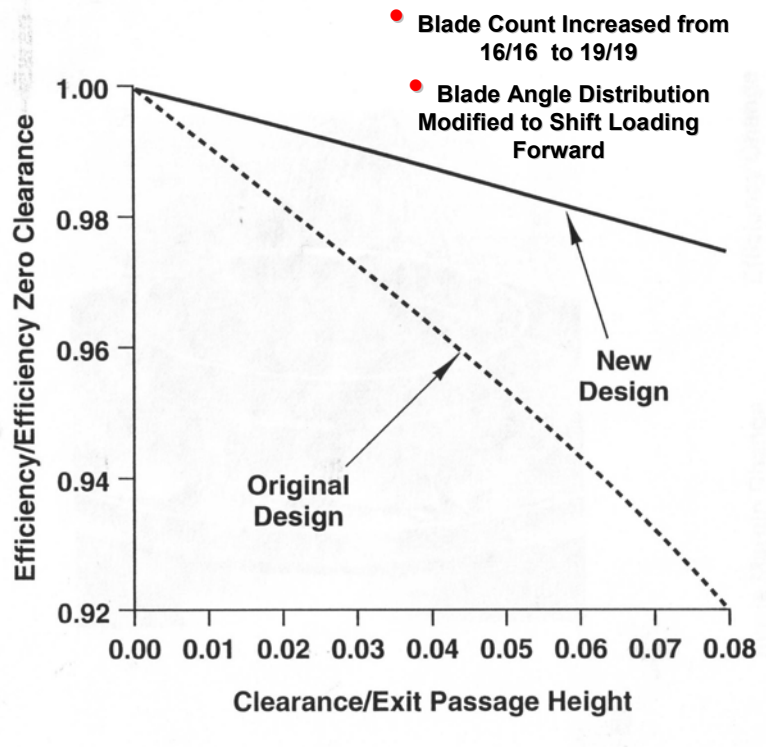

Figure B.54: Improved Clearance Sensitivity by Reduced Blade Loading.

This figure compares the clearance sensitivity of an original 16 main blade/16 splitter bladed second-stage impeller to a new design having 19 main blades/19 splitters. Clearly, the reduced impeller loadings due to increased blade count and revised blade angle distribution has had a significant effect on the rate of efficiency loss with increasing axial tip clearance. The low clearance sensitivity allows the second stage to operate efficiently at a robust 6 percent axial clearance-to-exit blade height needed for the extremely rapid helicopter acceleration requirements for this particular application.

B.1.2.3 Effects of Surface Roughness on Performance

Centrifugal compressor performance is significantly affected by the stationary shroud surface roughness over a rotating impeller. The small clearance gap makes this scrubbing flow very sensitivity to the surface roughness of the shroud. This sensitivity is illustrated in **Figure B.55** taken from Palmer and Waterman's ASME paper, **[B.30]**. Using a pipe-flow analogy for a centrifugal stage, the characteristic length for similarity is the hydraulic diameter (which is nearly equal to the impeller exit tip width). On this basis, centrifugal compressor Reynolds number effects can be correlated, as shown in the figure, to illustrate the effects of surface roughness at high Reynolds numbers. The Reynolds number of the selected second stage compressor is indicated on the figure (Reb = 3.5 x 10^5). As can be seen, the second stage lies in the hydraulically rough regime with a roughness of 350 micro-inches and in the transition region between hydraulically rough and hydraulically smooth with a roughness of 70 micro-inches. The predicted change in efficiency is 4.0 points which converts to approximately 1.6 points in the overall two-stage efficiency for the compressor configuration. The tested performance change for the overall two-stage efficiency was 2.0 points at the design point, verifying the criticality of stationary shroud surface roughness on compressor performance.

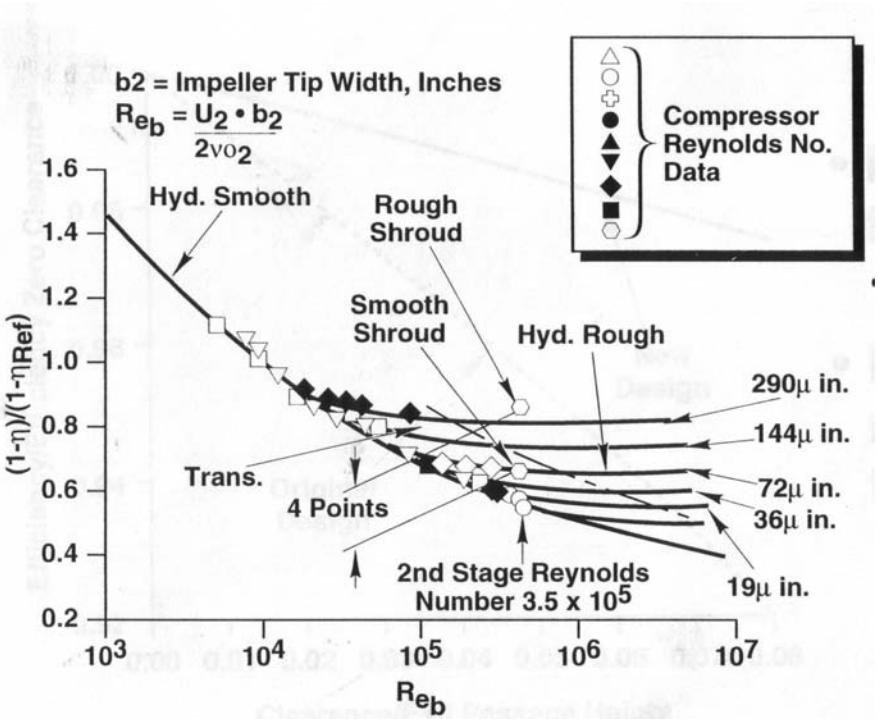

Figure B.55: Single-stage Centrifugal Compressor's Loss versus Reynolds Number.

B.1.2.4 Effect of Erosion on Performance

The effect of erosion, particularly sand erosion can have a large performance impact on turbomachinery components. Axial compressors are more sensitive to erosion compared to centrifugal stages for the same material. Quite often the first stage of axial compressors will be manufactured from steel if the compressor is utilized in a helicopter application. This section describes the results of a 50-hour sand ingestion test on a helicopter engine as reported in [B.30]. The engine was subjected to a 50-hour C-spec sand ingest test, an AC-fine sand test, and an AC-course sand test. The C-spec sand is generally considered to have the most potential for damage due to the high percentage of large particles. This test encompassed 50 hours of engine operation at maximum continuous rated power with sand contaminant introduced into the engine inlet at 53 mg per cubic meter of engine inlet air. The engine was equipped with an integral particle separator with a very high separation efficiency, therefore, most of the sand did not reach the compressor. However approximately 2.39 pounds of sand went through the engine core.

Engine performance deterioration was less than 5 percent horsepower at 25 hours and 10 percent at 50 hours. Diagnostic analysis of the pre- and post-test data indicated the compressor efficiency degraded over the range of 85 to 100 percent speed and was the major cause of the engine performance loss.

Post-test inspection of the compressor hardware showed:

- The leading edges of the first stage impeller blades were eroded as shown in **Figure B.56** with higher value near the hub.
- A slight channel on the pressure side of each blade and splitter at the exducer of the first-stage impeller.
- An increase in roughness on the first-stage shroud abradable coating.
- No visual signs of second-stage impeller leading edge erosion was noted.

- The second-stage shroud had a polished appearance.
- Only minor evidence of erosion was noted on the first- and second-stage diffusers and deswirl assembly.

This example shows the robustness of centrifugal compressors to sand and dust erosion.

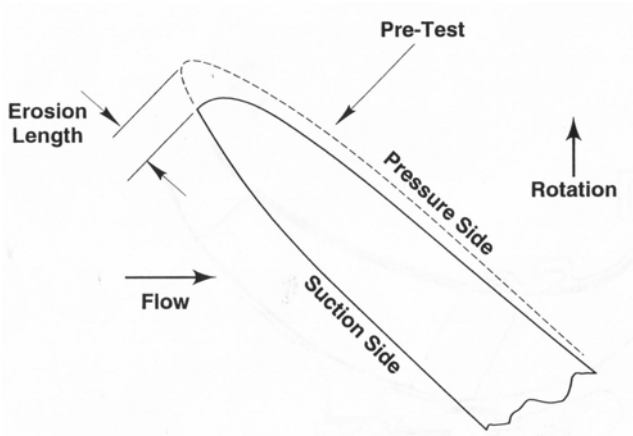

Figure B.56: First-Stage Impeller Leading Edge Sand Erosion.

B.1.2.5 Effect of Inlet Plenum on Performance

With the "buried" installations of APUs and with some helicopter applications, the effect of the inlet on compressor performance can be significant. The typical inlet plenum for an APU is shown in **Figure B.57**. The two most significant parameters that can impact compressor performance are:

- The ratio of the impeller inlet annulus area to the inlet plenum area (B x W); and
- The inlet plenum aspect ratio (B/W).

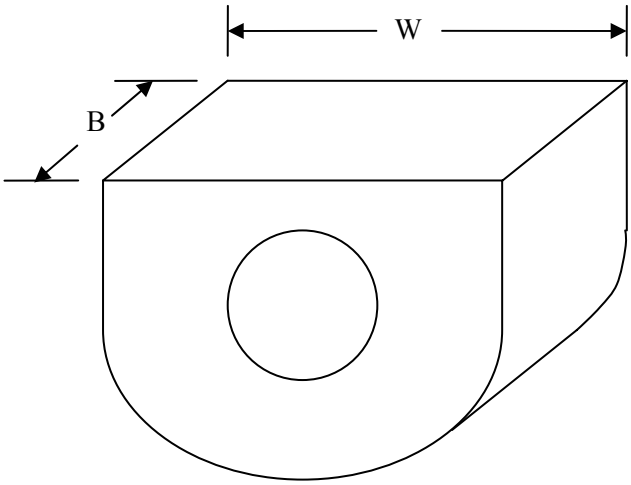

Aspect Ratio = B/W
Area Ratio = Impeller Eye/B·W

Figure B.57: Inlet Plenum Cross-Section.

Systematic testing with an inlet plenum flow rig that measured the pressure loss across the plenum is presented in **Figure B.58** and shows the rapid increase in plenum loss when the aspect ratio is less than 0.4. Keeping the aspect above 0.4 is essential to minimize plenum effects. In addition to aspect ratio, the plenum area ratio is the other significant parameter. This effect is best evaluated by comparing the efficiency of the entire compressor configuration including the inlet plenum. The reason for this is that the inlet distortion from the plenum affects the basic performance of the compressor in addition to the inlet plenum loss. **Figure B.59** shows that compressor efficiency can decrease as much as 3+ points in efficiency when a plenum with a poor aspect ratio (B/W = .27) and Area Ratio of 0.25 is added to a base compressor. This data is not necessarily in disagreement with data presented by Colin Rodgers **[B.31]**. He states that area ratios of .25 or smaller result in low loss plenums. This paper does not reference the aspect ratio of the plenum tested. The above data indicates that both parameters are important.

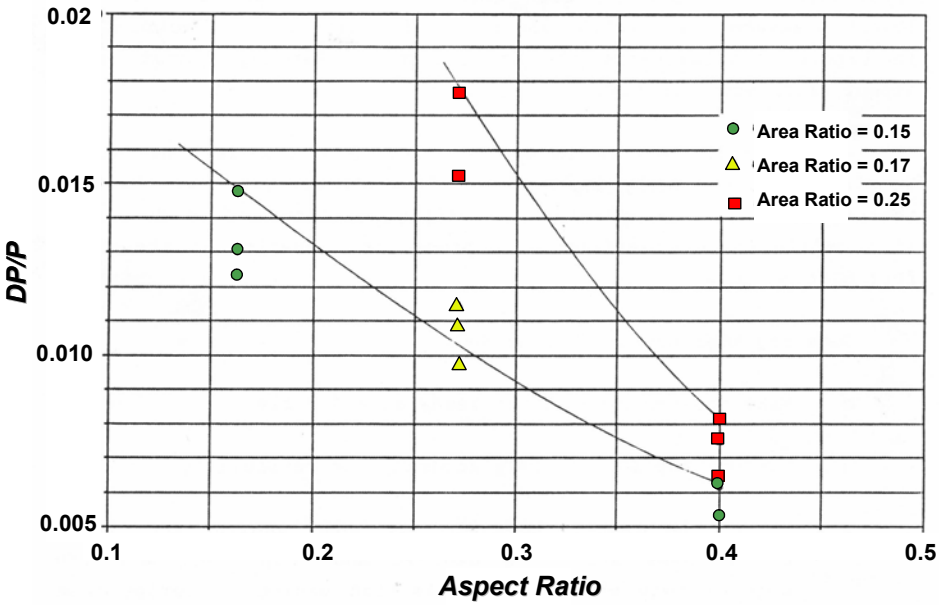

Figure B.58: Effect of Plenum Aspect Ratio and Area Ratio on Plenum Loss.

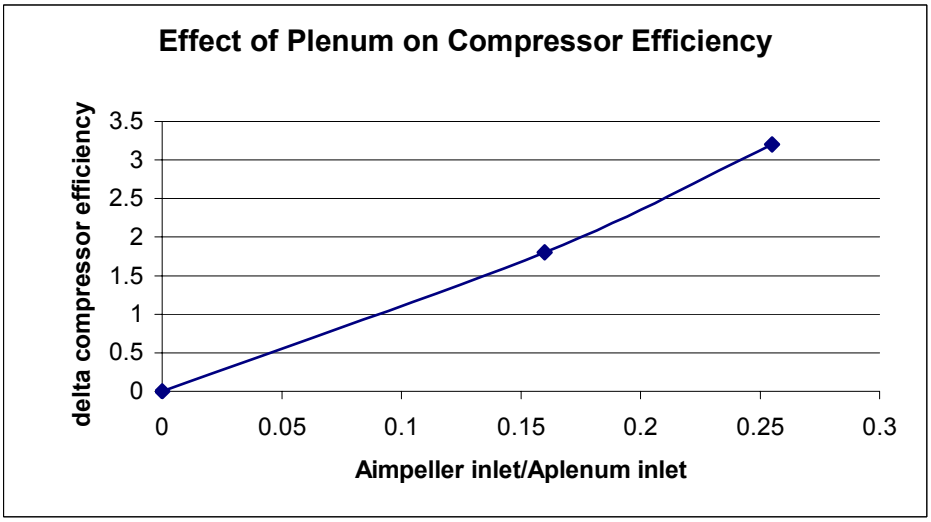

Figure B.59: Effect of Plenum Area Ratio on Compressor Efficiency.

B.1.2.6 Effect of Leakage on Performance

Due to the high pressure ratio achieved with centrifugal compressors, leakage can have large effects on compressor efficiency. There are two types of leakage that are most serious, recirculation and diffuser endwall leakages. These leakage paths are indicated in **Figure B.60**. Recirculation leakage can be from the exit of 1 component back to the inlet of that component or back to the inlet of the compressor. Another type of recirculation leakage can be from the turbine component to the backside of the compressor. All of these can result in loss of compressor flow capacity and or compressor efficiency. Testing has shown efficiency loss of over two points from just diffuser leakage from compressor exit back to diffuser inlet. This flow jetting back into the diffuser inlet region usually results in 2 – 4 percent loss in flow and pressure ratio along an operating line.

Diffuser endwall leakage can be just as serious. To minimize cost, compressors are manufactured with radial diffusers that are butted together at one endwall instead of brazing or securing the vanes to the endwall with studs or bolts. At operating temperature, the structures move significantly and diffuser endwall gaps develop especially near the leading edge region. Significant loss in diffuser pressure recovery was a result. A variable vane diffuser (via a button near the leading edge) was tested at various diffuser endwall clearances. The test results indicated over a 7-point reduction in compressor efficiency when the vane clearance gap was increased from zero to one percent of the diffuser vane height in order to be able to rotate the vanes. It is important to have minimal leakage in the compressor section. Developing and incorporating leakage models into engine simulation is critical to diagnosing the correct components to examine as engine performance changes with time.

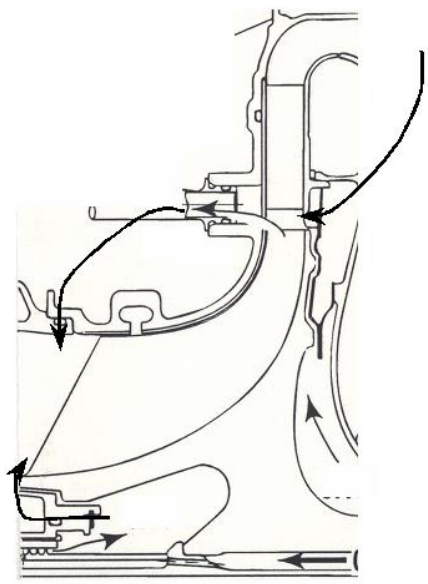

Figure B.60: Cross-Section of Centrifugal Stage Showing Leakage Paths.

B.1.2.7 Effect of Flowpath Steps

Conventional wisdom would say that flowpath steps should always be down, i.e. like a waterfall. However, looking at **Figure B.61**, which is reproduced directly from Hoener, **[B.32]**, the figure shows the drag coefficient for a variety of types of steps (steps up, steps down, blunt, rounded, etc.) on the sheet metal skin of aircraft, but is equally applicable to internal ducting of modern gas turbine engines. The higher the drag coefficient, the greater the loss in pressure.

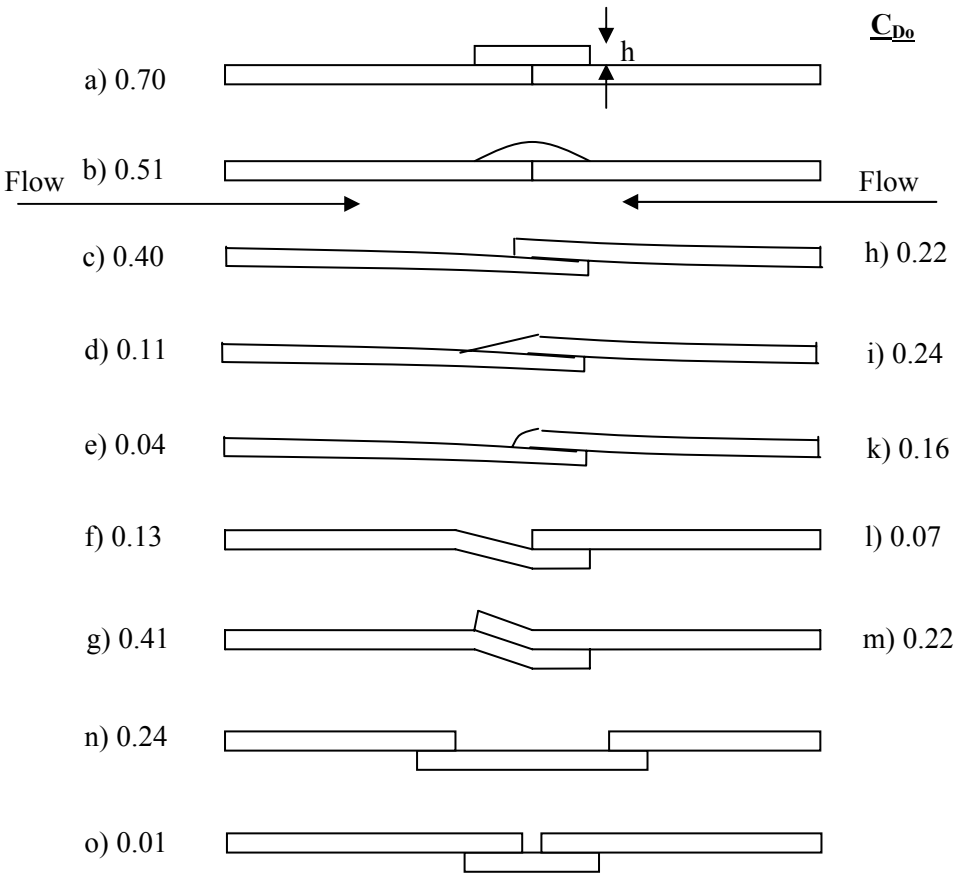

Figure B.61: Independent Drag Coefficient of Various Sheet Metal Joints, Based on Thickness, "h".

Drag coefficient is defined as

Cd = Drag / (q * S)

where q = velocity head (Ptotal - Pstatic or 1/2 * density *V^2)

S = a representative area (like wing area or a pipe area)

Note that coefficients are shown in the figure for flow from either direction, left or right, thereby for a step up or down. The following observations can be made:

- Comparing c (a blunt step up) to e (a rounded well treated step up) in the flowpath, the well treated step up reduces the drag by a factor of 10.
- Comparing h (a blunt step down) to e (the same rounded step up), the well shaped step UP is 5 times better than a step down.
- Even a 30 degree ramp (bevel) up (i) is half the drag of a beveled step down.

A "rounded well treated step up" is one that has the step shaped with a quadrant of an ellipse, preferably a 4:1 major/minor diameters (meaning blending the length over 2 times the height of the positive step). This is analogous to an entry bellmouth, which is continuously accelerating with little or no loss-producing diffusion. The above comparisons were made to counter the "conventional wisdom"; other comparisons are left to the reader (with an open mind). This data applies only to Mach numbers below

about 0.5 where there is little danger of local shocks forming on sharp corners, etc. Also, this applies only to small steps and ignores area changes.

B.1.3 Methodologies

We have so far been examining physical factors that impact the compressor performance and stability margin; these have been referred as compressor characteristic modifiers. In this section we will discuss analytical or computational models for assessing the effects of some of these characteristic modifiers on a quantitative basis. In principle one can proceed to build a correlative database for defining the effects these have on compressor performance through extensive testing. Such an approach, while of engineering utility, does not provide a rigorous scientific approach or basis that would allow one to predict changes in performance due to changes in the modifiers. Computational techniques have often been suggested as the ultimate means to predict component performance and its change with subsequent alteration of parameters such as tip clearance and operating conditions from those it is designed for. However as articulated by Adamczyk [B.1], the range of time scales and length scales encountered in flows through multi-stage compressors are so broad that it is unlikely that direct computation is feasible in the foreseeable future. Adamczyk suggested that one way to overcome this is to calculate fluid dynamic effects when the computational timescales are acceptable, and to model them on other occasions. Such an approach has been adopted by Adamczyk [B.1] and Rhie et al. [B.2] to develop procedures to compute the performance of a multi-stage compressor. In the following, methodologies to provide quantitative assessment of the impact of characteristic modifiers, via the simulation of flow phenomena in multi-stage compressors, are described.

B.1.3.1 Approximations at Global Level

In the development of techniques for simulating flow phenomena in multi-stage compressors with the aim of extracting quantitative information on compressor characteristics and its modifiers, there are two levels of approximation:

- Physical Approximations to problem under consideration; here we first ask the following question:
  - What is it that is important to include?
- Numerical approximations to partial differential equations (PDE) for the problem.

In general the various levels of physical approximation for flow phenomena can broadly be given as follows:

- Navier-Stokes equations (direct numerical simulation);
- Large eddy simulation;
- ‘Reynolds averaged’ Navier-Stokes equations – this would require the use of a turbulence model;
- Thin shear layer approximation;
- Inviscid Euler equations;
- Steady flow vs. unsteady flow;
- Three-dimensional vs. two-dimensional flow;
- Streamline curvature;
- Throughflow methods (hub-to-tip and blade-to-blade);
- Potential flow equations;
- Incompressible flow; and
- One-dimensional flow (control volume approach).

Because of the large range of length and time scales involved in the multi-stage environment, high-speed multi-stage turbomachinery flows are not presently amenable to direct numerical simulation (Adamczyk). Thus it is still necessary to develop multi-row geometry models that yield 'averaged' descriptions. These provide useful information that can be used to generate compressor performance maps and to quantify changes associated with characteristic modifiers. Hence we have to address the basic question of "What is the proper level to average at?" Furthermore the flow in multi-stage compressors is inherently unsteady. One is thus interested in assessing the time averaged impact of flow unsteadiness on compressor performance. (The characteristic modifier associated with changes in axial gap is a good example to illustrate this aspect of the problem.) In view of this it is useful to draw on the equation of hierarchy for turbomachinery flow given by Adamczyk:

- Navier-Stokes Equation – No closure, direct simulation;
- Reynolds-averaged Navier-Stokes Equation – Reynolds stresses, energy correlations;
- Time-averaged equations – Body forces, energy sources, correlations;
- Averaged passage equations – Body forces, energy sources, correlations;
- Axisymmetric equations – Body forces, energy sources, correlations; and
- Quasi-one-dimensional equations (control volume approach).

It is clear from the above that as one proceeds downward through this list, the degree of empiricism increases. Or more positively, one needs to do an ever better job of flow modeling. Conversely, the requirement for computational resources increases as one proceeds upward through the list.

B.1.3.2 Discrete Approximations to PDE

The result of physical approximation to the problem is a set of partial differential equations. To solve this set of PDE, one needs to discretize the PDE both on the spatial and on the temporal basis. These discretizations are summarized below:

- For spatial discretization:
  - Finite difference method (FDM);
  - Finite element method (FEM);
  - Spectral methods;
  - Finite volume method;
  - Hybrid method; and
  - Vortex methods – singularity methods.
- For temporal discretization:
  - Finite difference method;
  - Finite element method; and
  - Spectral method.

In the following, we will present examples that involve both levels of approximation for assessing changes in compressor performance.

B.1.4 Theoretical Model

The computed or predicted results shown as a solid line in **Figure B.16** and **Figure B.17** are based on the theoretical model of Hynes and Greitzer **[B.33]**. It addresses the behavior of two-dimensional flow-field

disturbances that have a length scale of the order of the compressor circumference (larger than the blade pitch). The model is thus strictly applicable only to situations where the flow through the compressor may be considered as radially uniform. In the model, the pressure rise across any blade row in the compressor is taken to consist of: that achieved in steady uniform flow, at the local inlet conditions plus that necessary to balance the acceleration of the fluid, within the blade row. The upstream and downstream flow-fields, and the overall flow system within which the compressor operates, are described in terms of the flow equations. In addition, the instantaneous loss across the blade-row lags the incidence changes with a timescale in the order of the convection time through the blade.

Assessing the effect of inlet distortion on flow stability through the compressor is inherently a nonlinear problem. This is apparent from the nonlinear relationship between compressor performance and flow coefficient. However the nonlinearity associated with the flow-fields upstream and downstream of the compressor are of lesser importance than those associated with the compressor performance. Hence a linear treatment is appropriate and is shown to be so, through assessment of the computed results from the model against measurements. Because the background flow is non-uniform the unsteady disturbance flow-field will not have a purely sinusoidal distribution round the annulus. Furthermore, the annulus averaged mass flow is not generally zero (in contrast to the situation of uniform background flow). This implies that the global compression system behavior is coupled to the local compressor behavior.

The compression system model essentially consists of a compressor pumping to a plenum that exhausts through an ideal throttle. The length of compressor ducting is assumed to be sufficiently long to ensure that there is no asymmetric potential flow interaction with the inlet and exit duct terminations. The inlet distortion, in total pressure terms, is specified as a function of circumferential position and time. This is at a location upstream of the asymmetric static pressure field ahead of the compressor. The background flow corresponding to the specified inlet distortion in the absence of flow instabilities can now be determined. To assess the stability of the compression system, an arbitrary small, unsteady flow disturbance is added to the background flow. If any such flow disturbance grows with time, the flow through the compressor is considered unstable. Such an approach is a standard technique in stability theory and constitutes an eigenmode and eigenvalue problem. The unsteady flow disturbances can be viewed as incipient stall cells when they propagate around the annulus and as small amplitude, surge-like system transients when they are predominantly one-dimensional in character.

The results of **Figure B.16** show that the computed stability degradation is in good agreement with the measurements for one-resonance-peak response compressor, implying that the stability margin degradation is associated with two-dimensional long circumferential-length-scale phenomena. However the model does not accurately capture the measured stability margin degradation for two-resonance-peak response compressors, **Figure B.17**.

When the model was applied to the determination of the overall compressor pressure rise characteristic in the presence of rotating distortion **[B.34]**, the compressor performance deteriorated with a drop in pressure rise capability and a decrease in stability margin as the distortion co-rotating speed increased. For a co-rotating speed of 0.3 rotor speed, there is only a small flow regime for which the compressor is stable. This is indicated by the progressive shift to the right of the neutral stability points indicated as solid circles. A drastic decrease in compressor stall margin can be the result when the inlet distortion is co-rotating at a speed corresponding to the propagating speed of the stall inception disturbance. An analogous drop in compressor stability margin occurs when:

- The system frequency (the one-dimensional surge-like instability mode) coincides with the frequency at which rotating stall would propagate.
- When the difference between the co-rotating speed of the imposed rotating inlet distortion and that of rotating stall coincides with the frequency of the one-dimensional surge-like mode **[B.34]**.

B.1.5 Application of CFD and Flow Models for Compressor Performance Assessment

In addressing the overall performance of multi-stage axial compressors, it is useful to characterize the flow variation on the following two length scales:

- The blade pitch; and
- The scale through which the blade row components interact, which is larger than the blade pitch.

In the following, we describe an approach used to develop a methodology that allows one to address flow instabilities in a multi-stage compressor in a practical manner. The procedure has the potential of establishing the design characteristics of each blade row so that the multi-stage compressor may have more desirable stability properties. This offers the possibility of designing a local component for optimal performance of the integrated system.

In essence, the approach takes advantage of modern CFD where it is appropriate to do so, and would take advantage of modeling the response and dynamics of the component when it is expeditious to do so. The modeling of the response and dynamics of the component can be implemented through the use of modern CFD tools. For instance, the pressure rise characteristic and the loss characteristic of a blade row can be established through local blade-row calculations. This information can then be used to represent each blade row as an appropriate body force distribution for compressor stability analysis or simulation. The flow-field in the blade-free regions can be described by the Navier-Stokes equations so that the presence of each blade row then appears as a source term to the Navier-Stokes equation. The aerodynamic coupling among the components would perceive the presence of the blade as a region of continuous body force distribution, rather than the detailed events in the individual blade passage. This is so because the interaction occurs on a length scale larger than the spacing between the blades.

However, the effects of the blade passage event should be reflected in the representation of the blade row by a continuous body force distribution. Thus, in the stability analysis of the multi-stage axial compressor, local calculations are made, for components such as the fan, fan exit guide vane, and rotor-stator pair, to establish the physical information needed for representation of a body force distribution (see **Figure B.62** local to system level). This is then used in the multi-stage compressor-stability calculations **[B.35]**.

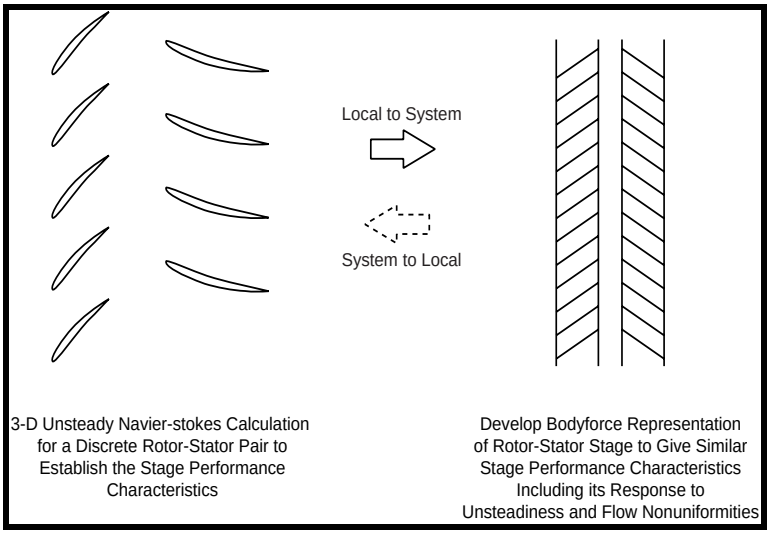

Figure B.62: Duality of Local and System Calculations.

Conversely, the multi-stage compressor-stability calculation can be used to establish the desired design characteristics of each blade row that will result in a compressor design that has the desirable stability

properties. This is then followed by a detailed design of the blade row to yield the desired design characteristics.

In summary, the proposed approach consists of two levels of analysis or simulation:

- Global system level analysis/calculation: The blade rows are represented as a body force distribution appearing as a source term to the flow equation describing the flow through the system. This has been applied successfully at the MIT Gas Turbine Laboratory to the development of a computational model for simulating inception and development of three-dimensional aerodynamic instabilities in a multi-stage compressor and its response to inlet distortion [B.35].
- Local level CFD calculation at the component level: This is used to establish information for use in the representation of the blade row as a body-force (i.e. local to system level). Likewise, this can also be used to design the blade row to yield the desired component characteristic to result in a compressor with good operability characteristics (i.e. system to local level).

To assess the impact of adjacent blade rows or adjacent stages, we can first implement unsteady 3-D flow in a discrete rotor-stator environment. (The computed results in this situation can be post-processed to examine the influence of adjacent blade rows on the resulting unsteady blade loads associated with rotor tip vortices and blade wakes.) The computed results for a discrete rotor-stator can then are used to establish the equivalent body force representation.

Now we can envision embedding a discrete rotor-stator pair in a multi-stage environment with the remaining stages represented as body force distribution as indicated in **Figure B.63**. Computed results from this situation can be assessed against calculations from the discrete rotor-stator pair alone to quantify multi-stage effects on time-average performance. For instance, the aero forces and moments as dictated by the multi-stage environment on a specific blade row can be viewed as an input for local aeroelastic calculation (as implied in **Figure B.62**). The local aeroelastic calculation would now redistribute the body force representation of the specific blade row under consideration. This is then in turn used in the multi-stage environment to update the flow-field and the associated blade response. Thus, this provides a conceptual model for implementing multi-stage aeroelastic calculations on a consistent basis. For application of this methodology for assessing the stability properties of multi-stage compressor, the reader is referred to [B.35].

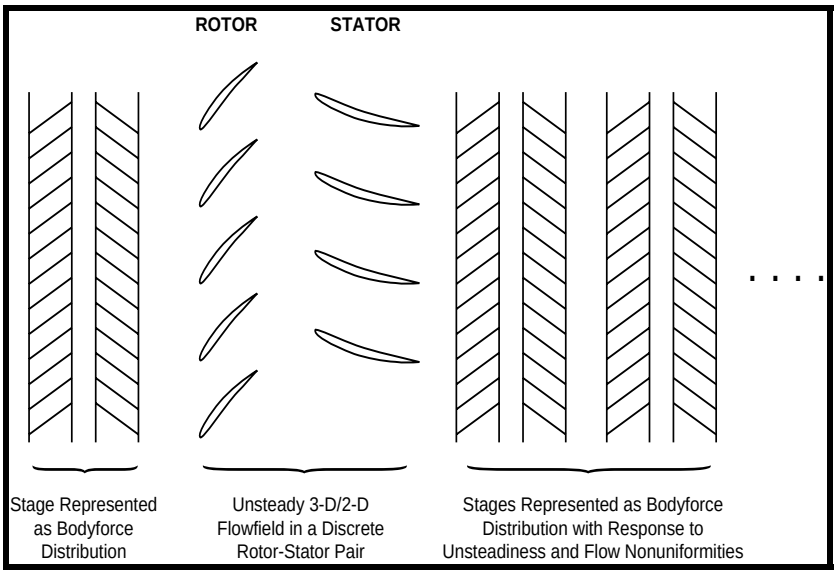

Figure B.63: Physical Model of Multi-Stage Compressor.

On a conceptual basis one can even extrapolate the methodology to the computation of compressor characteristics as delineated in **Figure B.5** provided a rigorous basis has been established for linking the factors that modify the characteristics for inclusion in the body force representation. Presently streamline curvature with correlative data base is routinely used to generate the compressor characteristics though modern CFD is playing an increasingly important role in this.

The methodology described in this section can readily be integrated seamlessly into an airframe-inlet-engine system for simulating the dynamic behavior of such a system.

B.1.6 Different Levels of Modeling

There are essentially three levels of physical approximations that one can use to generate compressor characteristics and/or its modification; these can be broadly classified as follows.

- System lumped parameters level (low-order) models:
  - 1-D model (ordinary differential equations); and
  - 2-D model with compressor represented as single actuator disk (ordinary differential equations or rudimentary partial differential equations for flow distortion problem in compressor and compression system dynamics).
- Macro-level model:
  - 3-D model with blade-row by blade-row body force representation (i.e. actuator duct representation for each blade-row) (partial differential equations).
- Physical level model:
  - 3-D distributed model with discrete blades in each blade row; and
  - 3-D flow simulation in multi-blade and multi-blade rows environment (partial differential equations).

B.1.6.1 Lumped Parameter (Low-Order) Models

This type of model captures all key system dynamic behavior but does so:

- With fast calculations (preferably analytical, rather than numerical);
- In a form that permits the designer to assess any effects of design variation;
- In a form suitable for incorporating into system level simulation for:
  - Assessing whether dynamic behavior requirements are met, and
  - Developing active control techniques for instability avoidance or performance enhancement.

B.1.6.2 Attributes of Macro-Level Models

This level of model satisfies physical laws on a blade passage average basis:

- Mass, momentum, energy conservation; and
- Entropy production in dissipative systems.

It has the correct dependencies on engine geometry and is preferably directly usable by designers. The results should agree with results of 3-D flow simulation and physical experiments.

B.1.6.3 Physical Level Model

At this level the method uses the full 3-D geometry that includes:

- Blade geometry details;
- Multi-blade passages; and
- Multi-blade rows.

This constitutes a full unsteady 3-D flow simulation in the complex geometrical configuration of a modern compressor.

B.1.6.4 Role of Each Level of Modeling

System designers specify component dynamic-behavior requirements while component designers specify constraints (what is feasible and what is not). Thus, the different levels of modeling enable system and component designers to communicate with one another on a rational basis.

B.1.7 Compressor Overall Summary

In this section we have reviewed the impact of tip clearance, stationary and rotating flow distortion, flow unsteadiness (axial spacing), Reynolds number, and blade surface roughness on compressor performance. We have also reviewed effects of thermal origin, and effects associated with blade untwist in high-speed fans. Recent progress made in the development of techniques for simulating and predicting flow effects that affect the operability of the compressor is also discussed. These techniques take advantage of modern CFD but physically model those aspects of the flow phenomena that are still beyond the feasibility of currently available computational resources.

B.1.8 Cited References for Compressor Section

[B.1] Adamczyk, J.A., “Model Equation for Simulating Flows in Multistage Compressor,” ASME Paper # 85-GT-226, 1985.

[B.2] Rhie, C.M. et al., “Development and Application of a Multistage Navier-Stokes Solver: Part I”, ASME Journal of Turbomachinery, Vol. 120, No. 2, April 1998.

[B.3] Cumpsty, N.A., “Compressor Aerodynamics”, Longman Scientific & Technical, 1989.

[B.4] Wisler, D.C., “Advanced Compressor and Fan Systems”, GE Aircraft Engines, Cincinnati, Ohio, USA. Copyright @ 1988 by General Electric Co. USA, All Rights Reserved. (Also 1986 Lecture to ASME Turbomachinery Institute, Ames Iowa)

[B.5] Smith, L.H., “Casing Boundary Layers in Multistage Compressors”, Proceeding of the Symposium on Flow Research on Blading, Brown Boveri & Co. Ltd, Baden, Switzerland 1969, In Dzung, L.S. (ed) Flow Research on Blading, Elsevier Publishing Company, 1970.

[B.6] Khalid, A. et al., “Effect of Tip Clearance on Compressor Endwall Blockage and Pressure Rise Capability”, Presented at 43rd IGTI Conference, Stockholm, 1998.

[B.7] Freeman, C., “Effect of Tip Clearance Flow on Compressor Stability and Engine Performance”, VKI Lecture Series 1985-05, 1985.

[B.8] SAE Aerospace Information Report, AIR-1419, “Inlet Total-Pressure Distortion Considerations for Gas Turbine Engines”, May 1983.

[B.9] SAE Aerospace Recommended Practice, ARP-1420, "Gas Turbine Engine Inlet Flow Distortion Guidelines", March 1978.

[B.10] Schmucker, J. et al., "Erosion, Corrosion and Foreign Object Damage Effects in Gas Turbines", AGARD-CP-558, 1994.

[B.11] Mazzawy, R.S., "Multiple Segment Parallel Compressor Model for Circumferential Flow Distortion", ASME J. Engineering for Power, 99, pp. 288-296, 1977.

[B.12] Reid, C., "The Response of Axial Flow Compressors to Intake Flow Distortions", ASME Paper # 69-GT-29, 1969.

[B.13] Ludwig, G.R., Nenni, J.P. and Arendt, R.H., "Investigation of Rotating Stall in Axial Flow Compressors and Development of a Prototype Stall Control System", Technical Report USAF-APL-TR-73-45, 1973.

[B.14] Kozarev, L.A. and Federov, R.M., "Aspects of the Appearance and Elimination of Breakdown in an Axial-Flow Compressor in the Presence of a Rotating Non-Uniformity at the Inlet", Izevstinya vuz Aviatsionnaya Tekhnika, 26(1), pp. 33-37 (translated), 1983.

[B.15] Longley, J.P., Shin, H.-W., Plumley, R.E., Silkowski, P.D., Day, I.J., Greitzer, E.M., Tan, C.S. and Wisler, D.C., "Effects of Rotating Inlet Distortion on Multistage Compressor Stability", *ASME Journal of Turbomachinery*.

[B.16] Silkowski, P.D., "Measurements of Rotor Stalling in Matched and Mismatched Multistage Compressor", MIT Gas Turbine Report No. 221, Massachusetts Institute of Technology, 1995.

[B.17] Day, J.J., "Stall Inception in Axial Flow Compressors", *ASME Journal of Turbomachinery*, Vol. 115, pp. 1-9, 1993.

[B.18] Hodder, B.K., "An Investigation of Engine Influence on Inlet Performance", NASA CR-166136, 1981.

[B.19] Graf, M., Wong, T., Greitzer, E.M., Tan, C.S., Marble, F.E., Shin, H.-W. and Wisler, D., "Effects of Asymmetric Tip Clearance on Compressor Stability", accepted for publication in ASME Journal of Turbomachinery, 1997.

[B.20] Hetherington, R. and Morritz, R.R., "The Influence of Unsteady Flow Phenomena on the Design and Operation of Aero Engines", in Unsteady Phenomena in Turbomachinery, AGARD CP-144, 1977.

[B.21] Mikolajczak, A.A., "The Practical Importance of Unsteady Flow Phenomena on Design and Operation of Aero Engines", in AGARD CP-144, Unsteady Phenomena in Turbomachinery, 1977.

[B.22] Smith, L.H., "Wake Dispersion in Turbomachines", ASME Journal of Basic Engineering, September 1966.

[B.23] Smith, L.H., Discussion of ASME Paper # 96-GT-029, Birmingham, United Kingdom, June 1996.

[B.24] Koch, C.C., "Stalling Pressure Rise Capability of Axial Flow Compressor Stages", ASME Paper # 81-GT-3, 1981.

[B.25] Valkov, T.V., "The Effect of Upstream Rotor Vortical Disturbances on the Time-Average Performance of Axial Compressor Stators", MIT, GTL, Report # 227, August 1997.

[B.26] Schaffler, A., "Experimental and Analytical Investigation of the Effects of Reynolds Number and Blade Surface Roughness on Multistage Axial Flow Compressors", ASME Paper # 79-GT-2, 1979.

[B.27] Suder, K.L., Chima, R.V., Strazisar, A.J. and Roberts, W.B., "The Effect of Adding Roughness and Thickness to a Transonic Axial Compressor Rotor", ASME Paper # 94-GT-339, 1994.

[B.28] Kandebo, S.E., "F100-PW-229 Failures Affect F-15E Readiness", Aviation Week and Space Technology, June 27 1994.

[B.29] Khalak, "Parametric Dependencies of Aeroengine Flutter for Flutter Clearance Applications", Phd Thesis, MIT Aero & Astro, 2000.

[B.30] Palmer, D.L. and Waterman, W.F., "Design and Development of an Advanced Two-Stage Centrifugal Compressor", ASME Paper # 94-GT-202, 1994.

[B.31] Rodgers, C., "Effect of Inlet Geometry on the Performance of Small Centrifugal Compressors", AIAA-88-2812, 1988.

[B.32] Hoener, S.F., "Fluid-Dynamic Drag", Published by the Author, 1965.

[B.33] Hynes, T.P. and Greitzer, E.M., "A Method for Assessing Effects of Inlet Flow Distortion on Compressor Stability", ASME J. of Turbomachinery, 109, pp. 371-379, 1987.

[B.34] Chue, R., Hynes, T.P., Greitzer, E.M., Tan, C.S. and Longley, J.P., "Calculations of Inlet Distortion Induced Compressor Flowfield Instability", *Int. Journal of Heat and Fluid Flow*, 10, pp. 211-223, September 1989.

[B.35] Gong, Y., Tan, C.S., Gordon, K. and Greitzer, E., "A Three-dimensional Computational Flow Model for Short Length Scale Instability in Multistage Axial Compressor", Submitted for consideration of publication in ASME Journal of Turbomachinery 1998.

B.1.9 Additional Bibliography for Compressor Section

Graf, M.B. and Sharma, O.P., "Effects of Downstream Stator Pressure Field on Upstream Rotor Performance", ASME Paper # 96-GT-507, 1996.

Walker, G.J., "The Unsteady Nature of Boundary Layer Transition on an Axial-Flow Compressor Blade", ASME Paper # 74-GT-135, 1974.

Pfeil, H., Herbst, R. and Schroder, T., "Investigation of the Laminar-Turbulent Transition of Boundary Layers Disturbed by Wakes", ASME Journal of Engineering and Power, 105, 1983.

Hodson, H.P., "Modeling Unsteady Transition and Its Effect on Profile Loss", ASME Journal of Turbomachinery, 112, October 1990.

Sharma, O.P. et al., "Assessment of Unsteady Flows in Turbines", ASME Paper # 90-GT-150, 1990.

Dong, Y. and Cumpsty, N.A., "Compressor Blade Boundary Layers: Part 1 – Test Facility and Measurements with Incident Wakes", ASME Journal of Turbomachinery, 112, 1990a.

Dong, Y. and Cumpsty, N.A., "Compressor Blade Boundary Layers: Part 2 – Measurements with Incident", ASME Journal of Turbomachinery, 112, 1990b.

Halstead, D.E., Wisler, D.C., Okiishi, T.H., Walker, G.J., Hodson, H.P. and Hsin, H.W., "Boundary Layer Development in Axial Compressors and Turbines – Part 1 of 4: Composite Picture", ASME Paper # 95-GT-461, 1995.

Halstead, D.E., Wisler, D.C., Okiishi, T.H., Walker, J., Hodson, H.P. and Hsin, H.W., "Boundary Layer Development in Axial Compressors and Turbines – Part 2 of 4: Compressors", ASME Paper # 95-GT-462, 1995.

Schulz, H.D., Gallus, H.E. and Lakshminarayana, B., "Three-Dimensional Separated Flow Field in the Endwall Region of An Annular Compressor Cascade in the Presence of Rotor-Stator Interaction – Part 1: Quasi-Steady Flow Field and Comparison with Steady-State Data", ASME Journal of Turbomachinery, 112, October 1990.

Kerrebrock, J.L. and Mikolajczak, A.A., "Intra-Stator Transport of Rotor Wakes and Its Effect on Compressor Performance", ASME Journal of Engineering and Power, October 1970, pp. 359-368.

Dawes, W.N., "A Numerical Study of the Interaction of a Transonic Compressor Rotor Overtip Leakage Vortex with the following Stator Blade Row", ASME Paper # 94-GT-156, 1994.

Valkov, T. and Tan, C.S., "Control of the Unsteady Flow in a Stator Blade Row Interacting with Upstream Moving Wakes", ASME J. Turbomachinery, 1995, Vol. 117, pp. 97-105.

Howard, M.A., Ivey, P.C., Barton, J.P. and Young, K.F., "Endwall Effects at Two Tip Clearances in a Multi-Stage Axial Flow Compressor with Controlled-Diffusion Blading", ASME Journal of Turbomachinery, 116, 1994.

Poensgen, C. and Gallus, H.E., "Three-Dimensional Wake Decay Inside of a Compressor Cascade and Its Influence on the Downstream Unsteady Flow Field: Part I – Wake Decay Characteristics in the Flow Passage", ASME Journal of Turbomachinery, 113, 1991a.

Poensgen, C. and Gallus, H.E., "Three-Dimensional Wake Decay Inside of a Compressor Cascade and Its Influence on the Downstream Unsteady Flow Field: Part II – Unsteady Flow Field Downstream of the Stator", ASME Journal of Turbomachinery, 113, 1991b.

Denton, J.D., "Loss Mechanism in Turbomachines", ASME Journal of Turbomachines, 115, No. 4, 1993.

Valkov, T. and Tan, C.S., "Effects of Upstream Rotor Vortical Disturbances on Time-Average Performance of Axial Compressor Stator: Part 1 – Framework of Technical Approach and Rotor Wakes – Stator Blade Interaction", Accepted for Presentation at 43rd International Gas Turbine and Aeroengine Congress and Exposition, Stockholm, June 1998.

Valkov, T. and Tan, C.S., "Effects of Upstream Rotor Vortical Disturbances on Time-Average Performance of Axial Compressor Stator: Part 2 – Rotor Tip Leakage and Discrete Streamwise Vortex – Stator Blade Interaction", Accepted for Presentation at 43rd International Gas Turbine and Aeroengine Congress and Exposition, Stockholm, June 1998.

Hendricks, G.J., Bonnaure, L.P., Longley, J.P., Gretizer, E.M. and Epstein, A.M., "Analysis of Rotating Stall Onset in High Speed Axial Compressors", AIAA Paper # 93-2233, 1993.

Hoying, D.A., Tan, C.S., Vo, H.D. and Greitzer, E.M., "Role of Blade Passage Flow Structures in Axial Compressor Rotating Stall Inception", Paper submitted for TurboExpo '98, Stockholm, Sweden, 1998.

Wisler, D.C., "Core Compressor Exit Stage Study, Vol. IV – Data and Performance Report for the Best Stage Configuration", NASA CR-165357, NASA Lewis Research Center, 1981.

Park, H.G., "Unsteady Disturbance Structures in Axial Flow Compressor Stall Inception", Master's Thesis, Massachusetts Institute of Technology, 1994.

LeJambre, C.R., Zacharias, R.M., Biederman, B.P., Gleixner, A.J. and Yetka, C.J., "Development and Application of Multistage Navier-Stokes Solver, Part II: Application to a High Pressure Compressor Design", ASME Journal of Turbomachinery, Vol. 120, No. 2, April 1998.

Dring, R.P., Sprout, W.D. and Weingold, H.D., "A Navier-Stokes Analysis of the Effect of Tip Clearance on Compressor Stall Margin", ASME Paper # 95-GT-190, 1995.

B.2 PERFORMANCE OF TURBINE SUB-SYSTEMS

B.2.1 Overview of Turbine Sub-System Performance

The turbine system of the gas turbine engine is a complex integration and balancing of the disciplines of aerodynamics, internal and external heat transfer, stressing, material properties, and manufacturing capability. During the design phase of the engine it is important to consider the expansion system in totality, i.e. high pressure turbine, interduct, low pressure turbine, exhaust diffuser and jet pipe. By so doing, the optimal engine may be derived. This may or may not mean that each turbine stage is at its peak aerodynamic performance point. Turbine interducts are potential sources of high losses, with high mach number swirling flow, highly rotational flow, and often with large radius changes. The turbine turbomachinery behaves in similar ways to that of the compressor's. Reynolds dependency on profile losses, shock-boundary layer interactions, tip clearance effects, and many of the references given under the compressor section are relevant to both environments.

This section of the report aims to give the reader an understanding of the way in which turbine performance is predicted, measured and analysed, highlighting areas of particular sensitivity.

B.2.2 High Pressure Turbines

B.2.2.1 General Performance

High pressure turbines operate for most of the time at a fixed expansion ratio with small changes in aerodynamic speed. Depending on the performance of the compressors, the LP turbine, the combustor pressure loss and efficiency, and the capacity and efficiency of the HP turbine, the turbine may, or may not, operate at its design expansion ratio and aerodynamic speed. In order to develop the engine it is important to have a characteristic of the turbine for use in the synthesis of the engine. In early design stages and simplified cycle calculations it is sufficient to hold a constant efficiency due to the relatively small variation in operating point.

The turbine has to convert energy from the hot gas stream to drive the compressor on the same shaft. In its simplest form, assuming constant flow through the gas turbine, the energy balance is:

Compressor enthalpy rise = Turbine enthalpy drop

In practice this is moderated in varying degrees by the following:

Compressor:

- External bleed bypassing the turbine;
- Internal bleed , partially or wholly bypassing the turbine;
- Leaks (i.e. from variable geometry vanes) bypassing the turbine; and
- Radiated heat from casings.

Secondary Air System:

- Windage losses on shaft and discs.

Bearings and Power Off-Take Shaft:

- Heat to oil and windage losses; power extraction.

Turbine:

- Position of cooling air return relative to rotor throat(s);
- Energy state of returned secondary air; and
- Heat losses through casings.

These modifiers of the simplified arrangement all need quantification for a real assessment of the turbine performance in the engine. Some of the above are amenable to direct measurement, whilst others are reliant on calculation and separate experimentation with subsequent superposition.

Two of the above are closely linked and are the two that are most difficult to assess. They are: 1) the secondary air system; and 2) the energy state of returned secondary air. Both these systems are driven by main gas stream pressure differentials, which are themselves subject to changes throughout the running range, and are strongly subject to engine deterioration. A typified cooling and secondary air system is indicated in **Figure B.64**.

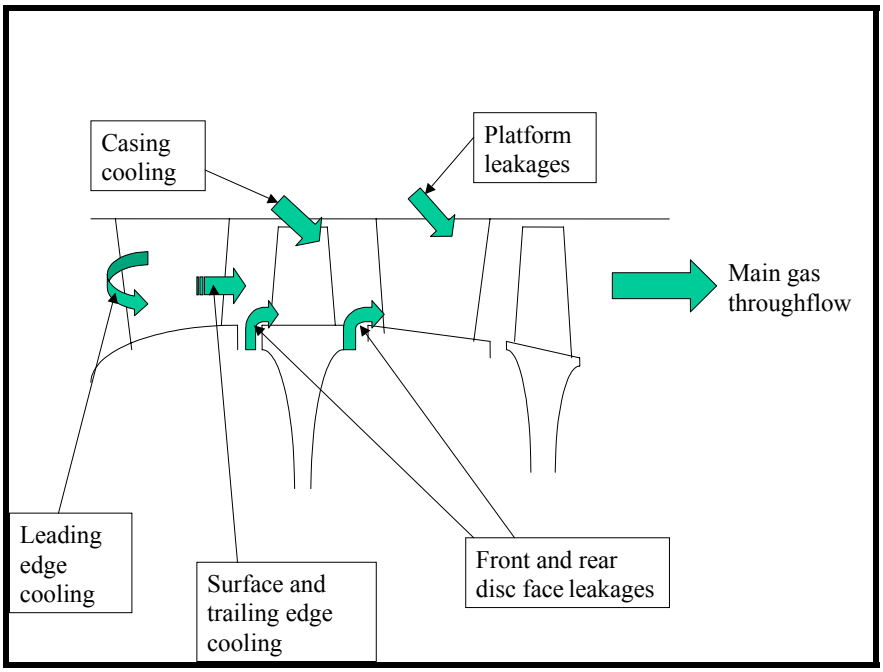

Figure B.64: Typical Secondary-Air-System Returns to Main Throughflow Bleed Network.

Nozzle:

- Airfoil leading edge cooling;
- Airfoil surface cooling;
- Airfoil trailing edge cooling;
- Platform cooling returned at platform trailing edge – inner and outer;
- Platform leakage, blade to blade direction, inner and outer; and
- Shroud well cooling.

Rotor:

- Airfoil leading edge cooling;
- Airfoil surface cooling;
- Airfoil trailing edge cooling;
- Front face of disc cooling;
- Front face of disc leakage;
- Rear face of disc cooling;
- Rear face of disc leakage;
- Platform leakage; and
- Overtip cooling flow.

It is normal convention that bleeds are treated in the following manner:

- Bleed flows introduced in the preceding blade row are treated as available for work in subsequent blade rows.
- Platform and disc bleed flows introduced upstream of the throat affect throat sizing, but are not available for work.
- Airfoil bleeds upstream of the throat contribute to the work in the turbine.
- Bleed flows downstream of the throat contribute no work in that blade row.

The astute reader will recognize that such a convention is not academically correct. This highlights the importance of clarity of the turbine efficiency definition being used.

B.2.2.2 Characteristic Generation

The potential efficiency of the turbine stage, or stages, is dependent on the basic velocity triangles, i.e. work, blade speed, and through-flow velocities. These have to be considered in the context of the turbine physical size and the hub/tip ratio of the stage concerned. Such physical considerations determine the effects of trailing edge thickness on the potential efficiency, the influence of tip clearance, and the Reynolds regime that the turbine will operate in.

Optimization of the airfoil profile, shock and secondary losses leads to the design point efficiency of the turbine, when the effects of cooling and secondary air flows have been incorporated. In order to generate a turbine characteristic for use in the synthesis of the gas turbine engine one of three actions can be taken.

Scaling of a previously measured turbine characteristic which has similar leading parameters, i.e. work, hub/tip ratio, through-flow axial mach numbers, and reaction.

Prediction based on blade row stacking. Based on regression analysis of previous turbines, the generic performance of the turbine can be predicted over a wide range of operation. Such methodology works adequately well with consistent and progressive small changes in the designs. It may however lead to substantive errors when more radical changes in design are pursued [B.36, B.37 and B.38].

Quasi 3-D/3-D simulation of the turbine stage(s). This methodology has proven itself capable of simulating widely different types of design with good results. The speed range and expansion ratio range is more limited than methods 1 and 2, normally due to the range of applicability of the boundary layer methods and calculation stability at off-design flow conditions. The flow conditions along the hub and casings allow better analysis of the secondary air system, and from the knowledge of the changes in lift distribution on the airfoil, so improved blade cooling assessments can be made [B.39]. This method does have the following added potential benefits: identifying the effects of upstream wakes, and downstream perturbations from struts or instrumentation; assessing the exit profile from the turbine at the various operating conditions. This is particularly important if inter-turbine ducts (especially with large radius change) are used, and if the downstream turbine is sensitive to pressure and temperature profiles.

B.2.2.3 Rig Testing

The HP turbine lives in a hostile environment and hence there are associated difficulties of measuring, as opposed to deducing, its in-engine performance. Consequently, much turbine development has used 'cold flow' rigs, which replicate the turbine unit and are operated at substantially lower temperatures. Without the complexity of combustor or following turbine, more accurate measurements may be taken over wide operating regimes, but which need accounting systems to transpose from the rig to the engine environment.

Four major types of rig have been used in the development of turbines, viz.

- **2-D or Annular Cascades** – These facilities are capable of high accuracy measurement of the aerodynamics of the airfoil over a wide range of operation and Reynolds number. The necessity to control the end wall boundary layer, and its effect on the mid height aerodynamics led to development of methods such as porous walls, and each tunnel has its own particular characteristic. Due to the potential of high quality test results these tunnels have formed the foundation of improvement to the analytical approach to airfoil design [B.40].

- This can be further subdivided into two sections:
  - **Internal Cooling** – Investigations of the effectiveness of internal cooling passage designs, including the residual pressure that is key to the selection of the location of the exhausting of the coolant , and its impact on the external aerodynamics [B.41].
  - **External Cooling** – Used to determine the optimum pitching and direction of the coolant ejection holes for effective filming of the surface. Such rigs also indicate the sensitivity of the film to the hole shape and the pressure ratio between the main gas passage and the source [B.42].

  Both of these rig types need to be able to evaluate the effects of corriollis forces from within the gas flow, and superimposed centrifugal forces, and their consequential effects on the localized heat transfer rates.

- **'Cold Flow' Turbine Rigs** – The cold-flow turbine rig simplifies the instrumentation and measurement difficulties that are encountered in the high temperature in engine situation. It allows for easier full spatial inlet, inter-blade row, and exit traverse, and can exercise the turbine over a wide of operation. As such these facilities provide the first insight to the measured performance of the turbine, as opposed to the predicted performance. There are corrections to be made to the

measured performance, such as disc windage and bearing losses, and gas conditions from rig to engine. In uncooled, or low flow cooled turbines the cold flow rig has close similarity to the engine environment. Most of the modern engines now rely on relatively high proportions of the main gas flow being used for cooling and secondary air systems. Consequently, the cold flow rig with solid blading has to attempt to emulate these effects. The experimenter can elect to maintain the blades as per the engine, test the turbine over the range of expansion ratios, and then manipulate the turbine results for the correct engine reaction. Alternatively, it may be preferred to redesign the nozzle, such that the correct reaction is achieved at the design expansion ratio. Such considerations are compounded with increasing stage numbers. Both approaches ignore the effects that cooling films have on the basic loss of the airfoil, and potential shock-interaction changes, and further modification to the measured characteristics must be made.

- **'Warm Flow' Turbine Rigs** – These facilities have the advantages of the cold flow rig plus the capability to introduce cooling and secondary air into the turbine. The spoiling effects of these return bleeds, their effects on disc windage and the blade row to blade row throat distribution and hence stage reaction, lead to a better simulation. Some facilities use vitiated cooling air that has been combined with other gases in order to better approximate the relative densities between the cooling and the main stream air. They therefore represent very closely the in-engine performance. Due to their complexity, the cost of the unit and plant on which the unit is tested is substantially greater than that of cold flow testing. Since the airfoils contain either engine or emulated engine cooling systems, the availability of these complex parts may be late in the lifespan of the engine development. So although good measurement of the turbine characteristic can be accomplished, the timing may be so late that the only gain may be an understanding of how to make improvements for the next mark of engine!

The experimenter must decide how best to run the unit to generate the required characteristics. Options include: running the cooling or secondary air at constant feed to re-entrant point pressure difference; or holding feed pressure constant over a small expansion ratio variation; varying the leading edge feed pressure in conjunction with trailing edge; or only varying trailing edge feed as expansion ratio changes. It must also be noted that as the feed pressures change, so may, the windage levels on the turbine disc and the thrust bearing losses. This depends on the detailed design of the rig.

Because of the cost of these units, their relative inflexibility, and the experimental accuracy available, the use of warm-flow turbine rigs is often reserved for exceptional occasions.

B.2.2.4 Engine Testing

In the engine environment the turbine experiences the radial and circumferential patterns generated by the combustor, and the upstream influence of the LP turbine. Both of these can lead to differences between cold and warm flow tests, usually in minor ways. The difficulty in engine testing is to achieve a high experimental accuracy on all of the parameters (see above), such that the resulting assessment of the turbine is of high integrity.

In order to measure correctly the energy state of the gas entering and exiting the turbine, full area traverses are required. These are difficult to achieve in the strictures of the engine architecture. This often leads to the use of separate engine core testing, without the LP spool, with greater access for measurement, and yet retaining the temperatures and secondary air systems and clearances as experienced in the whole engine. The quality of the primary factors in the calculation of turbine efficiency, mass flow, work in the compressor and average inlet and exit temperatures can all be substantially better than those of the engine.

Unlike the engine, where it is extremely difficult to change the operating point of the turbine, the HP spool vehicle enables the experimenter to explore a wide range of operation. Changes to the downstream control nozzle change the operating point, giving a limited turbine characteristic. If available, then alterations to

the compressor variable-geometry allow for a range of turbine aerodynamic speed to be assessed. Extra turbine load can be added by absorbing power at the power off-take shaft. This is normally done by use of hydraulic motors. Whilst these investigations are underway it remains important for the secondary air and cooling air system to be monitored, along with changes in tip clearance in order to gain a correct assessment of the turbine.

The table below summarizes the methods of turbine characteristic measurement and gives guidance to the validity of the resulting performance map.

Table B-1: Method of Turbine Characteristic Measurement

Method	Representative Conditions	Measurement or Sampling Difficulty	Measurement Accuracy	Nett Assessment	
				HP Turbines	*LP (uncooled) Turbines*
Cold Flow Rig	Poor	Low	High	No. 5	No. 2
Engine Parts Cold Flow Rig	Good	Low	High	No. 3	Best
HP Spool	Best (with intermediate op. range)	Intermediate	Intermediate	No. 2	N/A
Direct on Engine	Best (but limited range)	High	Intermediate	No. 4	No.4
On Engine with performance simulation	Best (but limited range)	High	Intermediate	Best	No.3

B.2.2.5 Transient and Abnormal Operations

During rapid throttle movement, the combustor may not complete the combustion process. Hence, the gas entering the turbine may also contain a relatively high degree of unburned fuel. This causes insignificant blockage of the turbine throat and does not affect engine matching. The major area of concern under transient operation is that of tip clearance, and the effect on turbine efficiency. Time constants for the tip clearance changes are substantially greater than those of the gas flow are. Consequently, turbine performance can be treated as pseudo steady state with the effects of the tip clearance changes added by superposition.

Whilst the aerodynamicist will be able to justify the use of continuous curvature on the blade surfaces, and the use of polished surfaces to gain that last point of efficiency, once developed, turbines are generally extremely resilient to damage. It is not infrequent that operators will only detect damaged turbines either by boroscope visual inspection or by indicated out of balance. Missing blades, burnt trailing edges of nozzles, impact damaged leading edges, erosion by volcanic ash, all are found in service and have to be severe to reduce the engine performance. It is essential though to maintain the mechanical integrity of the engine.

B.2.3 Low Pressure Turbines

B.2.3.1 General Performance

The low pressure turbine of aero gas turbines operates over relatively wide aerodynamic speed ranges and expansion ratios. It is therefore more important to have a characteristic that reflects the turbine performance

when engine performance calculations are made. Two different types of turbine need to be considered. They are:

- **High Specific Thrust Engines –** These turbines, often single-stage units, are usually cooled, and due to the effects of the reheat system, variable final nozzle and the wide flight regime, operate over a wide range of aerodynamics.
- **Low Specific Thrust Engines** – These multi-stage units are usually uncooled, at least in the airfoil, and changes in expansion ratio reflect the changes in aerodynamic speed. Generally, the aerodynamic excursions of the blades are substantially less than the high specific thrust units.

A modern exception to the above is the 'Remote fan' solution for one of the contenders in the Joint Strike Fighter – Vertical landing scenario. In this gas turbine, a clutched fan is driven by a low-pressure turbine that also drives the main engine low-pressure compressor. For up and away flight the turbine operates as a lightly loaded unit and is subject to normal high specific thrust engine changes of operation. In the vertical land mode the turbine operates as a highly loaded, but low specific thrust unit. At similar aerodynamic speeds the turbine changes its expansion ratio by approximately 2:1 as the load of the 'Remote fan' is demanded from the turbine. Similar operations have been considered for civil low noise supersonic engines. These ranges of operation demand that representative characteristics are available early in the project design phase as critical thrust conditions have to be met in both methods of operation.

The exhaust diffuser is the last aerodynamic unit before the gas enters the jetpipe. It has an arduous task, taking swirling flow from the exit of the turbine, turning it to the axial direction and diffusing from typically 0.6 Mn to 0.2 Mn. As the turbine aerodynamic loading varies so does the swirl and mach number into the diffuser. Since the performance analyst is primarily concerned with jetpipe gas conditions, it is often convenient to incorporate the losses of the exhaust diffuser into the LP turbine characteristic. Otherwise it is necessary for the diffuser losses to be expressed as a function of the turbine operating point, i.e. exit swirl, Mach number.

B.2.3.2 Characteristic Generation

Methods for estimating or measuring the LP turbine performance are essentially the same as for the HP turbine. Due to the variation in aerodynamic operation of the LP turbine, the cooling flow source to sink pressure ratios are not as constant as for the HP turbine. Consequently, it is important to include the variations in the 'warm flow' testing that may be done. As an alternative, the influence, normally by calculation, of the varying cooling flows can be superpositioned on the test results of a solid bladed 'cold flow' rig result.

B.2.3.3 Rig and Engine Testing

Similar requirements and concerns exist for LP turbine testing as those of the HP turbine. The cooled LP turbine may be subjected to the same options for rig tests as those for the HP turbine. Uncooled LP turbines, usually associated with the high power civil engines generate large powers, and need large capital investment in facilities if they are to be tested at engine conditions. It had been common practice to use scaled models of these units to overcome these difficulties. When model rigs are used it remains important to emulate the blading of the turbine as it will exist in the full scale unit. This means that representative features, such as trailing edge thickness and tip clearances are replicated in the rig. Due to the change of centrifugal and gas bending loads it is usually necessary to design such that the scaled turbine is representative at design aerodynamic speed, and account the small variances that will be present at off-design aerodynamic speeds. With modern blading methods that are strongly Reynolds number, turbulence level and unsteadiness level dependant, the use of model LP turbines is reducing. **[B.43]**

Engine testing of the LP turbine has a variety of technical areas that need consideration. The necessary quality measurements of the gas parameters, both inlet and outlet are difficult to achieve, as per the HP

turbine. The work done by the turbine is attributed from the analysis of the low pressure compressor, and the working mass flow is deduced from the analysis of the core engine. These factors accumulate such that the of the turbomachinery analysis the LP turbine performance has the highest uncertainty. However given these reservations, with careful analysis over a series of engine tests, then changes in efficiency and capacity of the turbine over a reasonably wide operation can be established.

B.2.4 The Exceptions

B.2.4.1 Variable Area Turbines

The concept of the variable area turbine has been considered for a variety of applications. Classically such turbines are designed to reduce their inlet flow usually by changing the stagger of the nozzle, whilst maintaining specific work at near fixed inlet temperatures. In order to predict their characteristic it is essential to have robust off-design incidence calculations of the blading. It is usual to compromise on the rotor ~ stator-throat ratios so that as the turbine is increased in flow so the flow controlling cascade remains the stator. Such modes of operation challenge the computational capabilities, especially at high or low incidence where separation bubbles can be generated on either the suction or pressure surface. Normal design and operation of turbines is given to eliminating such features from the blading. Modern variable bypass military engines use the variable turbine in conjunction with the variable geometry in the core compression system to improve the matching between the supersonic inlet characteristics, the propulsion nozzle drag characteristics and the flow ~ speed ~ combustion temperature relationships of the gas turbine. Since the benefit to the propulsion system is dominated by the inlet efficiency and exhaust losses, the compromise is sometimes to operate the turbine at less than optimal aerodynamics.

Alternative use of variable turbines is to improve spool matching, or to thermodynamically down flow the engine, whilst retaining overall pressure ratio and turbine temperature. This enables the lower power to be achieved with similar thermal efficiencies to the full power. Significant reductions in part power specific fuel consumption can initially be calculated, but changes to the internal bleed network, and reduction of component efficiencies at off-design conditions can rapidly erode initial indicated advantages. It remains the responsibility of the turbine designer to be able to predict with reasonable accuracy the performance at these extremes of operation.

A variety of potential solutions for changing the throat size of the turbine have been tried ranging from:

- Variable stagger (complete vane or trailing edge);
- Moving casing;
- Variable camber (or profile);
- Switchable high pressure air bleed at the throat; and
- Physical obstruction at the throat.

Many of the test results remain either company proprietary or classified.

B.2.4.2 Statorless Contra Rotating Turbines

Adoption of an expansion system where there is no direct control of the LP turbine flow capacity by use of a fixed nozzle between the HP and LP spools has seen limited application. There are clear advantages by deletion of the inter-turbine vane, such as the length, weight, and cooling flow savings along with potential aerodynamic improvements in the net expansion system efficiency. These turbines benefit from having close axial spacing, but this may be in conflict with the disc designs, which usually demand a reasonable disc width at the hub to accommodate the stressing and life requirements. Close coupling of the discs also leads to air system losses as the contra rotating discs create high shearing forces between their faces.

This can, in turn demand higher intercavity flows to prevent excessive heat build up and the possibility of induced disc vibrations from the secondary air flow behavior.

Prediction of these turbines is more complex than for nozzled turbines. The entry conditions for the following turbine are dependent on the through flow and work level of the preceding turbine as these determine the swirl angle and Mach number of the flow. It is therefore necessary to generate a turbine characteristic that is dependent on the compressor performance. This characteristic will vary with degradation, distortion and build scatter, and where an appropriate influence of variable vane and bleed off-take schedules, including tolerances, have been included.

B.2.5 Cited References for Turbine Section

Also refer to the Compressor section.

[B.36] Ainley, D.G. and Matheson, G.C.R., "A Method of Performance Estimation for Axial Flow Turbines", Aeronautical Research Council, R & M 2974 (1957).

[B.37] Craig, H.R.M. and Cox, H.J.A., "Performance Estimation of Axial Flow Turbines", Proc Inst. Mech. Engrs, Vol. 185, 32/71, 1971.

[B.38] Kacker, S.C. and Okapu, U., "A Mean-Line Prediction Method for Axial Turbine Efficiency", ASME Paper # 81-GT-58, 1981.

[B.39] Various, "Loss Mechanisms and Unsteady Flows in Turbomachinery", AGARD CP-571, 1996.

[B.40] Various, "CFD Validation for Propulsion System Components", AGARD AR-355, 1998.

[B.41] Ardoy, Fottner, Beversdorff and Weyer, "Laser 2-Focus Measurements on a Turbine Cascade with Leading Edge Cooling", AGARD CP-598, 1998.

[B.42] Guo, Lai, Jeony, Jones and Oldfield, "Use of Liquid Crystal Techniques to Measure Film Cooling Heat Transfer and Effectiveness", AGARD CP-598, 1998.

[B.43] Various, "Unsteady Aerodynamic Phenomena in Turbomachinery", AGARD CP-468, 1990.

B.3 COMBUSTOR SYSTEMS

B.3.1 Flowpath and Exit Temperature

One of the main issues for combustor design and performance is compliance with the high-pressure distributor and turbine specifications for durability and thermodynamic efficiency. Life and durability specifications are directly linked with the limiting thermal and mechanical point-stresses of the turbine nozzle and rotating parts and their associated cooling requirements. The circumferential and radial temperature and velocity profile envelopes and maximum temperature threshold compliance conditions at the exhaust of the combustor derive from these limits. These requirements are generally established in accordance with extreme design points for the engine operation and various representative fuelling mode effects, especially for staged or double combustors.

Additionally, profile distortions at the exit of the combustor can be generated during transient phases of the engine operation. These distortions due to air supply and air-to-fuel ratio variations can directly impact the global thermodynamic efficiency of the engine, through combustor and HP-turbine efficiency variations. Of course, these specifications have also to take into account the machining and tooling variations from both

the turbine and combustor points of view. The cost-effectiveness and technological compromise between the two modules also affects the outcome.

For design points, 1-D and 2-D engineering methods and 3-D CFD reactive calculations for isolated combustion, or coupled with the turbine nozzle module, are currently used to determine the most effective interface compliance conditions. Transient aspects are generally considered through 1-D and 2-D transient global modeling of the engine fitted on experimental data resulting from core engine tests and combustion rig tests on other engines. Inert and reactive 3-D and 2-D CFD calculations can also be considered for fuelling transient considerations.

B.3.1.1 Modeling

Classically, the design requirements have been obtained through numerous tests, leading to the practice where all of a manufacturer's experience is recorded and codified and some rules are given as advice. In the last ten years, CFD has been used to reduce the number of tests needed, but one is always kept as a reference point for calibrating the various constants involved in the different models. Today the main goal for the manufacturer is to design new concepts for advanced combustion, which usually represent technological progress regarding in-house experience and ability. Consequently, a better understanding of all the involved physical phenomena, combined with related improvements in CFD tools is greatly needed. Although all phenomena are linked in turbulent two-phase reactive flow the prediction of a good temperature field is of primary importance. Without a correct temperature field, a correct flow-field cannot be obtained. (Because the density is false the solution of the conservation equation for momentum is false.)

Two phenomena are particularly crucial in the prediction of all the performances related to combustion. These are:

- Two phase flow in turbulent combustion; and
- The interactions between turbulence and chemistry.

Both need to be represented simultaneously, with accuracy, by the model to get reliable CFD tools.

The most attractive approach for modeling turbulent combustion is the laminar flamelet concept. Within the laminar flamelet concept, a turbulent flame is regarded as an ensemble of stationary laminar, locally one-dimensional flame elements, stretched and distorted by the turbulent flow.

Two assumptions are commonly introduced: the reaction zone is thin in comparison to the typical length of the turbulent flow, and the chemistry is fast in comparison to diffusion and convective transport. Then the reaction zone can be modeled as a one-dimensional reaction diffusion layer. This method is based on the local mixture fraction, and includes an extinction mechanism due to high local strain.

In applications of flamelets, stationary laminar flame solutions are stored in a flamelet library. During the CFD calculation, the flamelet library is consulted to determine the local distribution of reactants.

However, laminar-flamelet concept drawbacks are:

- This method works well only if the reaction zone is small compared to turbulent lengths; and
- The turbulence influence appears through a presumed PDF (Probability Density Function) that required an 'a priori' knowledge of the composition PDF.

The second approach concerns the calculated PDF method. The main characteristic is that this method combines an exact treatment of chemical reactions with the influence of turbulence. It does so by solving a

balance equation for the one-point composition PDF wherein the chemical reaction terms are in closed form. All PDF codes use notional particles that obey stochastic differential equations, solved by a Monte Carlo method.

The PDF contains random variables representing all chemical species at a particular spatial location. However, it contains no information concerning local fluctuations in the scalar gradient (2-point information). Thus, a model is needed for this micromixing term.

PDF codes are more CPU intensive than moment closure, but still tractable for process engineering calculations. In order to predict pollutants, detailed kinetic mechanisms can be combined with composition PDF, but this application is restricted by CPU and computer memory limits on laboratory flames. Since the reaction rates usually vary by several orders of magnitude, a stiff ODE (Ordinary Differential Equations) solver is required, and complex kinetics involving many reactants can be computationally intensive. In principle, the number of scalars is limited to five or six reactants with a reduced chemical mechanism, and with a reaction look-up table.

Presently, considerable effort is being applied to develop reliable models for micro mixing and to represent the effect of the evaporation of the droplets.

B.3.1.2 Dissociation/Recombination/Emission

Because of strict environmental regulations for aircraft engines, emissions from carbon monoxide, unburned hydrocarbons, oxides of nitrogen and smoke must be reduced. Moreover, especially at high combustion temperatures (>1800 K), dissociation of CO_2 and H_2O into CO and H_2, result in a decreased heat release.

The combustion system is more affected by concerns about pollutant emission than any other part of a gas turbine. The combustor can be separated into two zones:

- A relatively small primary zone, where fast reactions produce radicals (H, OH). High temperatures are reached in this zone, which corresponds to the CO production region.
- A bigger secondary zone downstream, where CO is oxidized into CO_2 and NO_x appears.

CO and NO_x emissions from combustion chamber are influenced by engine power setting. First, carbon monoxide and hydrocarbon emissions are lowest at full throttle operations. As thrust is increased, inlet temperature and pressure in the combustion are higher, as is fuel-air ratio. The increased fuel flow results in improved fuel atomization, and a higher combustion inlet temperature increases the vaporization rate. Because of the greater fuel-air ratio (FAR), the flame temperature increases and the chemical reaction rates responsible for CO and HC consumption are also sharply increased. Secondly, oxides of nitrogen emissions are greatest at high power operating conditions. NO_x formation is extremely temperature sensitive. Since the combustion inlet temperature and consequently the stoichiometric flame temperature is increased with the power setting, the NO_x emission level is important for high design. Hence, new combustion concepts are being developed in order to reduce NO_x and CO emissions, with respect to their conflicting trends.

Combustion efficiency is a parameter of paramount importance for the performance engineer. It is customary to define the combustion efficiency as the ratio of the released energy to the maximum possible energy that can theoretically be released during the combustion process.

Hence, it is common practice in cycle decks to use the combustion efficiency as the ratio of the ‘actually burned’ fuel to the input fuel. The fuel air ratio (FAR) used for all subsequent calculations up to the engine exit is then based on this ‘actually burned’ fuel. The ‘remaining fuel’ (which has not been burned)

disappears from the engine thermodynamic calculation, with the exception of the Specific Fuel Consumption (SFC).

Until recently, because combustion efficiency was close to the maximum and exit combustion temperature (T4) was not very high, this way of working suited engine performance calculations. In recent years, the maximum cycle pressures and temperatures of jet engines have increased considerably. When temperatures are in excess of 1650 K, the dissociation effects become important.

The combustion inefficiency can be measured from the percentages of the exhaust products containing chemical energy (i.e. unburned hydrocarbons, carbon monoxide and hydrogen). To obtain the combustion inefficiency, only the amounts in excess of those formed at dissociation at equilibrium are considered (we cannot blame the combustion designers for the dissociation at equilibrium…). These concentrations in excess of those formed at equilibrium may be due to the non-uniformity of the temperature or combustion profile.

The dissociation energy at equilibrium can be very important, depending on the pressure and final temperature. At 39 bars and 2200 K the energy of dissociation accounts for 0.76% of the total fuel energy; at 2600 K the dissociation energy rises to 6%.

At these high temperatures, it is necessary to account for the molecular dissociation and recombination mechanism beyond station 4, because recombination is an exothermic reaction.

The engine makers frequently use one of two extreme assumptions:

- Local equilibrium is assumed (i.e. infinitely rapid chemical kinetics); and
- A frozen composition is assumed (i.e. no recombination) from the combustion exit to the engine exhaust.

From an engine test-analysis viewpoint, the assumption on the chemical composition is closely related to the turbine efficiency. Let's say that on a test bed there is an engine running at a very high turbine-entry temperature. If the frozen assumption is used to analyze the test data, the energy available for the turbines is less than the energy available if the local equilibrium assumption is used. Therefore, the turbine efficiency will be higher with the frozen assumption than with the local equilibrium assumption. Of course, the engine SFC is the same, what changes is the trade-off between chemical composition and turbine aerodynamics. This means that there is no clear cut-off (station 4) between the combustion (i.e. chemical reactions) and the turbine designer.

As has been mentioned above, the energy of dissociation becomes very important at high temperatures, making it is necessary to determine how much energy is recovered by the recombination reactions downstream of the combustion. There are few publications dealing with aerodynamics and chemistry through the turbine expansion. The cited publication is based on one-dimensional flow in the first nozzle (without cooling flows). This study shows that, except for the NO concentration, local equilibrium is attained at the exit of the nozzle.

Because NO has a much slower reaction rate, in this reference it is assumed that the concentration at equilibrium cannot be achieved at the end of the combustion. However, as the fluid progresses through the nozzle more NO is produced. In order to guarantee low emissions, turbine designers should consider NO formation.

From a performance viewpoint, the combustion efficiency is not enough, the chemical reactions downstream of the combustion cannot be ignored. The problem is very complex, aerodynamics and chemistry are involved, and 3-D effects may be important. The turbine blade cooling technique may have a strong influence on the recombination mechanism.

B.3.1.3 NO_x Modeling

NO_x is defined by the regulatory authorities as the sum of nitric oxide (NO) and nitrogen dioxide (NO_2). Many mechanisms have been developed to represent NO_x formation under a variety of thermo-chemistry conditions. In classical combustion, characterized by the presence of diffusion flames 'Thermal NO_x' is the principal route to NO_x formation. It is well described by the Zeldovich equations.

$N_2 + O \Leftrightarrow NO + N$ (R1)

$N + O_2 \Leftrightarrow NO + O$ (R2)

$N + OH \Leftrightarrow H + NO$ (R3)

A combustion kinetics model for NO_x, with a classical hypothesis of steadiness and partial equilibrium, is applied as a post-processing step after a converged two-phase turbulent reactive computation has been obtained. The model for turbulent combustion is based on a presumed PDF approach where chemistry is very fast compared to the turbulent micro-mixing and where liquid fuel is represented by an ensemble of droplets in a Lagrangian framework. From the expression of the chemical reaction rate we can see that two characteristics of the flow-field have to be very well predicted by the reactive computation. They are the temperature and equivalence ratio fields. Temperature acts directly on the k's constants while equivalence ratio is used to estimate the equilibrium values for all the radicals. This method is currently applied in the design process at Snecma and the other engine manufacturers use similar methods. All the users have demonstrated that this approach works well only for high level pressures (>30b), and that more information about chemistry must be included in the combustion model as a first step, and in the NO_x mechanism as a second step. The reasons for the method breaking down when finite-rate chemistry effects become important (when the pressure is reduced) lie principally in the combustion model. If we try to apply a very fast chemistry turbulent combustion model to situations where we get a false temperature field the consequence is a bad flow-field associated with a bad equivalence ratio field. Super equilibrium concentrations for the O radical have been frequently observed or computed with more powerful tools. This is directly the consequence of slow three body recombination reactions. Only the integration of more detailed chemistry to the turbulent combustion model can give us solution to this problem. This is currently the case at Snecma where work has been oriented toward the use of the PDF techniques associated with complex chemistry.

Applied to a research tubular combustor the simplified method has given the following results, which are a good illustration of the considerations above.

Table B-2: Simplified Method Results

$EINO_x$ Computed	$EINO_x$ Measured	Pressure	Equivalence Ratio	Error %
5	7	15.6	8.6	28,6%
5	8	15.5	9.8	37,5%
5,5	10	15.3	13.7	45,0%
20	20	32.9	11.2	0,0%
22	27	32.6	15.3	18,5%
27	35	33.4	18.4	22,9%
28	28	37.6	12.8	0,0%
31	31	37.6	13.7	0,0%
32	38	37.3	16.8	15,8%

Improvements can be obtained in the framework of PDF transported methods using the coupled kinetics of kerosene and NO_x, and taking into account more information about the NO_x production mechanism. Although NO_x modeling is compatible with flamelet model capabilities, it seems CO prediction is limited by this assumption. The flamelet approach for CO prediction can be improved by the inclusion of turbulent and chemistry models. However CO formation is very complex, and flamelet hypothesis is not necessarily appropriate for this pollutant.

In combustors, CO oxidation can take place in lean post-flame zones, far from the flame front, where the flamelet approach may be incorrect. CO emissions are greatly influenced by high mixing rates in combustors, so the statistics of fluctuations need to be well predicted.

Therefore, the PDF transport method, which is able to model the non-equilibrium effects, works well for CO predictions, and should improve results. Finally, two aspects are important for CO modeling: the kinetic mechanism must be enough detailed, and the PDF method must be accurate with scalar fluctuations, and account for finite rate and non-equilibrium effects.

B.3.1.4 Hail and Water Ingestion

Exposed to various climatic conditions, the jet engine ingests different forms of water contained in the atmosphere: vapor, liquid, hail, snow; and ice crystals. The operating conditions where these forms of water can be met are below 20,000 ft. For higher altitudes, the atmospheric water content is insignificant. Depending upon flight speed (i.e. the ratio between the free stream area and the inlet area) and engine rotor speed, the fluid flow at the compressor outlet might include water vapor, liquid or solid water. The lower the corrected speed, the more important these phenomena are. The impacted flight phases are then low altitude cruise, taxiing, and descent. Engine performance predictions and risk assessments for flight safety in severe climatic conditions require an understanding of the different factors characterizing the behavior of the combustion chamber. If the working fluid has a high water content, the specific fuel consumption (SFC) rises and the operational range of the aircraft decreases. With liquid water at the combustion inlet, several cases must be considered. With low liquid water content, vaporizing takes place in the combustion chamber, but combustion efficiency is deteriorated. The fuel flow rate must then be increased. Beyond some threshold, extinction might occur.

Two modeling approaches are required:

- Modeling of reductions in flame temperature and efficiency as a function of water content; and
- Calculation of extinction limits due to the presence of liquid and solid water in the combustor.

B.3.2 Transient and Dynamic Modeling

B.3.2.1 Flame Blow-Out and Relight

The engine operational envelope at high altitude or during fast transient or descent operations can be severely restricted by flame blow-out and combustor re-light capabilities (see **Figure B.65**). For example, flame blow-out effects can lead to very high thermal stress on turbine elements, nozzles and other parts located at the rear of the combustor.

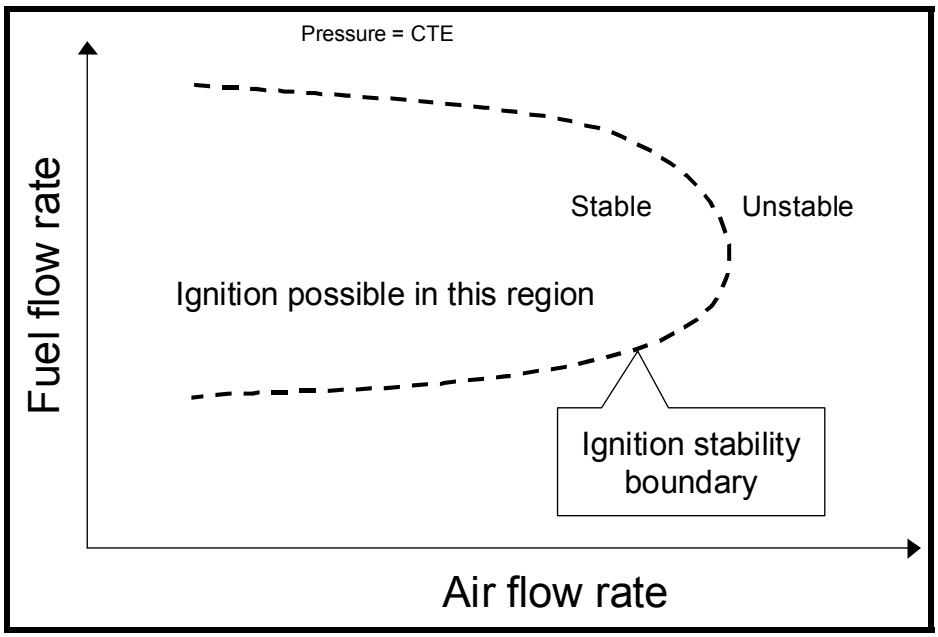

Figure B.65: Region of Stable Ignition.

Due to flight safety considerations and civil regulations, combustor ignition capability and operability requirements are generally defined through sub-domains and included in the flight envelope specifications. Complementary specifications on fuel temperature and atmospheric conditions such as temperature and hygrometry, rain and hailstone precipitation are also taken into account. Thermal limitations of the pumps and injection systems require minimal fuel flow rates for cooling and these can also reduce the operability of the combustor.

From the control system view of the combustor, these constraints are translated into fuelling and actuation laws that are dependent on engine operating conditions. All these conditions must be integrated in the global engine performance model in order to specify module performance and control systems, and help to define in-flight emergency procedures. Sensitivity to various control options, especially for staged or double combustion, have also to be considered: commutation laws between pilot, main and mixed modes in combustor fueling have to be considered in order to prevent such effects. Sensitivity to power off-take and air bleed, which can induce fuel–air ratio variations, also must be taken into account.

A re-light control system needs simulation models of extinction and light up capacities of the combustion. These transient models have to provide extinction detection and light up information. They integrate time-delay modeling for fuelling and spark operations, and combustion energy efficiency, which is correlated with the compression efficiency, fuel flow and engine power setting of the engine. Alarm temperature on turbine parts and engine rotor speed information generally is considered in this loop in order to detect a blow out risk or light up failure.

A particular aspect of the problem is the windmilling starting process, which requires:

- A precise knowledge of the airflow conditions at the combustor entry (pressure and temperature).
- After re-light, a good understanding of thermal and kinetic inertia of all other parts of the engine.

Of course, the control system and engine performance models have also to take into account the global variations in the quality of components such as the compressor, fueling system, combustor, sensor systems and others elements of the core engine.

Regarding the operational limits of the combustion, operation capacities and flame-out performances can be expressed in terms of fuel-air ratio and air-loading envelopes These stability and re-light performance envelopes are determined from 3-D CFD combustion calculations, experimental results and engine tests. As spark energy intensity and frequency at the ignition plug system has a direct influence on the combustion re-light and light up performance, it is also taken into account by 3-D CFD. The windmilling envelope re-light capacity is directly derived from this, incorporating the compressor effects through a simulation model of the engine for these particular conditions.

Unsteady and instability effects of the combustion preceding the flame-out event are currently incorporated in these models. Due to recent progress in computing, Large Eddy Simulation CFD calculations are progressively supplying an improving representation of these phenomena and providing new methodologies for building such simulation models.

On another point, blow out and relight performances are directly affected by the variation in quality of components and fueling and air flow distortions at the combustor inlet. CFD simulations and specific rig tests of the hydraulic chain including pump, manifold, valves and injectors currently provide models for the fuel system. However, a multi-module coupled CFD analysis from compressor to the combustor exit is needed to provide a sensitivity analysis of blow out risk and relight capacity to component variations and flow distortions.

B.3.2.2 Modeling Relight

Today, empirical rules are used to determine the primary zone airflow rate required for an acceptable altitude relight capability. The size of an aircraft combustor is, for the major part, fixed by this capacity. Ignition begins when power is supplied to the igniter plug to make a spark inside the combustor. We can then distinguish four steps, which are necessary in order to restart the engine:

- The kernel formed by the spark must be able to burn. This is the result of the competition between energy losses (turbulent conduction outside the kernel, conduction to the droplets inside the kernel, evaporation, heat release chemical kinetics) and the source of energy for the kernel (density of energy injected by the spark, energy coming from initiated combustion).
- Once the kernel is burning it must be captured by a stable eddy to maintain stable combustion. This process may be tuned by positioning of the igniter combined with the general flow organization.
- The flame, which is anchored to one sector of the combustor, must propagate to the whole combustor.
- When the flame has been established throughout the entire combustor, the combustion efficiency must be sufficient to ensure that the engine will accelerate. (Inertia and turbine/compressor power balance).

Failure of one single step will cause failure of the engine restart or re-light. For example doubling the energy to the igniter has no influence on the final ignition if step two fails. On the other hand optimizing the location of the igniter is a bad strategy if step one fails.

With only empirical rules that do not lead to any understanding of the underlying mechanism, significant improvements in ignition capability cannot be obtained. Note that if we are able to reduce the size of the combustor while keeping the ignition capacity constant, or improving it, we will have gains related to mass and weight because combustor chamber may be made more compact. For civil aircraft engines a reduction of combustor size can lead to reduction in NO_x emissions.

Making predictive models for this phenomenon becomes very hard when we try to connect the spark process through the related kernel growth to the turbulent flow inside the combustion. Many length scales

are involved with at least four orders of magnitude of difference. It is then impossible in the same computation to represent all those scales except with DNS (Direct Navier-Stokes) tools. Unfortunately due to CPU limitations DNS is not at present a viable strategy for the calculation of turbulent reactive two-phase flows with complex geometry in industrial applications, where Reynolds numbers are always high.

Once again, two-phase flow has a major role in the ignition process. If we consider step one in more detail we can see that the distribution of droplet size inside the ignition kernel will affect its future growth. This distribution is a function of the injector system and the location of the igniter inside the combustor. As already mentioned, the precise representation of the evaporation process inside the kernel is a key to success in building a reliable predictive computational tool. The method chosen at Snecma consists of: computing a two-phase flow with 3-D code to represent all the fields in the combustor related to engine windmilling before starting; applying a 1-D code at every point to determine the minimum ignition energy.

Although it is theoretically possible to make those computations by means of the PDF transport equation associated with detailed chemistry, we must keep in mind that we have to compute ignition curves corresponding to many points in the plane (fuel flow, air flow). Therefore, simplified methods are preferred.

B.3.2.3 Combustion Efficiency and Compressor Limits

Combustion efficiency is mainly controlled by evaporation, mixing and chemical reaction. When the chemical reactions govern the combustion process, the theta parameter (air loading) obtained by A.H. Lefebvre [B.44], which is based on the burning velocity model in the primary zone, allows correlation of efficiency to the main operating variables (pressure, temperature, mass flow and geometry). J. Odgers [B.45] has also obtained an empirical correlation, which allows combustion efficiency to be represented as a function of the fuel loading.

When mixing governs the combustion process, a quasi-empirical correlation due to Tipler and Wilson [B.46] is very often used. It has been claimed by A.H. Lefebvre that at low pressures (100 KPa), combustion is governed by chemical reactions and at high pressures (>300 KPa), combustion is dominated by mixing. As jet engines operate in a wide range of operating conditions, combustion efficiency may be determined by chemical reactions, mixing or both at the same time.

During transient operation, fuel evaporation may become important when dealing with rapid or severe (slam acceleration) transients. Evaporation rates depend strongly on the Sauter Mean Diameter (SMD), which in turns depends on the fuel properties, flow rate, geometry, etc. A.H. Lefebvre gives some correlation to obtain the combustion efficiency when evaporation is predominant. Moreover during a transient, there is a heat flux between the gas and the surrounding material (convection and radiation). This heat transfer affects combustor efficiency. When predicting compressor surge, it is very important to know accurately the combustion efficiency. Compressor surge is a very fast process, therefore all factors affecting combustion must be taken into account.

Compressor surge is a major consideration in the design of gas turbine engines and their control systems. The compliance with specified operability constraints requires a high level of agreement between the different component characteristics (aerodynamics, thermal conduction…) and the related control commands. It is customary to use both transient simulation tools and rig tests (components, HP core, and bench engine). The prediction of the surge and operating lines during various fast transients is therefore required.

Models for engine transient behavior prediction are required for the determination of:

- The fuel and stator schedules during acceleration and deceleration, with the computation of the operating and surge lines.

- The available surge margin.
- Process viability, for example fuel cut-off and re-light transients, for surge recovery.

Stability margins are evaluated on the engine to ensure that sufficient margin is available to meet the operational requirements. Compression system surge lines may differ on the engine from the rig test because of differing dimensional, thermodynamic and dynamic properties. To characterize the engine installed HP compressor surge line position or shift the following method is commonly used. The fuel step technique allows HPC operating point to be moved very quickly towards the HPC surge line. By using the continuity equation in the choked turbine nozzle the compressor mass flow is then solved.

With the aforementioned applications in mind, the following investigations are of interest:

- Modeling of outlet temperature, efficiency, stability domain, relaxation time, and heat soak characteristics as a function of gradients in fuel, FAR, and inlet conditions.
- Method to analyze compressor operating line excursions during fuel step transients.

B.3.3 Reheat System

B.3.3.1 Stability and Blow-Out

As for main combustors, fast transient from idle to full throttle operations can be severely restricted by flame blowout and instability in reheat system. There are different risks linked with this. From the pilot's viewpoint, and depending on the flight point considered, this phenomenon can be felt as an important and instantaneous lost of operability. This may lead to safety issues during heavily loaded take-off or dog-fight phases of flight. Less critical issues, such as thrust loss during supersonic operations, may also appear.

From the engine point of view and depending on the engine control system loop, the criticality of instability or a blowout varies. A local extinction or a local blow out of the combustion between different gutters of the flame holder system may have limited impact on the combustion efficiency and the thrust efficiency. However, due to consequential exhaust nozzle operation, the engine rating, the internal pressure of the reheat pipe, and eventually the compressor stall margin, the internal cooling distribution and the integrity of the liner, may all be affected. Due to the fuel release, it may also induce uncontrolled re-light phenomena in the nozzle or in the plume with undesirable effects on the infrared signature.

Reheat operability requirements expressed in terms of fuel-rate-range are generally defined through sub-domains and included into the flight envelope specifications, together with aircraft incidence parameters. These specifications have to integrate for instance the compressor stall margin transcribed in terms of maximum fuel rate and nozzle section amplitude. Complementary specifications on fuel temperature, and atmosphere conditions such as temperature and hygrometry also have to be taken into account.

All these conditions must be integrated in the global performance engine model in order to specify module performances, and control systems operation, and help to define in-flight re-light procedures. Sensitivity to various control options, especially for staged fueling and distribution laws of the fueling of the various manifolds and gutters of the flame-holder systems have also to be considered. Transient models have to integrate time-delay modeling for fuelling, spark and nozzle operations, reheat system energy efficiency variation and correlation with internal pressure, nozzle section, and fuel flow and engine speed.

Of course, these models have also to take into account the global variations in quality of components such as the fueling system, flame-holder geometry, by-pass ratio and nozzle section variations, regulation measurement systems and other elements of the engine.

With regard to the isolated module view of the reheat system, stability and blow out performance can be expressed in terms of fuel-air ratio and air-loading envelopes or limits. Specific sub-domains concerning fuel-staging modes of the different gutters and flame-holder regions are generally associated with these limits.

These stability and blow-out envelopes can be determined both from 3-D CFD calculations and experimental results on sub-components and engine tests.

Unsteady and instability effects of the combustion preceding the blow out or the unsteady process are currently incorporated in these models. Due to recent progress in computing, Large Eddy Simulation CFD calculations are progressively supplying a better representation of these phenomena and providing new methodologies for building such compartmental models. These may be further developed to take into account the influence of the aircraft incidence and the consequences on fan efficiency and combustion quality.

Blowout and stability performances are directly affected by the variations in the components of the fuelling system, by-pass ratio variations, and the vitiation and airflow distortions in mixer regions. CFD simulations and specific rig tests of the hydraulic chain including pump, manifold, valves and injectors currently provide compartmental models for the fuelling system.

B.3.3.2 Screech and Rumble

Screech and rumble phenomena in reheat systems may impose severe mechanical stress on the engine and may rapidly create safety issues for the engine and the aircraft. Due to combustion and acoustically coupled effects, the combustion amplified energy release may induce extensive physical to the exhaust duct structure. Because of the closeness of fuel pipes and fuel tanks, these problems can directly affect aircraft safety.

These instabilities can suddenly appear during transient operations, like fuel staging or engine acceleration, and continue until the pilot or the control system switches off the reheat mode. These phenomena are generally amplified in regimes of high fuel-air-ratio. Hence, free-screech and free-rumble operating conditions have to be precisely defined in the engine cycle models. These conditions can be transcribed from terms of fuel rate and air-fuel ratio interaction limits into fuel operating and staging regulation and intake airflow conditions. These limits have to take into account fuel flow restrictions or staging options directly connected to the fuel-system operating-regime, and include margins for distortion effects and component variations.

Screech and rumble margin safety domains can be transcribed into fuel-air ratio or air-loading envelopes or limits. Specific sub-domains concerning fuelling staging modes of the different gutters and flame holder regions are generally associated with these limits.

Experiments on full-scale engines and sub-component tests are required to determine these limits and build compartmental models for the whole flight envelope. Large Eddy Simulation CFD calculations are also useful to confirm these limits.

Screech and rumble sensitivity are affected by variations in components which may influence the fuelling regions, the by-pass ratio variations, and the vitiation and air flow distortions at the core and bypass mixer. CFD simulations and specific rig tests of the hydraulic chain including pump, manifold, valves and injectors currently provide compartmental models for the fuelling system.

Transient aspects are generally considered through 1-D and 2-D transient global modeling of the engine. This is typically based on experimental data resulting from full engine and reheat component tests on other

engines. Inert and reactive 3-D and 2-D CFD calculations can also be considered for fuelling transient considerations.

B.3.3.2.1 Modeling

The problem of combustion instabilities is classical, difficult and critical. It is classical and has been under study for at least sixty years. The first large effort on the subject was in the area of rocket propulsion with solid fuel during the two decades following WWII. It is difficult because the same term in fact applies to a wide variety of mechanisms, coupling several physical phenomena such as combustion itself, convection, fuel atomization and vaporization, mixing, hydrodynamic instabilities and acoustics. It should be noted that instabilities are generally named after the way they sound to the ear, and not after the underlying mechanism, which is often complex and ill understood. Examples are groaning, screech, organ noise, chugging, and growl. The problem is critical because combustion oscillations may lead to very large disturbances that jeopardize combustor operability, especially for advanced, low-emission designs.

It is useful to consider a classification of instabilities in three groups:

- Intrinsic combustion instabilities;
- Chamber instabilities; and
- System instabilities.

Intrinsic instabilities deal with the combustion process itself. The LBO limit, and flashback or auto-ignition phenomena may be treated within this class. By definition these instabilities do not involve complex coupling between various physical phenomena, and the modeling challenge is not as difficult as with the two other types, which will be our main concern from now on.

Chamber instabilities involve, in a strong way, the acoustic eigenmodes of the combustor. Given the scales typically encountered in aeronautical combustors, these instabilities can also be identified as high frequency instabilities, which are based on a coupling between acoustics and combustion. Indeed the frequency range is related to the acoustic characteristic frequency c/L, where c is the speed of sound and L the size of the combustor. The speed of sound is the highest velocity scalar available, especially at high temperature, and frequencies tend to be high.

System instabilities involve the whole combustion system, which not only includes the combustor itself, but also the fuel line, injection system and exhaust. In the case of a full engine, the system can go as far as including elements of the compressor and turbine. This type of instability is the most difficult to tackle since the first difficulty is to choose the limit of the 'system' under study. These instabilities can also be referred to as low frequency instabilities. The time scale is defined either by the acoustics of the system, with longer length scales than the combustor alone, or by slower physical processes, such as hydraulics, convection or vaporization.

B.3.3.3 High Frequency Instabilities

We will identify high frequency instabilities with instabilities based on a strong coupling of the combustion with the cavity modes of the chamber. These instabilities have been known for a long time in rocket engines, and in jet engine reheat systems. As far as the main chamber of a jet engine is concerned, 'high frequency' instabilities could be relevant to organ noise problems, related to the first circumferential modes of an annular combustor.

Modeling approaches for these problems are typically based on writing a classical acoustic equation where the combustion influence is relegated to a source term **[B.47]**:

$$\nabla(c^2\nabla p) - \frac{\partial^2 p}{\partial t^2} = H \qquad \textbf{Eq. B-3}$$

Generally speaking the source term, H, is complex, and some techniques aim at providing a model for H. Before detailing this, it is useful to derive an acoustic energy transport equation, with a source term relating to **[B.48]**:

$$S \propto p'\dot{q}\,, \qquad \textbf{Eq. B-4}$$

where p' is the acoustic pressure and $\dot{q}$ the unsteady heat release rate. By integrating this over time, the classical Rayleigh criterion is obtained. A combustion oscillation tends to amplify if the heat release is in phase with the pressure. One approach consists in writing the heat release and pressure correlation in the (n,τ) form initially proposed by Crocco **[B.49]**:

$$\dot{q}(t) = n.p(t-\tau) \qquad \textbf{Eq. B-5}$$

where n is a sensitivity factor and τ a time lag accounting for the time it takes for the flame to respond to a pressure perturbation. This time lag typically includes convection or vaporization time, and could be measured. In principle, it is then possible to build instability models. The only information that needs to be evaluated is the (n,τ) couple. However, the theory has the drawback that it implies a simple causal relationship between pressure or velocity fluctuation and flame response, while in a real instability the coupling is highly non-linear. Therefore, even with more complex definitions, the (n,τ) nomenclature remains a formal description, which is more useful in forming a visual representation of the phenomenon of high frequency instabilities rather than in actually predicting it.

As high frequency instabilities are strongly linked to the acoustic eigenmodes of the combustor, these modes are useful information in themselves. Computing the modes will give no information as to which modes will actually be excited, but will at least identify the higher risk frequencies. Moreover, the spatial structure of these modes can suggest locations where passive-damping techniques may be more efficiently applied. The extraction of the acoustic modes of a cavity is a classical problem with well-known solutions for an homogeneous medium in basic geometric configurations. For application in combustors, more general solving techniques have been developed for arbitrary geometric configurations with a non-homogeneous base temperature (hence speed of sound) field **[B.50]**. Let us recall that the computed eigenmodes are the solution of equation (1) with no source term: it is supposed that the combustion oscillation simply locks onto a cavity mode, without strongly affecting it, which is of course a strong assumption.

A more difficult problem is to define boundary conditions, while it is relatively simple to define boundaries themselves. The only boundaries that are easily handled are rigid solid boundaries, or zero pressure conditions, which are both energy conserving. The nozzle throat or turbine in the case of rocket engines or afterburners, and the compressor and turbines in the case of the main combustor in a jet engine, lead to complex boundary conditions. Generally speaking they involve frequency-dependent impedance conditions, which are not so easily modeled. Models are available for various types of problem **[B.51]**, but the boundary problem remains a critical point in these approaches.

Given that the basic acoustic modes were accurately captured, attempts have been made to account for a complex non linear interaction with combustion, namely by actually keeping the source term H in equation (1) and decomposing the perturbed modes on the free acoustic eigenbase. This is essentially Culick's approach **[B.52]**. Given the free cavity modes Ψn(x) associated to frequencies ω n:

$$\nabla(c^2\nabla\Psi_n) + \omega_n^2\Psi_n = 0 \qquad \textbf{Eq. B-6}$$

The solutions perturbed (by combustion) are decomposed on the Ψn base:

$$p(x,t) = \sum_n a_n(t)\Psi_n(x) \qquad \textbf{Eq. B-7}$$

Applying **Eq. B-3**, the amplitudes $a_n(t)$ are solution of the following equation:

$$(\frac{d^2}{dt^2} + \omega_n^2)a_n(t) = \int H.\Psi_n dV \qquad \textbf{Eq. B-8}$$

Of course, with zero source term, a_n is a simple sine wave with frequency ωn. Let us assume that a_n has the form

$$a_n(t) = \exp(-i\omega t) \qquad \textbf{Eq. B-9}$$

With no source term we recover of course $\omega=\omega_n$. The source term represents the influence of combustion and will therefore lead to a frequency shift (real part of the frequency), and a growth or decay (imaginary part of the frequency) of the eigenmode. Starting from an unperturbed acoustic mode computation, this method is therefore able to predict the alteration of the combustor acoustic modes by interaction with combustion, and provides the amplification factor of each modified mode. These are attractive features of the approach. On the other hand, all the difficulty consists in evaluating and modeling H, and more precisely response functions in the form H/a_n.

B.3.4 Liner Cooling

Because of the interactions resulting from the reheat chamber pressure and the air flow distribution between the liner and the reheat system, it is necessary to consider a coupled approach to modeling the liner cooling and the mixing of the core and fan flows.

These two functions directly influence the reheat combustion efficiency, the global pressure drop performances and the cooling efficiency. They also may influence the core rating and performances.

1-D models can be sufficient to give an average representation of the exhaust and liner flow rates. However, because recent non axisymmetric flame-holder geometries and cooling configurations may also induce local pressure drop and flows distortions in the exhaust pipe, 2-D and 3-D CFD analyses may be necessary to build a derived compartmental model.

B.3.5 Cited References for Combustor Section

[B. 44] Lefebvre, H., “Gas Turbine Combustion”, Second Edition 1999 Taylor & Francis.

[B.45] Odgers, J. and Carrier, C., “Modelling of Gas Turbine Combustors; Considerations of Combustion Efficiency and Stability”, Journal of Engineering for Power, pp. 105-113, April 1973.

[B.46] Tipler, W. and Wilson, A.W., “Combustion in Gas Turbines”, Paper B9 in Proceedings of the Congrès International des Machines à Combustion (CIMAC), Paris, pp. 897-927, 1959.

[B.47] Schönfeld, T. and Rudgyard, M.A., “Steady and Unsteady Flow Simulations Using the Hybrid Flow Solver AVBP”, AIAA Journal, 37(11), November 1999, pp. 1378-1385.

[B.48] Schönfeld, T. and Rudgyard, M.A., “COUPL and Its Use within Hybrid Mesh CFD Applications”, Proc. of the 10th Intl Conference on Parallel CFD 98, pp. 433-440, Eds A. Ecer, D. Emerson,

J. Periaux and N. Satofuka, Elsevier Science Publishers, 1998, AIAA 98-1027, 36th AIAA Aerospace Sciences, January 12-15, 1998, Reno.

[B.49] Crocco, L. and Cheng, S.-I., "Theory of Combustion Instability Liquid Propellant Rocket Motor", AGARDograph No. 8, 1956.

[B.50] Colin, O., Ducros, F., Veynante, D. and Poinsot, T., "A Thickened Flame Model for Large Eddy Simulations of Turbulent Premixed Combustion", Physics of Fluids 2000, In Press.

[B.51] Cazalens, M., Lecourt, R. and Quintilla, V., "Predicting Ignition Performance for Altitude Relight", XV ISABE 2001, September 2-7 2001, Bangalore, Inde.

[B.52] Culick, F.E. and Yang, V., "Overview of Combustion Instabilities in Liquid-Propellant Rocket Engines", Progress in Astronautics and Aeronautics, 169, 1995.

B.3.6 Additional Bibliography for Combustor Section

Bray, K.N.C., "The Challenge of Turbulent Combustion", 26th Symposium (International) on Combustion, The Combustion Institute, Pittsburgh, 1996, pp. 1-26.

Pitsch, H., Chen, M. and Peters, N., "Unsteady Flamelet Modeling of Turbulent Hydrogen-Air Diffusion Flames", 27th Symposium (International) on Combustion, The Combustion Institute, Pittsburgh, 1998, pp. 1057-1064.

Barths, H., Peters, N., Brehm, N., Mack, A., Pfitzner, M. and Smiljanovski, V., "Simulation of Pollutant Formation in a Gas-Turbine Combustor Using Unsteady Flamelets", 27th Symposium (International) on Combustion, The Combustion Institute, Pittsburgh, 1998, pp. 1841-1847.

Dopazo, C., "Turbulent Reacting Flows", (Libby, P.A. and Williams, F.A., Eds), Academic Press, London, 1994, pp. 375-474.

Larroya, J.C., François, C., Cazalens, M. and Vervisch, L., "Testing a New Monte Carlo Method for Solving PDF Equation in Turbulent Combustion", In 5th International Conference on Technologies and Combustion for a Clean Environment, Vol. I, pp. 177-183, 1999.

Leide, B. and Stouffs, P., "Residual Reactivity of Burnt Gases in the Early Expansion Process of Future Gas Turbines", Gas Turbine and Power.

Visser, W.P.J. and Kluiters, S.C.M., "Modelling the Effects of Operating Conditions and Alternative Fuels on Gas Turbine Performance and Emissions", Research and Technology Organisation, RTO-MP-14, 1999.

Ravet, F. and Vervisch, L., "Modelling Non-Premixed Turbulent Combustion in Aeronautical Engines using PDF Generator", AIAA Paper # 98-1027, 36th AIAA Aerospace Sciences, January 12-15, 1998, Reno.

Cazalens, M., Beule, F. and David, E., "Design of Advanced Low Emission Combustor", CEAS European Propulsion Forum Programme 2001.

Angelberger, C., Veynante, D., Egolfopoulos, F. and Poinsot, T., "Large Eddy Simulations of Combustion Instabilities in Premixed Flames", Proc. of the Summer Program 1998, Center for Turbulence Research, Stanford.

Williams, F.A., "Combustion Theory", Menlo Park: Benjamin/Cummings, 1985.

Laverdant, Poinsot, T. and Candel, S., "Influence of the Mean Temperature Field on the Acoustic Mode Structure in a Dump Combustor", J. Propulsion and Power, 2, pp. 311-316, 1986.

Vuillot, F. "Acoustic Mode Determination in Solid Rocket Motor Stability Analysis", AIAA Journal, July-August 1987.

B.4 EXHAUST NOZZLE COMPONENT SYSTEMS

The nozzle exhaust system is a major component of an aircraft gas turbine powerplant. It is the device by which the energy from the gas generator is converted into useful thrust. It has efficiency just like other components. Turbofan and turbojet engines are especially sensitive to nozzle losses in because they operate on all of the flow from both an airflow and thrust standpoint. Careful design to keep losses low is necessary to achieve goal performance.

The exhaust nozzle component system serves the following functions in the aircraft gas turbine powerplant:

- The exhaust nozzle component contains the exit throttling area (throat) of the powerplant. It meters flow and sets the turbine back-pressure, thereby controlling turbine work. It is one of the primary metering areas in the engine, regulating the cycle. For the case of a dual stream bypass engine, the exit nozzle is the principle controller of the back-pressure to the fan thereby setting fan pressure ratio.
- The nozzle functions as an aerodynamic component that accelerates the gas exiting the turbine to produce thrust from available energy (see **Figure B.66**).
- A variable area nozzle plays an important role in providing optimum performance and assuring engine operability. Variable throat area is essential for control of engine matching and fan back-pressure during augmentation.
- A variable geometry nozzle can be designed to generate pitch and yaw forces to control the air vehicle.
- The exhaust nozzle can be designed to produce reverse thrust.

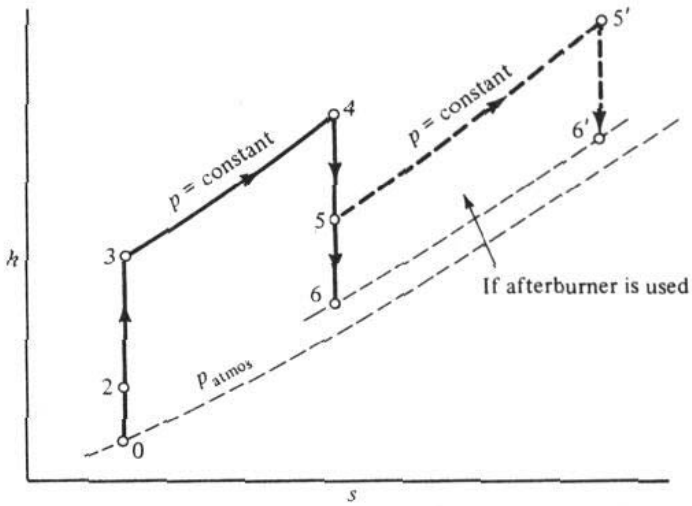

Figure B.66: Energy Available to Produce Thrust from Thermodynamic Cycle.

This chapter will develop and define the standard theory and practice for assessing exhaust system performance in aircraft gas turbine engine analytical simulations. That is, the analytical determination of

the efficiency of the exhaust and nozzle systems in passing flow and producing thrust. We begin with a simple single-stream turbojet and continue to more complex dual stream and variable geometry examples.

B.4.1 Zero Dimensional Analysis

B.4.1.1 Definition of Nozzle Coefficients

Definition and evaluation of the gross and specific thrust and flow coefficients requires a definition of 'ideal' thrust. The ideal thrust can be defined on a basis of an ideal convergent/divergent nozzle, an ideal convergent nozzle, or variations in between. It is recommended that the ideal thrust be defined based on fully expanded convergent/divergent nozzle theory.

The true performance of the nozzle system remains of course unchanged by the choice of the ideal definition; often the ideal definition is simply a choice of a reference datum for bookkeeping purposes. However, it is also a measure of maximum potential of the nozzle component to produce thrust. Insight into potential nozzle system improvements may be gained by analysis and understanding of the various real gas and mechanical design effects causing the actual thrust and nozzle coefficient to be less than ideal.

B.4.1.2 Single Stream Exhaust System

Gas turbine rotating machinery produces hot gas at the turbine exit, station 5, shown schematically for a single-stream turbojet engine in **Figure B.67**.

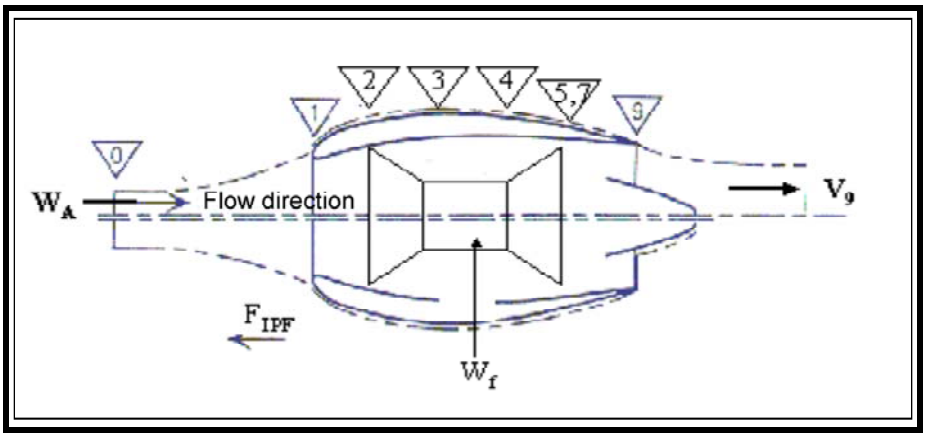

Figure B.67: Turbojet Schematic Showing Engine and Nozzle Station Designations.

For this simple configuration the forward boundary of the nozzle component, Station 7 (also called the nozzle 'charging station'), coincides with the turbine exit Station 5. The nozzle throat is designated Station 8 and the nozzle exit, Station 9. Station designations between 5 and 7 are reserved for ducting, mixers, and augmentors in more complicated engine configurations.

The gas flow at the turbine exit consists of combustion products produced by air entering the engine minus any leakage and customer bleed prior to Station 7 plus the fuel flow entering the combustor.

$$W_{g7} = W_2 - W_{bl} + W_f \qquad \textbf{Eq. B-10}$$

The total energy available for thrust is equal to $W_{g7} * h_{t7}$ where h_{t7} is the total specific enthalpy of the turbine exit gas.

The gas expands through the nozzle to ambient pressure at Station 9 for a fully expanded ideal convergent/ divergent nozzle. This acceleration process transforms available heat energy in the gas to kinetic energy in the expanding jet, which produces useful thrust to propel the aircraft.

The flow velocity at the nozzle exit will be:

$$V_{9,ideal} = \sqrt{2*(h_{t7} - h_{amb})} \qquad \textbf{Eq. B-11}$$

The resultant ideal gross thrust is:

$$F_{g9,ideal} = W_{g7} * V_{9,ideal} \qquad \textbf{Eq. B-12}$$

The ideal gross thrust can also be evaluated as a function of nozzle pressure ratio:

$$F_{g9,ideal} = W_{g7} * M_9 * a_9 = W_{g7} * \sqrt{T_{t7}} * f_1(\gamma, R, P_{t7} / P_{amb}) \qquad \textbf{Eq. B-13}$$

Where M_9 and a_9 are the corresponding Mach number and speed of sound for the exhaust gas expanded to ambient conditions at the nozzle pressure ratio, P_{t7}/P_{amb}.

$$F_{g9ideal} = \left[F_{g9} / (W_{g7} * \sqrt{T_{t7}})\right]_{ideal} W_{g7} * \sqrt{T_{t7}} \qquad \textbf{Eq. B-14}$$

$[F_{g9}/(W_{g7}*\sqrt{T_{t7}})]_{ideal}$ developed in **Eq. B-14** is called the 'ideal specific thrust parameter' and is an analytic function of isentropic exponent, gamma, gas constant and nozzle pressure ratio.

An alternate equivalent expression for gross thrust, based on full expansion, is

$$F_{g9ideal} = \left[F_{g9} / (A_8 * P_{amb})\right]_{ideal} * A_8 * P_{amb} \qquad \textbf{Eq. B-15}$$

$[Fg/(A_8*P_{amb}]_{ideal}$ in **Eq. B-15** is called the 'ideal thrust function' and is a second analytic function of gamma, gas constant and nozzle expansion ratio.

These definitions are used for both converging and converging/diverging (C/D) nozzles, both choked and unchoked. The definitions assume that the controlling area of the nozzle is at station 8. However, for an unchoked C/D nozzle, the controlling area shifts to station 9. Because of this shift, it is not unusual to calculate nozzle throat flow (discharge) coefficients greater than unity for unchoked C/D nozzles.

The expansion process in real nozzles is not isentropic. Losses occur relative to the ideal, because of real gas effects and other reasons listed below:

- Leakage;
- Cooling;
- Thermal expansion;
- Reverser links;
- Steps and gaps;
- Surface roughness and friction;
- Acoustic treatment;

- Gas mixing;
- Temperature profile;
- Pressure profile;
- Non-axial exit flow vector;
- Swirl;
- Over or under expansion;
- Shock losses; and
- Separation.

Because of these losses, the actual thrust is less than the ideal.

The nozzle gross thrust coefficient that quantifies this loss is defined as:

C_g is called the 'gross thrust coefficient' and can be expressed as

$$C_g = F_{g9_{actual}} / F_{g9_{ideal}} \qquad \textbf{Eq. B-16}$$

C_g can also be expressed as:

$$C_g = [F_g /(A_{8,actual} * P_{amb})]_{actual} /[F_g /(A_{8,ideal} * P_{amb})]_{ideal} \qquad \textbf{Eq. B-17}$$

Actual nozzle gross thrust can be evaluated using **Eq. B-18** if C_g is known.

$$F_{g9,actual} = [F_{g9} /(A_8 * P_{amb})]_{ideal} * C_g * A_8 * P_{amb} \qquad \textbf{Eq. B-18}$$

The actual gas flow will also be less in a real nozzle than in an ideal nozzle. The 'flow' coefficient, C_d, quantifies this loss**, Eq. B-19**.

$$\begin{aligned} C_d &= W_{g7,actual} / W_{g7,ideal} = A_{8,ideal} / A_{8,actual} \\ &= \left[W_{g7} * \sqrt{T_{t7}} /(A_8 * P_{t7})\right]_{actual} /\left[W_{g7} * \sqrt{T_{t7}} /(A_8 * P_{t7})\right]_{ideal} \end{aligned} \qquad \textbf{Eq. B-19}$$

The specific thrust coefficient, C_v is defined in **Eq. B-20**.

$$C_v = [F_{g9} /(W_{g7} * \sqrt{T_{t7}})]_{actual} /[F_{g9} /(W_{g7} * \sqrt{T_{t7}})]_{ideal} \qquad \textbf{Eq. B-20}$$

An alternate equivalent method to calculate gross thrust uses the 'specific thrust coefficient', C_v.

$$F_{g9} = [F_{g9} /(W_{g7} * \sqrt{T_{t7}})]_{ideal} * C_v * W_{g7} * \sqrt{T_{t7}} \qquad \textbf{Eq. B-21}$$

Actual gross thrust expressions defined by equations 8 and 11 are equivalent.

$$C_v = \frac{F_{g9,actual} /\left(W_{g7} * \sqrt{T_{t7}}\right)_{actual}}{F_{g9,ideal} /\left(W_{g7} * \sqrt{T_{t7}}\right)_{ideal}} = C_g * \frac{\left(W_{g7} * \sqrt{T_{t7}}\right)_{ideal}}{\left(W_{g7} * \sqrt{T_{t7}}\right)_{actual}} = \frac{C_g}{C_d}$$

The relationship between the coefficients is given by **Eq. B-22**.

$$C_g = C_v * C_d \qquad \textbf{Eq. B-22}$$

From the definition of C_g, **Eq. B-17**, the following correlation may be derived:

$$C_g = F_{g9,actual} / F_{g9,ideal} = [W_{g7} * V_9]_{actual} / [W_{g7} * V_9]_{ideal}$$
$$= C_d * [V_{9,actual} / V_{9,ideal}] \qquad \textbf{Eq. B-23}$$

Comparing **Eq. B-22** with **Eq. B-23**, shows that:

$$C_v = [V_{9actual} / V_{9ideal}] \qquad \textbf{Eq. B-24}$$

Therefore the specific thrust coefficient, C_v, is also the ratio of actual to ideal jet velocity and is commonly referred to as the 'velocity coefficient', **Eq. B-22**. This relationship is very useful to adjust to actual thrust in cycle-match computer simulations where the ideal jet velocity is calculated from energy deltas, **Eq. B-11**.

B.4.1.3 Thrust Definitions

A control volume for a single stream turbojet is shown in **Figure B.68**.

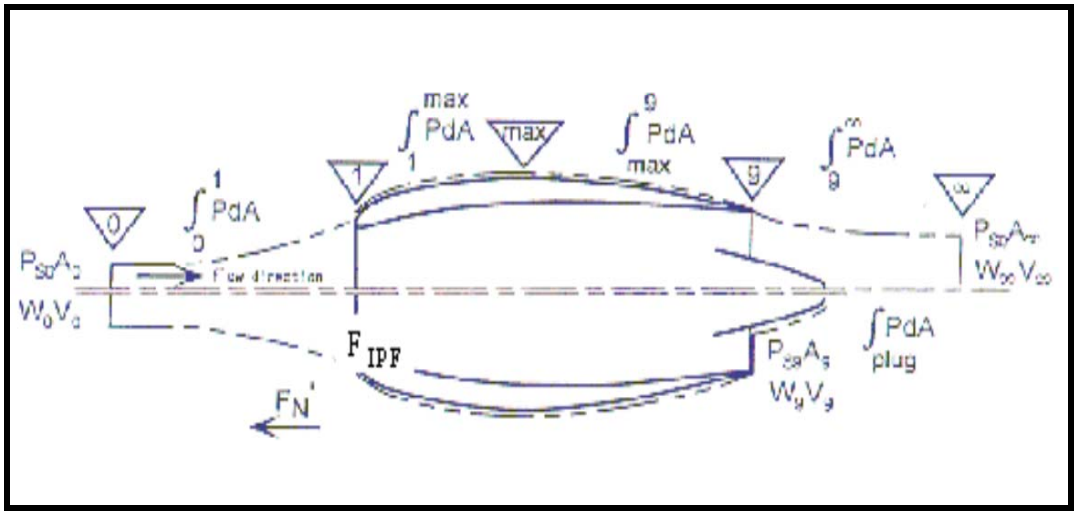

Figure B.68: Single Stream Control Volume for Thrust Definition.

The sum of the forces called 'Installed Propulsive Force', (F_{IPF}), acting on the single stream turbojet control volume shown in **Figure B.68** is

$$F_{IPF} = -A_0 P_{amb} - W_0 * V_0 + \int_0^1 P_s * dA + \int_1^{max} P_s * dA + \int_{max}^9 P_s * dA + A_9 * P_{s9} + W_9 * V_9 + \int_{plug} P_s * dA \qquad \textbf{Eq. B-25}$$

Friction has been set to zero to simplify the equation.

Algebraic adjustment, to refer pressure forces to ambient, yields:

$$F_{IPF} = -W_0 * V_0 + \int_0^1 (P_s - P_{amb}) * dA - \int_1^{max} (P_s - P_{amb}) * dA + \int_{max}^9 (P_s - P_{amb}) * dA$$

$$+ A_9 * (P_{s9} - P_{amb}) + W_9 * V_9 + \int_{plug} (P_s - P_{amb}) * dA \qquad \textbf{Eq. B-26}$$

The terms in **Eq. B-26** are also known as:

Ram Drag $\quad -W_0 * V_0$

Additive Drag $\quad \int_0^1 (P_s - P_{amb}) * dA$

Lip Suction $\quad \int_1^{max} (P_s - P_{amb}) * dA$

Exhaust Recompression Force ΔF_{EXH} $\quad \int_{max}^9 (P_s - P_{amb}) * dA$

Engine Gross Thrust F_{gg} $\quad A_9 * (P_{s9} - P_{amb}) + W_9 * V_9 + \int_{plug} (P_s - P_{amb}) * dA$

Spillage drag ΔF_{INL} is the sum of additive drag and lip suction.

$$F_{IPF} = \underbrace{\underbrace{-W_{a0} * V_0}_{\text{RAM DRAG}} + \underbrace{\int_0^1 (P_s - P_{amb}) dA}_{\text{ADDITIVE DRAG}} \underbrace{- \int_1^{max} (P_s - P_{amb}) dA}_{\text{LIP SUCTION}}}_{\text{INLET SPILLAGE DRAG}} + \underbrace{\int_{max}^9 (P_s - P_{amb}) dA}_{\text{EXHAUST RECOMPRESSION FORCE}}$$

$$\underbrace{+ A_9 (P_{s9} - P_{amb}) + W_9 * V_9 + \int_{plug} (P_s - P_{amb})\, dA}_{\text{ENGINE GROSS THRUST}} = F_{IPF} \qquad \textbf{Eq. B-27}$$

$$= F_{G9}$$

Eq. B-26 and **Eq. B-27** do not account for friction forces. Including friction uses the definition of Φ which describes the axial force component of the combined pressure and friction force on a surface in axisymmetric flow:

$$\Phi = \int_{surface} \left[(P_s - P_{amb}) + \tau * \cot\Theta \right] * dA \qquad \textbf{Eq. B-28}$$

where, Θ = angle between free stream flow direction and plane tangent to the surface element ds

τ = shear stress acting on surface element ds

dA = sinΘ ds = area of a surface element ds projected on a plane normal to the free stream flow direction

Rewriting **Eq. B-28** including friction forces leads to **Eq. B-29**:

$$F_{IPF} = -W_0 * V_0 + \int_0^1 (P_s - P_{amb}) * dA - \Phi_{inlet} + \Phi_{Exhaust} + A_9 * (P_{s9} - P_{amb}) + W_9 * V_9 + \Phi_{Plug} \qquad \textbf{Eq. B-29}$$

The installed propulsive force F_{IPF} acting on the pylon consists of engine net thrust reduced by nacelle drag and is equal to the airframe system drag, D_{afs}, **Eq. B-30**. SAE AIR 1703, **[B.53]**.

$$F_{IPF} = F_{g9} - W_0 * V_0 - \Delta F_{INL} - \Delta F_{EXH} = D_{afs} \qquad \textbf{Eq. B-30}$$

The powerplant net thrust, F_n, is defined in **Eq. B-31**.

$$F_{net} = F_{g9} - W_0 * V_0 \qquad \textbf{Eq. B-31}$$

Summarizing for the single stream turbojet:

$$F_{g9} = [W_9 * V_9]_{actual} - A_9 * (P_{s9} - P_{amb}) + \int_{plug} (P_s - P_{amb}) * dA \qquad \textbf{Eq. B-32}$$

$$= [F_{g9} / (A_8 * P_{amb})]_{ideal} * C_g * A_8 * P_{amb} \qquad \textbf{Eq. B-33}$$

$$= [F_{g9} / (W_{g9} * \sqrt{T_t})]_{ideal} * C_v * W_{g7} * \sqrt{T_{t7}} \qquad \textbf{Eq. B-34}$$

$$= W_{g7,actual} * V_{9,ideal} * C_v \qquad \textbf{Eq. B-35}$$

$$= W_{g7} * C_v * \sqrt{2 * (h_{t7} - h_{amb})} \qquad \textbf{Eq. B-36}$$

A representative plot of the nozzle coefficients is shown in **Figure B.69**.

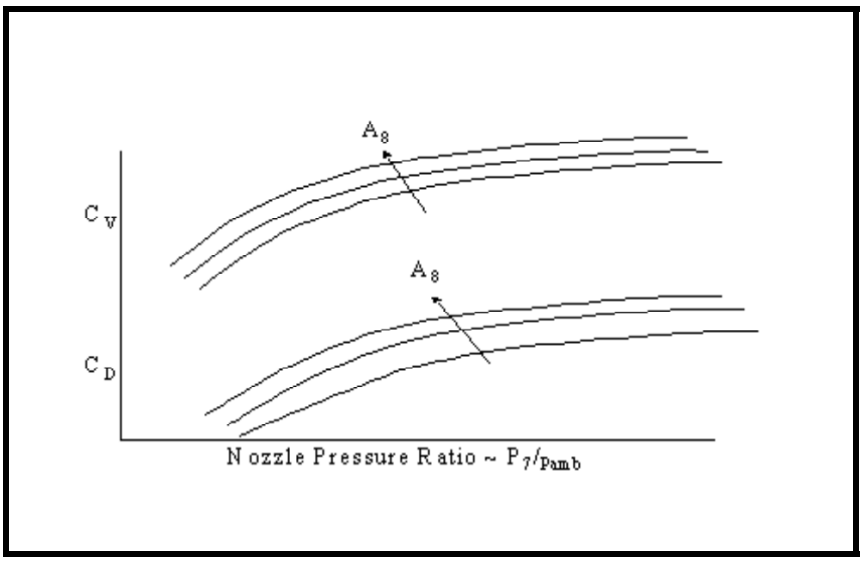

Figure B.69: Representative Thrust and Flow Coefficients vs. Nozzle Pressure Ratio.

B.4.1.4 Dual Stream Engine Configuration

The foregoing relationships can be extrapolated to dual-stream by-pass engines (see **Figure B.70**). Station numbers in the bypass stream are similar to those in the primary stream but increase by ten; e.g. station 9 primary becomes station 19 in the by-pass duct. Force accounting and thrust definitions are shown in **Eq. B-38**, the no friction case.

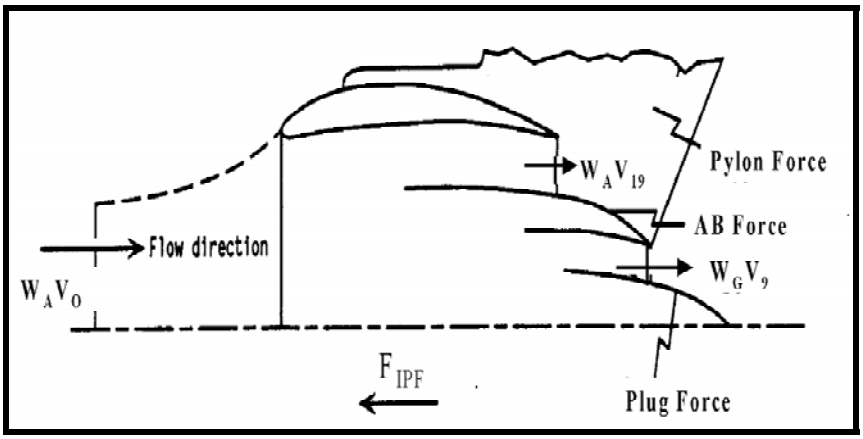

Figure B.70: Schematic of a Dual-Stream Bypass Engine.

$$F_{IPF} = \underbrace{-W_{a0} * V_0}_{\text{RAM DRAG}} + \underbrace{\int_0^1 (Ps - P_{amb})dA}_{\text{ADDITIVE DRAG}} \underbrace{- \int_1^{max} (P_s - P_{amb})dA}_{\text{LIP SUCTION}} + \underbrace{\int_{max}^9 (P_s - P_{amb})dA}_{\text{EXHAUST}}$$

RAM DRAG $= F_R$

INLET SPILLAGE DRAG $= \Delta F_{INL}$

EXHAUST RECOMPRESSION FORCE $= \Delta F_{IXH}$

$$\underbrace{+ A_9 (P_{s9}-P_{amb})+W_9*V_9 + \int_{\text{external plug}}(P_s-P_{amb})dA}_{\text{PRIMARY STREAM GROSS THRUST} = F_{G9}}$$

$$\underbrace{+ A_{19} (Ps_{19}-P_{amb}) + W_{19}*V_{19} + \int \text{core cowl } (P_s-P_{amb})dA}_{\text{BYPASS STREAM GROSS THRUST} = F_{G19}} \qquad \textbf{Eq. B-37}$$

$$F_{IPF} = -W_0 * V_0 + \int_0^1 (P_s - P_{amb}) * dA + \int_1^{max} (P_s - P_{amb}) * dA + \int_{max}^9 (P_s - P_{amb}) * dA$$

$$+ A_9 * (P_{s9} - P_{amb}) + W_9 * V_9 + \int_{plug} (P_s - P_{amb}) * dA \qquad \textbf{Eq. B-38}$$

$$+ A_{19} * (P_{s19} - P_{amb}) + W_{19} * V_{19} + \int_{core\,cowl} (P_s - P_{amb}) * dA$$

The terms in **Eq. B-38** are also known as:

Ram Drag	$-W_0 * V_0$
Additive Drag	$\int_0^1 (P_s - P_{amb}) * dA$
Lip Suction	$\int_1^{max} (P_s - P_{amb}) * dA$
Exhaust Recompression Force ΔF_{EXH}	$\int_{max}^9 (P_s - P_{amb}) * dA$
Primary Stream Gross Thrust F^*_{g9}	$A_9 * (P_{s9} - P_{amb}) + W_9 * V_9 + \int_{plug} (P_s - P_{amb}) * dA$
Bypass Stream Gross Thrust F^*_{g19}	$A_{19} * (P_{s19} - P_{amb}) + W_{19} * V_{19} + \int_{core\,cowl} (P_s - P_{amb}) * dA$

Spillage drag ΔF_{INL} is the sum of additive drag and lip suction.

If friction forces are included, then **Eq. B-38** becomes

$$F_{IPF} = -W_0 * V_0 + \int_0^1 (P_s - P_{amb}) * dA - \Phi_{inlet} + \Phi_{Exhaust} + \\ + A_9 * (P_{s9} - P_{amb}) + W_9 * V_9 + \Phi_{Plug} \\ + A_{19} * (P_{s19} - P_{amb}) + W_{19} * V_{19} + \Phi_{core\ cowl} \qquad \textbf{Eq. B-39}$$

Inlet and exhaust system forces defined in installed propulsive force equations (**Eq. B-25**, **Eq. B-30**, and **Eq. B-39**) have been accounted entirely as thrust terms to the propulsion system for bookkeeping. They are customarily apportioned partially to the propulsion system and partially to the airframe system depending on the scope of scale model tests done to define the thrust-drag bookkeeping system. Further details may be found in references SAE AIR 1703 **[B.53]** and SAE AIR 5020 **[B.54]**.

A PW4000 two-stream separate nozzle flow example is shown in **Figure B.71**.

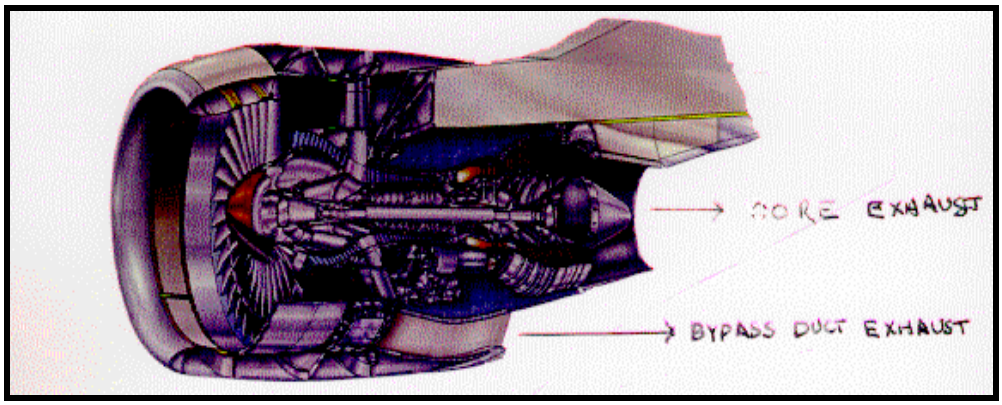

Figure B.71: PW4000 Example of Dual-Stream Exhaust System.

B.4.1.5 Mixed Flow Example

A schematic of a two-stream mixed flow powerplant is shown in **Figure B.72**. For this case, the primary and by-pass flows mix before they enter the nozzle. The mixing process in a particular configuration is further complicated if augmentation is also present. These processes must be precisely defined to produce average pressure, temperature, and gas constituents entering the nozzle charging station. Systematic errors in these calculations will be transferred to the nozzle and complicate understanding between measured (real) and ideal conditions. The mixed configuration is then handled the same as for a single stream engine. **Figure B.73** and **Figure B.74** show examples of mixed flow configurations. **Figure B.75** shows an example with an augmentor in the F100.

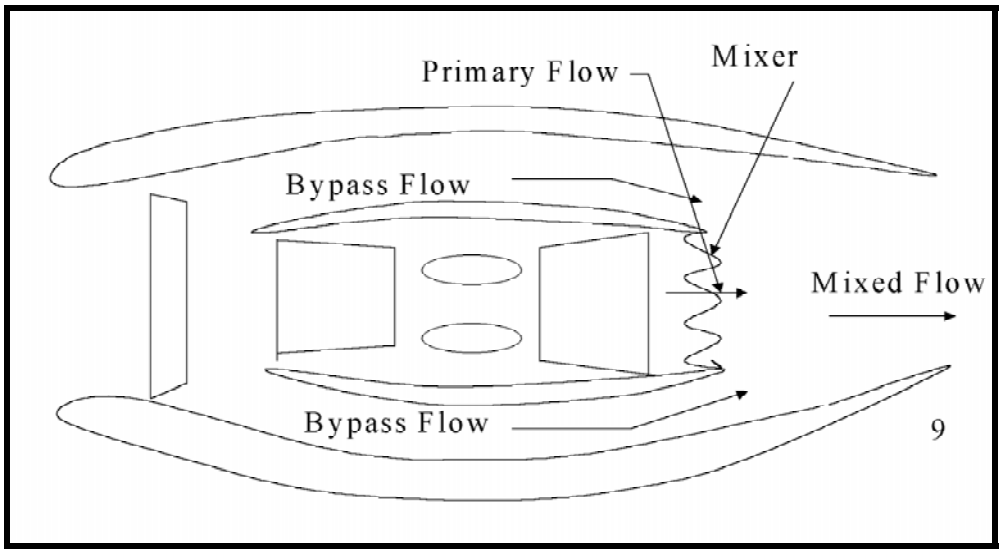

Figure B.72: Schematic of Mixed Flow Turbofan Engine.

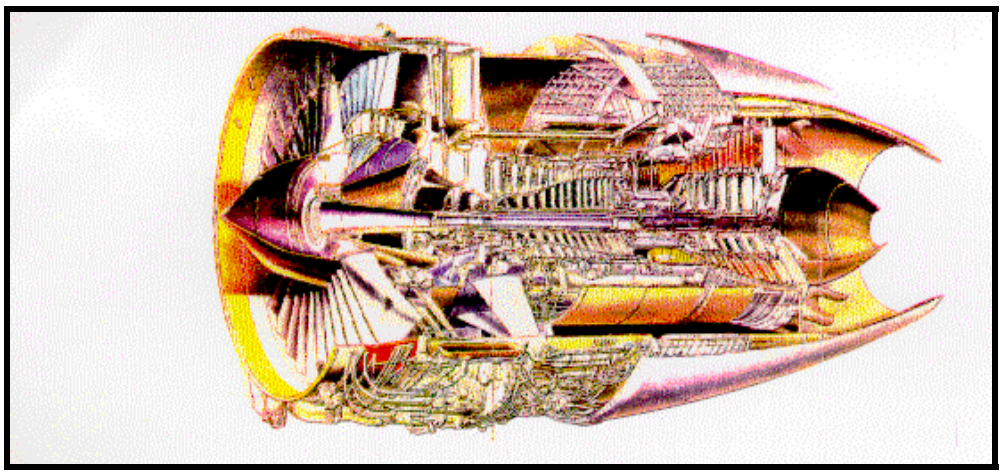

Figure B.73: Mixed Flow Configuration Example, PS-90P.

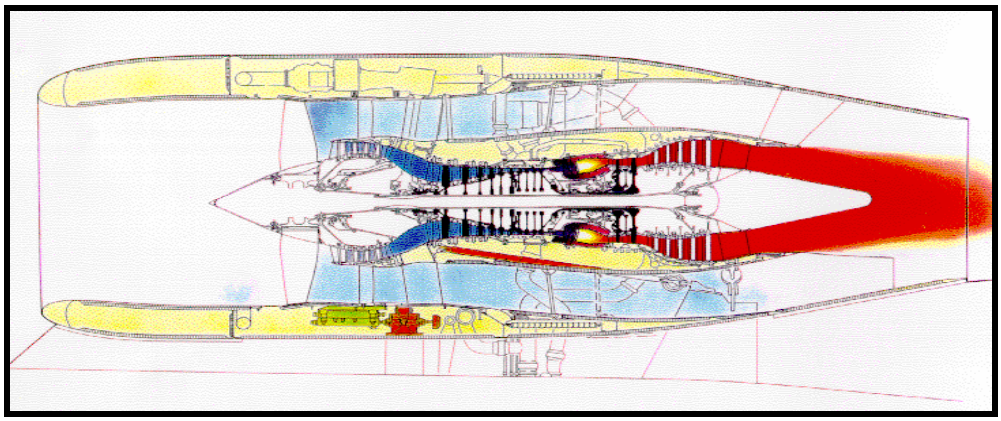

Figure B.74: Mixed Flow Example, V-2500.

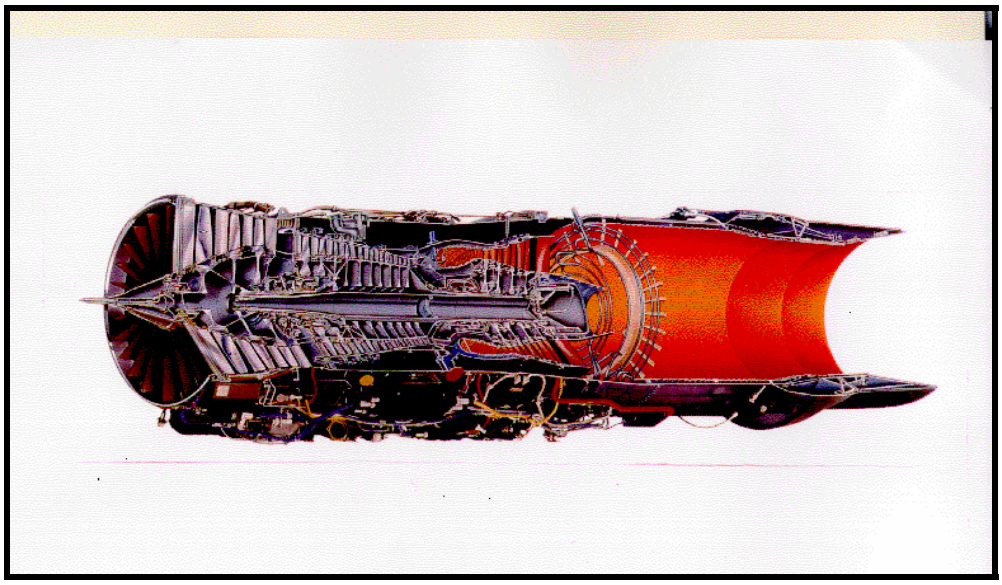

Figure B.75: Military Mixed Flow with Augmentor Example, PW-F-100.

Modern military aircraft need extensive cooling in the nozzle, which must be accounted for in the definition of ideal thrust and flow coefficients.

B.4.1.6 Evaluation of Nozzle Coefficients

Nozzle coefficients discussed in the foregoing paragraphs are measured using a full-scale engine testing in sea level and altitude test facilities, **Figure B.76** and **Figure B.77**. They are also measured using sub-scale models tested in rigs and wind tunnels. Methodology for doing this utilizes the same definitions and equations as discussed above. For evaluation testing, however, the thrust and airflow are measured and the nozzle coefficients calculated. The coefficients are then used in the engine simulation and aircraft in-flight thrust determination process. Methods and examples for determining nozzle coefficients are described in detail in references **[B.53**, **B.54** and **B.55]**.

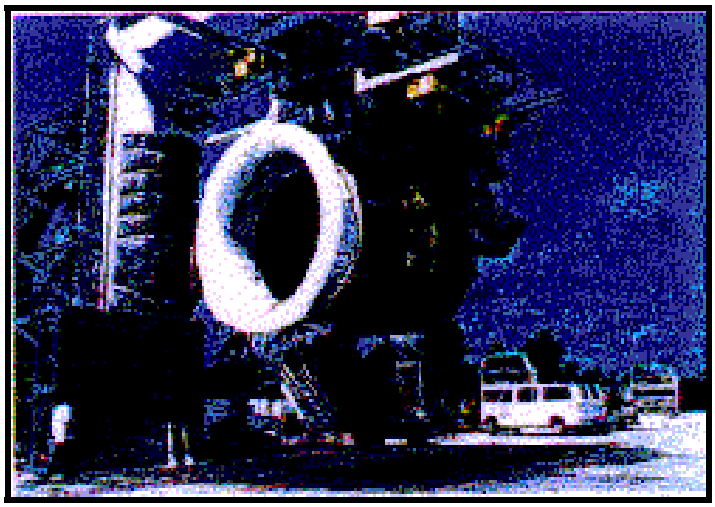

Figure B.76: Sea Level Engine Test Facility to Measure Thrust, Airflow and Nozzle Coefficients.

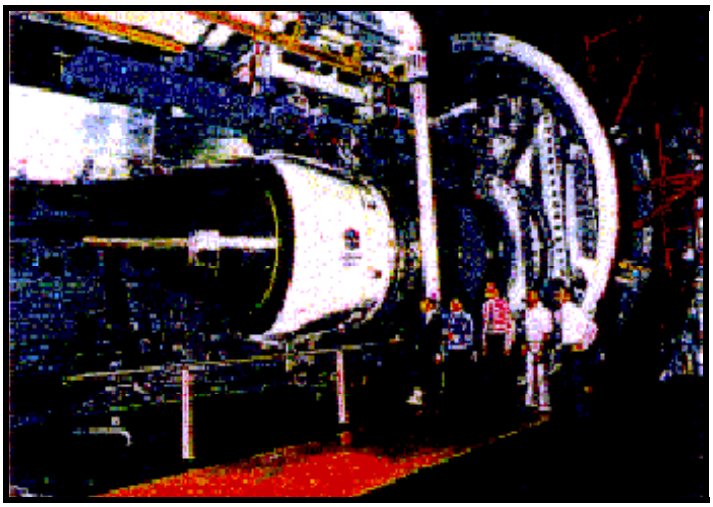

Figure B.77: Altitude Engine Test Facility to Measure Thrust, Airflow, and Nozzle Coefficients.

When measuring nozzle coefficients, in either the full-scale engine or sub-scale model, the test measurement and data analysis process must account for the differences between the test article and the flight engines, see the earlier list. Scale models must be corrected to (adjusted to full scale) and measurements in full-scale engines must be designed to provide, or be adjusted to, an average one-dimensional T7 or P7 value, for example. Any error in adjusting the measurements will be propagated to the nozzle coefficient through the calculation of ideal thrust and airflow, [B.55].

B.4.1.7 Variable Nozzle Benefits and Examples

The calculation for thrust and performance for all foregoing definitions are applicable for variable geometry nozzles. The nozzle coefficients are a function of both nozzle expansion ratio and jet area. The coefficients must be measured during full-scale engine or sub-scale model testing. The F-100 military-turbofan engine, shown in **Figure B.75**, provides an example of a variable geometry nozzle.

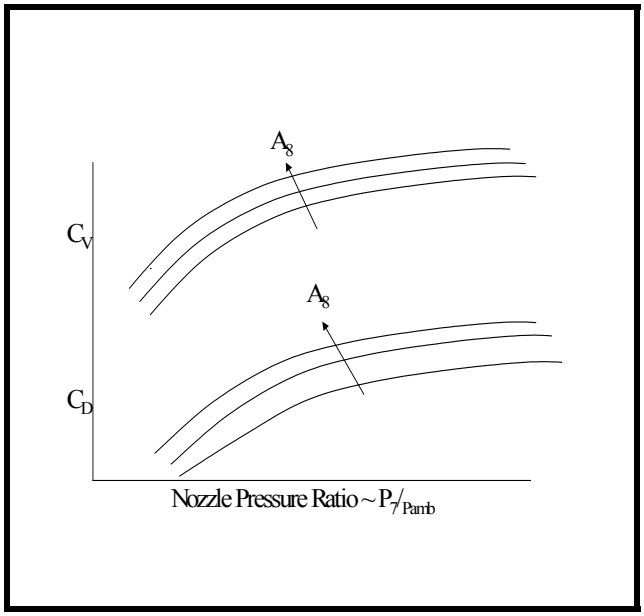

Figure B.78: Nozzle Coefficients with Variable Jet Nozzle Area.

A variable jet nozzle area is of benefit to aircraft gas turbine engines for three reasons:

1) **Operability** – The variable geometry nozzle is used to regulate the backpressure to the fan thereby maintaining stall free operation throughout the operating envelope. This is especially important for an engine with augmentation. The jet area must be increased when the afterburner is operating to maintain stall free fan operation. This accomplished with modern control systems by closed loop logic, where pressure ratio measured with high response transducers, is maintained by control of a variable nozzle area.

2) **Performance Optimization** – Since the nozzle throat meters the exit flow, it regulates the backpressure of the gas generator. Variation of the backpressure affects the cycle match and therefore powerplant thermal efficiency. The throat area also affects jet velocity, which impacts propulsive efficiency. A variable throat area may be optimized to provide best performance at a given flight condition. Generally, non-augmented engines require minimal or no throat area variation to optimize engine thrust. Augmented engines, however, require throat areas as much as 100% larger than the corresponding non-augmented area.

   Improved performance may also be obtained from a variable expansion ratio (exit area) convergent/divergent nozzle when a large operating range of nozzle pressure ratio (NPR) is required (most transonic/supersonic vehicles), see **Figure B.78**. The maximum thrust that the nozzle can produce for a given expansion ratio is obtained when the nozzle flow is fully expanded to ambient pressure at station 9 (see **Figure B.79**). The potential improvement for a convergent-divergent nozzle relative to a convergent nozzle is a function of nozzle pressure ratio. It may be calculated as the ratio of the ideal thrust functions and is shown in **Figure B.80**. The actual improvement for a convergent /divergent section will be reduced because of additional pressure loss. Inspection of **Figure B.78** shows that the convergent nozzle is better than the C/D nozzle at low nozzle-pressure ratios. The improvement for a C/D nozzle occurs when the C/D nozzle over-expansion losses are less than the convergent nozzle under-expansion losses.

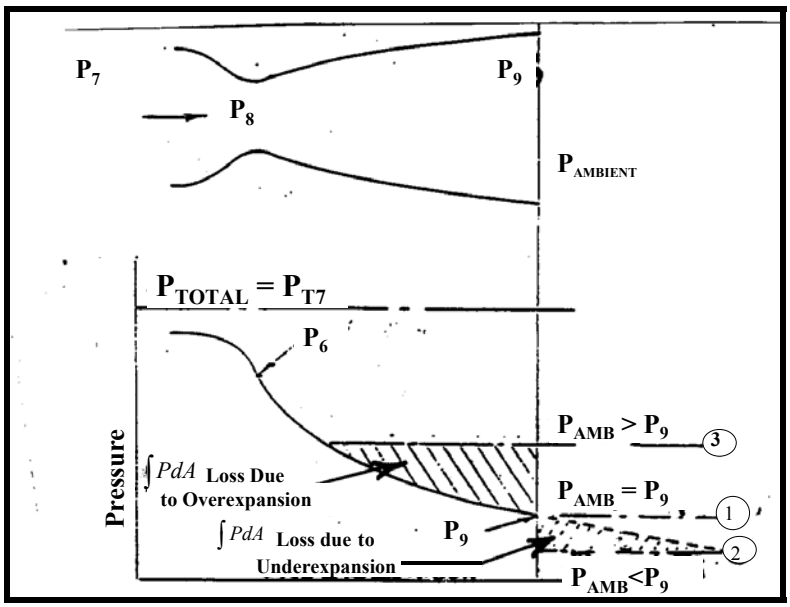

Figure B.79: Schematic Showing Pressure-Forces on C-D Divergent Section.

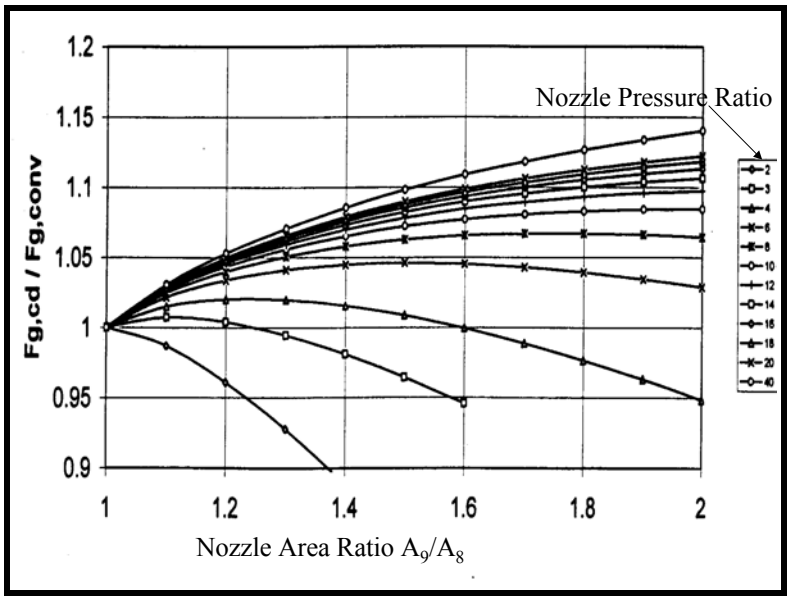

Figure B.80: Theoretical Improvement for C-D Relative to a Convergent Nozzle.

Commercial and transport engines are normally high bypass – low nozzle pressure ratio configurations to maximize propulsive efficiency and reduce fuel consumption. They do not have augmentors or operate over a large range of nozzle pressure ratio so variable nozzle areas are not required. The optimum nozzle is usually a convergent or fixed convergent/divergent with a small area ratio.

High thrust-to-weight ratio military engine configurations operate over a much wider range of nozzle pressure ratios and flight Mach numbers, and benefit greatly from variable-area-ratio nozzles.

3) **Air Vehicle Maneuverability** – The nozzle may be designed to turn the exhaust thrust vector to provide forces in the pitch and yaw directions as well as the normal thrust direction. This feature may be used by the pilot to direct additional pitch and yaw control to the aircraft. Special configurations may also provide lift control. An example is provided by the F-119-PW-100 shown in **Figure B.81**.

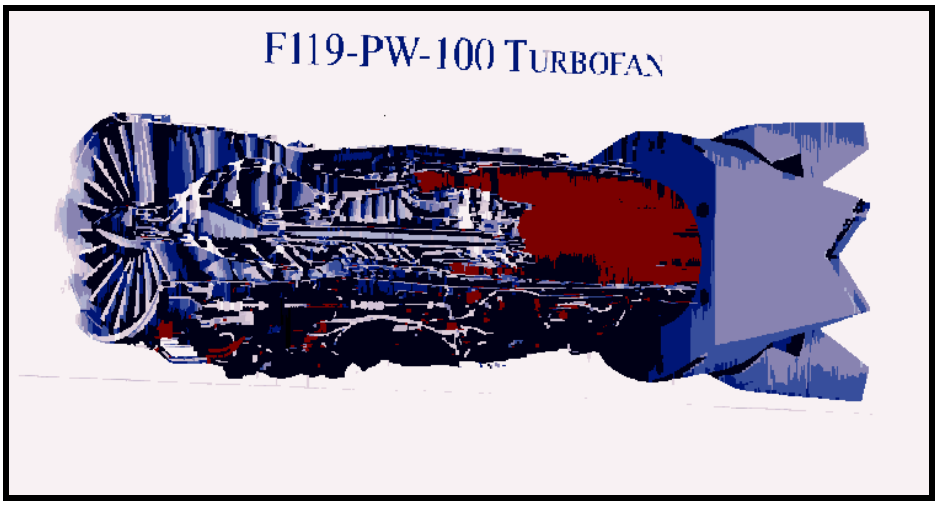

Figure B.81: F-119 Example.

B.4.2 Multi-Dimensional Considerations for Variable Area Nozzle Simulation

The foregoing discussions have been focused on a 'zero' dimensional simulation of the nozzle wherein all nozzle losses have been accounted for in the thrust and flow coefficients, based on an ideal flexible convergent/divergent nozzle. Simulation of an engine with variable geometry nozzles (which include all engines with reheat) may be sufficiently complicated as to require consideration of the true nozzle geometry, internal nozzle mechanical characteristics and aerothermodynamic processes for accurate results. For that case, a one (or greater) dimensional treatment of the nozzle is necessary to obtain reliable and robust calculation of the match points and efficiencies in the rotating machinery and augmentor. This applies to both predictive simulations and simulations used in the test data reduction process. These nozzle exhaust system requirements are similar to those which drive improvement from 'zero dimensional' compressor and turbine maps to higher dimensional 'physics based' FD representations of rotating components.

B.4.2.1 Multi-Dimensional Representation of Convergent Nozzles

B.4.2.1.1 Flow

The effective area of the nozzle is the product of the geometric area and the discharge flow coefficient, A_8C_d, as defined by **Eq. B-19** referenced to station 8, (nozzle exit and throat). The magnitude of C_{d8} depends on the nozzle pressure ratio, P_7/P_{amb}, and the nozzle design features, e.g. relative petal length (L/D), and petal angle, α. **Figure B.82**. For the case where the pressure loss between Stations 7 and 8 is small then P_7/P_{amb} is approximately equal to P_8/P_{amb}. The development below is based on this assumption.

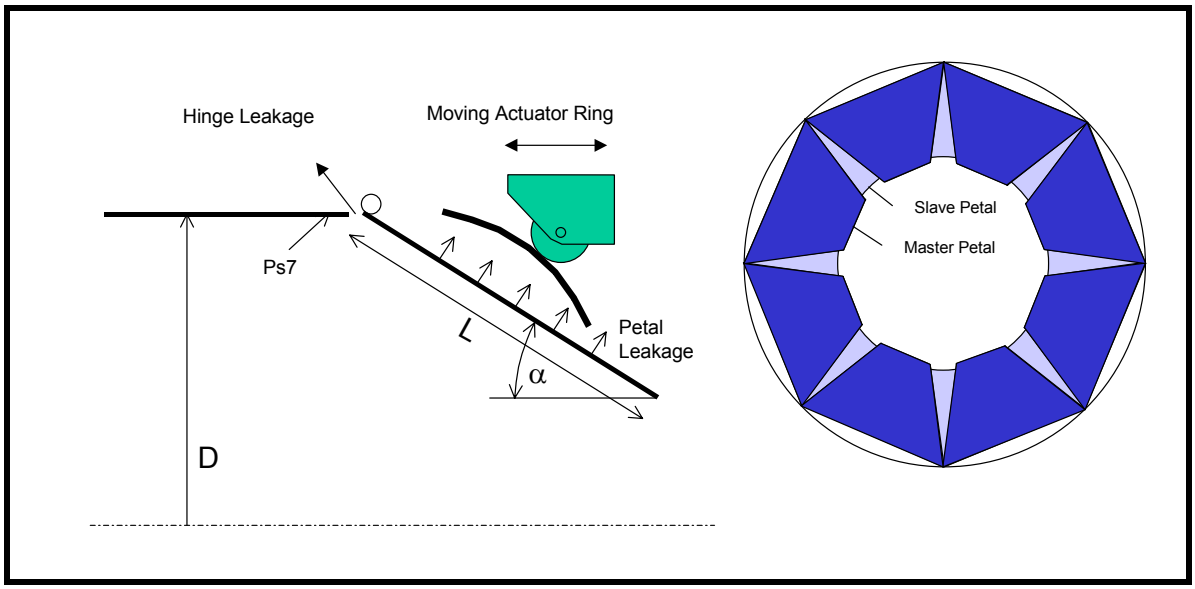

Figure B.82: Schematic of Variable Convergent Nozzle.

Note that in the text below, the total pressures and temperatures are designated without the subscript, t.

The flow at the nozzle throat W_8 may be calculated from P_8/P_{amb}, T_8 and A_8 from the formulae for isentropic flow.

B.4.2.1.2 Engine Test Analysis Method

Design to calculate nozzle exit area, A_8, from other measured parameters and sub-scale model correlations:

- Calculate T_8 from measured W_2, W_f, overboard leakage, and main burner efficiency utilizing conservation of energy considerations. This calculation utilizes an iteration which begins with an initial value for petal angle (α) (see **Figure B.82**).
- P_7 and P_8 are determined from sub-scale model correlations of $P_7/P_{s7} = f(\alpha)$ and $P_{s7}/P_{s7wall} = f(\alpha)$.
- $A_8 * C_{d8}$ is then calculated from W_8, T_8, and P_8.
- Actual A_8 is calculated from Step 3 and sub-scale model correlation of $C_d = f(P_7/P_{amb}, \alpha)$.
- Solve (iterate) till A_8 and petal angle,(α), are consistent.

B.4.2.1.3 Simulation and Measurement Validation Criteria

The calculated and measured nozzle jet areas A_8 are compared. The difference can be used to 'calibrate' the nozzle jet area measurement process. If the difference is large and unexpected then a re-evaluation of the simulation and measurement process should be undertaken. A detailed uncertainty analysis should be available to assist in evaluating the result, Ref. SAE Aerospace Information Report 1678, **[B.55]**.

B.4.2.1.4 Scale Model Basis for Flow and Thrust Coefficient Definition

For a given design the discharge flow coefficient may be measured as a function of nozzle pressure ratio and petal angle during sub-scale model tests encompassing the full range of pressure ratio and petal angle. Good practice requires that model nozzles be made of one piece to preclude leakage during the tests. Furthermore, it is good practice to measure $P_{s7,wall}$ upstream of the petal hinge to establish the correlation, $P_{s7}/P_{s7,wall}$ to be used to determine Ps_7 from measured $P_{s7,wall}$ during full scale test analysis.

B.4.2.1.5 Nozzle Leakage Considerations

To calculate airflow at the nozzle charging station, it is necessary to account for flow path and nozzle leakage. Proper accounting requires accurate inlet airflow, fuel flow and main burner efficiency correlation which must be determined/calibrated from dry engine test results over the full range of nozzle inlet conditions.

For the full scale variable nozzle there will be some leakage at the hinge of the petals as well as at the intersection of adjacent petals between the hinge and the throat, **Figure B.82**. The analytical model must account for this leakage in order to obtain consistency between the scale model and full scale flow and thrust coefficients, C_d and C_g . Further discussion of the thrust and thrust coefficients is contained in the next section.

The leakage at the hinge can be calculated from the pressure ratio across the hinge, Ps_7/P_{amb} and the effective area of the leakage path. Along the petals between the hinge and the throat, there is a straight-line contact between the 'master' (outer) and 'slave' (inner) petals. The effective leakage gap height and area decreases with increasing pressure difference, $P_s - P_{amb}$. Since the static pressure inside the nozzle varies significantly along the petals, it is recommended to subdivide the leakage calculation into several parts.

B.4.2.1.6 Nozzle Area Measurement Considerations

Accurate measurement of a variable nozzle throat area is a difficult task. One method utilizes a Moving Actuator Ring (MAR). It is positioned by hydraulics or air motor, and has rollers running on curved tracks which are mounted on master petals. Measurement of the axial position of the MAR is used with a correlation to determine actual nozzle throat area, A_8. This measurement is very difficult to perform because the position sensor is located in a very harsh environment. Moreover, if there is only 1 MAR sensor, any misalignment of the MAR relative to the nozzle centerline will result in additional

measurement error. The widely varying mechanical loads and metal temperatures are elements causing an additional nozzle-area measurement error. A large resulting error in nozzle-area will propagate to unacceptably large uncertainties in calculated and measured airflow and thrust.

B.4.2.1.7 Nozzle Position Sensor Calibration

The nozzle position sensor requires calibration, which can be done utilizing the full-scale static pressure at the nozzle charging station (inlet) P_{s7wall}, and the P_{s7wall}/Pam and Cd from sub-scale model tests (or alternatively CFD calculations).

B.4.2.1.8 Thrust

The gross thrust of a convergent nozzle may be defined as

$$Fg_{8\ actual} = A_8\,(P_{s8}-P_0)+W_8*V_{8,ideal}*C_{v8} \qquad \textbf{Eq. B-40}$$

This equation is consistent with the thrust-accounting control volume for a single stream convergent exhaust system shown in **Figure B.67** and **Eq. B-25** adjusted to a convergent throat at station 8. The nozzle coefficient is defined here as the ratio of the actual to the ideal jet velocity of a convergent nozzle.

For the example of **Figure B.82**, the velocity coefficient, C_{v8}, is a function of nozzle design, the petal angle, the nozzle pressure ratio, and many other loss causing effects.

B.4.2.1.9 Mixing

Incomplete mixing of the gas streams in a turbofan engine will result in a thrust loss, which is properly assessed against the mixer, not the nozzle. This loss has been accounted as a 'mixer efficiency', **Eq. B-41**.

$$\eta_{\ mix} = (F_{g8}-F_{g8,unmixed})/(F_{g8\ fully\ mixed} - F_{g8\ unmixed}) \qquad \textbf{Eq. B-41}$$

The application of $\eta_{\ mix}$ requires the calculation of the fully mixed and unmixed thrust, i.e. separate expansion of the cold and hot streams. This makes the nozzle calculation complex because one must now define two nozzle entry stations: one for the hot and one for the cold expansion. In addition, the nozzle area must be apportioned for the hot and cold streams. Inconsistencies in throat Mach number for the separate streams also arise due to gas property effects. When different turbofan cycles or different mixers are to be compared, the concept of partial mixing is very useful, both to describe and to help understand effects on thrust. On an existing engine, although it is much simpler to book-keep the effects of non-uniform temperature and pressure to the nozzle thrust coefficient, it must be recognized that a significant contributor to the level of the thrust coefficient derives from an effect generated outside the nozzle.

B.4.2.1.10 Clear Definition of Ideal Thrust Required

It is important in any particular program to avoid ambiguity by clear understanding and agreement at the outset among all stakeholders regarding the definition of nozzle ideal thrust.

A common definition for the ideal expansion process is to ambient pressure in an ideal convergent/ divergent nozzle. Other definitions are possible depending on how the averaging calculations at the nozzle charging station, the flow mixing calculations, bleed and leakage calculations, and multi-stream evaluation are handled. The definitions may become complicated especially as the complexity (dimensionality) of nozzle model increases.

The actual thrust for an existing engine will not change regardless of how the ideal nozzle coefficient is defined. Understanding of the components including the nozzle can be improved by more complex 'physics based' nozzle component representations.

B.4.2.2 Multi-Dimensional Representation of Convergent-Divergent Nozzles

The addition of a divergent section to the exhaust nozzle increases the usefulness and in some cases need for one plus dimensional analysis and simulation of the system. For the example discussed here, **Figure B.83**, a precise description of the geometry for all positions is necessary. The primary petal angle is an important parameter; the metal temperature of the primary petal is also important. Thermal expansion of the primary master petals causes an increase in A_9. This happens because the length of the strut which holds the divergent petals remains unchanged because its temperature does not change, **Figure B.83b**. The multi-dimensional geometry model is necessary to properly evaluate the values for the throat area, A_8 and the exit area, A_9, and thus nozzle area ratio A_9/A_8 for all operating conditions.

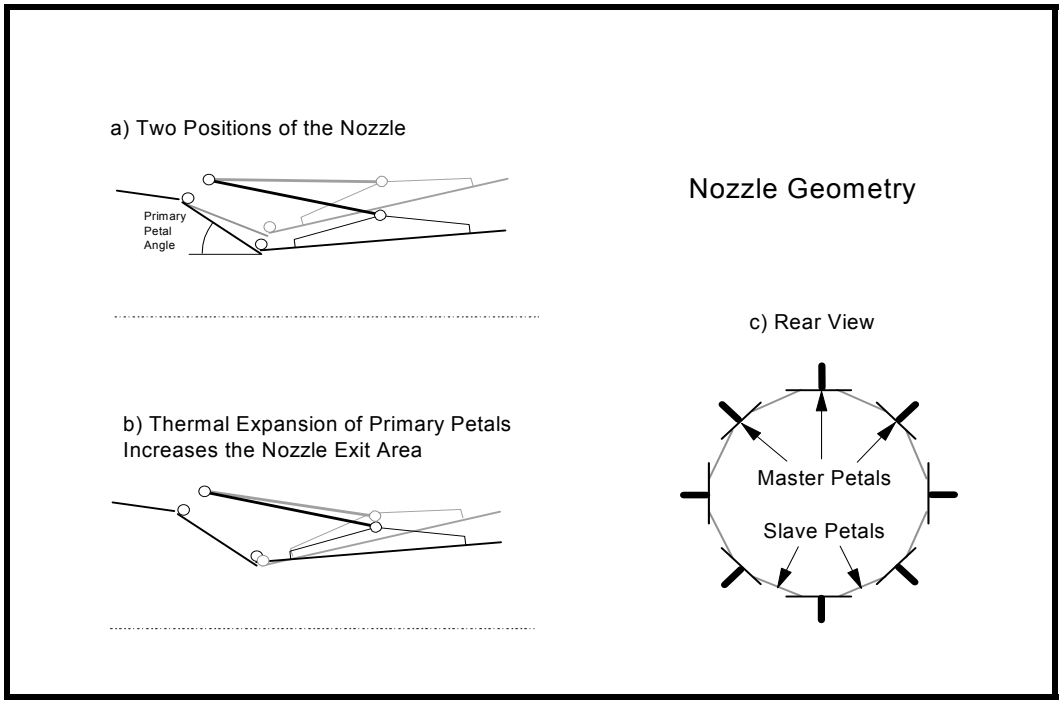

Figure B.83: Geometry of Variable Convergent Divergent Nozzle.

Once the geometry is determined from the mathematical model, the static pressure along the nozzle inside surface can be calculated. In the convergent section, the static pressure along the wall can be calculated from the local area ratio A_{local}/A_7 and one-dimensional isentropic relationships. In the divergent section, the wall pressures can be determined from isentropic relationships with corrections, Rebolo et al. (1993) **[B.56]**.

B.4.2.2.1 Flow

The flow characteristics of a convergent/divergent nozzle can be described according to **Eq. B-42**.

$$C_d = W_{g-actual} / W_{g-ideal} = A_{8-ideal} / A_{8-actual}$$
$$= \left[W_g * \sqrt{T_t} / (A * Pt)\right]_{actual} / \left[W_g * \sqrt{T_t} / (A * Pt)\right]_{ideal} \qquad \textbf{Eq. B-42}$$

In order for the definitions of equation 9 to be valid, flows, temperatures and pressures must be consistently calculated at Station 8.

When the ideal flow, $W_{g8,ideal,}$ is calculated from W_8-W_{leak}, the total temperature T_8 and pressure ratio P_8/P_{amb}, a flow coefficient calculated from $C_d = W_{act}/W_{ideal}$ will provide coefficients greater than 1.0 at low pressure ratios. Proper physics in the computation of the coefficient will always result in a value less than 1.0. More realistic computation, of the flow-conditions at the throat, is no additional burden for this simulation because it is needed for the calculation of forces and nozzle leakage.

At sufficiently high nozzle pressure ratios (when the flow is under-expanded or only slightly over-expanded) the discharge flow coefficient can be closely approximated as a function of petal angle (α) only, **Eq. B-43**.

$$C_d = -1.25*10^{-5} * \alpha^2 - 0.001425 * \alpha + 0.995 \qquad \textbf{Eq. B-43}$$

When the pressure ratio is low, the flow in the divergent section of the nozzle detaches and C_d becomes a function of both α and P_8/P_{amb}.

The nozzle exit discharge flow coefficient C_{D9} is very nearly constant and has a value of ~ 0.995, for under expanded operation and becomes a function of pressure ratio and area for low P_8/P_{amb}.

B.4.2.2.2 Leakage Considerations

The leakage through the hinges and between the master and slave petals depends on the difference between the pressures within and around the nozzle. A description of how to evaluate the pressure distribution inside the convergent part of the nozzle can be found in the foregoing description.

As long as the pressure outside the nozzle is lower than inside, the effect of leakage can be directly evaluated. However, there are many operating conditions, sea level static for example, for which static pressure in the throat and divergent sections is lower than pressure outside, and air is consequently sucked in.

During engine testing of the EJ200 (a mixed flow turbofan engine), for example, one could easily identify when the pressure inside the divergent nozzle section is lower than outside. Inspection of **Figure B.84** shows that the slave petals are sucked in and a gap opens between the master and the slave petals.

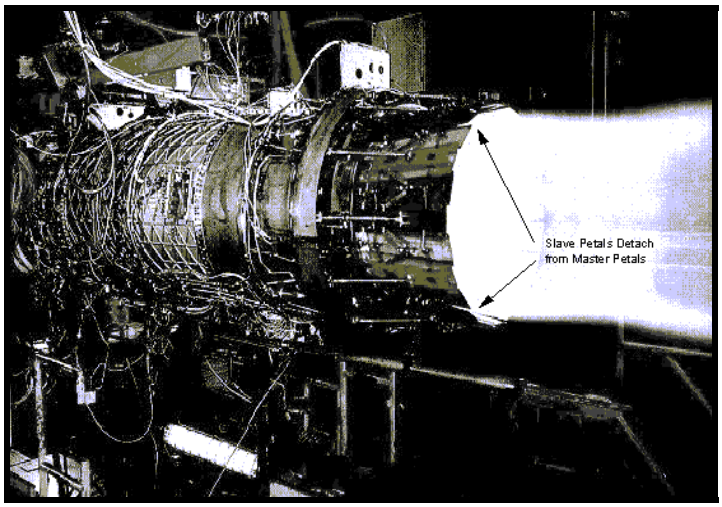

Figure B.84: Over-Expanded Operation of a Convergent-Divergent Nozzle.

B.4.2.2.3 Thrust

A nozzle located downstream of a mixed flow turbofan gas-generator will have non-uniform pressure and temperature profiles at the nozzle inlet Station 7. It is possible to model the thrust loss caused by the non-uniform flow conditions by using the mixing efficiency approach described in the previous convergent nozzle discussion. However, the calculation process of the unmixed flow conditions in the convergent/ divergent nozzle becomes unnecessary complex. It is much better to base the calculation of the ideal nozzle performance on the fully mixed flow and properties at the nozzle entry charging station 7. Losses due to incomplete mixing can be addressed by the nozzle thrust coefficient.

B.4.2.2.4 Definition of Thrust Coefficient

The performance of a convergent/divergent can be characterized by the thrust coefficient C_g defined in **Eq. B-44**, repeated.

$$C_g = F_{g9_{actual}} / F_{g9_{ideal}} \qquad \textbf{Eq. B-44}$$

The thrust coefficient C_g can also be calculated consistent with the flow coefficient.

$$C_g = [F_g /(A_8 * P_{am})]_{actual} /[F_g /(A_8 * P_{am})]_{ideal} \qquad \textbf{Eq. B-45}$$

The gross thrust coefficient compares the actual thrust (measured) with an ideal definition of thrust produced by an ideal expansion to ambient pressure. C_g will also be a function of nozzle throat to exit area ratio, A_8/A_9.

B.4.2.2.5 All Stake-Holders Should be Aware of Thrust and Coefficient Definitions

The definition of ideal C_g based fully expanded variable geometry results in a lower numerical value for the calculated real nozzle system. This is because it is not possible for the nozzle to fully expand to ambient pressures at off-design conditions. Several experimenters have opted to define the ideal coefficient as the maximum achievable for a given hardware geometry. This has the advantage, that the thrust respectively velocity coefficient becomes a true measure of nozzle flow quality. The coefficient defined in such a way is independent from nozzle area ratio A_9/A_8, pressure ratio P_8/P_{amb} and nozzle leakage provided a sufficiently detailed mathematical model of the nozzle is employed.

Although other definitions for ideal thrust are possible, they are generally non-standard and should only be used for sound reasons, related to a particular geometry. All parties should fully understand and use the definitions including nozzle designers, sub-scale modelers, analytical simulation engineers, test analysis engineers, technical manager/system evaluators, customers and sometimes suppliers.

An alternate formulation of the thrust equation reported in the literature is shown in **Eq. B-46**.

$$Fg_{9\ actual} = A_9 (P_{s9}-P_{amb})+W_9*V_{9\ ideal} * C^*_{v9} * C_a * C_f \qquad \textbf{Eq. B-46}$$

In this formulation C_a is the angularity coefficient from the Reference **[B.57]** Fig. 5 – 12 that accounts for the losses due to non-axial exit flow velocity. The coefficient C_f from the Reference **[B.57]** Fig. 5.13 accounts for the effect of boundary layer momentum loss caused by friction in the nozzle. Both these coefficients depend on the nozzle area and the primary petal angle. The velocity coefficient C^*_{v9} is held to represent a nozzle efficiency. The advantage to define the coefficient is this way is discussed in the next section.

Note that in the turbofan engine this coefficient accounts mainly for losses due to incomplete mixing of the core flow, bypass flow and nozzle cooling air and is not the same as the velocity coefficient C_v as defined earlier.

B.4.2.3 Special Considerations for Multi-Dimensional Modeling and Simulation of Nozzles

B.4.2.3.1 High Nozzle-Pressure Ratios

When the nozzle pressure is large, and the flow is under-expanded, the flow tends to remain attached to the nozzle 'wall' and follow the contours of the divergent petals. Using a nozzle analytical model based on geometry provides excellent correlation with test results. An example of velocity coefficient C^*_{v9} test results for a turbofan engine measured over a wide range of engine ratings, altitude and Mach number flight conditions is shown in **Figure B.85**. When the nozzle pressure ratio is greater than 3.5, the velocity coefficient has a unique value of 0.99. The 1% reduction from the ideal value of 1.0 is caused by incomplete mixing of the core and bypass gas streams, and losses due to nozzle cooling.

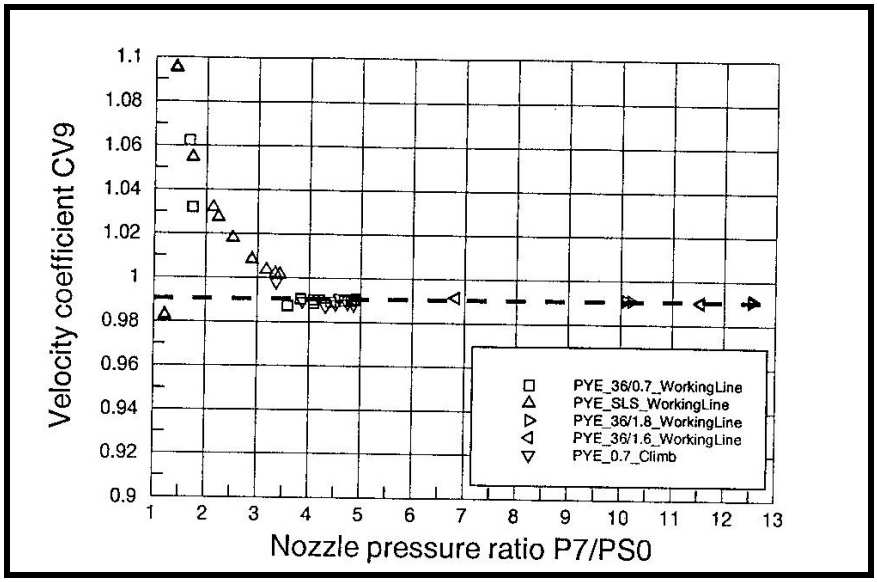

Figure B.85: Test Result for Nozzle Velocity Coefficient Using 1-D Geometry Model.

For high-pressure ratio nozzles with significant cooling flow, the assumptions in treating the cooling flow can change the nozzle thrust coefficient. Typically cooling air entering upstream of the nozzle throat is treated as part of the primary flow, even if the injection location does not allow for effective mixing and the momentum of the flow is not considered. Cooling flow on the expansion flaps is generally not included in the thrust calculation. As cooling becomes more significant, the modeler may choose to treat these cooling flows as separate streams with their own thrust contribution and thrust coefficient, rather than try to develop a thrust coefficient representation to cover the nozzle behavior over a wide range of cooling flow and nozzle pressure ratio levels.

B.4.2.3.2 Low Nozzle-Pressure Ratios

When the nozzle pressure ratio is less than 3.5 to 4.0 the C^*_{v9} increases rapidly as nozzle pressure-ratio decreases, **Figure B.85**. This occurs because the calculated force on the struts holding the secondary petals becomes negative. In turn, this is because the pressure inside the divergent section is lower than ambient causing the forces on the divergent master petals to exert a "pull" on the struts, see **Figure B.86**. Under

these conditions, the slave petals detach from the master petals as can be clearly seen in **Figure B.84**. Airflows from outside to inside the nozzle, which reduces the effective nozzle exit area ratio A_9/A_8. This results in a better match of the effective nozzle area ratio at the low-pressure ratio condition and the nozzle appears to perform better than calculated with the standard assumption, $C_d = 0.995$.

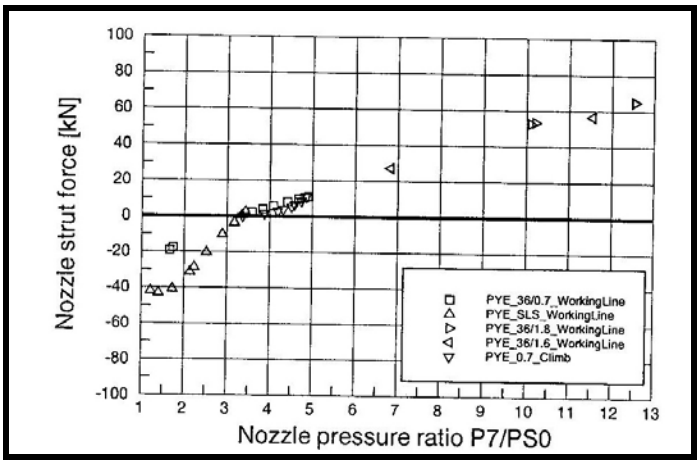

Figure B.86: Nozzle Strut Forces; Positive when Struts are Compressed.

This point is illustrated in **Figure B.87** in which the calculated thrust coefficient, (C_g) is plotted as a function of nozzle pressure ratio for lines of constant nozzle area ratio. For example, when the flow follows the nozzle geometry at a pressure ratio of 2.4 and nozzle area ratio of 1.35 the ideal thrust coefficient is 0.95. If the flow were detached in the divergent section leading to an effective area ratio of only 1.2, the gross thrust would improve by 3.0%.

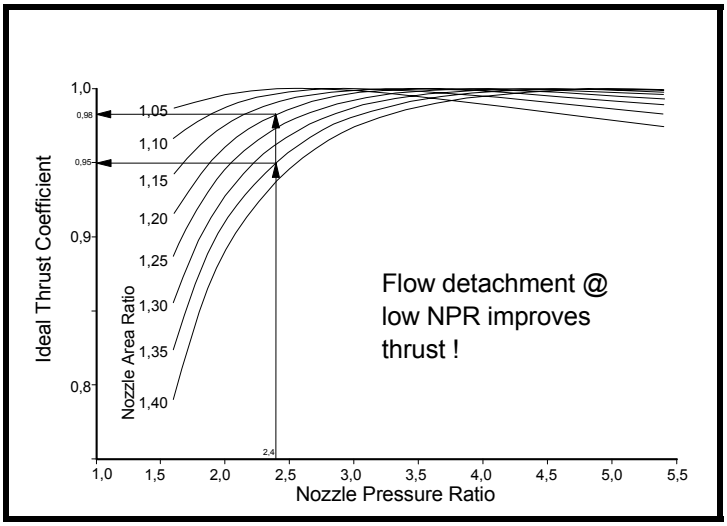

Figure B.87: Thrust Gain Due to Flow Detachment at Low Nozzle Pressure Ratios.

B.4.2.3.3 Operation at Windmilling Conditions (ISABAE Paper Excerpt on Windmilling)

For separate flow high bypass engines at very low nozzle pressure ratios and extreme bypass ratios (windmilling conditions), the assumption of independent expansion of the two exhaust nozzles begins to break down and the thrust coefficient characteristics begin to vary significantly. Mixed flow nozzles thrust

coefficient characteristics tend to be less sensitive since they have already captured this effect in the mixing calculation. To allow continued use of the base nozzles thrust coefficient characteristic at windmilling conditions, a base drag term is often added for separate flow engines to approximate the thrust impact of the downstream mixing of the two streams. (ISABAE paper reference with chart on relative effect).

B.4.2.3.4 Partially Mixed Nozzles

Most low to medium bypass turbofan engines incorporate mixed flow nozzles. Very high-bypass ratio engines are typically separate flow. Use of mixed flow nozzles on high bypass engines often results in behavior that does not match well with the results from a fully mixed nozzle analysis. Rather than trying to capture this behavior in a unique thrust coefficient characteristic, a partially mixed nozzle analysis may be used. In this case, the results from a separate flow and mixed flow nozzle analysis are used and the results are interpolated using the two limiting cases.

B.4.2.3.5 Useful Correlation from Test Results

Improved understanding of the characteristics of the divergent section of the nozzle may be achieved from analysis of correlation of the ratio of static pressure measured at the nozzle exit wall to P_{amb}, $P_{s9,wall}/P_{amb}$. vs. nozzle pressure ratio, P_7/P_{amb}, **Figure B.88**. Test results for a turbofan engine are plotted in **Figure B.89**. Also plotted in the figure are of constant divergent section area ratio, A_9/A_8, based on one-dimensional analysis with $C_{d8} = C_{d9} = 1$. Note that the range of the constant-area-ratio lines extends well below 1.0. The lower limit of the measured pressures for this example is approximately 0.91.

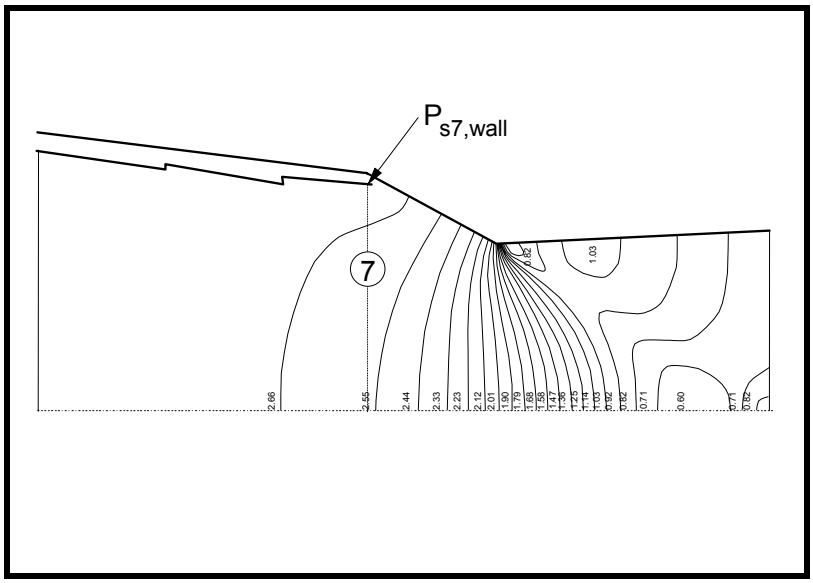

Figure B.88: Schematic of Divergent Nozzle Wall Section with Pressure Instrumentation Locations.

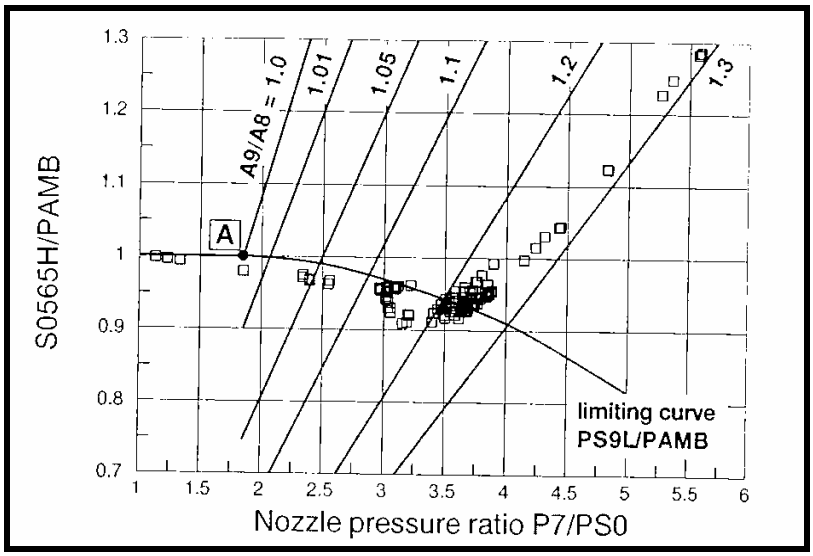

Figure B.89: Correlation of Static Pressure near the Nozzle Exit with Nozzle Pressure Ratio.

If one hypothesizes the requirement that the Nozzle throat area, A_8, always controls the flow, i.e. the effective nozzle area ratio, A_{e9}/A_{e8}, is always greater than 1, an empirical correlation to calculate nozzle exit discharge coefficient, C_{d9}, may be defined. In this example the nozzle operates much like a convergent nozzle and expands the flow to ambient pressure for nozzle pressure ratios below the sonic limit of ~1.8, (P_{s9wall}/P_{amb} = ~ 1.0. At nozzle pressure ratios above 1.8 the level of measured P_{s9wall}/P_{amb} trends lower. The curve labeled P_{s9L}/P_{amb} in **Figure B.89** is a best-fit curve through the measured data; it represents the lower limit of the P_{s9}/P_{amb} for the given nozzle. Lines of constant divergent nozzle area ratio calculated from one-dimensional considerations are also shown in the figure.

The limiting curve of $P_{s9L}/P_{amb} = f\,(P_7/P_{amb})$ is used in the simulation in the determination of C_{d9} as follows:

1) Assume $C_{d9} = 0.995$ and calculate a tentative value for P_{s9}.
2) If P_{s9}/P_{amb} is greater than the limiting value from **Figure B.89**, then $C_{d9} = 0.995$.
3) If P_{s9}/P_{amb} is lower than P_{s9L}/P_{amb} In **Figure B.89**, then use the theoretical $(A_9/A_8)_{eff}$ from the limiting curve.
4) Calculate the required C_{d9}, and recalculate the exit flow conditions.

This procedure requires that the static pressure at the nozzle exit never be lower than that consistent with the limiting curve; therefore the simulation calculations may be slightly different than the measured values for C_d. The method provided good consistency of the thrust coefficient, C^*_{v9}, however, and therefore provides a useful correlation for characterizing nozzle thrust performance, **Figure B.90**.

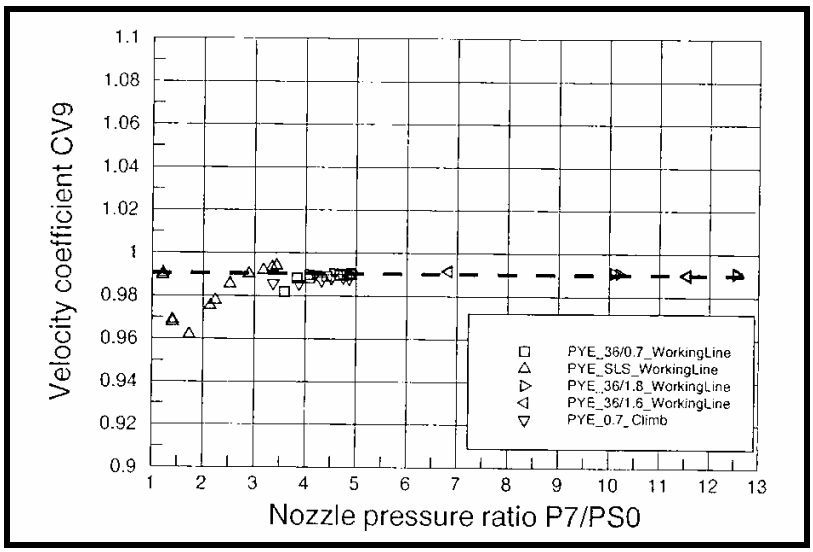

Figure B.90: Adjusted Correlation for Nozzle Velocity Coefficient.

B.5 INLET SYSTEMS

The inlet aerodynamic design characteristics of the powerplant have significant effects on the engine performance and stability and are of vital concern to the engine designer. Inlets are designed to guide required engine flow into the front face of the engine with minimum loss and distortion. For sub-sonic flight velocity this generally means properly faired inlet surfaces to minimize flow separation. For supersonic flight velocity, the design must minimize losses due to formation of shock waves. In any case to assure engine stability, the inlet design must provide low flow distortion and, in the supersonic case, stable shock structures. The inlet design will also have important effects on overall flight vehicle drag.

The inlet functions as follows in the overall powerplant system:

- It accelerates or decelerates ambient air to the engine forward flange station to achieve the entering flow Mach number that will provide most efficient operation of the engine turbomachinery.
- It is part of the cycle compression process.
- It transforms the dynamic pressure generated by flight velocity to increased cycle static pressure.
- It produces total pressure loss in the outer bypass stream.
- It produces total pressure loss in inner core stream by means of spinner scrubbing.
- It affects distortion entering the engine.
- It affects noise generated by powerplant.
- It contains instrumentation required for power setting and engine control.
- It produces ‘spillage drag force’ due to non-isentropic effects.
- It produces additional air vehicle drag due to scrubbing and pressure forces generated by free stream flow over the external cowl.

Inlet drag and pressure loss should be faithfully modeled in the engine simulation to calculate accurate average total pressures for the core stream and the bypass stream at the fan inlet face. Clear definitions are required for thrust-drag bookkeeping.

B.5.1 Diffusion and Acceleration of Airflow into the Propulsion System

The inlet is designed to induct air into the powerplant with minimum loss at the aircraft design flight condition. For subsonic and low supersonic aircraft the design is usually a fixed inlet area with significant external diffusion and accompanying rise in static pressure, see **Figure B.91**. The energy contribution of the velocity of the airflow to the engine cycle is depicted in the H-S diagram shown in **Figure B.92**. A typical subsonic aircraft design condition would have the inlet area approximately 20% larger than the area of the entering stream tube far upstream of the engine where the flow which will enter the engine is unaffected by air vehicle velocity. The diffusion process from station 0 far upstream to station 1 at the inlet lip is very nearly isentropic at the design condition and the static pressure rise is an ideal function of the flight velocity, equation 22 and **Figure B.92**.

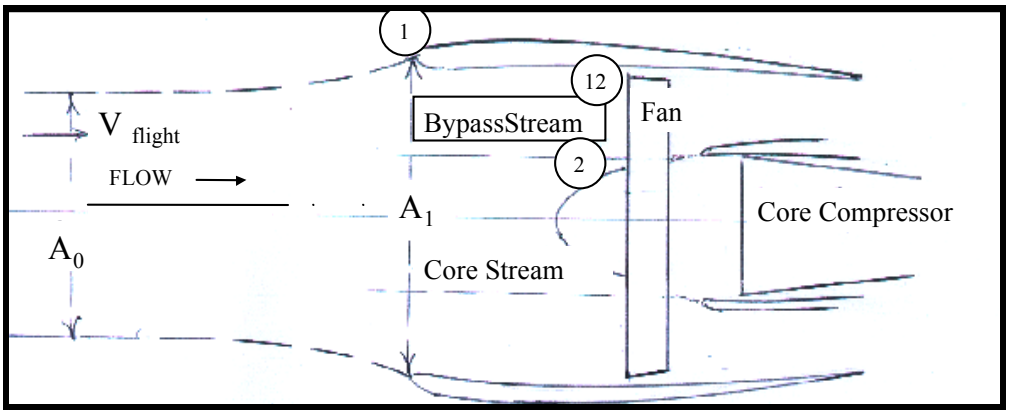

Figure B.91: Fixed Inlet Area Schematic.

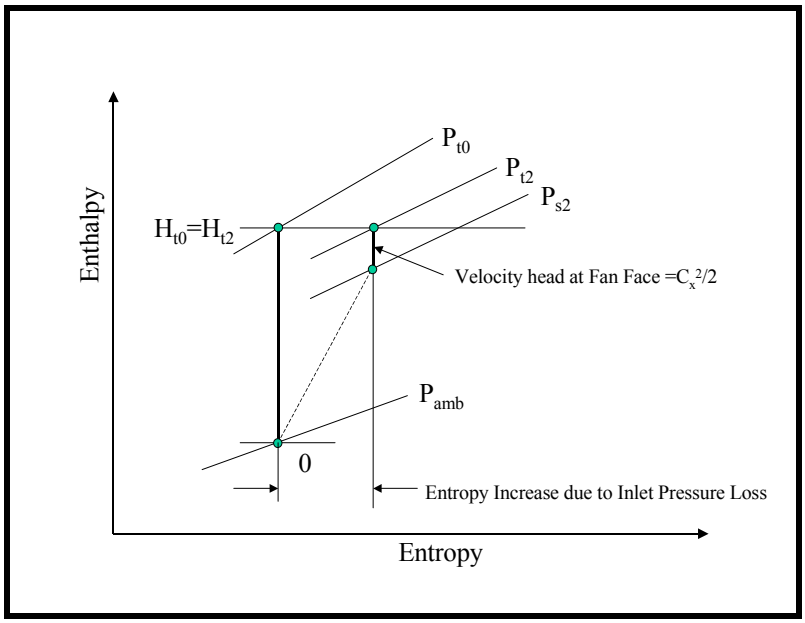

Figure B.92: Flight Velocity and Inlet Contribution to Engine Cycle.

An exception to this would be off-design conditions like sea level static where the engine flow required is very large relative to the inlet area and some of the entering flow comes from behind the inlet and may actually intersect the ground. Engine test installations minimize this effect by using a bellmouth inlet

which is designed to minimize lip overspeed, **Figure B.93**. Another exception at the aircraft design condition would be a case where external heating of the flow occurs due to hot gas ingestion from a missile. For supersonic inlets losses due to shock wave formation internal and external to the inlet must be considered and will be discussed below.

$\Delta h = V^2/2$ **Eq. B-47**

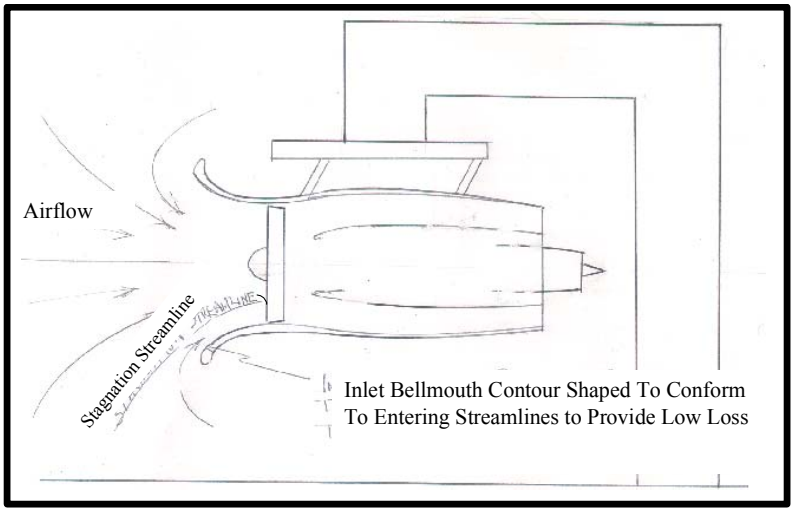

Figure B.93: Schematic of Sea Level Test Inlet.

B.5.2 Inlet External Loss: Spillage Drag

Forces are generated on the inlet cowl from pressure differentials along the external surface and from viscous effects such as scrubbing skin friction, flow separation at the inlet lip, and shock losses. The sum of these forces defines the total drag of the Inlet.

The 'INLET SPILLAGE DRAG' force term consists of three components:

- Additive drag, which is the force from the static pressure integral along the entering streamline from station 0 far upstream to the engine inlet lip, Station 1;
- Lip suction, which consists of the static pressure force integrals along the external surface from the inlet lip , Station 1 to the rear if the inlet cowl, Station MAX; and
- Scrubbing Friction.

B.5.2.1 Subsonic Case

For ideal non-viscous flow the additive drag is balanced by the forward force generated by low pressures on the forward facing surface of the inlet lip. In real (viscous) flow the "lip suction force is reduced from the ideal due to turbulence and separation effects and a net force in the drag direction occurs which is defined as 'spillage drag', equation 23. Spillage drag is minimized by proper inlet design, at the primary aircraft operating condition. The spillage drag is a result of the viscous losses generated at the inlet lip and increases when the flow Mach numbers around the lip increase. These losses are a function of inlet mass flow ratio, (Area of inlet at lip)/(Area of entering stream tube), see **Figure B.94**.

Additive Drag + Lip suction + Scrubbing Friction = Spillage Drag **Eq. B-48**

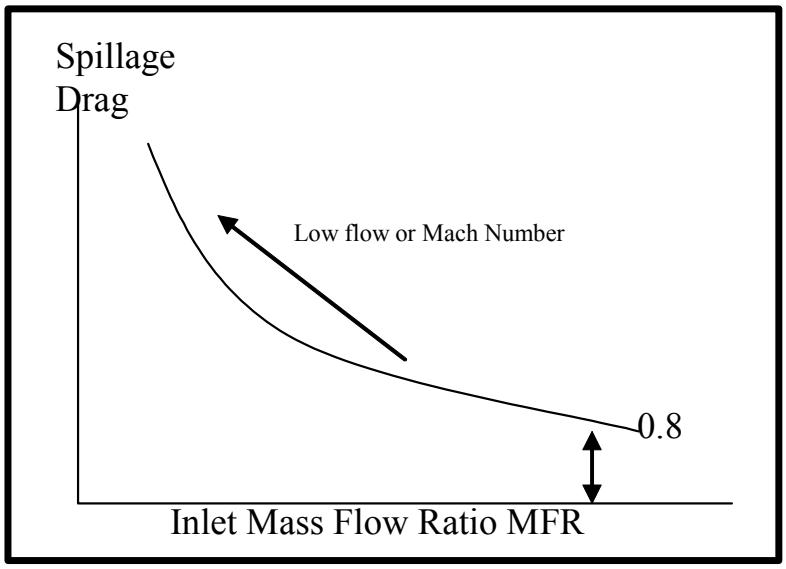

Figure B.94: Inlet Spillage Drag is a Function of Mass Flow Ratio.

B.5.2.2 Supersonic Case

For supersonic flight velocity, a shock wave can form at the inlet lip. At velocities higher than the inlet design condition, the shock may be positioned forward of the inlet, **Figure B.95**. The supersonic inlet lip design will generally be sharper than for the subsonic case and will not support a forward lip-suction force. A portion of the flow in the potential 'inlet capture area' will spill around the lip with little or no flow acceleration around the lip generating compensating 'lip suction'. The resultant spillage drag will be large and approximately equal to the additive drag,.

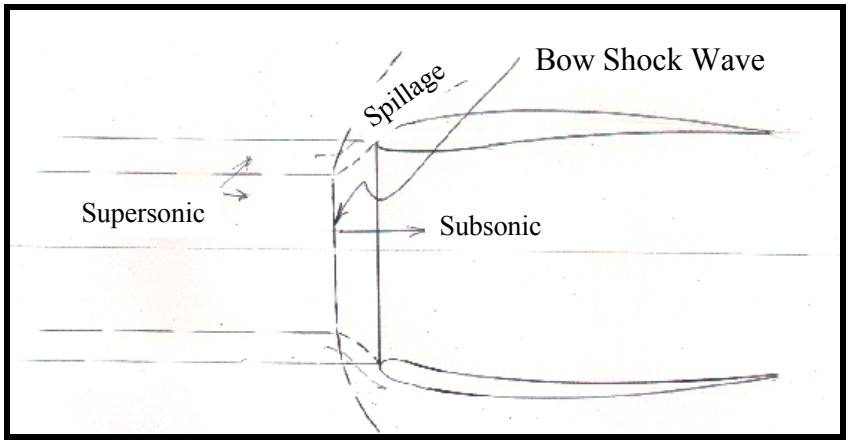

Figure B.95: Fixed Area Inlet in Supersonic Flow.

Fixed inlet area normal shock losses are generally acceptable for Mach numbers up to about 1.6. To reduce the shock losses at higher flight Mach numbers, the inlet is designed with external centerbody ramps that compress the flow externally. The ramps create a series of oblique shocks having lower total loss than a single normal shock near the inlet lip. Forward force can also be generated on a center inlet plug, **Figure B.96**. For Mach numbers above about ~2.5 optimum inlet loss can be obtained using an inlet design having both external and internal compression, **Figure B.97**.

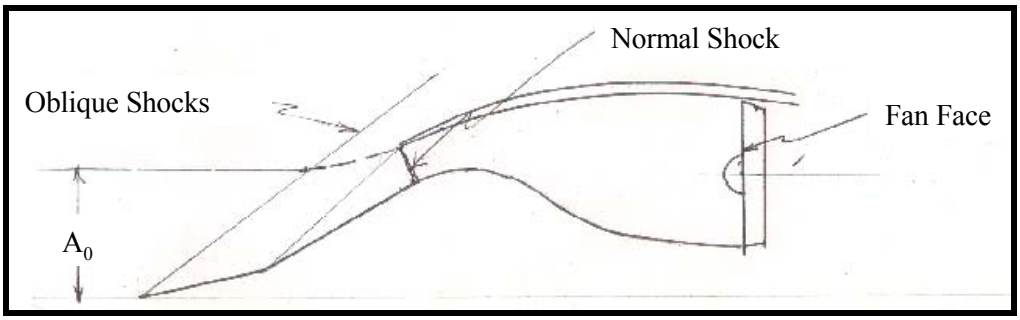

Figure B.96: Supersonic Inlet with External Compression.

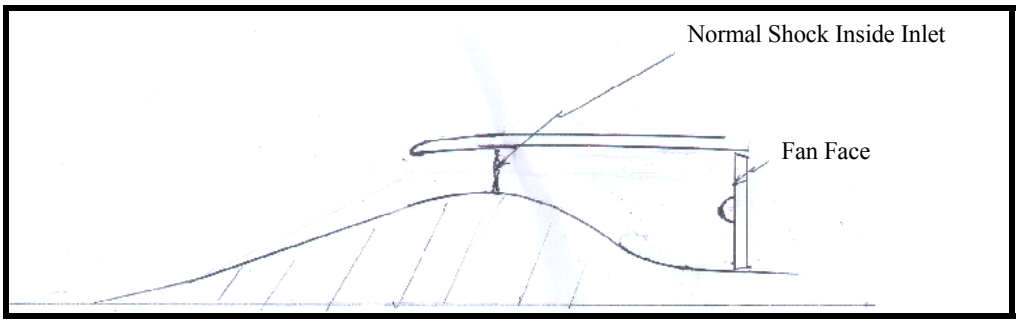

Figure B.97: Supersonic Inlet with External and Internal Compression.

Simulation of the propulsion system requires accounting for all shock and other viscous losses between Station 0 and Station 1. External forces must be accounted for between Station 2 and the inlet max-external diameter. Internal drag forces must be accounted for between Station 1 and the fan face.

B.5.3 Inlet Internal Losses: Inlet Recovery

The entering flow stream tube has a stagnation point at the inlet lip. Flow within the stream tube enters the engine and scrubs the inner surface of the inlet creating a boundary layer and reducing the effective total pressure of the flow in the fan tip region. Additional loss due to flow distortion may be generated by inlet lip-separation effects. The flow also scrubs the center spinner producing an additional pressure loss in the core stream. These losses reduce P12 and P2 at the fan face inlet, and are correlated for simulation as functions of the corrected airflow. This is shown schematically in **Figure B.98**.

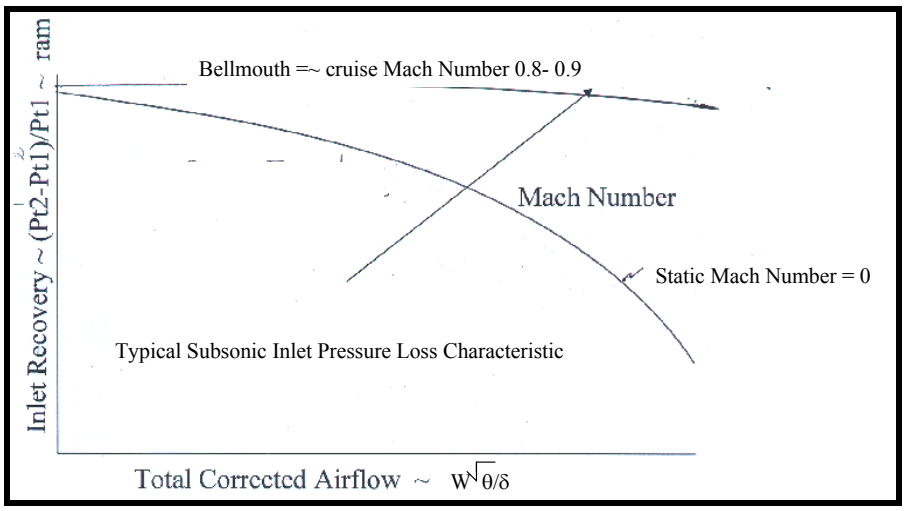

Figure B.98: Inlet Recovery Loss.

For sea-level testing a special bellmouth inlet is used to reduce inlet recovery loss. These losses correlate with inlet airflow, and are shown in **Figure B.98**.

For supersonic applications in the early design stage, the inlet recovery is estimated using a convention shown in **Eq. B-49** which is taken from Mil-E-5007D.

$$Pt2 = 1.0 - .075\,(M_0 - 1)^{1.35} \qquad 1.0 < M < 5.0 \qquad \textbf{Eq. B-49}$$

$$Pt2 = 800/(M_0^4 + 935) \qquad M > 5.0$$

B.5.4 Cited References for Nozzles and Inlets

[B.53] SAE Standard, IR1703: In-Flight Thrust Determination.

[B.54] SAE Standard, AIR5020: Time Dependent In-Flight Thrust Determination.

[B.55] SAE Standard, AIR1678: Uncertainty of In-Flight Thrust Determination.

[B.56] Rebolo et al., “Aerodynamic Design of Convergent-Divergent Nozzles”, AIAA-93-2574, 1993.

[B.57] Oates, G., “Aircraft Propulsion Systems Technology and Design”, AIAA Education Series, 1989.

B.6 AERODYNAMICS OF AIR SYSTEMS

B.6.1 Introduction

Three important subjects of the physics of air systems have been chosen:

- Part 1: Tappings/Bleeds and Pre-Swirl Systems;
- Part 2: Rotating Holes and Two Phase Flow; and
- Part 3: Labyrinth Seals.

In these fields, many new papers are available. Correlations out of the literature for the discharge coefficients, which include the most important parameters are compared and discussed. For two-phase

flow, simple correlations for engineering purposes are recommended, especially for vent lines of aero engines. It is concluded that much more effort is required in order to push knowledge beyond the state of current literature that is partly controversial and not comprehensive enough for computerized engineering.

The aim of this review is to collect the major aspects for air systems calculations. It does not contain all the different correlations out of the literature. The choice presented in the following is based on a subjective judgment of the authors based on their experience. Furthermore it is aimed to keep it simple; therefore, the effects of only the most important parameters are taken into account.

B.6.2 Tappings/Bleeds

Air is tapped off outwards for several purposes: Cooling air (C/A), engine bleeds, i.e. for starting or for pneumatic purposes and customer bleeds. Inwards the air is only used for cooling purposes.

In order to minimize the performance impact of the tapped air on the engine cycle, it is important to choose the lowest possible compressor stage. The purpose for which the air is used dictates a certain pressure level and necessitates tapping off with a minimum of pressure losses. On the other hand, from a design point-of-view it is required to keep the number of tappings to a minimum.

To calculate overall engine secondary-air-system characteristics with a computer program, accurate correlations for all flow elements are necessary. For tappings they are usually presented in form of Cd-values as a function of pressure ratio.

Results from rig tests or from numerical calculations are usually from three-dimensional models and a transformation into 1-D correlations is necessary. In this process a lot of information is lost, this and further reasons are responsible that only moderate accuracy can be expected.

B.6.2.1 Outward Tappings

The following geometries are encountered:

- Plain;
- With a step;
- Radiused;
- With subsequent diffuser; and
- Between vanes.

Plain tappings are the most common ones, but they have relatively high pressure losses.

A stepped design can only be adopted, if there is a permanent bleed, since otherwise the pressure losses in the main channel become high. If there is space for a radius at the upstream corner or a subsequent diffuser the pressure losses of the tapping configuration can be significantly reduced. (**Figure B.99** gives an example of a tapping with a step, a radius and a subsequent diffuser). Tapping in between vanes has high-pressure losses and leads to an elaborate design but it minimizes the axial length of the compressor.

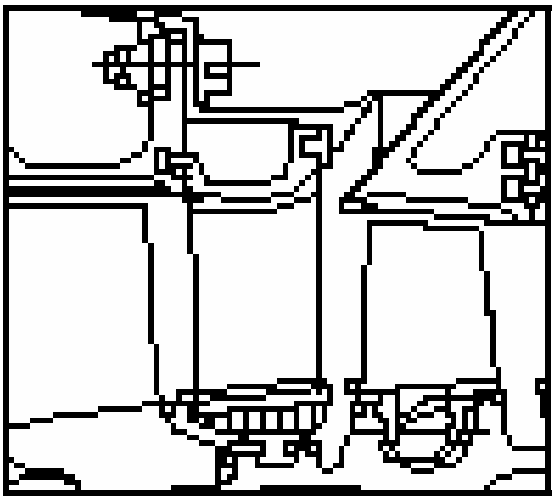

Figure B.99: Example for an Outward Tapping.

The following correlations are commonly used:

$Cd = m_{ol} / m_{id}$ **Eq. B-50**

$$m_{id} = \frac{P_{t1} \cdot A_{bl}}{\sqrt{R \cdot T_{t1}}} \left(\frac{P_{s2}}{P_{t1}} \right)^{\frac{1}{\kappa}} \sqrt{\frac{2\kappa}{\kappa - 1} \left[1 - \left(\frac{P_{s2}}{P_{t1}} \right)^{\frac{\kappa - 1}{\kappa}} \right]}$$ **Eq. B-51**

$Cd = f(DAB)$ **Eq. B-52**

$$DAB = \frac{P_{t1} - P_{s2}}{P_{t1} - P_{s1}}$$ **Eq. B-53**

In order to fit all configurations it is convenient to base the DAB-parameter on total upstream and the static downstream pressure. Otherwise, if the upstream static pressure is used it becomes difficult in case the downstream static pressure is higher than the upstream one.

The influence of a diffuser can be seen from **Figure B.100**, details can be obtained from Möller (1990) **[B.58]**. In **Figure B.101** the Cd-values of rectangular holes are compared with those of angled holes. The influence of slot length and lip height can be seen on **Figure B.102** and **Figure B.103** for tappings with a step, details again from Möller (1990). Further characteristics can be obtained from Dittrichs and Graves (1956) **[B.59]** and Rohde et al. (1996) **[B.60]**.

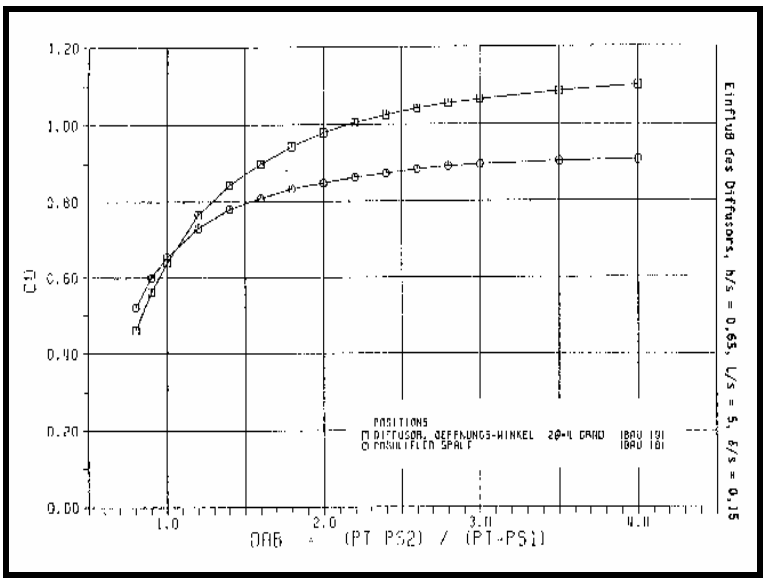

Figure B.100: Influence of a Diffuser on the Cd-Value.

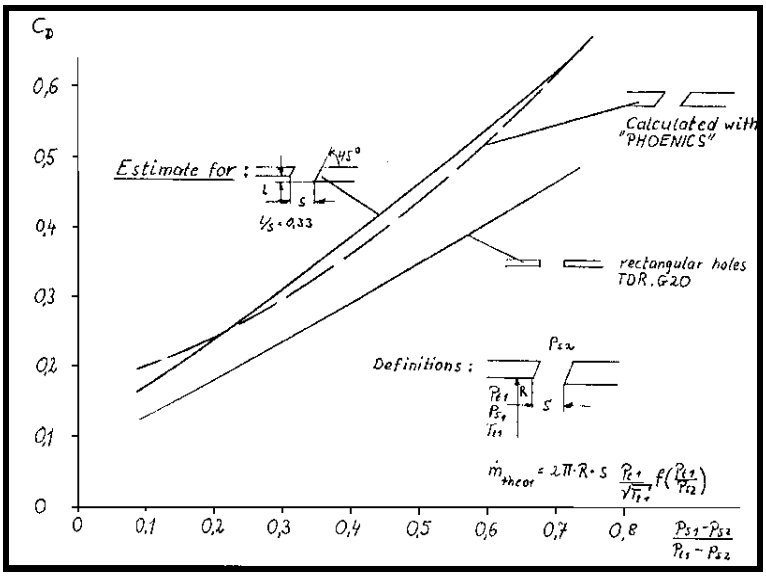

Figure B.101: Comparison of a Rectangular with an Angled Hole.

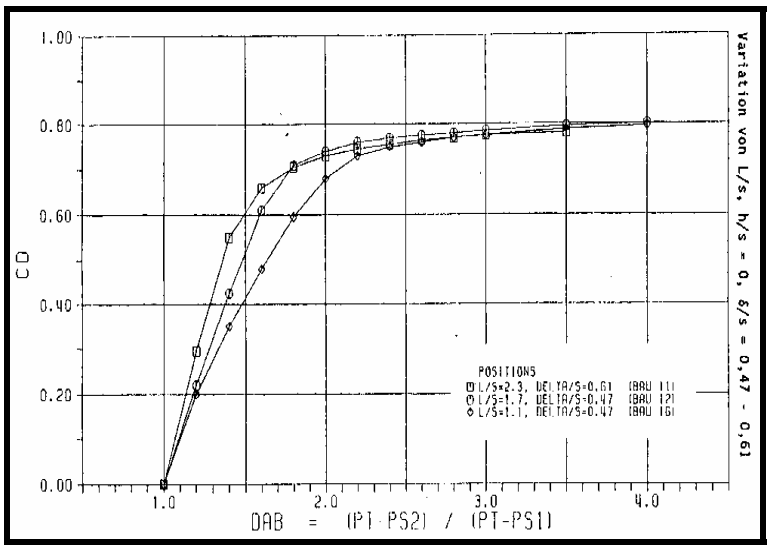

Figure B.102: Influence of Slot Length on the Cd-Value.

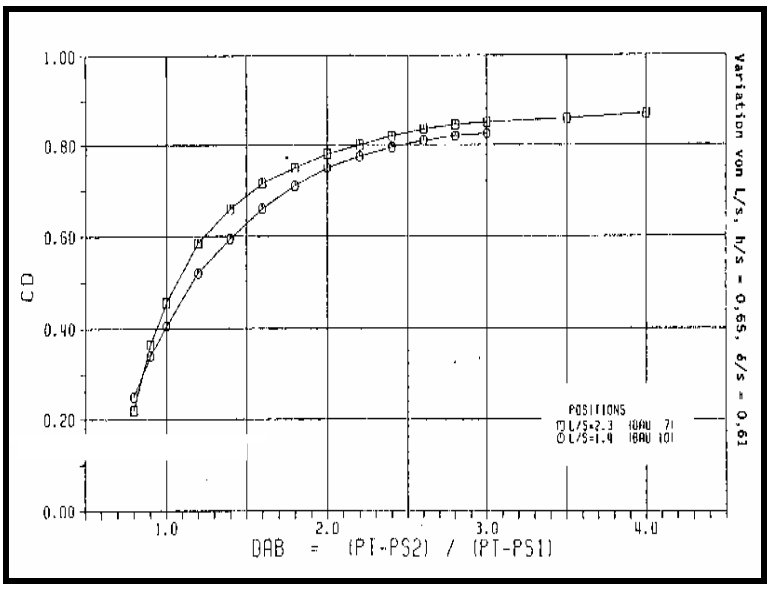

Figure B.103: Influence of Step Height and Slot Length on the Cd-Value.

For a bleed port with diffuser, assuming that $P_{t1} = P_{t2}$

$$DAB_{dif} = DAB * (1 - Cp) = \frac{P_{t1} - P_{dif,s2}}{P_{t1} - P_{s1}} \qquad \textbf{Eq. B-54}$$

$$Cp = \frac{P_{dif,s2} - P_{dif,s1}}{P_{dif,t1} - P_{dif,s1}} \qquad \textbf{Eq. B-55}$$

Assuming further that the diffuser behaves like an ordinary one, i.e. the distortion of the inlet velocity profile is neglected, bleed port characteristics with a diffuser can be obtained from the basic DAB with a Cp from diffuser charts and vice versa. Of course, DAB could be derived from DAB_{dif}.

B.6.2.2 Inward Tappings

To design an efficient inward tapping needs much more sophisticated skills than the outward case. This results from aerodynamic as well as from mechanical reasons and the relevant engine and rig tests are very expensive.

An example for an inward tapping of air is presented in **Figure B.104**. There are several difficulties encountered in designing such a system: The swirl between the inner radius of the main stream an the rotor drum must be known to get the correct inlet conditions for the holes in the drum. Next, the swirl originating from the holes and its development down to the inlet of the tubes influence the pressure drop in the upper cavity and the inlet losses to the tubes. The tubes are used to avoid the high-pressure drop of a free vortex, which would strongly limit the amount of flow which can be bled inward. The radial position of the tube entry can be optimized to the end that the circumferential velocities of the tube and the entry swirl are matched. On the other hand a stream tube between the holes and the entry of the tubes may form without diffusing the radial velocity.

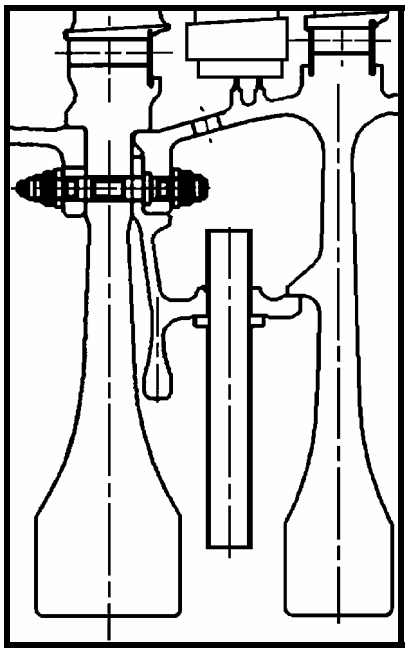

Figure B.104: Inward Tapping with Tubes.

This situation can best be investigated with the help of CFD (computational fluid dynamics). This should be done already in the design phase, where normally only correlations are used. But the swirl changes and entry losses into the tubes can only roughly be calculated using correlations. The pressure changes and losses inside the tubes could as well be calculated by CFD, though this might not be worthwhile. To generate correlations from model tests will not yield results that can be generalized and applied to all engine conditions.

It is considered that this is the only case in internal engine aerodynamics, where mainly CFD is recommended. Variation calculations should be performed for different swirl levels and tube positions.

Stable inward tapping without tubes is only possible for a small amount of bleed and the pressure drop calculation is not at all accurate which leads to a considerable uncertainty of the calculated bleed flow. A calculation method can be based on Farthing et al. (1989) **[B.61]**, but their investigation was done for low Reynolds and Rossby numbers only.

B.6.3 Pre-Swirl Systems

Two types, radial and axial pre-swirl systems are in use. There was an opinion, that the two types of systems should behave considerably different. Rig tests have shown that for practical applications it is fair enough to apply the same correlations for both. The whole problem can be divided into four parts:

- Characteristics of the pre-swirl nozzles.
- Swirl loss and mixing in of boundary layer fluid in the pre-swirl chamber.
- Pressure and swirl losses in the receiver.
- Cover plates.

The second point might be different for radial and axial pre-swirl systems, but there are not enough test results available to quantify the matter. Uncertainties arise from rig results, which are specific to engine configurations and up to now no telemetry tests results are available. Furthermore, it is recommended to agree on a nomenclature and the basic theory in order to facilitate comparisons.

The temperature drop into the rotating system is:

$$T_t - T_{t,rel} = C^2 / 2Cp - W^2 / 2Cp = U * C_{ta} / Cp - U^2 / 2Cp \qquad \textbf{Eq. B-56}$$

with $C_{ta} = C * \cos\alpha$ **Eq. B-57**

Using for C according to Meierhofer and Franklin (1981) (see ***Section B.6.8*** for full reference):

$$C = f_s * C_n \qquad \textbf{Eq. B-58}$$

and $C_n = C_v * C_{id}$ **Eq. B-59**

it follows $C = C_v * f_s * C_{id}$ **Eq. B-60**

with $$C_{id} = \sqrt{\frac{2\kappa}{\kappa - 1} R * T_t \left[1 - \left(\frac{P_{s,n,2}}{P_{t,n,1}} \right)^{\frac{\kappa-1}{\kappa}} \right]} \qquad \textbf{Eq. B-61}$$

Cv depends on nozzle shape, surface roughness and pressure ratio, it is in the order of 0.9 to 0.95. The swirl factor f_s comprises wall friction and turbulence losses and mixing in of boundary layer fluid. It is in the order of 0.8.

B.6.3.1 Pre-Swirl Nozzles

The shape of the nozzles can be optimized by CFD methods without big effort. It is important to get a nearly rectangular velocity profile, in order to get a good discharge coefficient and, more important, a good velocity coefficient, which is coupled with the Cd-value. The discharge coefficient in itself is not so important as there is usually enough space available to have the required amount of pre-swirl nozzles. A low velocity coefficient, however, would reduce the pre-swirl with the consequence of higher temperatures in the rotating system. An important means of achieving a high Cd and Cv is a low roughness of the pre-swirl nozzles.

B.6.3.2 Pre-Swirl Chamber

The size of the chamber is not very important, but the distance nozzle exit and receiver entry should at least be larger than 1.2 d_n to avoid an interaction between the two flow-fields: that of the nozzle jet and that of the receiver.

Radial nozzles have the advantage that there is no boundary layer due to disk pumping which can mix into the receiver flow.

The swirl loss results from a complex 3-D flow structure including a powerful chamber vortex.

B.6.3.3 Receiver

The receiver holes are normally large and consequently the pressure losses small.

If the swirl can be utilized, i.e. if there is a coverplate or an annular space for a free vortex downstream of the receiver the swirl losses are of importance.

The swirl loss of the receiver is a function of length over diameter ratio of the holes and of the ratio of receiver to nozzle area. The receiver swirl factor is defined as:

$$f_{s,rec} = W_{ta,rec2} / W_{ta,rec1} \qquad \textbf{Eq. B-62}$$

The pressure loss can be described by a Cd-value:

$$Cd = m / m_{id} \qquad \textbf{Eq. B-63}$$

or by a pressure loss coefficient:

$$\zeta = \frac{P_{t,rel,1} - P_{t,rel,2}}{\frac{\rho}{2} \cdot W_{rel,1}^{\ 2}} \qquad \textbf{Eq. B-64}$$

The difficulty is, to define a pressure ratio across the receiver. A pressure loss is a total pressure difference and would have to be determined by averaging the velocity profiles up- and downstream of the receiver. Normally these profiles are not available, furthermore the pressure losses are small and the pressure profiles very uneven which would render these results questionable. In Schmitz [B.62] and Popp et al. [B.63] the pressure and swirl losses of different receiver configurations are plotted.

B.6.3.4 Coverplates

In Hasan et al. [B.64], and Zimmermann [B.65] it is shown, that the free vortex flow between coverplate and turbine disc can be fairly well calculated by CFD, the same applies for a forced vortex. Many engine applications have no coverplate, i.e. the swirl is lost by the transition into the disc. The main reason for having a coverplate is to enable good seals on both sides of the swirl chamber in order to minimize leakages and to achieve a sufficiently high pressure for a good blade cooling air supply.

B.6.3.5 Conclusions for Tappings

- For outward tapings correlations are available.
- For designing inward tapings CFD is recommended.

- To get reliable coverplate receiver characteristics, more investigations are necessary.
- On the whole more research is required.

B.6.4 Labyrinth Seals

Most companies in the turbomachinery industry have a wealth of unpublished test results, which are partly transformed into company restricted correlations. Therefore, the opinion in this review is necessarily based on the knowledge of the authors. If this paper initiates more research and exchange of ideas, or even correlations, the authors would meet part of their targets.

This chapter comprises labyrinth seals. There are several books for these subjects, e.g. Trutnovsky [B.66] and others. Since there is a good basis, progress needs much effort, but there are still some geometrical and physical parameters, which are not fully covered up to now.

On the other hand, seal clearances will hardly be known very accurately and there are other uncertainties, which overall results in moderate accuracy of air system calculations.

It is important to cover the main parameters for optimizing purposes and to give analytical engineers more confidence into their calculations.

Labyrinth flow has been a subject of research for more than 100 years. Therefore a wealth of literature exists, but complete combined correlations for all parameters are missing. In this paper it is aimed to give a set of correlations for practical applications. Contributions from other authors to complete or improve this set are welcomed.

The authors have produced several quite different methods of correlating labyrinth seal leakage, but only one method each for straight through and stepped seals will be described.

For straight through labyrinth seals most of the important geometrical parameters can be covered, for stepped seals there are significant gaps of knowledge. In this paper, it is not intended to quote every investigation into the effects of the different geometrical parameters. Only if there is a correlation that covers a large fraction of the field of practical application, is it taken into account. It is considered that the forthcoming correlation method based on ideal labyrinth flow, carry over factors (in case of straight through seals) and Cd-values are most useful. A disadvantage of that method is, that ideal labyrinth correlation and carry over factors are strictly speaking not fully correct models. Therefore, many corrections have to be bundled in a Cd-value, if not, for the benefit of better practical application of a simpler model, slightly larger discrepancies from reality are accepted.

B.6.4.1 Straight Through Labyrinth Seals

Figure B.105 shows the flow function for the ideal labyrinth, derived from the linearized gas dynamic equations, as a function of pressure ratio. It can be seen that for 1 fin up to conditions of maximum flow function the difference between linearized and compressible flow functions are small. Therefore, the forthcoming correction factors are based on the linearized functions:

$$Q_{id} = \sqrt{\frac{1-(P_s/P_t)^2}{R(n-\ln(P_s/P_t)}} = \frac{m_{id}\cdot\sqrt{T_t}}{A\cdot P_t} \qquad \textbf{Eq. B-65}$$

$$\mathrm{m} = k_2 \cdot Cd \cdot m_{id} \qquad \textbf{Eq. B-66}$$

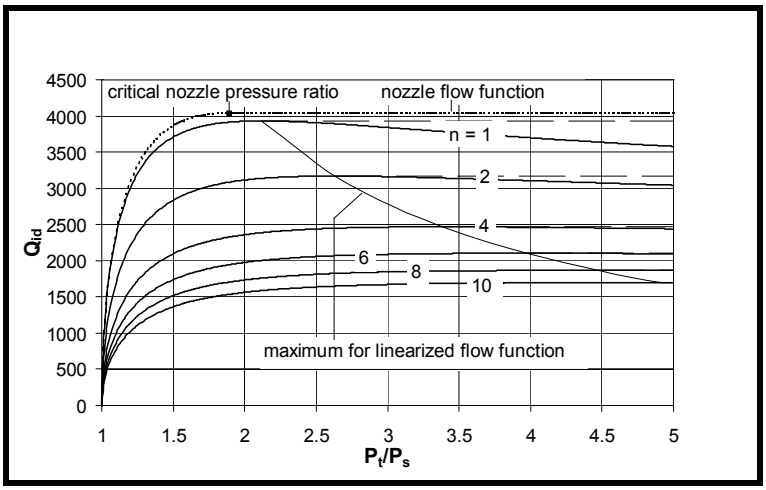

Figure B.105: Ideal Labyrinth Flow.

Eq. B-65, **Eq. B-66**, and **Figure B.105** are based on the so-called 'Martin Equation' for a series of identical restrictions with vertical fins. **Eq. B-66** defines k_2 and Cd.

B.6.4.1.1 Carry-Over Factor

The ideal labyrinth flow functions (**Figure B.105**) imply one dynamic head pressure loss downstream of each fin. The carry-over factor should account for the effect that only a fraction of the dynamic head is lost, i.e. some dynamic head is carried over. Test results have shown, that this effect depends on the number of fins, which can easily be understood, because the first and the last fin play an extra role and thus it is important how many fins are in between.

Figure B.106 shows the carry-over factor from Hodkinson **[B.67]** and **Figure B.107** shows correction factors as a function of number of fins.

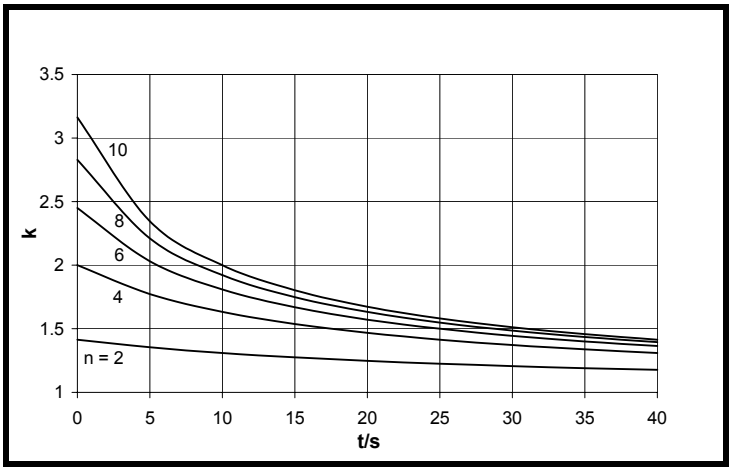

Figure B.106: Carry-Over Factor from Hodkinson.

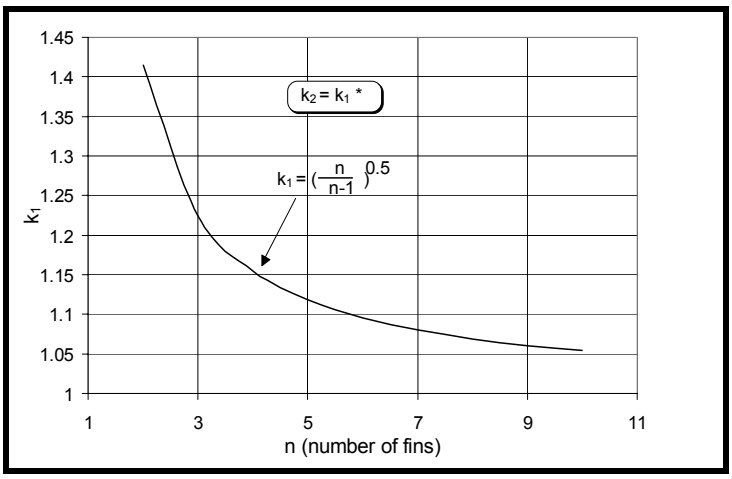

Figure B.107: Correction Term for Carry-Over Factor.

The carry-over factor proposed by Hodkinson **[B.67]** is:

$$k = \sqrt{\frac{1}{1 - \frac{n-1}{n} \cdot \frac{s/t}{s/t + 0{,}02}}} \qquad \textbf{Eq. B-67}$$

With the new correction factor from unpublished test results:

$$k_1 = \sqrt{\frac{n}{n-1}} \qquad \textbf{Eq. B-68}$$

A revised carry-over factor k_2, which describes better the effect of n, than the correlation k from Hodkinson **[B.67]**, is obtained by:

$$k_2 = k_1 \cdot k \qquad \textbf{Eq. B-69}$$

Carry-over factors derived from CFD calculations as tabulated in Zimmermann and Wolff **[B.68]** compared with those from equivalent conditions in **Figure B.106** and **Figure B.107**, are in the same order, i.e. they are in line with physical understanding.

B.6.4.1.2 Coefficient of Discharge

The Cd-values in **Figure B.108** and **Figure B.109** comprise the effect of flow contraction and various corrections, they are plotted against the stream-wise Reynolds number ($Re = U \bullet d_h / \nu$ with U, the velocity at the fin tip). Above $Re = 2x10^4$ there is only an effect of s/b for small seal clearances, where friction losses are of larger influence.

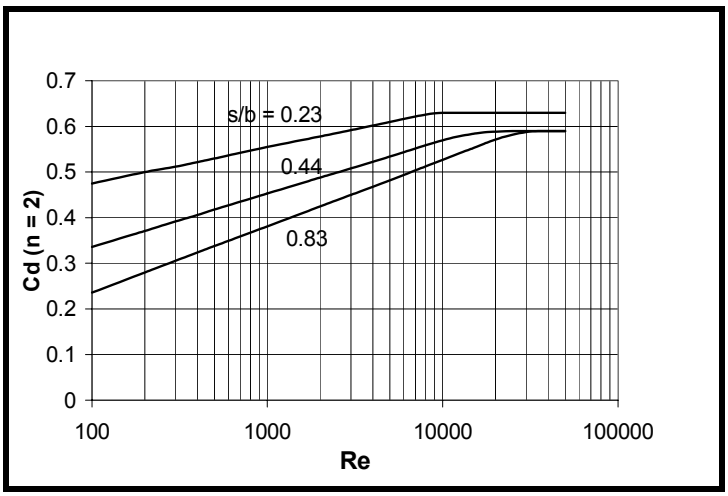

Figure B.108: Discharge Coefficients for n = 2.

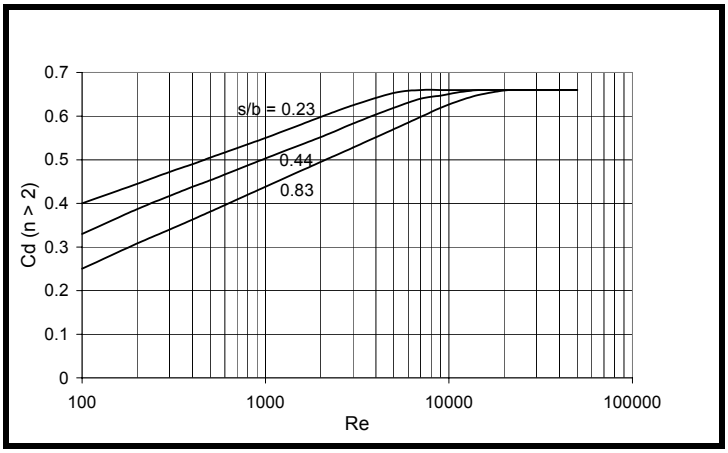

Figure B.109: Discharge Coefficient for n > 2.

The plotted correlations represent test results from a data bank, containing a mixture of test results from literature and company owned data. It is considered, that for low Reynolds numbers, friction factors would give better correlations.

B.6.4.1.3 Grooves

With the use of coatings on the stator, the design is often such, that running into the liner is allowed under certain extreme operating conditions. Therefore, it is important to know the performance of a labyrinth seal running in a groove. **Figure B.110**, derived from Zimmermann et al. **[B.69]**, shows a correction factor for Cd-values without grooves as a function of the groove depth related to gap width and with the groove width related to groove depth as parameter. It can be seen that large increases of the throughflow up to a factor of approximately 2.5 can occur.

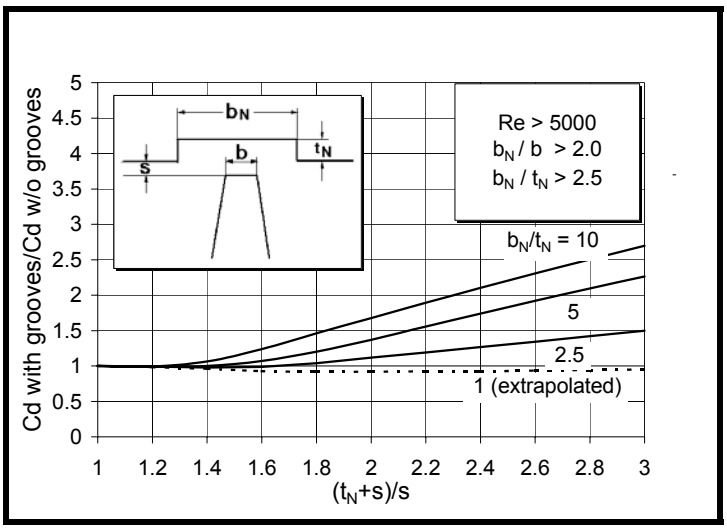

Figure B.110: Correction Factor for Straight-Through Labyrinth Seals with Stator Grooves.

Honeycomb on the stator layers with three different sizes as a function of labyrinth gap width related to cell size, where delta m is the increase or decrease of the leakage flow induced by the honeycomb. The correction is derived from Stocker [B.70] and agrees well with company owned data. For big seal clearances the negative delta arises from the increased roughness of the outer wall. For small seal clearances, the effective gap is enlarged. **Figure B.111** shows a correction for honeycomb.

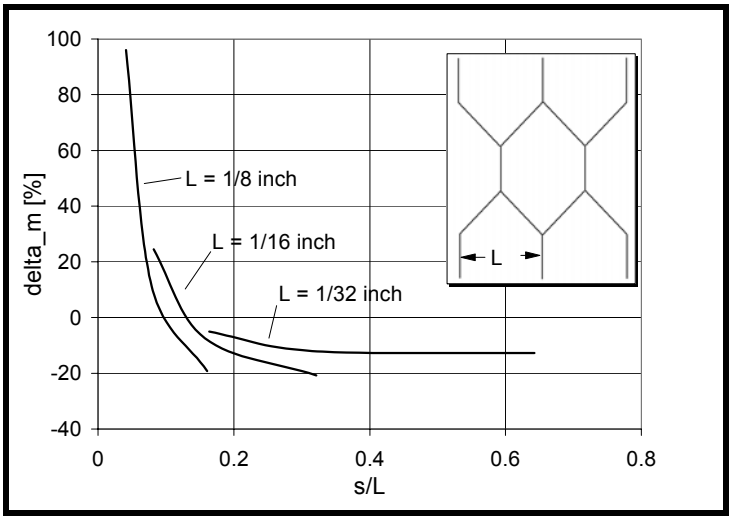

Figure B.111: Mass Flow Differences for Honeycomb Layers on the Stator.

B.6.4.1.4 Corner Radius

The effect of corner rounding on Cd can be obtained from Zimmermann et al. and is shown in **Figure B.112**. The correction factor on Cd is plotted versus corner radius related to hydraulic diameter for an orifice, for stepped and straight through labyrinth seals. Because of the carry-over effect in straight through labyrinth seals, the effect of the corner radius is much smaller than for stepped seals. A relative small rounding of $r/d_h = 0.2$ yields already most of the effect.

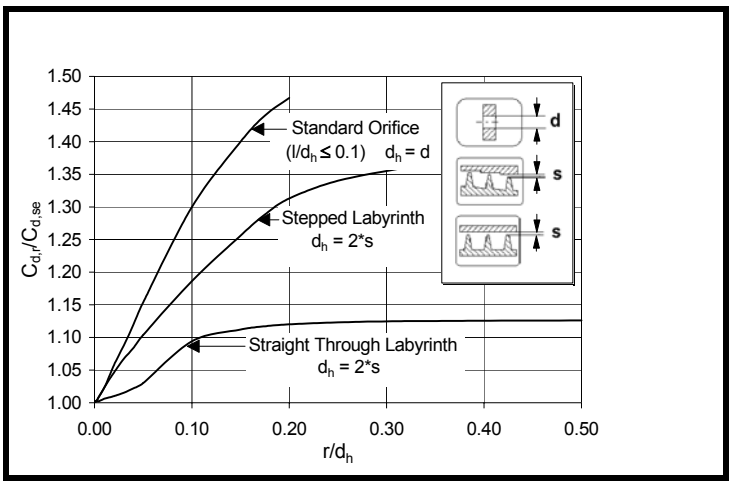

Figure B.112: Effect of Rounding Radius.

B.6.4.1.5 Chamber Depth

In **Figure B.113** the influence of chamber depth on the labyrinth through-flow from Trutnovsky and Komotori **[B.66]** is shown. It can be seen that up to 15 % improvement can be obtained. As the minimum is independent of gap width always at h/t = 0.25 it is possible to realize it on an engine and to sustain the effect under all operating conditions. But very likely will not be realized in practice, because shorter teeth tend to be thermally unstable in a rub case, i.e. the situation might escalate into a failure case.

B.6.4.1.6 Labyrinth Seal Windage

A set of formulae is from McGreehan and Ko **[B.71]**, a verification by test results can be found in Millward and Edwards **[B.72]**. This effect, however, is not directly related to the calculation of labyrinth seal leakage. Therefore, it is not discussed here in more depth.

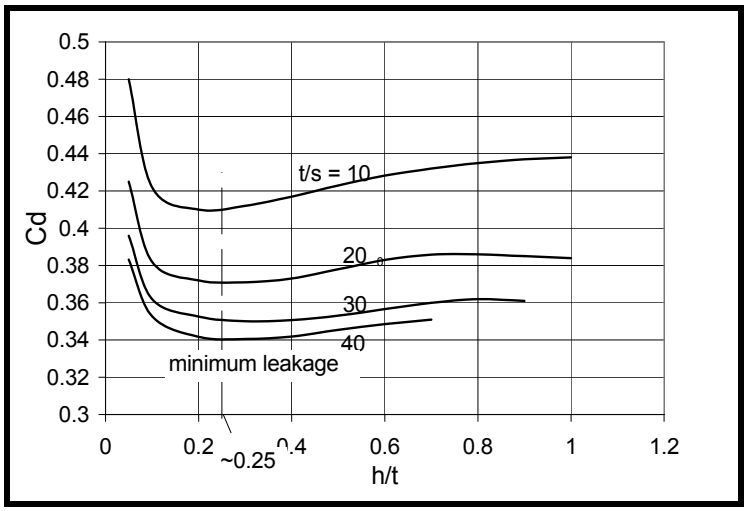

Figure B.113: Effect of Chamber Depth.

B.6.4.1.7 Rotation

From Waschka et al. **[B.73]** it can be seen that for Re =10000 the influence of rotation on throughflow is negligible. But for laminar flow, especially for low Reynolds numbers the effect is high. As the pressure

losses for laminar flow are due to increasing friction losses with decreasing Reynolds numbers they depend on surface area and form. Therefore, a generalized correlation cannot be very accurate.

B.6.4.2 Stepped Labyrinth Seals

The flow function of the ideal labyrinth in **Figure B.105** is as well valid for stepped seals.

$$m = k_s \cdot Cd \cdot m_{id} \qquad \textbf{Eq. B-70}$$

with Cd from **Figure B.114** and k_s from **Figure B.115**.

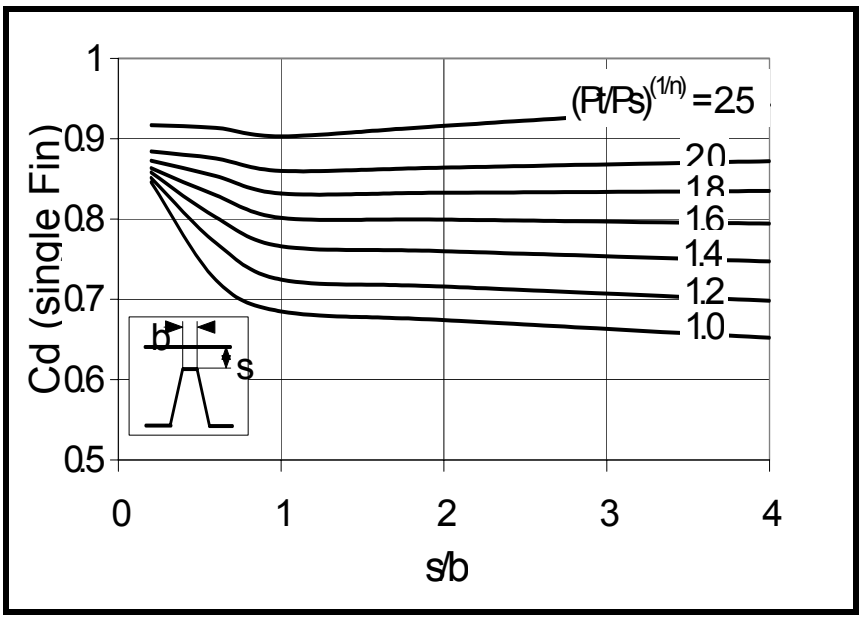

Figure B.114: Discharge Coefficients for Stepped Labyrinth Seals (single fin).

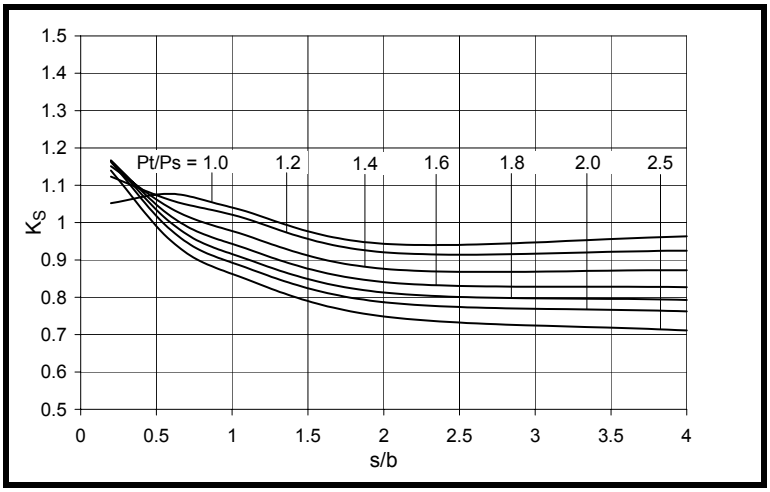

Figure B.115: Correction Factor for Cd.

Though the literature is manifold, there is not enough information available to cover all influencing parameters.

B.6.4.2.1 Ideal Cd-Values

Figure B.114 contains the Cd-values for single fins derived from Snow **[B.74]** to be applied for stepped seals because of the assumption that there is a one dynamic head loss after every fin. It is furthermore assumed that the pressure ratios are equal for each fin.

B.6.4.2.2 Cd Correction Factor

As the assumption above is not fully applicable, a correction factor is necessary. **Figure B.115** shows this factor as a function of gap width related to fin width. It represents test results with +/- 5 % accuracy.

B.6.4.2.3 Corner Radius

See **Figure B.112** and the associated section, where the effect of corner rounding for stepped seals is included.

B.6.4.2.4 Flow Reversal

From Waschka **[B.73]** it can be seen that the influence of flow reversal on the Cd-value of stepped labyrinth seals is small. Only for $Re \leq 10^3$ there is an effect of approximately 10 to 20%, but that rarely occurs with stepped seals in aero engines, see Zimmermann et al. **[B.69]**.

B.6.4.2.5 Rotation

Waschka et al. **[B.73]** have shown that for approximately $Re \geq 3.10^2$ the influence of rotation on through-flow is negligible.

B.6.4.2.6 Step Height

Figure B.116 based on unpublished company owned data shows that there is a flat minimum at H/t equal to 0.075. It is recommended to place practical applications around that value. For decreasing s/b $Cd*k_s$ increases, because in the then relatively longer gap the flow reattaches and thus increases Cd.

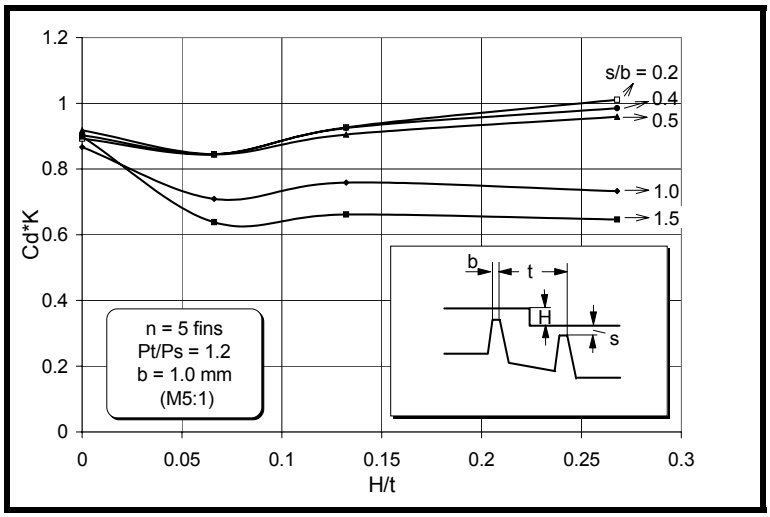

Figure B.116: Influence of Step Height.

B.6.4.3 Conclusions for Labyrinth Seals

- For both, stepped and straight through labyrinth seals the influence of Reynolds number is only significant for laminar flow.
- It is advantageous to design straight through labyrinth seals with flat chambers. But the thermal stability of the fins in a rub situation has to be watched.
- It is as well advantageous to realize flat steps and small chambers for stepped labyrinth seals. The influence of flow reversal on the Cd-values of stepped seals is small.
- There is a strong need for further research, especially concerning whole models and correlations for all important parameters.
- All correlations in this paper could be refined.
- Better or new correlations are required for Reynolds number effect, influence of rotation, especially at low Reynolds numbers, furthermore for the influence of chamber depth (or step height) and for the axial displacement of stepped seals.
- There is a wealth of literature but it is difficult to create complete correlations from individual research projects that do not fit together.

B.6.5 Rotating Holes

The aim of this review is to collect the major aspects for systems calculations. It does not contain all different possibilities out of the literature, thus it is based on a subjective judgement of the author. For simplicity, only the effects of the most important parameters are taken into account.

Rotating holes are often the bottleneck to sections of the air system network, because the discharge coefficients are small. Consequently, large areas in rotating pieces are required which is often critical, especially with respect to the stressing of these parts. For rotating holes the final method of correlation has yet to be found. Therefore, in this chapter four methods are compared to each other and discussed.

B.6.5.1 Sharp-Edged Holes

For sharp edged holes with small l/d all sources quote similar test results. The more it is astonishing that for the other cases there are so large discrepancies.

B.6.5.2 Rounded Holes

There is only little and contradictory literature available on the influence of the rounding radius and the interaction with the l/d effect.

Several methods of correlation are in use. The definitions of Cd are the following:

$$Cd = \frac{m}{m_{id}} \qquad \textbf{Eq. B-71}$$

$$m_{id} = A \cdot P \sqrt{\frac{1}{RT}} \sqrt{\frac{2\gamma}{\gamma - 1} \left(\frac{Ps_\infty}{P}\right)^{\frac{2}{\gamma}} \left(1 - \left(\frac{Ps_\infty}{P}\right)^{\frac{\gamma-1}{\gamma}}\right)} \qquad \textbf{Eq. B-72}$$

P and T may be expressed either in the absolute or in the relative frame of reference. In the absolute frame of reference, P and T are P0 and T0, whereas in the relative frame of reference Prel and Trel have to be used:

$$P_{rel} = P_0(1+\frac{\gamma-1}{2}Ma^2)^{\frac{\gamma}{\gamma-1}}$$ **Eq. B-73**

$$T_{rel} = T_0(1+\frac{\gamma-1}{2}Ma^2) \quad \text{with}$$ **Eq. B-74**

$$Ma = \frac{U}{\sqrt{\gamma \cdot R \cdot T_0}}$$ **Eq. B-75**

Samoilowich [B.75], Meyfarth and Shine [B.76] and McGreehan and Schotsch [B.77] plot Cd in the absolute system against U/Cax,id:

$$Cax,id = \frac{m_{id}}{\rho A} = \sqrt{\frac{2\gamma}{\gamma-1}RT_0(1-(\frac{P_{s\infty}}{P_0})^{\frac{\gamma-1}{\gamma}})}$$ **Eq. B-76**

More recently Weissert [B.78] presents Cd in the relative frame of reference versus Cax:

$$Cax = \frac{Cd \cdot m_{id}}{\rho A}$$ **Eq. B-77**

For ρ, the density in the vena contracta has to be used. This necessitates iteration and the first Cd has to be guessed. Another method would be to plot Cd in the relative system against U/Wid with:

$$W_{id} = \sqrt{\frac{2\gamma}{\gamma-1}RT_{rel}(1-(\frac{P_{s\infty}}{P_{rel}})^{\frac{\gamma-1}{\gamma}})}$$ **Eq. B-78**

Because U/Wid approaches 1 for U approaching infinity, U/Wid is limited between 0 and 1 and not between 0 and infinity as is the case with U/Cax and U/Cax,id. Therefore, U/Wid is advantageous, especially if limited test data have to be extrapolated.

In the following diagrams the different correlations are transformed to the same basis, in order to allow a comparison. The upstream total equals the static condition. From **Figure B.117** it can be seen that in the absolute frame of reference Cd,rot,abs may exceed 1. This is the more the case the greater Rk/D is. Cd,rot,rel in the relative frame of reference.

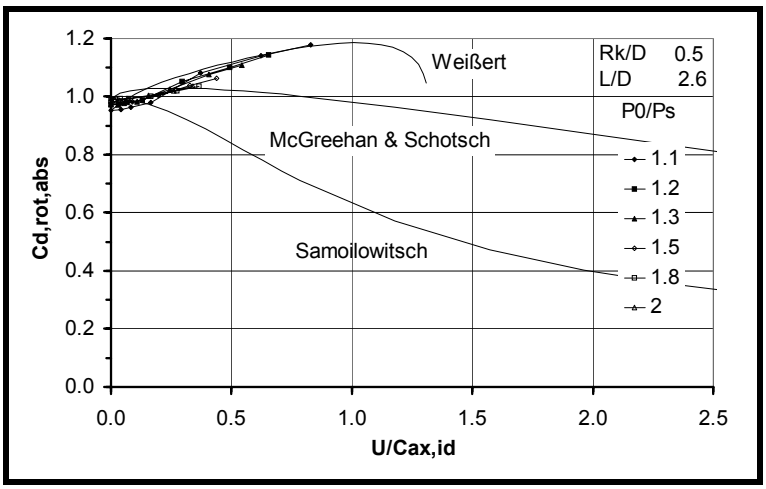

Figure B.117: Comparison of Different Cd Correlations, Absolute Frame of Reference.

Figure B.118 on the contrary stays at or only slightly above 1 which is in line with the notion of an engineer, that such ratios describing a comparison to an ideal condition should stay below 1.

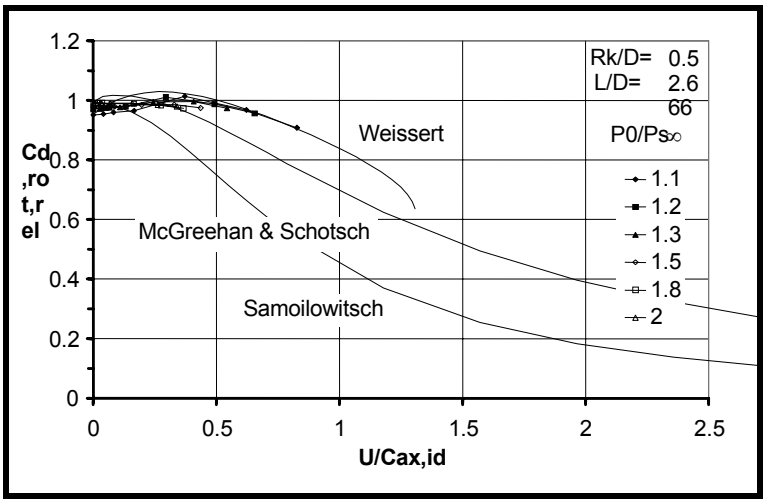

Figure B.118: Comparison of Different Cd Correlations, Relative Frame of Reference.

In the forthcoming figures Cd,rot,rel will be related to the static Cd which is labeled as Cd,0. This has the advantage, that the scatter of the test results is reduced. From **Figure B.119** and **Figure B.120** it can be seen that the rotating Cd for low U/Cax,id is higher than the static Cd, because of the work done to the distorted flow with strong secondary vortices.

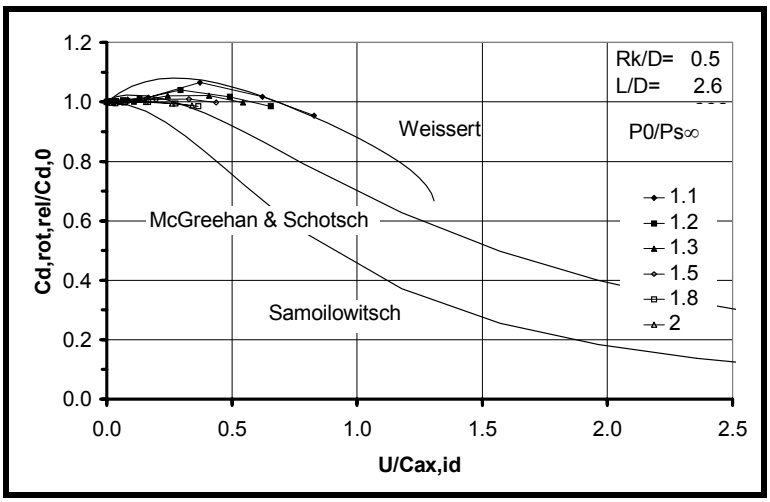

Figure B.119: Cd,rot,rel Referred to Cd,static as Function of U/Cax,id.

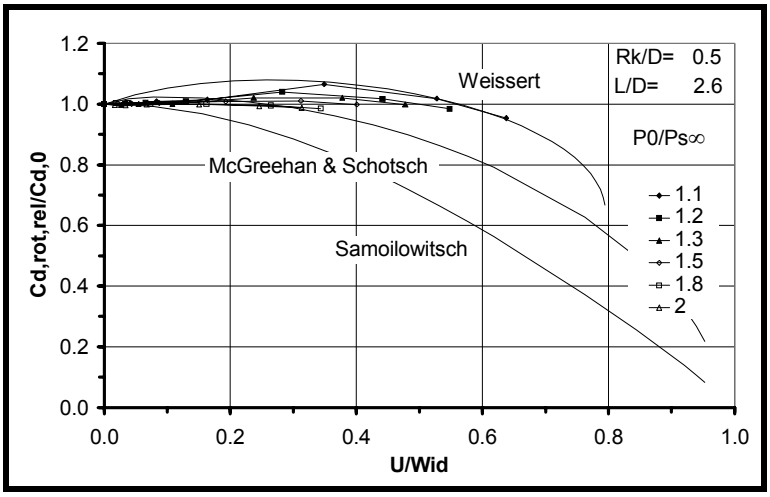

Figure B.120: Cd,rot,rel Referred to Cd,static as Function of U/W,id.

With large L/d the work done is mainly independent of the corner radius, but influences the efficiency, i.e. the conversion into pressure rise which yields higher Cd-values than for shorter L/d. In **Figure B.117** to **Figure B.119** the Cd-values are plotted against U/Cax,id, whereas in **Figure B.120** against U/Wid. This has the clear advantage that the Cd-values have to approach different Cd Correlations 0 at U/Wid = 1 on the abscissa. This is advantageous if, due to the limited extent of available test data, extrapolations become necessary. The difference between the three compared correlations partly results from the difference in the test results. Only Weissert **[B.78]** has modeled the maximum in the relative system on the left hand side of the diagrams which is due to the work done to the secondary flows.

B.6.5.3 Discharge Coefficient Correlations

In this section four methods to correlate discharge coefficients will be described and discussed. They differ by the use of different test results. All four methods could be improved and developed to the preferred one in practical use.

B.6.5.3.1 Method by McGreehan and Schotsch (1987)

This method is mainly based on test data of stationary holes, i.e. Rohde et al. (1969) **[B.60]**, with inlet tangential velocity. For small U/Cax,id the correlations were checked by McGreehan and Schotsch **[B.77]** against test results from rotating holes, Grimm (1969) **[B.79]**, Meyfarth and Shine (1965) **[B.76]**. For U/Cax,id between 0 to 1, where most of the practical applications are placed, the maximum as shown in Weissert (1997) **[B.78]**, is not modeled adequately, whereas for U/Cax,id from 2 to 5 it can be seen from the original paper that the correlation should yield smaller Cd-values. All this could be adjusted in the light of more recent test results or CFD calculations.

B.6.5.3.2 Method by Weissert (1997)

The Thesis of Weissert (1997) **[B.78]** will not yet be known to most of the readers. It contains very useful CFD results, which show the complex flow pattern in rotating holes and, here of more interest, presents a Cd correlation.

In **Figure B.121** the related Cd-values are plotted against U/Cax, which on the first sight shows no difference to **Figure B.119**, a plot against U/Cax,id. When **Figure B.120** and **Figure B.122** are analyzed, it becomes evident, especially on **Figure B.122** that Wid derived from Cax can lead to erroneous values. This is insofar as it tends to show a maximum and will not reach the theoretical limit of 1.

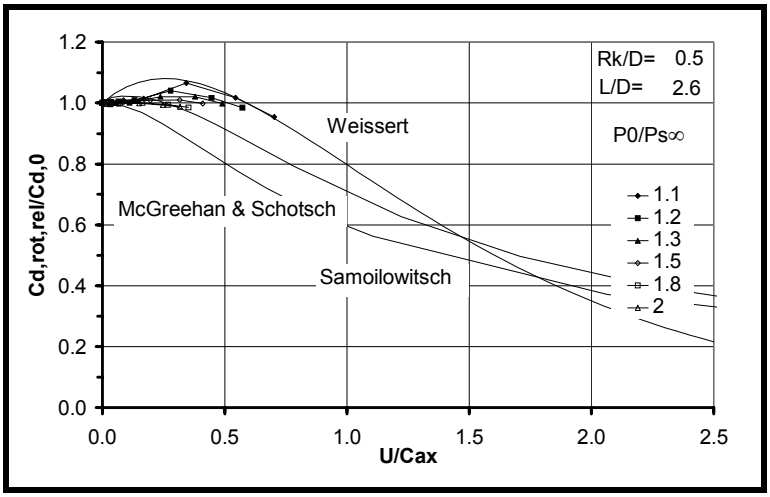

Figure B.121: Cd,rot,rel Referred to Cd,static as Function of U/Cax.

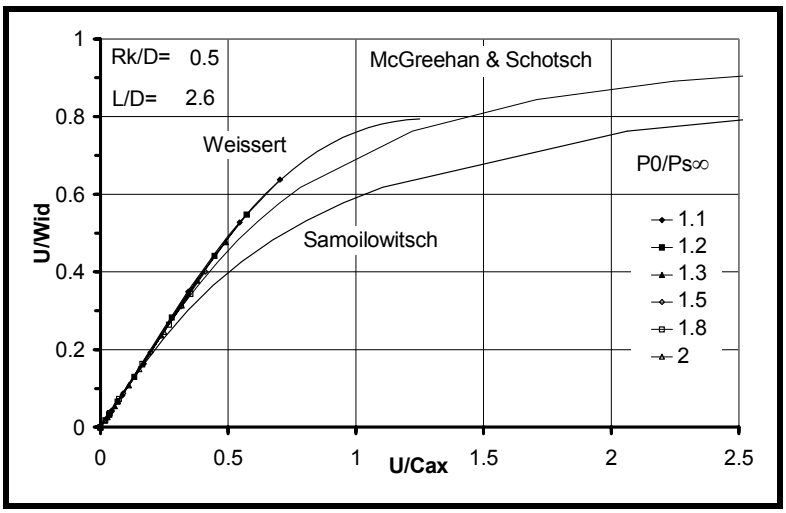

Figure B.122: Comparison of U/Wid vs. U/Cax.

It can be shown that Cax = Cd ∗Wid. With Cd = f(U/Cax) it follows that U/Wid = U/Cax ∗f(U/Cax). Because U/Wid approaches 1 for U/Cax,id or U/Cax approaching infinity, as mentioned already above, only such functions Cd=f(U/Cax) are allowed which do not produce a maximum of U/Wid, i.e. the slope dCd/d(U/Cax) has to be greater than -1. Therefore, the validity of the correlation from Weissert (1997) **[B.78]** has to be limited to U/Cax < 1.5, where most of the practical applications take place. In order to obtain Cax, a Cd-value is required, the relevant iteration can lead to big discrepancies with the test results the correlation is based on.

B.6.5.3.3 Method Based on Samoilowich [B.75]

A previous method of MTU is fully based on Samoilowich (1957) **[B.75]** and, therefore, is somehow superseded by more recent publications. The following correlation has been developed:

$$Cd_{rot,abs} = (Cd,0^{-1/z} + 2 \cdot (U/Cax,id)^2)^{-z} \qquad \textbf{Eq. B-79}$$

with:

<u>l/d 0 0.5 1.0 1.5 2.0 2.5 3.0 3.50</u>

z 0.65 0.65 0.65 0.65 0.53 0.44 0.38 0.33

<u>l/d 4.0 4.5 5.0 5.5 6.00</u>

z 0.30 0.28 0.26 0.25 0.24

The influence of a corner radius is taken from McGreehan and Schotsch (1987) **[B.77]**. The correlation (equation 23) has been included as the test data from Samoilowich are still the most comprehensive ones and can be used to check the other methods. It is easier to do the comparison with a formula that can easily be programmed, than to use test results from diagrams, which are often not very clear.

B.6.5.3.4 Method by Reichert et al. (1997) [B.80]

This method can only be recommended for long orifices. It differentiates between three parts: Entry losses, friction losses in the middle and exit losses. Details can be obtained from the paper.

This method should be used as a basis for a new method of correlating all three parts (entry, friction, and exit losses) separately, mainly as a function of RPM. Weissert (1997) [B.78] has demonstrated by CFD calculations that the velocity profiles are heavily distorted. The entry losses can be described by a flow contraction defined as a Cd-value and a subsequent expansion loss (Carnot shock). The exit loss is as well determined by a Cd-value, which describes the contraction. A full dynamic head pressure loss from the velocity in the restricted area then yields the exit loss.

It is considered that a method where all three parts are assessed separately would yield better results than a complex formula with all three parts mixed.

B.6.5.4 Comments on the Correlation Methods

Each method has its merits, the main difference among method 1 to 3 may arise from the test results used. It is not understood why the discrepancies are so large, which is not the case for sharp edged holes. In Samoilowich (1957) [B.75], the test arrangement was different to that of Weissert (1997) [B.78] with respect to the pre-swirl and the pre-swirl was varied. With static test data, i.e. McGreehan and Schotsch (1987) [B.77] the pre-swirl effect is excluded. For rotating holes with corner rounding the pre-swirl is much more important than for sharp edged holes.

Furthermore, it is suggested to differentiate between disc windage and the associated flow-field and flow through rotating holes. Both are at least to a small extent coupled according to the design of the different test facilities. The disc windage yields the boundary conditions for the rotating holes and both should be assessed separately (laser measurements). It is mainly important to know the core rotation factor and to use it as input to calculate the Cd-value of the rotating holes from the amount of pre-swirl.

B.6.5.5 Conclusions for Rotating Holes

- It is recommended to plot related Cd-values in the relative frame of reference against U/Wid.
- If U/Cax is used on the horizontal axis, errors due to the coupling with Cd can occur in case the correlation is used for extrapolating beyond the test data.
- The difference between the various test results is not understood.
- New test results are required to clarify the latter point and to refine the correlations.

B.6.6 Two Phase Flow

Only those correlations are chosen for this chapter which are easy to handle for engineering purposes and as there is not much experience in this field, test data are added to give more confidence into the application.

In Zimmermann et al. (1991) [B.81] a review was published mainly based on water/air test results. Since then, new correlations have come forward and oil/air test results are available. Because of limited space the formulas or basic diagrams are not reproduced, they have to be taken from the references. The air/oil test data are taken from an ongoing research program and a forthcoming thesis from R. Fischer.

B.6.6.1 Pipe Flow

The Lockart and Martinelli (1949) [B 82] correlation is still in use, therefore it has been compared with those of Storek and Brauer (1980) [B.83], Friedel (1978) [B.84] and air/oil test results (**Figure B.123**). As already stated in Zimmermann et al. (1991) [B.81] the correlation of Friedel is recommended.

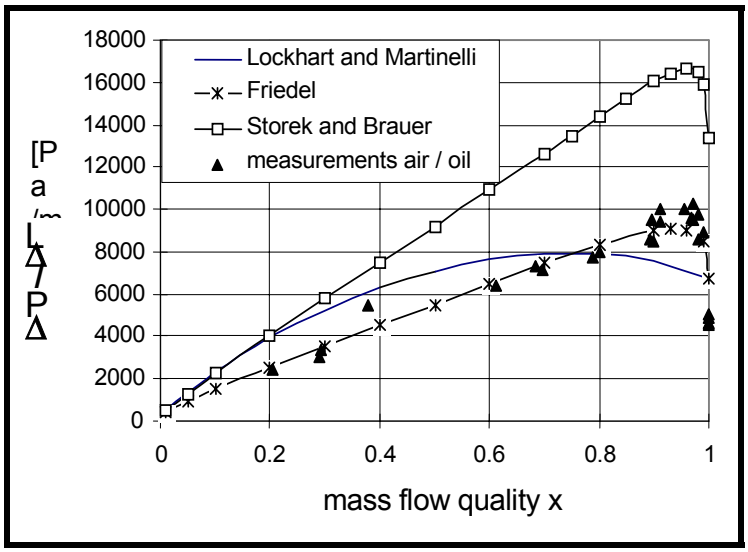

Figure B.123: Comparison of Available Correlations with Air/Oil Measurements.

B.6.6.2 Bends

In order to take into account the effect of de-mixing the pressure loss in the exit line has to be considered. For bends two calculation methods are available, which both are simple combinations of pure bend losses, Chisholm (1980) [B.85], and pipe losses Friedel (1978) [B.84] or Storek and Brauer (1980) [B.83]. It can be seen from **Figure B.124** that both have their shortcomings if it is assumed that the test data are representative for engine conditions.

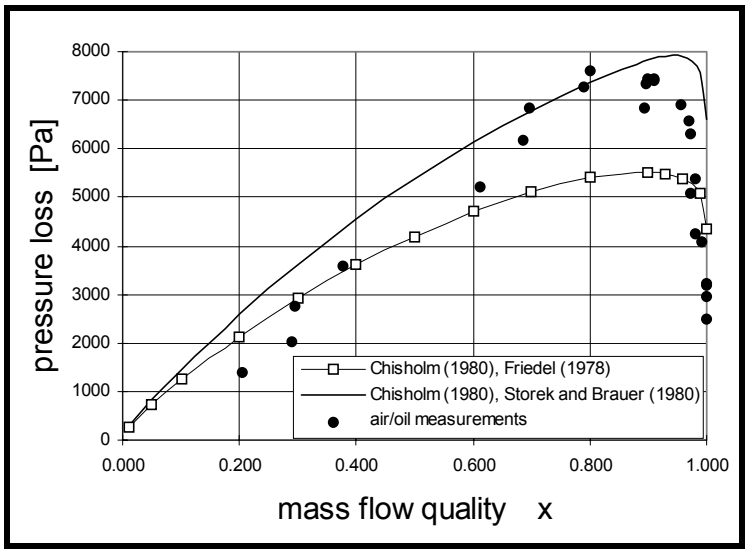

Figure B.124: Pressure Loss of a 90° Bend –
Comparison of Available Correlations with Air/Oil Measurements.

B.6.6.3 Mitre Bends

Figure B.124 shows the pressure loss comparison of a 90° mitre bend with correlations from Chisholm (1980) [B.85] and from Theissing (1980) [B.86], it can be seen that the Chisholm correlation fits better but for pure air there is a big discrepancy. For a 60° mitre bend the situation is very similar, **Figure B.125**.

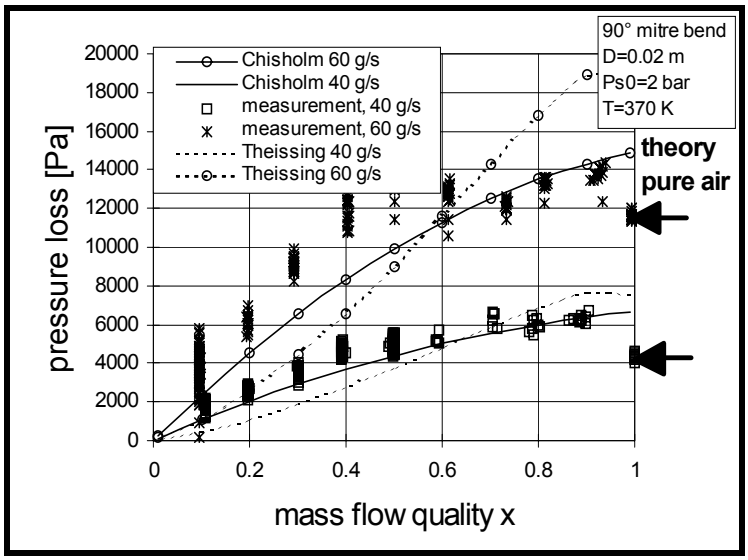

Figure B.125: Pressure Loss of a 90° Mitre Bend.

B.6.6.4 Stationary Orifices

In **Figure B.126** the data resulting from Fischer (1995) **[B.87]** are compared to air/oil test data. It can be seen that the comparison is favorable. The measurements are obtained from a mixture of sharp edged and chamfered entry configurations of the orifice. It seems that the oil smoothes the edges and, therefore, it is questionable whether there is a vena contracta at all.

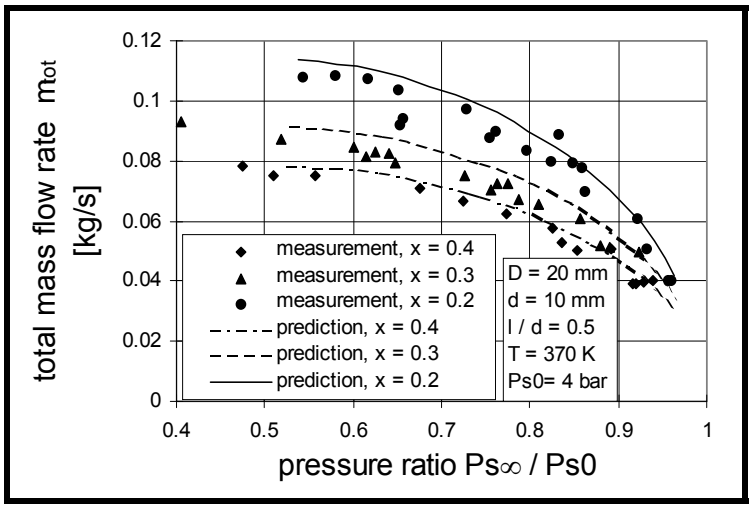

Figure B.126: Subcritical Mass Flow Rate through an Orifice – Comparison between Prediction and Measurement.

Figure B.127 shows the critical mass flow rate as a function of mass flow quality. Again, it can be seen that there is no difference between sharp edged and chamfered orifices. The comparison is very good.

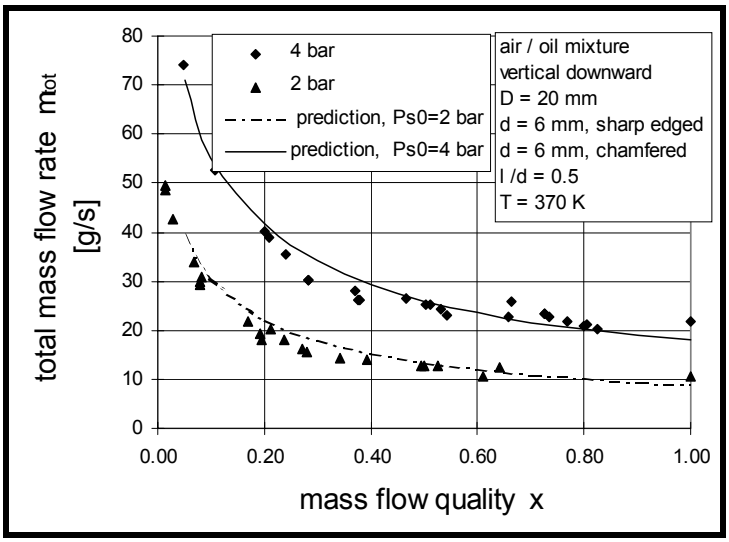

Figure B.127: Critical Mass Flow Rate through an Orifice – Comparison between Prediction and Measurement.

The two phase flow through orifices can be described by the following formula:

$$\left(\frac{m\,x^{0.44}\sqrt{T}}{Po\;A}\right) = Cd\,'\cdot\left(\frac{Ps\,,\infty}{Po}\right)^{1/\gamma}\sqrt{\frac{2\gamma}{R\,(\gamma-1)}\left[1-\left(\frac{Ps\,,\infty}{Po}\right)^{\frac{\gamma-1}{\gamma}}\right]} \qquad \textbf{Eq. B-80}$$

Cd' can be obtained from pure air correlations for instance from Parker and Kercher (see ***Section B.6.8*** for full reference).

The relevant critical mass flow function equals:

$$\frac{mx^{0.44}\sqrt{T}}{Po\cdot A} = 3322.1 = Qcrit \qquad \textbf{Eq. B-81}$$

Figure B.128 summarizes all the test results, which show a scatter band of approximately +/- 10 % which is not bad for two phase flow.

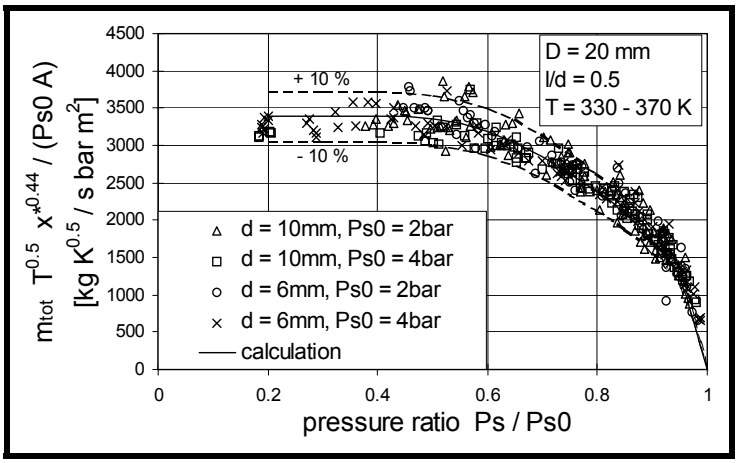

Figure B.128: Two Phase Orifice Flow Characteristic.

In **Figure B.129** the critical mass flow for orifices from different authors are compared to rig and engine measurements, which are in line with the already quoted value of Qcrit of 3322.1. It is considered that the difference arises from the method of generating air/oil mixtures. In the literature, frozen conditions are the objective. The rig results from the forthcoming thesis are obtained from a rig set up which simulates the engine conditions.

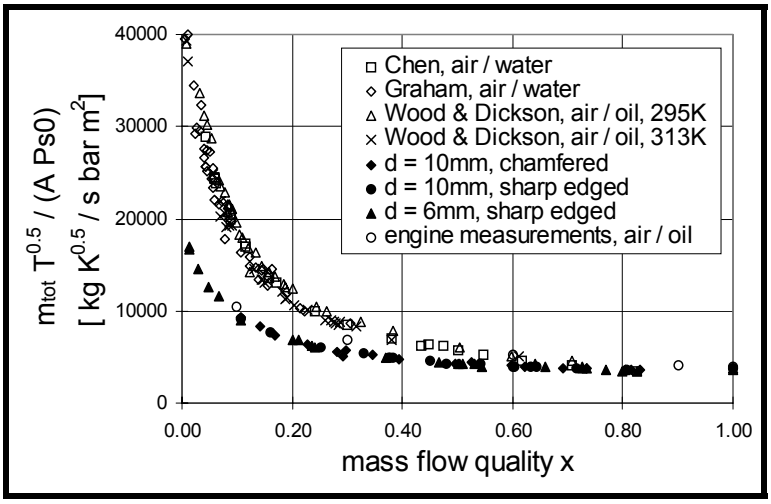

Figure B.129: Mass Flow Function of Critical Orifice Flows.

B.6.6.5 Conclusions for Two Phase Flows

- For straight pipes the correlation of Friedel (1978) **[B.84]** is recommended.
- The correlations for bends are not satisfactory. More research is required.
- The correlations for mitre bends from Chisholm (1980) **[B.85]** have to be adjusted for pure air.
- For orifices satisfactory correlations for practical applications are put forward.

B.6.7 References for Aerodynamics for Air Systems

[B.58] Möller, M., "EJ 200: Durchflußbeiwerte für Spaltabzweigungen in Verdichtern", Technischer MTUBericht, Liu, X., 1997, "Flow in a Corotation Radial Inflow Cavity Between Turbine Disc and Coverplate", ASME Paper # 97-GT-137, 1990.

[B.59] Dittrich, R.T. and Graves, C.C., "Discharge Coefficients for Combustor-Liner Air Entry Holes: Circular Holes with Parallel Flow", NACA-TN3663, 1956.

[B.60] Rohde, R.E., Richards, H.T. and Metger, G.W., "Discharge Coefficients for Thick Plate Orifices with Approach Flow Perpendicular and Inclined to the Orifice Axis", NASA TN D- 5467, 1969.

[B.61] Farthing, P.R., "The Use of Deswirl Nozzles to Reduce the Pressure Drop in a Rotating Cavity with a Radial Inflow", ASME Paper # 89-GT-184, 1989.

[B.62] Schmitz, D., "Analyse von Axialen und Radialen Vordralldüsensystemen", Technischer MTU Bericht, 1995.

[B.63] Popp, O., Kutz, J. and Zimmermann, H., "CFD-Analysis of Coverplate Receiver Flow", ASME Paper # 96-GT-357.

[B.64] Hasan, J.C., "Flow in a Cover-Plate Pre-Swirl Rotor-Stator System", ASME Paper # 97-GT-243, 1997.

[B.65] Zimmermann, H., "Some Aerodynamic Aspects of Engine Secondary Air Systems", ASME Paper # 89-GT-209, 1989.

[B.66] Trutnovsky, K. and Komotori, K., "Berührungsfreie Dichtungen", VDI – Verlag, 1981.

[B.67] Hodkinson, B., "Estimation of the Leakage Through a Labyrinth Gland", Proceedings Inst. Mech. Eng. Vol. 141, pp. 283-288, 1940.

[B.68] Zimmermann, H. and Wolff, K.H., "Comparison between Empirical and Numerical Labyrinth Flow Correlations", ASME Paper # 87-GT-86, 1987.

[B.69] Zimmermann, H., Kammerer, A. and Wolff, K.H., "Performance of Worn Labyrinth Seals", ASME Paper # 94-GT-131, 1994.

[B.70] Stocker, H.L., "Determining and Improving Labyrinth Seal Performance in Current and Advanced High Performance Gas Turbines", AGARD-CP-273, 1978.

[B.71] McGreehan, W.F. and Ko, S.H., "Power Dissipation in Smooth and Honeycomb Labyrinth Seals", ASME Paper # 89-GT-220, 1989.

[B.72] Millward, J.A. and Edwards, M.F., "Windage Heating of Air Passing Through Labyrinth Seals", ASME Paper # 94-GT-56, 1994.

[B.73] Waschka, W., "Zum Einfluß der Rotation auf das Durchfluß- und Wärmeübergangsverhalten in Labyrinthdichtungen und Wellenduchführungen", Dissertation, Universität Karlsruhe, 1991.

[B.74] Snow, E.W., "Diskussionsbeitrag", Proc. Inst. Mech. Engrs., Vol. 166, 1952.

[B.75] Samoilowich, G.S., "Coefficients of Flow Through Pressure Equalizing Holes in Turbine Discs", D. S. I. R. Translation C. T. S. No. 541, 1957.

[B.76] Meyfarth, P.F. and Shine, A.J., "Experimental Study of Flow Through Moving Orifices", J. of Basic Engineering, pp. 1082-1083, 1965.

[B.77] McGreehan, W.F. and Schotsch, M.J., "Flow Characteristics of Long Orifices with Rotation and Corner Radiusing", ASME Paper # 87-GT-162, 1987.

[B.78] Weissert, I., "Numerische Simulation reidimensionaler Strömungen in Sekundärluftsystemen von Gasturbinen unter besonderer Berücksichtigung der Rotation", 1997, VDI Fortschrittsbericht, Reihe 7, Nr. 313.

[B.79] Grim, R.E., "Fluid Flow Characteristics Through Orifices in Enclosed Rotating Discs", M.S. Thesis, AFIT, 1969.

[B.80] Reichert, A.W., Birillert, D. and Simon, H., "Loss Prediction for Rotating Passages in Secondary Air Systems", ASME Paper # 97-GT-215, 1997.

[B.81] Zimmermann, H., Kammerer, A., Fischer, R. and Rebhan, D., "Two-Phase Flow Correlations in Air/Oil Systems of Aero Engines", ASME Paper # 91-GT-54.

[B.82] Lockart, R.W. and Martinelli, R., "Proposed Correlation of Data for Isothermal Two Phase, Two Component Flow in Pipes", Journ. Chem. Eng. Progr., Vol. 45, pp. 39-48, 1949.

[B.83] Storek, H. and Brauer, H., "Reibungsdruck-verlust der Adiabaten Gas/Flüssigkeits- Strömung in Horizontalen und Vertikalen Rohren", VDI Forschungsheft Nr. 599, 1980.

[B.84] Friedel, L., "Druckabfall bei der Strömung von Gas/Dampf-Flüssigkeits-Gemischen in Rohren", Chem. Ing. Technik, Vol. 50, pp. 167-180, 1978.

[B.85] Chisholm, D., "Two-Phase Flow in Bends", Int. J. Multiph. Flow, Vol. 6, pp. 363-367, 1980.

[B.86] Theissing, P., "Eine allgemeingültige Methode zur Berechnung des Reibungsdruckverlustes der Mehrphasenströmung", Chemie-Ing.-Techn. 52, Heft 4 (1980).

[B.87] Fischer, R., "Calculation of the Discharge Characteristic of an Orifice for Gas-Liquid Annular Mist Flow", Int. J. Multiph. Flow, Vol. 21, 1995.

B.6.8 Additional Bibliography for Aerodynamics for Air Systems

Idel'chic, I.E., "Handbook of Hydraulic Resistance", Atomic Energy Com. And Nat. Science Found, AEC - TR 6630, 1960.

Oates, G., "Aircraft Propulsion Systems Technology and Design", AIAA Education Series, 1989.

Chen, D.K., Chen, Z.H., Zhao, Z.S. and Zhua, N., "The Local Resistance of a Gas-Liquid Two-Phase Flow through an Orifice", Int. Journal of Heat and Fluid Flow, Vol. Nr. 3, pp. 231-238, 1986.

Graham, E.J., "The Flow of Air-Water Mixtures through Nozzles", NEL Report, No. 308, 1967.

Parker, D.M. and Kercher, D.M., "An Enhanced Method to Compute the Compressible Discharge Coefficient of Thin and Long Orifices with Inlet Corner Radiusing", HDT- Vol. 183, Heat Transfer in Gas Turbine Engines, ASME 1991.

Meierhofer, B. and Franklin, C.J., "An Investigation of a Preswirled Cooling Airflow to a Turbine Disc by Measuring the Air Temperature in the Rotating Channels", ASME Paper # 81-GT-132, 1981.

Wood, J.D. and Dickson, A.N., "Metering of Air-Oil Mixtures with Sharp-Edged Orifices", Dep. Mech. Eng. Rep., Heriot-Watt University, Ricarton, Edinburgh, UK, 1973.

B.7 CONTROL SYSTEMS MODELING

B.7.1 Requirements for Modeling Control Systems

The standard of fuel system and actuator modeling that is required depends on the objective for the work. When the objective is to analyze and develop a control-system, then very detailed models of the hardware and software will be required. When the basic control is functioning satisfactorily, and the objective is to evaluate engine performance and handling, the control system models can usually be simplified significantly.

Simplification of the control system models for engine handling and performance work is required to obtain acceptable run times for the model. The detailed control models normally require shorter integration time steps than are acceptable for engine handling work.

Acceptable control-system models for engine handling work can be developed using simple transfer-functions and the steady-state characteristics of the control. It may be necessary to change the coefficients of the transfer functions with engine operating conditions. The information required to define suitable transfer functions for the control systems can be obtained from the more detailed models that should have been built to facilitate control design.

Where control-system dynamics must be modeled accurately, then all dynamic valves need to be modeled as first or second-order systems. For all valves, fluid pressure, spring force, friction effects, leakage and the effect of fluid masses should be considered and included where appropriate. Fluid pressure-drop-to-flow relations and fuel compressibility should be modeled throughout the system. The effects of flow forces (Bernoulli Forces) should be included in valves that operate at low force levels.

It is not practicable to model the effects of heat transfer and other thermal effects in a dynamic control-system model. Where such effects are of interest, a separate model should be built for this purpose, using simplified control modeling.

The effect of manufacturing tolerances can be simulated, in a detailed control-system model, by changing parameters within the model. It is rarely practical to include terms for all components where tolerances could influence control performance, so engineering judgment must be used in determining how to model particular scenarios. The same constraints apply to modeling of failures within the control system.

Modern controls are built around electrohydraulic and electromechanical transducers and actuators. These can often be modeled satisfactorily using the manufacturer's declared characteristics and response data, but more detailed modeling is advisable if performance is marginal. It is also advisable to model delays incurred in the signal conditioning associated with many transducers.

Modeling of the DECU will depend on how detailed the control system models are and what the objectives for the model are. The engine control laws will normally be modeled, but the functionality associated with transducers and output devices may be omitted for the simpler models.

Clearly, control-laws, which are implemented digitally, are bespoke and modeling can only exist at a certain level for a given logical feature. However, a decision may be made to omit a certain branch of logic depending on the application of the model.

There will be other features of a fuel system, which require modeling at the appropriate level of detail, examples being heat-to-fuel, filtration, fuel chemistry changes, pressure losses, and compressibility effects.

B.7.1.1 Types of Models

There are two main types of pump used in modern fuel systems: the fixed displacement type and centrifugal flow pumps. Gear pumps are the most common form of fixed displacement pump and are widely used in modern, main-engine fuel-systems. Centrifugal pumps are used primarily in low-pressure fuel supply systems but are increasingly finding applications in reheat controls.

In the past, variable stroke piston pumps were used in many main engine fuel systems, and vapor core pumps (inlet throttled C.F. Pumps) were used for reheat applications. Although these pumps are to be found on many engines still in operation, they are unlikely to be used on new engine controls and are not described in this report.

B.7.1.1.1 Modeling the Fixed Displacement Pump

This type of pump is probably the simplest to model. The steady state characteristic, **Figure B.130** is used to determine pump delivery flow given pump speed and delivery pressure. There are no dynamics in the pump to be represented.

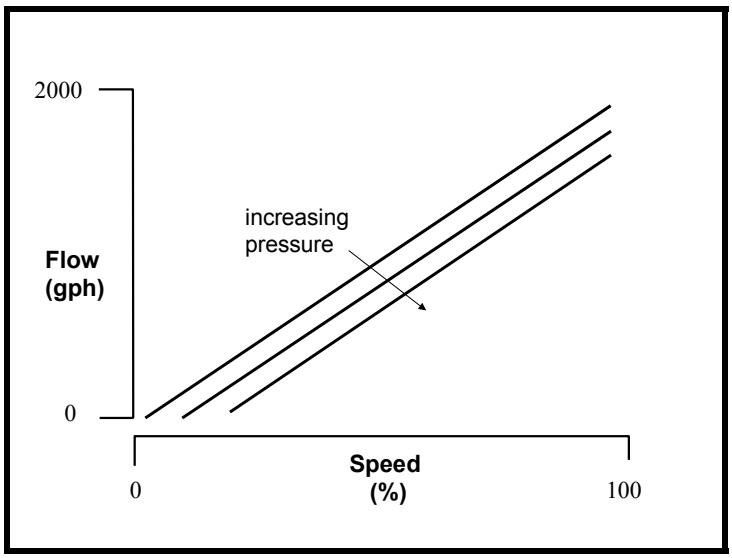

Figure B.130: Fixed Displacement Pump Characteristic.

B.7.1.1.2 Modeling the Centrifugal Pump

The CF pump characteristic (see **Figure B.131**) is more complex than for a fixed displacement pump. Modeling of pump dynamics is not necessary, and pump delivery pressure is determined from the pump characteristics for given speed and delivery flow rate.

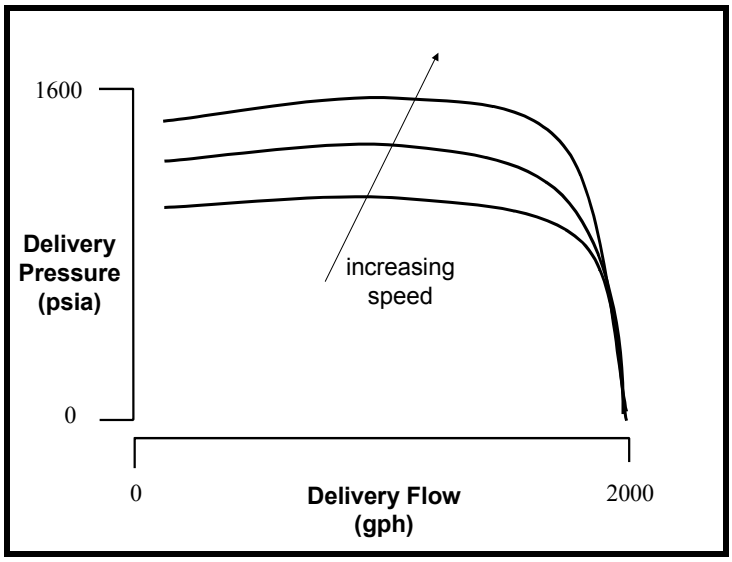

Figure B.131: Centrifugal Pump Characteristic.

To avoid algebraic loops in the model, it may be necessary to include a first order lag as shown in **Figure B.132**. The lag should not exceed 0.01 seconds.

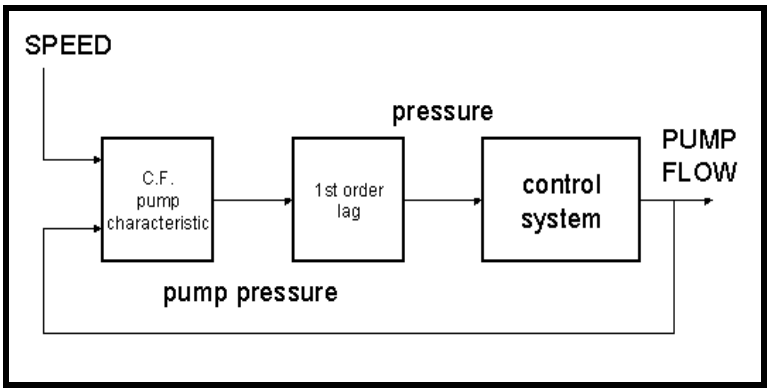

Figure B.132: Avoidance of Algebraic Loops.

B.7.1.2 Equations Used in Hydraulic Control Systems

The following equations are widely used in modeling aero engine control systems and components.

Where:

- Flow: Volume flow rate through orifice;
- Cd: Discharge coefficient;
- CSA: Orifice flow area;
- P: Pressure;
- ΔP: Pressure drop;
- ρ: Fluid density;
- Area: Pressure sensing area;
- Acc: Acceleration;
- Force: Applied force;
- Mass: Effective mass;
- K: Fluid bulk modulus;
- Qnet: Net flow into a chamber; and
- Vol: Volume of chamber.

The equations are valid for any consistent set of units (**Figure B.133**).

$$flow = Cd.CSA.\sqrt{\frac{2\Delta P}{\rho}}$$

$$force = P.area$$

$$acc = \frac{force}{mass}$$

$$P = \int K.\frac{Qnet}{vol}.dt$$

Figure B.133: Hydraulic Control System Equations.

B.7.1.3 Electro-Hydraulic Servo Valves

Modern engine control systems are operated using several types of electrohydraulic servo valve. The most common types are:

- Solenoid;
- Single stage servo valve – flapper, jet deflector and jet pipe types; and
- Two-stage servo valve – using one of the above first stages to drive a second stage spool.

Response of these servo valves can normally be ignored for engine handling work, as the bandwidth of the devices is typically above 100 Hz. For more detailed work, the manufacturer's response data can be used, and an example of a two-stage servo valve is shown later. For detailed analysis of the control systems, it is often necessary to model individual components within the servo valves, but this is beyond the scope of this document.

The solenoid valve is usually used for on-off operations and can often be treated as a simple switch. Where the response is critical, the device can be represented as a first order lag with a time constant obtained from the manufacturer's data.

A schematic of a single-stage flapper-valve is shown in **Figure B.134**, the jet deflector and jet pipe devices are similar, although the steady state characteristics need to be treated differently when detailed models are required.

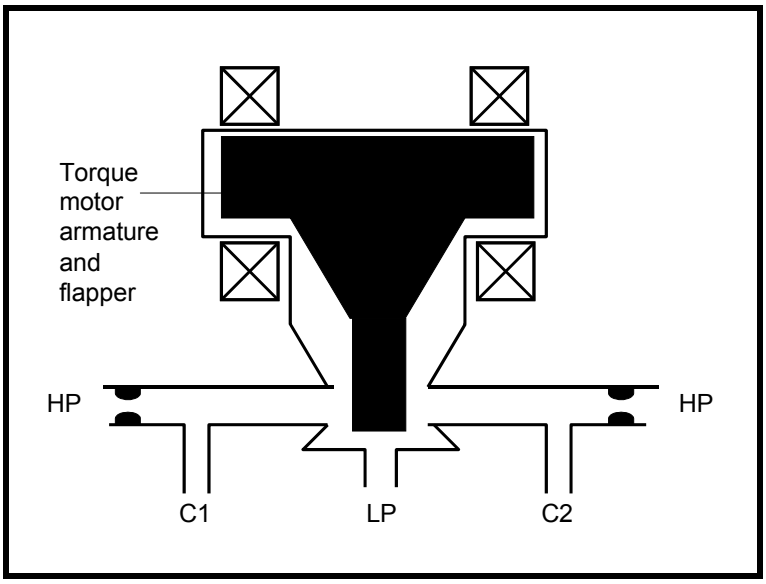

Figure B.134: Single Stage Flapper Valve.

For engine handling work the single stage servo valve response can normally be ignored, because the bandwidth is typically above 100 Hz. Use of a flapper-type servo-valve as the first stage of a two-stage servo valve is shown, as an example, in a later section.

B.7.1.4 Metering Valve

The metering valve (**Figure B.135**) is a variable orifice, usually controlled by a spool valve. The flow through the metering valve is proportional to the orifice area and the square root of the pressure drop across the orifice, which is set by a pressure drop regulator.

The metering orifice is normally machined in a sleeve and is opened and closed by varying the travel of a spool inside the sleeve (see below). An LVDT or other transducer measures the metering valve travel, and a single or two-stage servo valve controls it (see example of two-stage valve). The control loop is closed by the DECU.

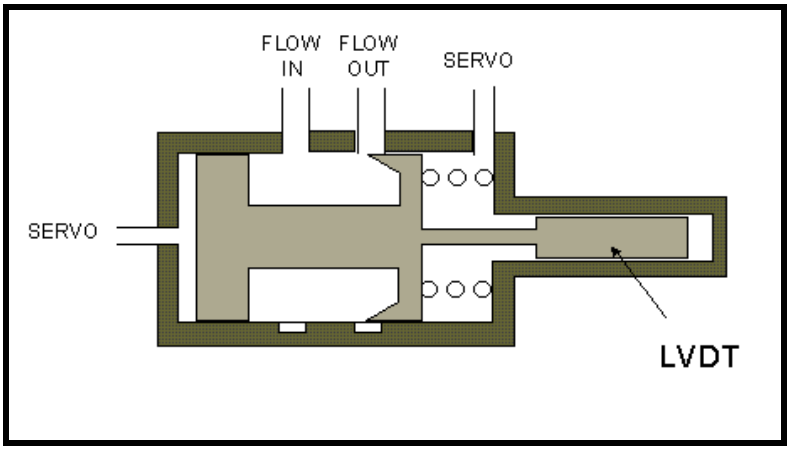

Figure B.135: Metering Valve.

The response of the loop will be a function of: the control algorithm in the computer, the response and gain of the servo valve, the diameter of the metering valve spool, the supply and return pressures available, and any loads on the metering spool.

Typically, the metering valve loop can be represented by a first order response with a time constant of 0.015 to 0.03 seconds. This should be adequate for engine handling work, but more detailed modeling is required to investigate any problems with the control.

B.7.1.5 Pressure Drop Regulator

The purpose of the pressure drop regulator is to set the required pressure drop across the metering orifice. The required pressure drop may be constant or, if correction for fuel temperature is required, the pressure drop may be made a linear function of fuel temperature.

The metering pressure drop is controlled by spilling excess flow when a fixed displacement pump is used, or by throttling when a C.F. pump is used. Both direct acting and servo pressure-drop regulators may be used.

The response of the pressure drop regulator is normally much faster than that of the metering valve, and can be ignored for engine handling work; only the steady state characteristics of the valve need be included. Where fuel system problems are to be investigated, a more detailed PDR model is required, but this is beyond the scope of this document.

B.7.1.6 Power Actuators

These are used to control IGVs, nozzle area and other engine components. Typically the power actuator is a ram, with the servo supply set by a two-stage servo valve (**Figure B.136**). An LVDT or other transducer measures Ram position, and a digital computer is used to close the loop. Provided that the control has been correctly designed, the response of the servo valve will be insignificant in the overall control loop. An acceptable model can be obtained by setting the ram velocity as a function of DECU drive current and available pressure drop across the servo valve, after allowing for the pressure required to overcome actuator loads.

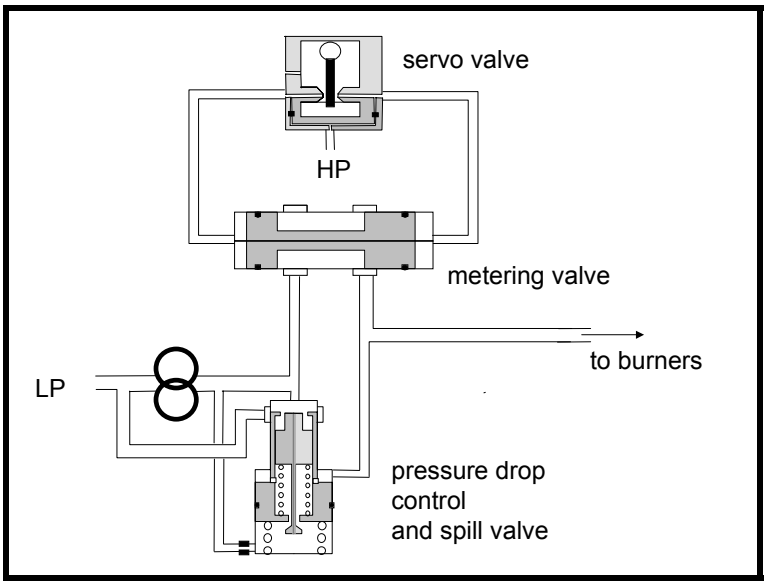

Figure B.136: Schematic of Main System Components.

B.7.1.7 Modeling a Two-Stage Servo Valve (Moog Type)

A schematic of the valve is shown in **Figure B.137**.

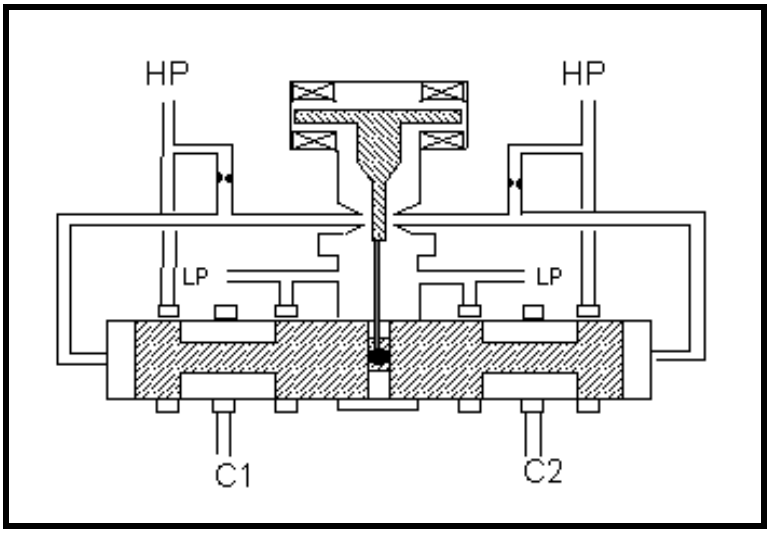

Figure B.137: A Two-Stage Moog Valve.

In the steady state condition, servo fluid, at servo supply pressure, passes through identical restrictors to the nozzles on each side of the flapper. The flapper is equidistant from each nozzle, so equal pressures and flows are generated at each side of the flapper. The pressures at the flapper are felt on the spool ends and, as the pressures are equal, the spool remains stationary.

When drive current is applied to the motor, it produces torque on the first stage, and the flapper and motor armature deflect. With the flapper deflected, the nozzle flows are no longer equal and the difference in flow results in spool displacement. As the spool displaces, it bends the feedback wire producing a torque at the armature to balance the motor torque. A new equilibrium position will occur when the flapper is

again centered between the nozzles and the feedback wire torque balances the motor torque, with the spool displaced from its null position.

As the spool moves, it varies the flow numbers between its output ports (C1 and C2) and the supply and return pressures. These flow numbers may vary linearly with spool travel or be profiled for custom applications.

An external driven device (e.g. a metering valve) will be connected to ports C1 and C2 so that the velocity of the driven valve will be a function of the control spool displacement, the supply and return pressures available and the loads on the driven valve.

Figure B.138 shows a relatively detailed model of the above valve and the equations **Figure B.139** used to build it. For any detailed dynamic analysis of engine and control systems, a model of this complexity will be required but, for engine handling work, the response of the valve may be reduced to a first-order transfer-function with break frequency = Kv rad/sec.

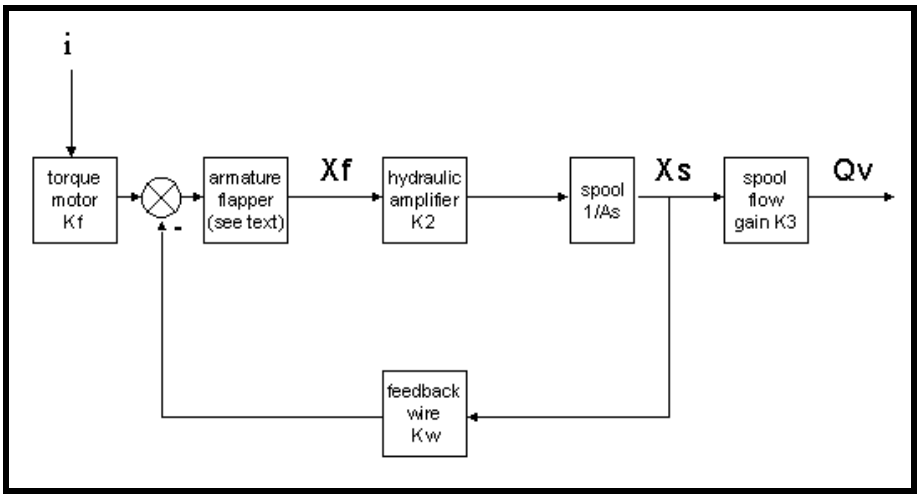

Figure B.138: Two-Stage Servo Valve Block Diagram.

Armature flapper characteristic

$$\frac{\frac{1}{Kf}}{1+\left(\frac{2\zeta}{\omega_n}\right)s+\left(\frac{s}{\omega_n}\right)^2}$$

where :

$\omega_n = \sqrt{\frac{Kf}{Lf}}$ first stage natural frequency

$\zeta = \frac{Bf}{2.Kf}.\omega_n$ first stage damping ratio

$Kv = \frac{K2.Kw}{Kf.A}$ servo valve loop gain

Figure B.139: Valve Control Laws.

Where performance variations of the valve need to be investigated, or a possible problem with the valve is suspected, the *hydraulic amplifier* block will need to be modeled in more detail, but the degree of complexity required is beyond the scope of this report.

The manufacturer for each valve design can supply the following data.

- I: Torque motor current;
- Xf: Flapper displacement at nozzles;
- Xs: Spool displacement;
- Qv: Servo valve control flow;
- K1: Torque motor gain;
- K2: Hydraulic amplifier flow gain;
- K3: Flow gain of spool;
- A: Spool end area;
- Kf: Net stiffness of armature/flapper;
- Kw: Feedback wire stiffness;
- Bf: Net damping on armature/flapper; and
- Lf: Rotational mass of armature/flapper.

B.7.2 Control Integration with Engine Model

Consider the *traditional* roles of the performance and controls engineers, in terms of the engine functional definition. The performance engineer determines the appropriate way to control the engine to meet certain performance requirements within thermodynamic constraints. This will cover both transient and steady state aspects of the engine performance. The controls engineer will determine suitable control laws to allow the engine to operate according to the identified constraints, such as control loops. There is, of course, a considerable *gray area* between the two, the extent of which increases with engine complexity. It is sometimes difficult to distinguish between the *performance requirements for engine control* and *feasible ways of controlling gas-turbine engines*. It is therefore important to remove as many of the working barriers between the two areas as possible, so that the functional definition process becomes co-operative, thus facilitating an iterative engineering approach. The final solution may be a compromise of the ideals perceived by each area.

Each area may use different computing environments and tools for the differing engineering tasks. *Pure* performance work is generally based around development of an engine understanding through synthesis and analysis of engine test data. Where a control-system model is required to support this work, it is usually of a known, bespoke standard. In the past it has been common to see control-system models coded independently in the performance area, without reference to any similar model existing in the controls area. Such a duplication of effort has clear disadvantages in operational, program and risk terms Marcus S Horobin May (1998) **[B.88]**.

There are two fundamental issues:

- Provision and interfacing of a single *engine model*, used across all functional engineering activities; and
- Provision and interfacing of a single *control-system model* used across all functional engineering activities.

B.7.2.1 Common Engine Model

Configuration control of the models is essential, and has the same importance as configuration control of the end products – engines. Engine models must be released to the controls area, and controller models must be released to the performance area. A central repository containing all models may be the ideal, but network constraints may force the use of copies in each area; this needs careful handling.

Figure B.140 shows the common scenario of an engine model supplied by a specialist area for control-system development work using a proprietary development environment such as MATRIXx or MATLAB.

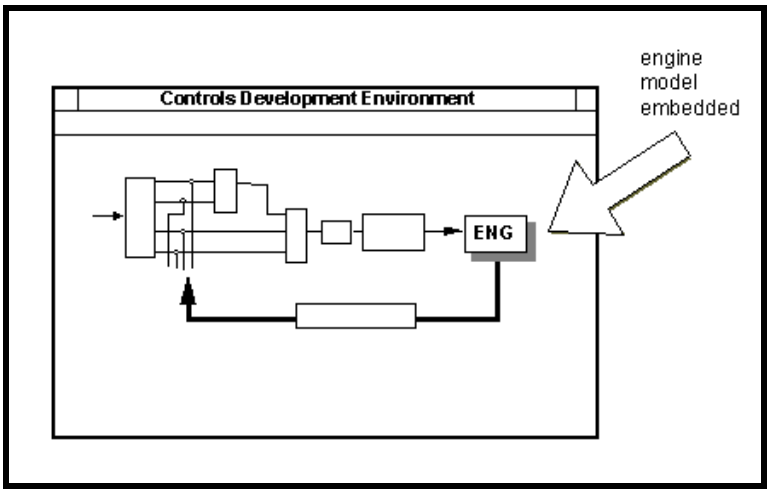

Figure B.140: Engine Model Imported (Embedded) in Controls Development Environment.

The main challenges arise from the interface of different modeling tools. Embedding sub-system models into other host environments is one approach; the use of shared memory or other inter-process communication interfaces such as CORBA (Common Object-Requested Brokerage Architecture) may be more appropriate. This is because it offers greater flexibility arising from the separate configuration of the models. A CORBA based model can be cross language, cross operating system and cross hardware platform. The combined model is not a single executable, but consists of separate elements that are based on object-oriented design. This has advantages in keeping the accountability for the subsystem models with the model creator. **Figure B.141** below shows the engine and controller each running in their home environments, communicating by shared memory. For the controls user, there is no significant difference to the setup as shown in **Figure B.140**. However, there is now the potential to drive the simulation from the performance environment as may be required (see below).

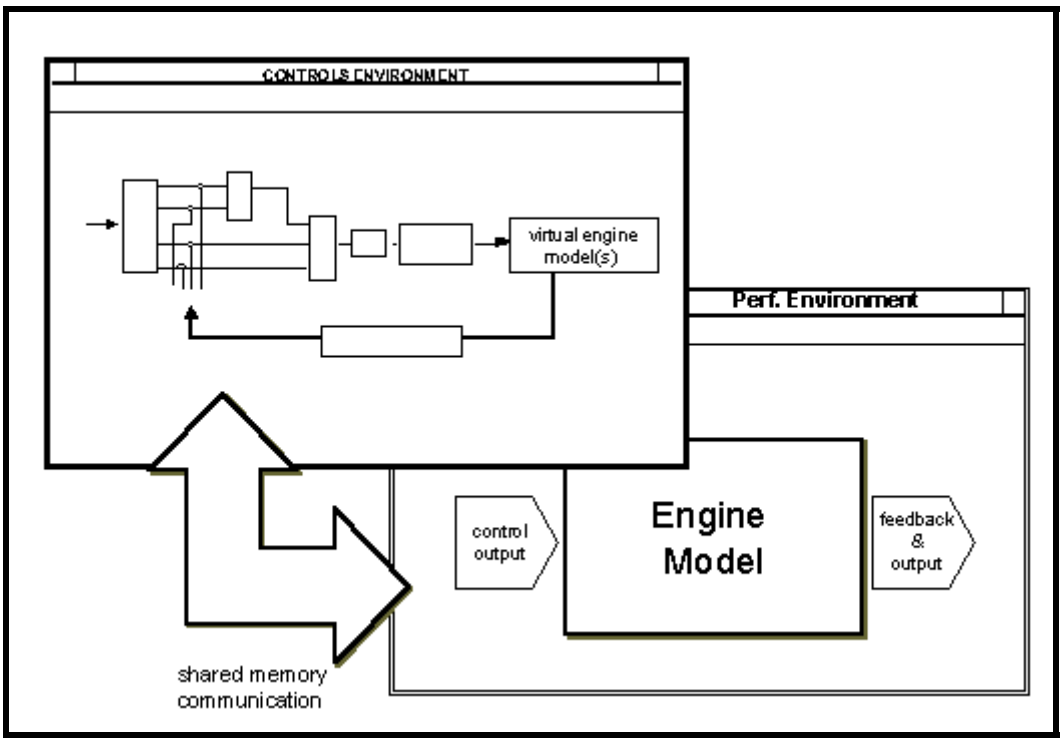

Figure B.141: Engine and Control-System Models Running Together with Inter-Process Communication.

It is common practice for engine models to be written in FORTRAN although the emphasis is shifting towards C. As such, an engine model may be imported into proprietary development environments in the form of a user code block. Custom interface routines may be required. The interface routines should allow easy routing of additional signals if required.

Development environments such as MATLAB or MATRIXx have suites of tools (toolboxes) with which the model must be compatible. It is common practice for all dynamic elements in a system to be numerically integrated by the host environment. Several integration algorithms are available; the most appropriate for the particular dynamics present, can be chosen. This said, some engine models might perform their own integration internally. Iterative techniques used in thermodynamic solutions facilitate implicit integration approaches that may have certain advantages in numerical stability. Engine models are also manipulated to generate linear models in state-space form.

In the early stages of a project, it is common to find that some control variables are not modeled as independent program input variables. For example, a variable mixer may be present in the engine concept, but early performance studies do not need a geometry-to-thermodynamic-effect calculation. This is because the model can be matched by prescribing what such a feature has to achieve, rather than predicting the effect of a specified geometry. Clearly, in the case of control-system design, a geometry model is required, although some simplification may be acceptable at the preliminary stage.

B.7.2.2 Using Performance (Cycle-Match) Models for Control-System Design and Analysis

Control engineers are perhaps most familiar with engine models presented in the form shown in **Figure B.142** below. The engine is a dynamic simulation, which requires the host environment to perform the numerical integration of state derivatives. Often explicit integration techniques are used such as Runge-Kutta 4th order. A model presented in this form is also able to be linearized (see below). Whereas this is the

standard model form used in many areas of dynamic modeling, it is one particular form (of several) in which a performance model may be presented. It can be thought as a *states-matching mode*. This reflects the model's function of finding a solution (by iteration) to a *question* posed in terms of specified values of inputs [u] and states [x].

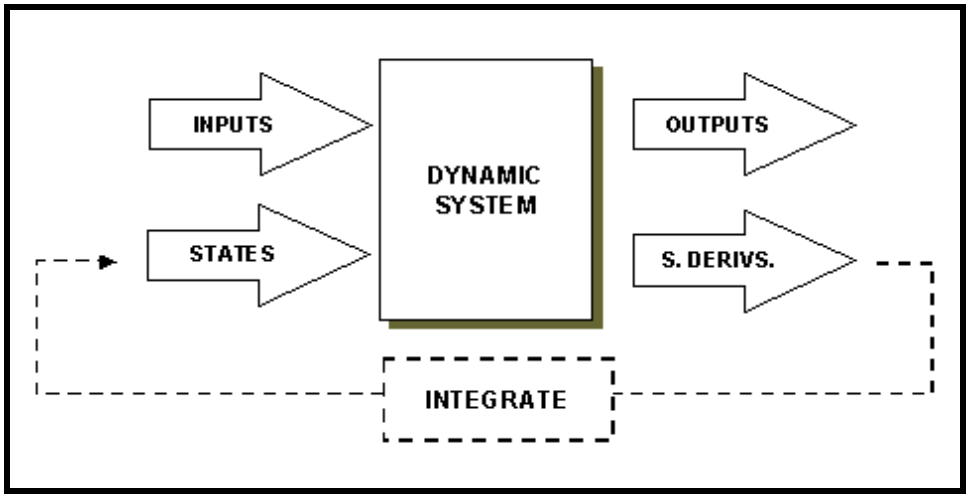

Figure B.142: A General Form of Dynamic Model using External Integration for Simulation.

- **Inputs** [u] are boundary terms, e.g. environmental temps, pressures, fuel-flows and geometry for an engine;
- **Outputs** [y] are parameters of interest, e.g. thrust, specific-fuel consumption, surge margin;
- **States** [x] are those parameters whose responses are governed by a differential (dynamic) equation, e.g. shaft speed; and
- **State Derivatives** [xdot] are the time differentials of the state variables.

B.7.2.2.1 Linearization

In order to linearize the engine model, it must be presented in this form – i.e. with states set up as program input, and state derivatives as output. Thus the model may be manipulated (by parametric perturbation of states and inputs) around a base point to generate the linear (partial-derivative or state-space) engine representation which is necessary for standard controller design and analysis methods.

B.7.2.2.2 Steady-State Synthesis (Initialization)

Consider the engine model presented as shown in **Figure B.143**. In order to generate a steady-state solution for a prescribed set of boundary conditions (inputs, e.g. fuel flow), the values of the state variables have to be ascertained. With a performance model, this is achieved by the iteration that is also used for the thermodynamic solution. With other types of engine model which do not use iteration, the initial values of states can be determined in several ways:

- By invoking an external iteration function, *trimming*, which varies the states to achieve a zero state-derivative (at fixed inputs).
- By running a *settling transient* where the states are initialized at arbitrary values and the simulation run over a period of time at constant inputs until steady state is achieved. Thus the initial combination of *arbitrary states* and *prescribed (fixed) inputs* combine to give a non-zero state-derivative. This is numerically integrated to predict the next time-step value of state variable. The model should eventually achieve steady state where xdot = 0.

- By using table look-ups of states vs. inputs for steady-conditions.
- By setting the inputs and states at values stored from a previous run (not necessarily a steady-condition), moving the input variables to the required values over a time-base, and allowing the model to achieve steady-state.

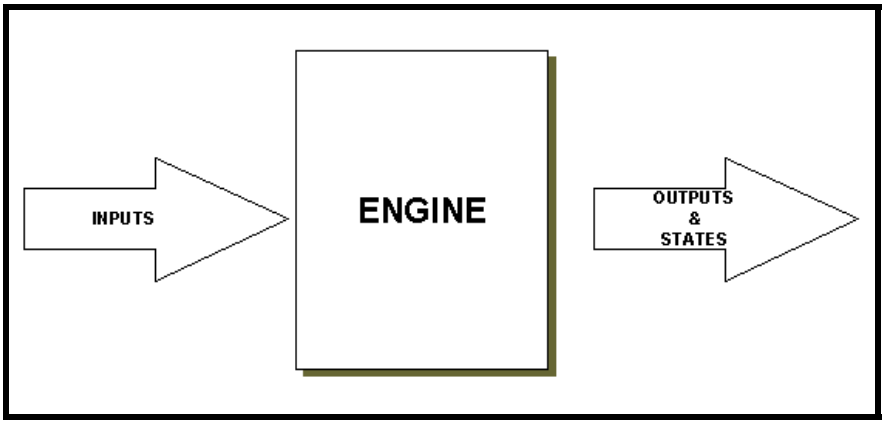

Figure B.143: Performance Model Showing Steady-State Mode.

None of this is necessary with a performance model running in *steady-state* mode.

Given fixed values of control inputs, a steady-state solution is generated. The steady condition may also be specified in terms of a specified level of output parameter (e.g. thrust) or internal engine parameter (e.g. compressor operating point).

Steady-state mode can be used to define the base points around which the model may be linearized. *States-matching* mode is selected after the steady-state point has been generated.

If a control-system model is present, this can be initialized separately or as part of the combined system using the methods described above.

B.7.2.2.3 Simulation (Dynamic or Transient Synthesis)

Although simulation can be achieved using *states-matching* mode (using the host system to integrate), performance models can simulate transients by performing integration internally. Iteration allows integration to be performed implicitly which gives certain advantages in numerical stability. Thus there is a third *transient* mode (**Figure B.144**).

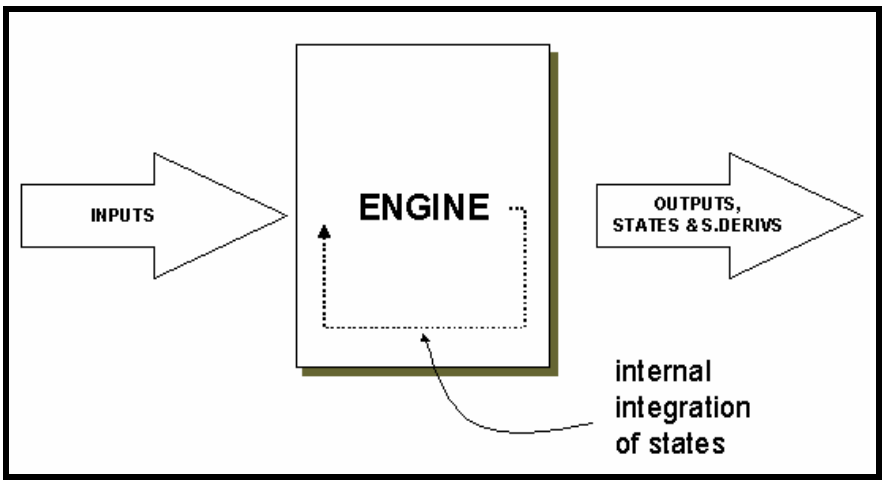

Figure B.144: A Performance Model Running in Transient Mode using Internal Integration.

The base points for linearization are not necessarily at steady-state conditions. Any mid-transient point (generated by *transient* mode) can be selected as a base point for linearization.

Generalization:

- The three modes are fundamentally distinguished by the iteration matching-scheme used to produce the solution in each case (which is transparent to the user). In addition, the dynamics routines are not called in steady-state mode.
- The steady-state matching-scheme is the simplest and does not allow excess power on any shaft, nor any stored W, P or T within a volume. This matching scheme is extended for the states-matching mode and for the transient mode, where an extra matching pair is added for each dynamic equation being considered. Ref. 1 expands on this using a simple example.
- Iterative models are not dependent on the solution of gas dynamics equations for dynamic or transient simulation – valid simulation can be achieved by modeling only the shaft dynamics. Modeling of gas dynamics (volume packing) can be added if required.
- When gas dynamics are *not* modeled, the model sampling frequency is around 5 Hz. With gas dynamics, the bandwidth is increased to 30 – 40 Hz.
- The performance process is largely preoccupied with the prediction and analysis of steady-state performance. Solution by iteration is essential for this type of work. Performance engineers often regard transient synthesis as an extension of the steady-state model. Controls engineers often see things the other way around with the steady state being a particular state of a dynamic system, which is perhaps never truly achievable. However regarded, the modeling techniques are the same.

B.7.2.2.4 Using Control-System Models in Performance and Operability Assessment

Integrated engine and controller models are seldom required in traditional performance activities. However, for operability studies, such as compressor stability assessment, a control-system model is essential. The emphasis is placed on the understanding of engine behavior in response to control-system action. Data interface requirements therefore differ – the performance engineer wants full visibility of internal engine parameters and engine analysis tools. It is also the case that other sub-systems, for instance the secondary air-system and oil systems, should be represented in the best possible way.

Clearly, if a controller model has been developed in a controls development environment, it is desirable that this should also run in the performance environment. Models constructed using Graphical User Interfaces

(GUI) can be represented in pure code forms using proprietary code-writing tools. This facility offers potential for inter-environment use. C and ADA are common languages for this task.

Figure B.145 shows a controller model derived using picture-to-code tool in a performance development environment.

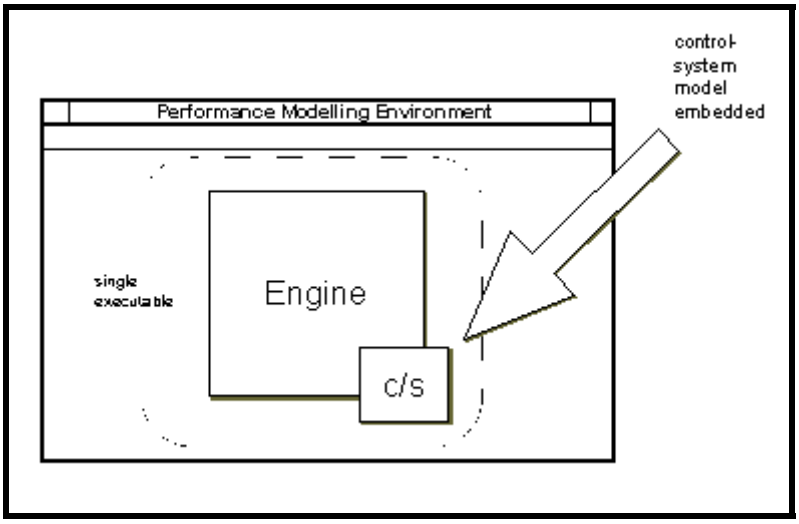

Figure B.145: Control-System Model Imported (Embedded) into Performance Modeling Environment.

Several issues arise:

- Interface of dissimilar languages (e.g. FORTRAN and C);
- Ideally, the control-system and engine model should be separately configurable items;
- The integrated model in this environment should be technically equivalent (in simulation terms) to the alternative scenario of the engine-model imported as a subservient element in the controls environment; and
- Initialization.

In the case of FORTRAN and C, there is little technological challenge in interfacing. It is more a case of careful handling of the different conventions used in the two languages. Naturally, the platform must support both languages.

It is possible to avoid embedding the controller within the engine model, by using the inter-process communication technique shown in **Figure B.141**. For work centered on performance studies, it is desirable that the combined model should be run from the performance domain.

Performance work often involves the prediction of nominal steady-state performance under the action of the control-system, at, say, a particular power demand or rating. For example, as expressed by a certain pilot-lever angle. Ideally, the full, integrated model should be used to generate these points. However, the computing task can become a burden because of the requirement to initialize certain dynamic terms in the combined model.

A control-system (or other engine sub-systems) can also be structured to take on the form in **Figure B.141**. Thus a combined controller and engine model, both exhibiting the form in **Figure B.141** and running in a

development environment (such as MATRIXx or MATLAB) can be initialized in the ways discussed above. Initialization is *not* so straightforward when:

- Any constituent part of a whole system is not in the standard form (**Figure B.142**);
- When constituent parts of the model are spread across different environments (**Figure B.141**); and
- When the whole model is running in an environment that does not feature the *trimming* function (**Figure B.145**).

1 is solved by providing ensuring a standard form, or providing models which are self-initializing.

2 ought not be a fundamental problem if 1) is solved; inter-process communication will be increased for the initialization phase.

3 becomes an issue when using combined models in the performance environment. Often, a *series* of steady-state flight points (for given values of pilot demand) is to be generated. This can require initialization for each point. In such a case, the settling transient method is an excessive burden on execution time. However, there are ways of alleviating this overhead. The transients are not of interest, so some dynamic terms can be muted or modified to reduce settling time (e.g. heat-soakage can be muted and shaft inertia reduced). A problem can arise if this measure is taken to extremes: the whole-system stability may be compromised and therefore prevent a steady condition being achieved! A *trimming* function may be used, however such a facility may not be available in all environments. Also, with an extended iteration scheme, there is a potential convergence hazard with the number of control-system states that may need initialization.

An alternative approach is to use a subset of the controller: the ratings structure, to establish the level of performance in terms of the engine rating parameters. An iterative engine model can be run to such parameters (with due regard to engine limit loops) and converge on a steady-state solution (either on the prescribed rating or on an overriding limit) without any settling period. From this point, the initial conditions in the controller may be determined either by back-calculation or by including controller terms in the iteration loop. The engine condition thus obtained should be identical (within iteration tolerance) to that obtained by transient settling. However, there are some situations when this approach is not feasible. Even with iteration; the time-settling technique is sometimes essential, for instance for engines with switching bleeds or with unusual 'pecking–order' of limits and ratings. The full model is, of course, the best means of determining the steady-state performance, if indeed such a condition exists.

Where the model is being used for *true* transient simulation, the execution time associated with the start point is less significant and so the transient settling method may be acceptable. It may be beneficial in this case to initialize the engine model at an arbitrary fuel flow first, thus giving the controller a feedback consistent with the initial engine input. The combined model can then *bootstrap* to the required steady-state condition, at which point the controller state variables (e.g. numerical integrators) are correctly initialized for the forthcoming maneuver of interest. From the user's point of view, the settling method can be made virtually transparent. The settling transient can be hidden and discarded after steady state has been achieved. The only symptom will be in the execution time.

The issues discussed above extend to other systems such as intakes and secondary air system that interact with the engine.

B.7.3 References for Control Models

[B.88] Horobin, M.S., "Cycle-Match Models Used in Functional Engine Design – An Overview", Presented at the RTO Symposium: Design Principles and Methods for Aircraft Gas Turbine Engines, May 1998.

B.8 EFFECT OF WATER/STEAM INJECTION ON THE PERFORMANCE OF POWER GENERATION GAS

B.8.1 Introduction

The increasing use of gas turbines in the power generation industry has created an additional incentive for the further improvement of their performances. In the last years several techniques have been proposed for gas turbine power and efficiency augmentation, such as steam or water injection at different locations along the gas path.

A first possible location for water injection is the compressor inlet duct. The fact that gas turbine output and efficiency drop during high ambient temperature periods, when demand usually increases, has led to the broad application of inlet air cooling through evaporation of water injected in the form of fine droplets, a technique called inlet fogging. Water injection at some location along the compression path is a means of compression intercooling for performance augmentation. Steam can be injected at a location along the expansion path, as for example between a high pressure and a low pressure turbine of a twin spool engine. The most widely used technique; however, is the injection of water or steam at the exit of the compressor.

Injection of water or steam in the combustion chamber of gas turbines is one of the means to reduce NO_x emissions while it leads to augmentation of power output. Steam injection, in particular, is also a means of improving efficiency. If it is produced with the use of the heat of the exhaust gases, it increases the net efficiency of the gas turbine cycle, by exploiting some of the heat that would otherwise be wasted through the exhaust gases. The term diluent will be used hereafter to denote either steam or water injected in the combustion chamber of a gas turbine.

The reduction of NO_x emission levels through diluent injection has been the subject of many studies. Reviews of such techniques have been reported in **[B.89**, **B.90** and **B.91]**. Relations between the amount of water used and the emissions reduction achieved have been presented in **[B.89** and **B.92]**. On the other hand, since steam injection has a beneficial effect on performance, study of its effects on the overall performance of gas turbine cycles has been the subject of many publications, as for example **[B.93**, **B.94**, **B.95** and **B.96]**. Summaries of the technology and the achievements up to the early nineties have been provided in **[B.97** and **B.98]**.

The effects of the injection on the performance of the gas turbine engine are qualitatively known, (see for example **[B.99]**). Curves of performance parameters dependence on the amount of injected water or steam have been presented by some authors (for example **[B.100** and **B.101]**). Such curves are usually produced with the aid of computational performance models for specific gas turbines. The effect of diluent injection is evaluated by introducing the appropriate parameters in a thermodynamic engine model and comparing the results to those with no injection. A study of this type was also reported in **[B.102]**.

Methods for evaluating the effects of water or steam injection on the performance of a gas turbine will be discussed in the following. The case of diluent injection in the combustion chamber will be covered in more detail, as it has been more extensively studied. Before presenting the techniques for evaluating effects on performance, it is useful to overview the physical mechanisms through which performance is altered.

B.8.2 The Physics of Operational Parameter Deviations

Water or steam injection at some station along an engine has the following consequences:

- Mixing of the injected media with the gas, alters the thermodynamic state of the main gas flow. The mixing can be considered to be at constant pressure. A small pressure drop due to mixing

may occur, but this drop is of small magnitude. Temperature change can be more significant, especially if liquid water is injected and it absorbs heat for its evaporation.

- The thermodynamic properties of the gases are different after the mixing, since their constitution changes, containing a larger amount of steam.
- The mass flow rate of the gases is larger by the amount of injected media after the injection position. The mass flow compatibility may lead to alteration of turbomachinery components (compressor or turbine) operating point.

Let's consider the case of injection in the combustion chamber in more detail. Injection of a diluent between the compressor outlet and the turbine inlet results in the change of several operational parameters. The way of change depends on the mode of operation. For example, different changes occur if the controller maintains a constant turbine inlet temperature (TIT) or if the load demand is kept constant. We will discuss here the changes for operation with given TIT, since this is the mode of operation used for defining turbine ratings.

Since the diluent is injected at a temperature that is lower than the TIT, some additional heat is needed to bring it to the required TIT level. The engine controller gives thus a command for additional fuel injection into the combustion chamber. The amount of additional fuel depends on the condition of the diluent. When water is injected, the amount of additional fuel is larger than for steam, since the heat needed includes the latent heat of evaporation of the water, which is of considerable magnitude.

Diluent injection results in an increase of the mass flow that has to pass through the turbine. This means that for a given TIT, the pressure has to increase (since the referred mass flow rate though the turbine is fixed). Therefore, the compressor is required to operate at higher pressure ratio. Compressor outlet pressure and temperature are thus altered, in comparison to operation with no injection. The movement of the operating point on the compressor map will depend on the shaft configuration, namely single or twin shaft.

The turbine is fed with a larger amount of gas, at a pressure higher than for dry operation. Additionally, this gas has a larger steam content, and therefore a larger heat capacity (the heat capacity of steam is roughly double that of air), while the isentropic exponent also changes. The expansion process is thus different and the turbine produces more power. The immediate consequence of these changes is that overall engine performance, namely power output and efficiency, are altered.

As a result of these changes, the matching between compressor and turbine is influenced, leading to different operating points on their corresponding characteristic curves. Typical positions of operating points on the compressor map of a single shaft gas turbine for different cases of operation are shown in **Figure B.146**. The three points correspond to the same TIT. It is observed that water injection drives the operating point to higher pressure ratio. The change is larger for larger amount of water.

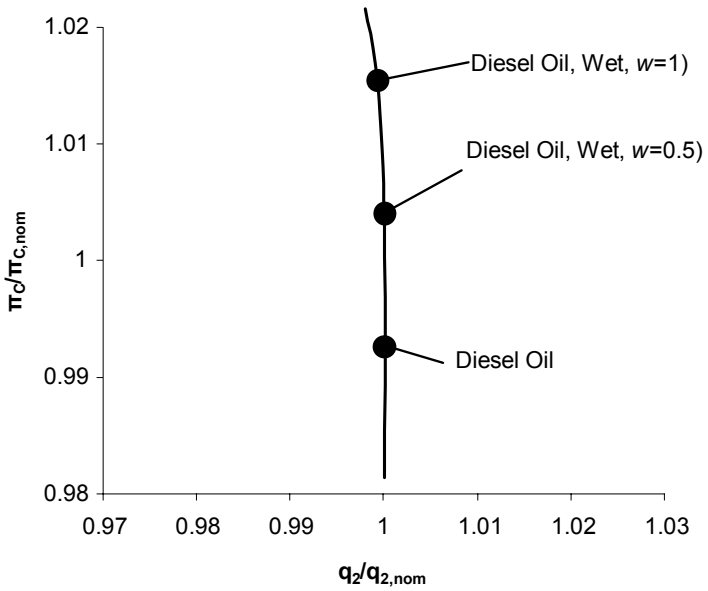

Figure B.146: Compressor Operating Point of a Single Shaft Gas Turbine. Constant TIT, Operation with Different Fuels and Water Injection.

B.8.3 Computer Models for Water Injected Operation

B.8.3.1 Constitution of a Performance Model

In order to build a performance model, a Gas Turbine is viewed as an assembly of different components (modules). Each component is identified according to the kind of process it accomplishes. The working fluid is assumed to be a perfect gas and its thermodynamic properties are interrelated through the compressible flow relations. If Y_{IN} is the vector of independent variables at a component inlet and Y_{OUT} the corresponding vector at its outlet, then in order to find the values at the components exit an equation of the following form must be solved

$$g(\overline{Y}_{IN}, \overline{Y}_{out}) = 0 \qquad \textbf{Eq. B-82}$$

This equation usually derives from conservation laws, as well as existing experience in components operation. It can be an analytical relation, possibly including empirical constants (e.g. duct pressure loss), or a set of curves (e.g. turbomachinery component maps). Additional equations express the compatibility between the different components operation. A set of equations which have to be simultaneously satisfied by the fluid parameters, is thus formed. The solution of this system of equations, non-linear in nature, is achieved numerically. Different types of numerical techniques can be employed, as for example described by Stamatis et al. [B.104]. The solution of this system for one operating point gives the full cycle details, and the performance parameters are uniquely defined.

A schematic representation of a twin spool gas turbine of interest to the present paper and its subdivision to individual components is shown in **Figure B.147**. The layout shown has provision for inlet cooling, intercooling, combustion chamber injection and interturbine steam injection.

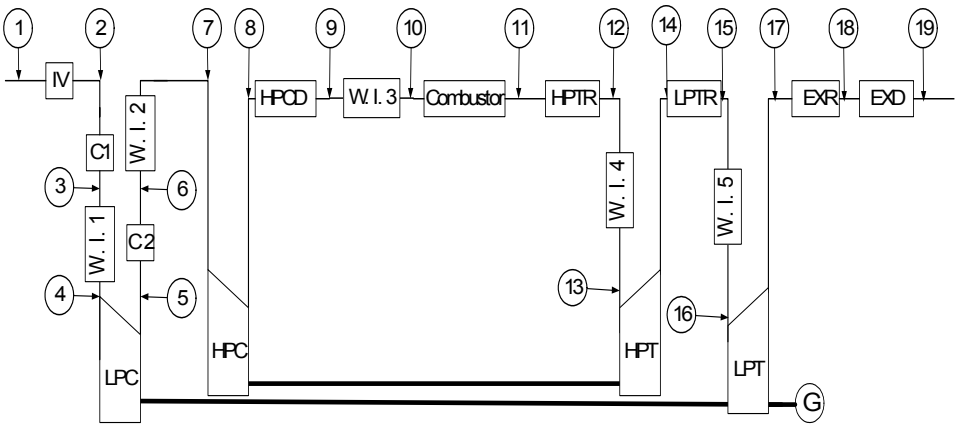

Figure B.147: Schematic Representation of a Twin Spool Gas Turbine and Discrimination of its Components.

B.8.3.2 Modelling for Water Injection

B.8.3.2.1 Gas – Water Mixing

Mixing of gas, namely air or combustion products, with water can take place at different stations along the engine: compressor inlet, between the compressors, at compressor outlet (in the form of liquid water or steam), steam between the turbines. In zero dimensional modeling it is considered that when water is injected, it is always fully evaporated before entering the downstream component. The way that properties are calculated for mixing at any of these stations is described below.

The flow in the cooling component is assumed to be steady, one-dimensional and adiabatic. The droplets partial pressure along with the volume occupied by the droplets is neglected. At cooling component inlet (station 1) the thermodynamic conditions of the air mixture and the injected water, are considered known.

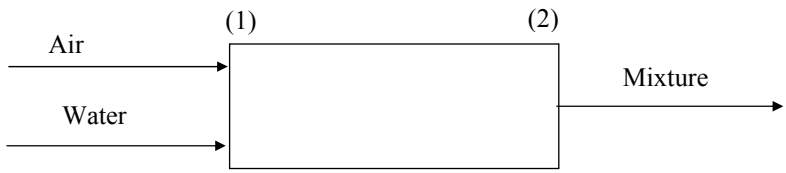

Conditions downstream of the cooling component (station 2) can be computed through the application of the conservation laws of continuity, energy and momentum which in the case of water injection form the following set of equations:

$$\dot{m}_{da}(h_{da1}+\frac{V_1^2}{2})+\dot{m}_{v1}(h_{v1}+\frac{V_1^2}{2})+\dot{m}_{w1}h_{w1}-\left[\dot{m}_{da}(h_{da2}+\frac{V_2^2}{2})+\dot{m}_{v2}\cdot(h_{v2}+\frac{V_2^2}{2})+(\dot{m}_{w1}-(\dot{m}_{v2}-\dot{m}_{v1}))\cdot h_{w2}\right]=0 \qquad \textbf{Eq. B-83}$$

$$p_1\cdot A_1+\rho_{m1}\cdot(V_1\cos(a_1))^2\cdot A_1=p_2\cdot A_2+\rho_{m2}(V_2\cos(a_1))^2\cdot A_2 \qquad \textbf{Eq. B-84}$$

$$\rho_{m1}\cdot V_1\cdot\cos(a_1)\cdot A_1=\rho_{m2}\cdot V_2\cos(a_1)\cdot A_2 \qquad \textbf{Eq. B-85}$$

Dry air enthalpy is a function of temperature while vapour and water enthalpy is a function of both pressure and temperature.

These relations can express the case that no full evaporation occurs, along with the case of possible condensation. A mixing component is assumed of constant cross-sectional area.

The non-linear algebraic equations are solved through a numerical procedure, taking into consideration the variation of the composition and the variation of thermodynamic properties of the mixture. The criterion whether saturation occurs is the correlation between vapour partial pressure and vapour saturation pressure at the temperature at component exit. In the case that the mixture is saturated vapour partial pressure is equal to vapour saturation pressure at the same temperature:

$$p_{v2} = p_{sat}(T_2)$$ **Eq. B-86**

B.8.3.2.2 Gas Properties

Calculations of thermodynamic processes use properties of a working medium, which is a mixture of gasses. The properties of individual mixture constituents are calculated by means of polynomial functions and the mixture properties are evaluated from its mass composition, through a relation of the form:

$$P = \sum_i X_i \cdot P_i$$ **Eq. B-87**

P is a property of the mixture and Xi, Pi is the mass composition and the corresponding property value for the i-element of the mixture respectively. Inlet air is handled as a mixture of gases, including steam due to ambient humidity. The composition of gases at the combustor outlet is computed on the basis of stoichiometric calculations, and depends on the composition of the fuel used. When water is injected, it also accounted for as an additional amount in the gas composition.

The variation of c_p of the mixture of combustion gases and steam, for the range of temperatures of interest to gas turbine applications, is shown in **Figure B.148**. The values have been calculated by considering the gases as a mixture of ideal gasses, and the properties of the constituents are derived by polynomial relations **[B.99]**. The variation of isentropic exponent γ is also shown.

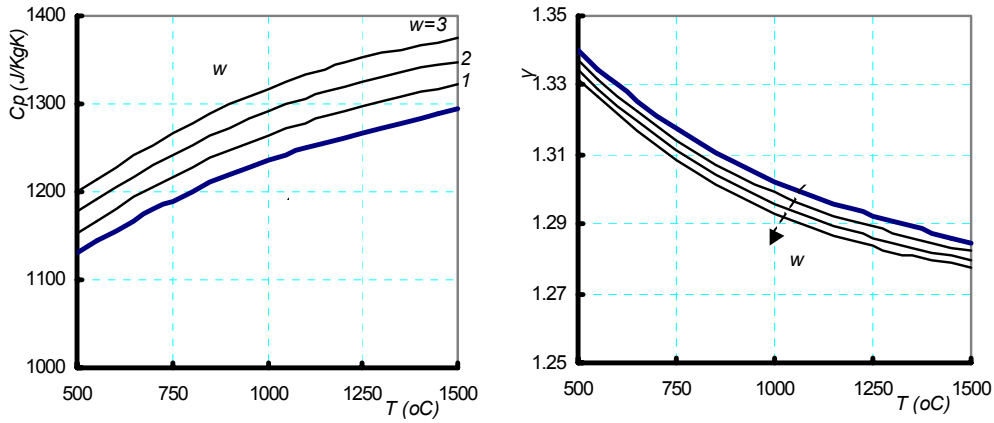

Figure B.148: Values of Specific Heat C_p and Isentropic Exponent *γ*, for Temperatures Usual in the Hot Section of Gas Turbines.

Variation of gas properties for typical rates of water injection is shown in **Figure B.149**. The changes of properties of gases after water is injected, with respect to the values with no water injected are shown.

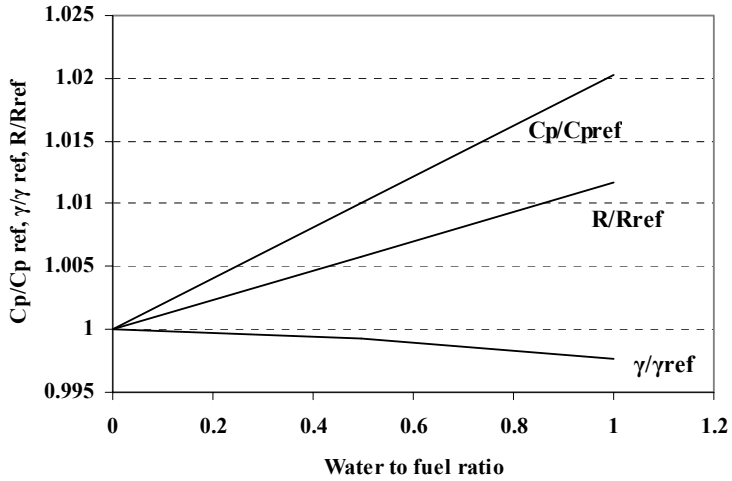

Figure B.149: Change in Gas Properties for Different Amount of Injected Water (f = 0.02).

B.8.3.2.3 Turbomachinery Components

Calculation of component performance parameters is based on performance maps for each component, which are expressed in a generalized form to account for the use of different gases. The quantities that remain invariant for a map can be found in many references (e.g. AGARD [B.105], Walsh and Fletcher [B.99], Mathioudakis and Tsalavoutas [B.106]). When the map is expressed in function of these parameters it remains unique, independently of the working medium.

For water/steam injection at the compressor outlet, the variation of the quantities related to the turbine is of interest, since it is the turbine that faces this gas composition changes. The quantities that remain invariable and are interrelated through the map, when gas composition changes are:

$$\left(\frac{N}{\sqrt{T}}\right) \Big/ \left(\frac{N}{\sqrt{T}}\right)_0 = \sqrt{R \cdot \gamma \cdot (1+\gamma_0) / R_0 \cdot \gamma_0 \cdot (1+\gamma)} \qquad \textbf{Eq. B-88}$$

$$\left(\frac{W\sqrt{T}}{P}\right) \Big/ \left(\frac{W\sqrt{T}}{P}\right)_0 = \sqrt{\frac{R_0 \cdot \gamma}{R \cdot \gamma_0}} \cdot \left(\frac{2}{1+\gamma}\right)^{\frac{\gamma+1}{2\cdot(\gamma-1)}} \cdot \left(\frac{1+\gamma_0}{2}\right)^{\frac{\gamma_0+1}{2\cdot(\gamma_0-1)}} \qquad \textbf{Eq. B-89}$$

$$\left(\frac{\Delta h}{T}\right) \Big/ \left(\frac{\Delta h}{T}\right)_0 = R \cdot \gamma \cdot (1+\gamma_0) / R_0 \cdot \gamma_0 \cdot (1+\gamma) \qquad \textbf{Eq. B-90}$$

Subscript 0 in all the above relations denotes properties of working medium at a condition that is considered to be the reference. The choice of reference condition depends on how the map was obtained. It could be dry air, combustion gases with dry air at the inlet and reference gas fuel or other.

It is worth noting here that the expression for reduced flow rate though the turbine, **Eq. B-89** can be used to understand some of the effects of fuel change or water injection. When the turbine is chocked (which is actually the case for most gas turbines today, at least for operating conditions in the vicinity of full load),

reduced mass flow remains constant. It can be easily shown that the term to the right of the radical, in the right hand side of **Eq. B-89** changes very little for the range of values obtained by γ. This means that the quantity that remains unchanged is:

$$q_4 = \left(\frac{W_4 \sqrt{T_4}}{P_4} \right) \sqrt{\frac{R}{\gamma}} \qquad \textbf{Eq. B-91}$$

Using this fact and also the fact that compressor inlet reduced mass flow changes very little ("vertical" characteristic on compressor map), changes in pressure ratio can be evaluated.

B.8.3.2.4 Sample Results of Effects on Performance

Once a model that can simulate engine performance in all these situations is constituted, it is possible to examine how water injection can influence engine performance. Before going into the detailed study, it is useful to remark that assessment of these effects can be done in two levels: It is possible to have an assessment using analytic relations. Such analysis for fuel changes has been presented by Mathioudakis **[B.106]** and for water injection effects by Mathioudakis as well **[B.107]**. They give an understanding of the related effects and the possibility for fast calculations, helpful for a quick engineering judgment. The accuracy of predictions can be good, especially if small deviations occur from what is considered to be the reference condition. Accurate calculations, irrespective of the size of deviations, necessitate the use of a non-linear computer simulation model.

B.8.3.3 Estimation of Performance Deviations using Analytical Relations

The information derived by computer models is valid for a specific gas turbine modeled, but it is not known how general the predictions are or what are the factors governing the phenomena studied. If another gas turbine is considered, it is not known to what extent information already available can be used for assessing these effects.

These drawbacks are overcome when explicit relations can be used. If such relations are available, then it is possible to study any given gas turbine, provided that the necessary design data are available. Additionally, the use of relations allows an understanding of the effect of diluent injection and provides a means for a quick estimation of such effects. Such relations have been published by Mathioudakis **[B.103]**, for studying the effect of water injection on the performance of a gas turbine. In the present paper, this approach is extended to study the effects of steam injection. The analysis is further extended to study the movement of the compressor operating point and thus allow implementation on twin shaft gas turbines. Differences for the effects of steam or water injection will be highlighted and explained. The study is concentrated on the behaviour of the gas turbine engine and it is shown that it can be used to interpret the changes observed on cycle performances.

B.8.3.3.1 Fuel/Air Ratio and Gas Properties Changes

An important mechanism behind overall performance parameter changes lies in the fact that additional fuel is needed for keeping the turbine inlet temperature constant, as mentioned above. The fuel to air ratio f ' when diluent is injected, with a proportion to fuel denoted by w can be evaluated from the ratio f without injection, through the following relation:

$$f' = \frac{f}{1 - r\,w\,f} \qquad \textbf{Eq. B-92}$$

Eq. B-92 can also be written as

$$\frac{\delta f}{f}=\frac{f'-f}{f}=\frac{rwf}{1-rwf} \qquad \textbf{Eq. B-93}$$

The parameter that determines how f changes with w is the relative enthalpy rise of steam r. This parameter takes characteristic values, which are different for water or steam, and do not change very much for practical gas turbine designs. Its value depends on TIT, compressor delivery temperature and the condition of the injected diluent. It can be shown that r does not vary very much for existing gas turbine designs and a typical value that can be used for steam injection is r≈2 and for water injection r≈5.

Predictions of fuel/air ratio for different diluent flow rates, using **Eq. B-93**, are shown in **Figure B.150**. They are compared to predictions of a detailed thermodynamic computer model. The test case of a single shaft gas turbine, the modeling of which has been reported in **[B.108]** was used. The predictions of **Eq. B-93** are shown to almost coincide with those of the full model, for either steam or water injection. The slope of the change for water is larger than for steam, due to the larger value of r, reflecting the larger amount of fuel needed to evaporate the water, as mentioned in the previous section.

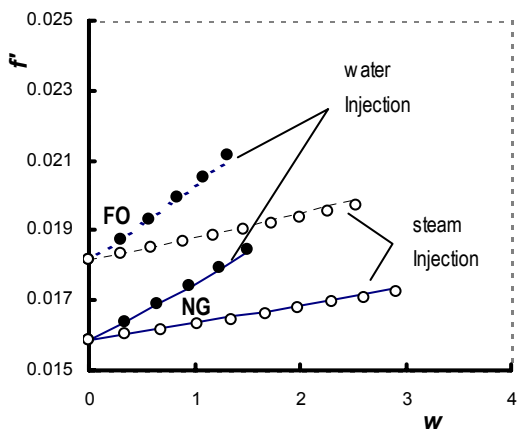

Figure B.150: Typical Variation of Fuel/Air Ratio, with Water and Steam Injection (TG20 Simulation). Operation with Fuel Oil and Natural Gas. Points: Computer Model, Lines: eq (1).

The range of variation of w for water injection is chosen narrower than for steam. This choice is made to reflect the fact that water is used mainly for NO_x abatement, and it is more effective than steam for that purpose (It is mentioned in **[B.90]** that the same level of emissions reduction can be achieved by steam using 1.6 times the amount of water). Typically, the maximum reduction can be achieved with a one-to-one proportion of liquid water to fuel. On the other hand, steam may be chosen to be used in larger amounts, not simply for NO_x abatement, but also for performance improvement purposes. For example, a large engine manufacturer uses a typical level of steam content for performance augmentation of the order of 5% of inlet airflow, while recent improvements have allowed increasing this level to 9%, as reported in **[B.109]**.

B.8.3.3.2 Gas Properties Changes

The derivation of Cp and γ from the dry combustion gas values can be evaluated by means of simplified relation. If property values are known for dry combustion gases, then the change of cp because of the injection of water or steam can be evaluated though the relation:

$$\frac{\delta c_{pg}}{c_{pg}} = war\ (\frac{c_{ps}}{c_{pg}} - 1)$$ **Eq. B-94**

The specific heat of the dry combustion products can be considered to be the same as the one before the diluent is injected. A similar relation can be derived for the change in the value of the gas constant R:

$$\frac{\delta R_g}{R_g} = war\ (\frac{R_s}{R_g} - 1)$$ **Eq. B-95**

The change in the isentropic exponent γ results from its definition and the previous expressions, to get:

$$\frac{\delta\gamma}{\gamma} = (\gamma - 1)\left(\frac{\delta R_g}{R_g} - \frac{\delta c_{pg}}{c_{pg}}\right) = (\gamma - 1)\left(\frac{R_s}{R_g} - \frac{c_{ps}}{c_{pg}}\right) war$$ **Eq. B-96**

The product (f ' w) appearing in these relations is equal to the water-to-air ratio war. If this quantity is substituted in the previous expressions, they could also be used for changes in inlet air properties due to varying ambient humidity.

We note that the above expressions can be further simplified for gas turbine combustion gases, by taking into account that the specific heat of steam is roughly double the specific heat of the combustion gases, as can be seen from **Figure B.151**. For the range of turbine inlet temperatures encountered in today's turbines, and representative values of fuel/air ratio, Cps/Cpg is shown to take values very close to **Eq. B-94**.

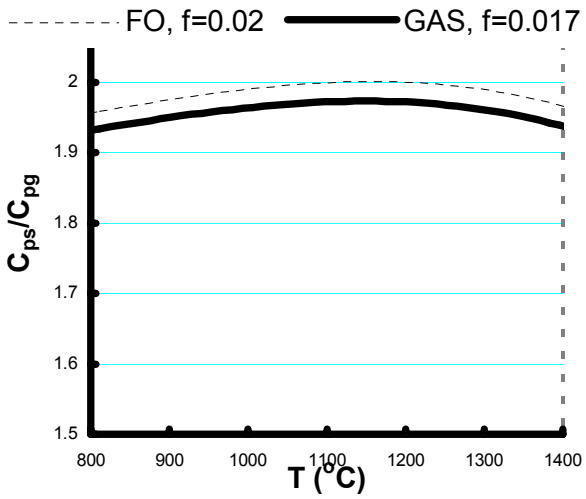

Figure B.151: Ratio of Specific Heats of Steam and Combustion Gases.

By virtue of this observation**, Eq. B-94** for Cp becomes:

$$\frac{\delta c_{pg}}{c_{pg}} \approx war$$ **Eq. B-97**

For the gas constant R, for Rs = 461.5 and Rg = 287, **Eq. B-95** gives:

$$\frac{\delta R_g}{R_g} = 0.61 war \qquad \textbf{Eq. B-98}$$

and for the isentropic exponent,

$$\frac{\delta \gamma}{\gamma} \approx 0.33(1.61 - 2) war = -0.13\, war \qquad \textbf{Eq. B-99}$$

B.8.3.3.3 Performance Deviations

With the help of the formulas for the fuel/air ratio and specific heat deviations, simplified expressions for the deviations of power output, and efficiency can be derived. We will show that use of such expressions allows the evaluation of the effects of diluent injection on the performance of a gas turbine. Power output and efficiency are examined first, followed by the effect on the compressor operating point and exhaust gas temperature.

B.8.3.3.4 Power Output

The fractional change in power output is given by the following approximate relation:

$$\frac{\Delta P}{P} = \frac{\Delta \dot{m}_2}{\dot{m}_2} + 2\frac{P_T}{P} f' w \qquad \textbf{Eq. B-100}$$

The first term is the fractional change of air mass flow rate caused by the change in the operating point of the compressor. The second term represents the change in power produced by the turbine, swallowing extra fluid, namely the injected diluent. The factor two comes from the fact that steam produces twice the power produced by the same mass flow rate of combustion gas, when expanding over the same temperature limits, due to its thermal capacity being double that of the combustion gas. can be modified to use only data from the dry operating point at the same TIT, by substituting f ‘ from **Eq. B-92**.

$$\frac{\Delta P}{P} = \frac{\Delta \dot{m}_2}{\dot{m}_2} + 2\frac{P_T}{P} \frac{f\, w}{1 - r\, w\, f} \qquad \textbf{Eq. B-101}$$

For a modern single shaft turbine used in electricity generation, operation with fixed compressor geometry implies almost no change in inlet mass flow rate. Therefore, the change in power will depend only on the water/fuel ratio w, since the first term on the right hand side of **Eq. B-100** will be almost zero. When variable geometry exists and is used for engine control, mass flow changes will have to be accounted for according to this relation. This also holds for a twin shaft gas turbine.

Variation of the power output of a single shaft gas turbine with constant IGV setting, as a function of the water–to-fuel ratio, is shown in **Figure B.152**. Results for operation with fuel oil or natural gas and injection of water or steam are shown. The lines represent the prediction using **Eq. B-100** and the points prediction of the same conditions with a detailed thermodynamic computer model of the engine considered **[B.108]**. It is shown that predictions with **Eq. B-100** are in very close agreement with the predictions of the full model, and thus **Eq. B-100** can accurately represent changes due to diluent injection for different fuels. It can also be used to interpret the differences in operation for the different cases, shown in **Figure B.152**.

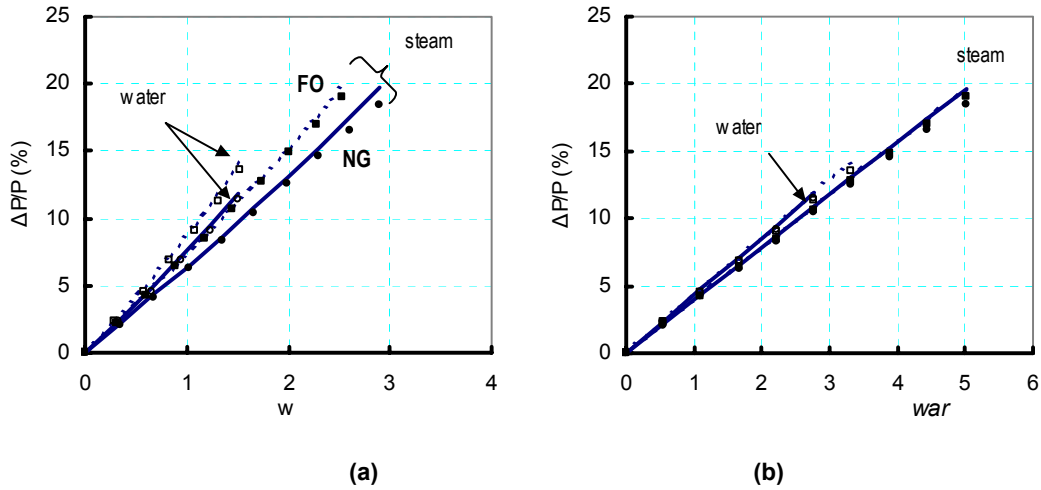

Figure B.152: Power Output Deviation with Diluent Injection. (a) As a Function of Water/Fuel Ratio, (b) As a Function of Water/Air Ratio. Points: Computer Model, Lines: eq (6).

Water injection produces a larger power output than the same quantity of steam, irrespective of the kind of fuel**. Eq. B-101** can be used to explain this trend: for a given operating point and fuel (given PT/P), the slope of the power increase versus w is higher in the case of water, since the parameter r takes a larger value, and thus the denominator in **Eq. B-101** becomes smaller. It is also observed in **Figure B.152**, that the change in power output is smaller when the fuel is gas, as compared to liquid. The reason for this behaviour is two fold: First, the term PT/P is slightly smaller (PT increases due to a larger gas specific heat and therefore PT/P(=1/(1-Pc/PT)) slightly decreases), and secondly, the slope is proportional to f which is smaller for typical natural gas (due to its LHV being about 20% higher than fuel oil). The difference is much smaller if war(=f ‘ w) is plotted on the abscissa, as shown in **Figure B.152b**. The use of this independent variable, virtually eliminates thus the dependence on the kind of fuel.

The values of the predictions presented in **Figure B.152**, are in very close agreement with data published by gas turbine manufacturers **[B.100** and **B.101]**.

B.8.3.3.5 Efficiency

The deviation of thermal efficiency is given by the relation:

$$\frac{\Delta(\eta_{th})}{\eta_{tth}} = (2\frac{P_T}{P} - r) f' w$$

Eq. B-102

which can be further transformed, using **Eq. B-92**

$$\frac{\Delta(\eta_{th})}{\eta_{tth}} = (2\frac{P_T}{P} - r)\frac{f\ w}{1 - r\ f\ w}$$

Eq. B-103

The efficiency deviation, as a function of the water–to-fuel ratio, is shown in **Figure B.153**, where data for water injection and different fuels are also included, similar to **Figure B.153**. The good agreement with predictions of the full computer model can be observed in this case too, while the trends predicted here are close to the trends published by engine manufacturers, shown in **Figure B.153**. In this case too, it can be shown that use of the water to air ratio as an independent variable produces curves which demonstrate a very weak dependence on the kind of fuel.

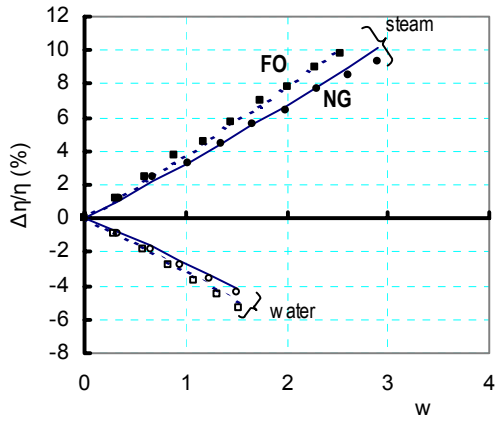

Figure B.153: Gas Turbine Efficiency Deviation with Diluent Injection.

The first observation is that while both steam and water injection result in an output increase, they have the opposite effects on efficiency: steam injection increases efficiency while water injection decreases it. The reason for this behaviour can be explained by looking at **Eq. B-102**. As discussed above, r is very large for water injection, and thus the coefficient in **Eq. B-102** becomes negative. It has a much smaller value for steam and hence the positive slope.

The change in efficiency can be further interpreted physically, as the resultant of two effects in opposite directions: More power is produced due to the increased flow through the turbine and increase in heat capacity. This power increase is achieved with an increase in the fuel consumed, to heat the diluent injected. This heat is proportionally higher than the extra power, in the case of water injection, as it includes the heat of vaporization. This proportionality is expressed by the value of r. For water r is very large, and offsets the advantage in power. It should be noted that this effect can also be seen from the cycle point of view: In the case of steam the average temperature of heat addition to the cycle is slightly increased, while the temperature of heat rejection is lowered, since part of the exhaust heat is used to produce the steam. In the case of water, the heat rejection is at the same temperature, while heat addition occurs at a lower temperature (a large part of it is used to evaporate the water).

B.8.3.3.6 Compressor Operating Conditions

Movement of the operating point on the compressor map is of interest for different operating conditions, mainly to monitor surge margins and to ensure that the risk of encountering unstable operation is minimized. The fact that steam injection reduces surge margin means that compressor operation has to be monitored, to avoid the occurrence of such conditions, as discussed in **[B.110]**.

The operating point of the compressor is defined by the pressure ratio πc and reduced mass flow rate q2. For operation without and with water injection and dividing the two equations gives:

$$\frac{\pi_c'}{\pi_c} = \frac{q_2'}{q_2} \frac{1+f'(1+w)}{1+f} \sqrt{\frac{R_4'}{R_4} \frac{\gamma_4}{\gamma_4'} \frac{T_4'}{T_4} \frac{T_2}{T_2'}} \qquad \textbf{Eq. B-104}$$

This relation can be used to predict the pressure ratio at any operating condition once the pressure ratio at one operating point is known (e.g. at base load) and can be applied to both dry and wet operation. It can be used to estimate the change in pressure ratio, which will result from the injection of water. For constant TIT, this equation gives:

$$\frac{\pi_c'}{\pi_c} = \frac{q_2'}{q_2}\frac{1+f'(1+w)}{1+f}\sqrt{\frac{R_4'}{R_4}\frac{\gamma_4}{\gamma_4'}} \qquad \textbf{Eq. B-105}$$

Using the small f ' w approximation and eq. (23), it can be transformed as follows:

$$\frac{\pi_c'}{\pi_c}\frac{q_2}{q_2'} \approx (1+f'w)(1+0.37f'w) \approx 1+1.37\frac{fw}{1-r\,w\,f} \qquad \textbf{Eq. B-106}$$

At this point it must be noted that operation of a single shaft configuration and a configuration with a free power turbine is different. The relations for change in pressure ratio, presented above, can be used to estimate the shift of operating points for the two cases.

B.8.3.3.6.1 Single Shaft Gas Turbine

The typical application for this configuration is electricity generation. In such applications the shaft mechanical speed is constant. This means that for given ambient conditions the compressor operating point will be moving along a constant speed line. For operation with constant geometry, namely with no variation of stator vane angles, it is usual that the nominal constant speed characteristic is approximately vertical to the flow axis, namely q2 = constant, especially for high pressure ratio transonic axial compressors. Operation at constant turbine inlet temperature, allows thus a further simplification of **Eq. B-105**:

$$\frac{\pi_c'}{\pi_c} = \frac{1+f'(1+w)}{1+f}\sqrt{\frac{R_4'}{R_4}\frac{\gamma_4}{\gamma_4'}} \approx (1+f'w)\sqrt{\frac{R_4'}{R_4}\frac{\gamma_4}{\gamma_4'}} \qquad \textbf{Eq. B-107}$$

This relation shows that pressure ratio changes as a result of two effects: change of mass flow though the turbine and change of gas properties as a result of increased water content. Therefore, diluent injection will force the pressure ratio to increase.

Eq. B-107 can be used to evaluate change in pressure ratio and thus estimate the new position of the compressor operating point. An example of a calculated change in pressure ratio is shown in **Figure B.154**, where it is also shown that predictions of **Eq. B-107** are in close agreement to those of a full computer model. The way the operating point moves is shown in **Figure B.154**.

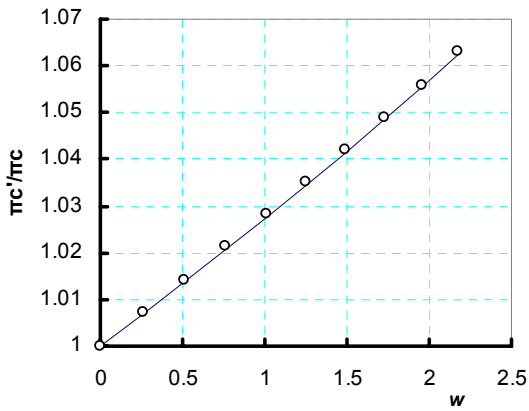

Figure B.154: Variation of Compressor Pressure Ratio as a Function of the Amount of Injected Steam for a Single Shaft Gas Turbine.

B.8.3.3.6.2 Twin Shaft Gas Turbine

For dry operation, the gas generator operating point moves along the operating line. For a single spool gas generator, the movement of the operating point can be assessed by using the power balance equation. This equation can be written as follows:

$$\pi_C^{\frac{\gamma-1}{\gamma}} - 1 = \frac{m_4}{m_2}\frac{c_{pg}}{c_{pa}}\frac{T_4}{T_2}\left(1 - \frac{T_{41}}{T_4}\right)\eta_{Cis} \qquad \textbf{Eq. B-108}$$

For operation with the power turbine choked, the temperature ratio of the gas generator turbine T41/T4 remains approximately constant (see for example [B.111]). If we consider operation with a given T4, write this equation for operation with and without injection, divide the two equations and use also eq (18), we get:

$$\frac{\pi'^{\frac{\gamma-1}{\gamma}}_C - 1}{\pi_C^{\frac{\gamma-1}{\gamma}} - 1} = \frac{1 + f'(1+w)}{1+f}\frac{c'_{pg}}{c_{pg}} \qquad \textbf{Eq. B-109}$$

This equation can be used to predict the change in pressure ratio. A comparison of prediction of this equation and prediction using a full computer model of a twin shaft gas turbine (the one described in [B.112]), is shown in **Figure B.155**.

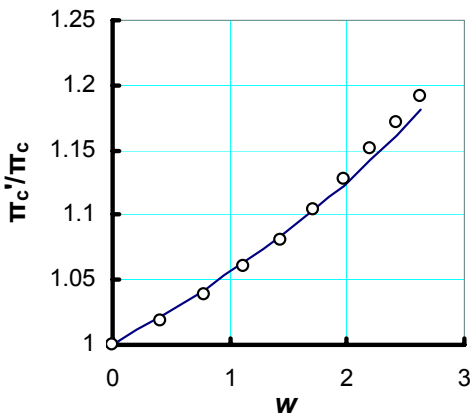

Figure B.155: Change of Compressor Pressure Ratio with Water Injection for a Twin Shaft Gas Turbine. Points: Computer Model, Line: Eq. B-109.

Once the pressure ratio is estimated, the compressor flow function q2 can be estimated using **Eq. B-105**. The movement of the operating point on the compressor map, corresponding to the predictions of **Figure B.155**, is shown in **Figure B.156**, where prediction of this equation are compared to those of the full computer model. It is observed that pressure ratio varies with mass flow rate and compressor speed. The increase in power caused by diluent injection drives the compressor to operate at higher rotational speed, the surge margin is however reduced.

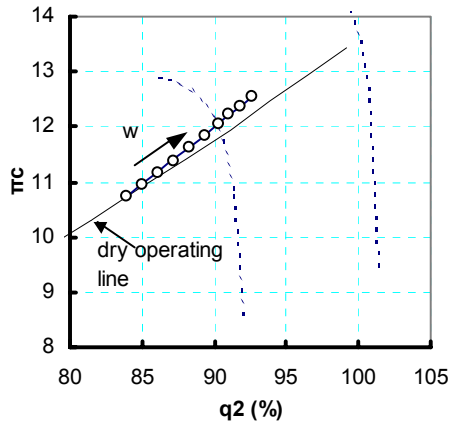

Figure B.156: Change of Compressor Operating Conditions with Diluent Injection for a Twin Shaft Gas Turbine. ° Operating Points when Water is Injected at Constant TIT.

The estimated deviations of the compressor flow function provide directly the deviations of mass flow rate from the value at the dry operating point. This means that both terms of **Eq. B-100** are known and thus the deviation in power output can be assessed for the case of the twin shaft gas turbine as well. A comparison of the deviation evaluated through **Eq. B-101** and the detailed computer model is shown in **Figure B.157**.

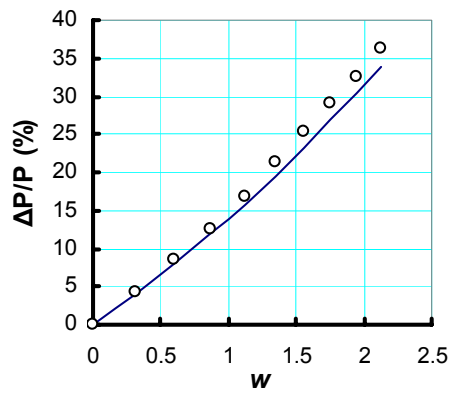

Figure B.157: Deviation of Power Output with Water Injection, for a Twin Shaft Gas Turbine.

B.8.4 Water/Steam Ingestion Effects Discussion

All the relations presented above for evaluating the deviations of performance parameters contain the term f ‘w . This term is equal to the water/air ratio, since:

$$f'w = \frac{m_f}{m_a}\frac{m_w}{m_f} = \frac{m_w}{m_a} = war \qquad \textbf{Eq. B-110}$$

This means that this parameter can also be considered as the governing parameter for the deviations. We have also shown that when this parameter is used, the change in power output and efficiency depends very little on the type of fuel, while when w is the independent variable, different slopes are observed for different fuels. On the other hand, the use of w may be preferable since this parameter is the one that determines the reduction in NO_x emissions, as discussed in the introduction.

The formulas for power output and efficiency are valid, independently of shaft arrangement. It was discussed previously that in the case of a single shaft gas turbine with constant geometry, the amount of water alone determines the power change. If variable IGVs are used their control law would need to be known, for evaluating the power change (this law would allow determination of the term Δm/m in **Eq. B-100**. For the twin shaft gas turbine, the mass flow change is evaluated from the power and flow matching relations, as discussed in the previous section.

It is interesting to examine how the sensitivity of power and efficiency variations are expected to vary for the range of design parameters encountered in today's gas turbines. The main parameters that influence sensitivity to diluent injection are the ratio of turbine power to power output PT/P and the relative enthalpy rise of the steam expressed by the parameter r. The range of values of these two parameters for today's gas turbines is discussed in ***Annex B***. On the basis of these values, the range of variation of the power versus water to air ratio for constant geometry single shaft gas turbines, is shown in **Figure B.158**. war is chosen as the abscissa, since the corresponding lines are then almost independent of the fuel type. It is observed that for a large variety of designs, the rate of power change with water-to-air ratio varies within a relatively narrow range. The range for water injection is also narrow with slightly higher slope. From this figure we could claim that for any gas turbine, a rule of thumb would be that there is an increase of 5% in power for every 1% of injected water or steam, expressed as a percentage of inlet air, for operation at nominal conditions.

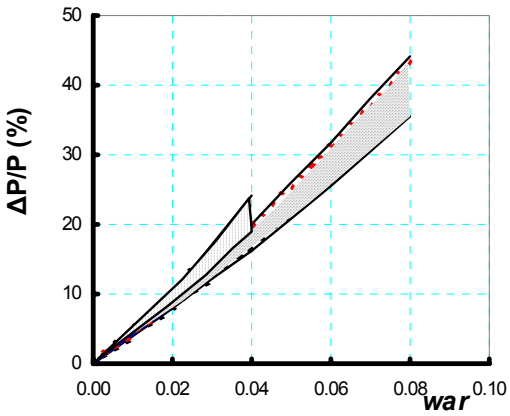

Figure B.158: Range of Variation of Power Deviation for Existing Gas Turbines. Single Shaft, Constant Geometry.

At this point it should be commented that the increase in output for a twin shaft gas turbine is larger, for the same amount of injected water or steam. For this case, diluent injection results in an increase of mass flow rate, resulting in an additional power increase, as indicated from **Eq. B-100**. The simultaneous increase in pressure ratio, results in general in larger values of the ratio PT/P, giving finally a larger increase of output per unit diluent mass flow injection. Analysis of **Eq. B-106** and **Eq. B-109** can show that for this case an additional output increase of about 1.5% per 1% of injected diluent, should be expected. We note here an increase of 6.5% per 1% of injected steam in a twin spool, twin shaft gas turbine was reported, which is in agreement with the previous observations.

The corresponding changes of efficiency are shown in **Figure B.159**. It is observed here that the efficiency increase due to steam injection is bounded within a relatively narrow band. The range of variation for the efficiency drop for water injection is rather wide however.

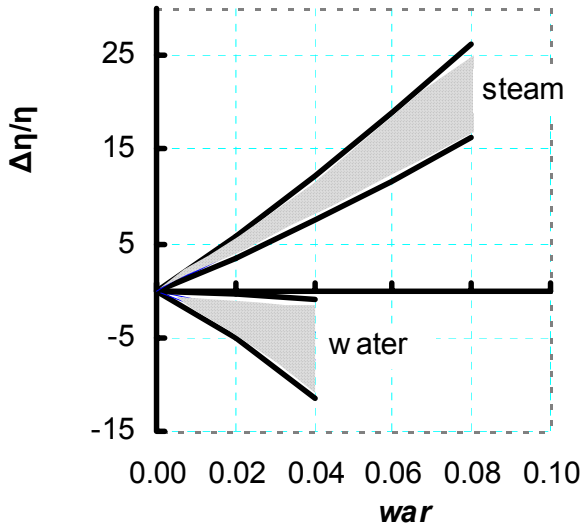

Figure B.159: Range of Variation of Efficiency Deviation for Existing Gas Turbines. Single Shaft, Constant Geometry.

Both **Figure B.158** and **Figure B.159** have been derived on the basis of design point data. When off-design operation of a given gas turbine is considered, the curves may differ considerably, since the parameter PT/P may change.

B.8.5 Conclusions for Water/Steam Ingestion

The possibility of predicting the main gas turbine performance parameter deviations due to the injection of water or steam into the combustion chamber, by means of simple analytical relations has been demonstrated. It was shown that with minimum design data, it is possible to predict deviations in performance with an accuracy comparable to that of more detailed models.

These relations allow an interpretation of the difference in behavior observed between water and steam injection, or even different fuels. It was thus explained why both water and steam injection have the same influence on output, while they produce opposite trends in efficiency.

Apart from the overall performance, it was shown that the movement of the operating point on the compressor characteristic can also be predicted.

The generality of the predictions was discussed and it was shown that some general trends exist for current gas turbine designs, as demonstrated by using published design data from a large number of industrial gas turbines.

It was also shown that the main parameters influencing the magnitude of the deviations caused by diluent injection are bounded within certain limits. Some generalized conclusions can thus be derived for any application.

B.8.6 Further Discussions

The layout of a gas turbine considered for the present study is shown in **Figure B.160**. This layout covers both types of shaft arrangement. For the twin shaft gas turbine, station 41 is the station between compressor and power turbine.

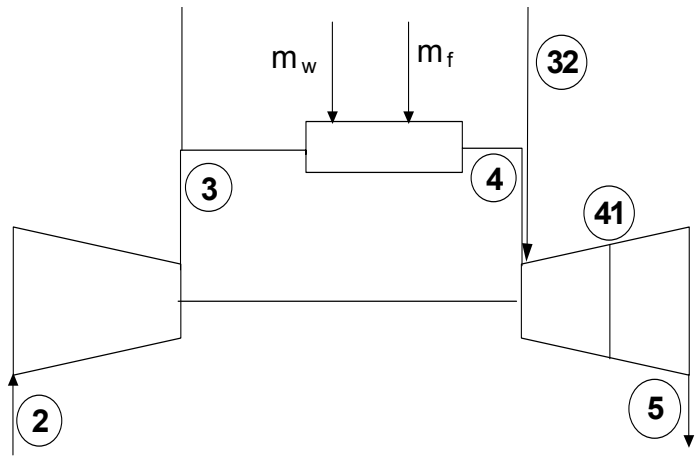

Figure B.160: Schematic of the Gas Turbine Layout Studied.

The formulas used to calculate performance parameter changes have been derived by the author in [B.103], for water injection. The approach followed is to consider an operating point without diluent injection and to derive formulas for the deviations of performances from the values at that operating point. From the derivation, it is deduced that they are applicable to steam injection as well. Injection at compressor outlet or within the combustion chamber are equivalent from a performance point of view.

Derivation of simplified relations becomes possible by taking advantage of the fact that the fuel air ratio f of a gas turbine is a small number, with a value usually around 0.02 for base load operation. Terms containing higher power of this quantity can thus be neglected without loss of accuracy. A summary of the procedure for derivation of the equations is given in the following.

B.8.6.1 Gas Properties

Diluent injection increases the steam content of the hot gases into the turbine, in comparison to the case with no diluent injection. The new specific heat can be calculated if the gas is considered to be a mixture of water vapour and gas produced from dry combustion:

$$c'_{pg} = \frac{(1+f')c_{pg} + f'wc_{ps}}{1+f'(1+w)} \qquad \textbf{Eq. B-111}$$

Taking into account that $f', f'w << 1$ this relation can be simplified to give:

$$\frac{c'_{pg}}{c_{pg}} \approx (1 + f'w(\frac{c_{ps}}{c_{pg}} - 1)) \qquad \textbf{Eq. B-112}$$

From this relation, **Eq. B-93** is derived.

B.8.6.2 Fuel-Air Ratio

The change in fuel flow rate when diluent is injected can be evaluated by applying the steady flow energy equation (SFEE) to the combustion chamber for operation with and without injection. The flows into and out of the combustion chamber are shown schematically in **Figure B.161**.

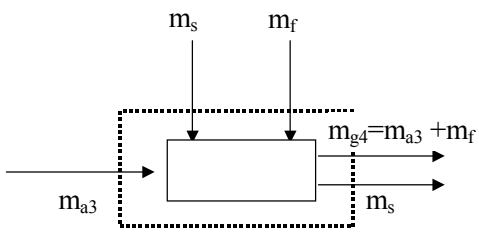

Figure B.161: Control Volume for Application of the SFEE over the Combustion Chamber.

The SFEE for the combustion chamber is:

$$(1+f')(h_{g4}-h_{g0})=(h'_{a3}-h_{a0})+f'\,LHV-wf'\,(h_{s4}-h_w) \qquad \textbf{Eq. B-113}$$

Writing this equation for dry and wet operation and eliminating the quantity LHV, gives the following relation for fuel air ratio:

$$\frac{f'}{f}=r\,w\,f'+a \qquad \textbf{Eq. B-114}$$

where

$$a=\frac{(h_{g4}-h_{g0})-(h'_{a3}-h_{a0})}{(h_{g4}-h_{g0})-(h_{a3}-h_{a0})},\quad r=\frac{h_{s4}-h_w}{(h_{g4}-h_{g0})-(h_{a3}-h_{a0})} \qquad \textbf{Eq. B-115}$$

The value of a in this relation is very close to unity. Compressor outlet enthalpy h'a3 differs from the dry value ha3 by a relatively small amount, compared to the enthalpy rise in the combustion chamber. The numerator and denominator of the fraction are therefore almost equal. We thus have:

$$\frac{f'}{f}\approx r\,w\,f'+1 \qquad \textbf{Eq. B-116}$$

which gives **Eq. B-92** of the main text.

We note that r expresses the relative specific enthalpy rise of the injected diluent with respect to the enthalpy rise for transformation of the air into combustion products.

B.8.6.3 Power Output

The deviation of power output has been derived in **[B.103]**. The derivation is also summarized here for completeness.

Power output is derived by relating the net output to the difference between the turbine and compressor power:

$$P=\dot{m}_2 C_{pa} T_2 \overbrace{\left[\frac{\dot{m}_4}{\dot{m}_2}\frac{c_{pg}}{c_{pa}}\frac{T_4}{T_2}\eta_{Tis}\left(1-\frac{1}{\pi_T^{\frac{\gamma_g-1}{\gamma_g}}}\right)-\frac{1}{\eta_{cis}}\left(\pi_C^{\frac{\gamma_a-1}{\gamma_a}}-1\right)\right]}^{P_h} \qquad \textbf{Eq. B-117}$$

This is a simplified expression, as it does not take into account the effect of parasitic flows, such as those used for cooling. It provides a better approximation when T4 is the ISO turbine inlet temperature (derived on the assumption of mixing parasitic flows at turbine inlet). Deviations, when water or steam is injected, are calculated more accurately, provided that the cooling flows remain unchanged. This is a good approximation, since these flows are driven by pressure differences which remain practically unaltered.

For given ambient temperature and turbine inlet temperature, taking logarithms and differentiating, we obtain:

$$\frac{\delta P}{P} = \frac{\delta \dot{m}_2}{\dot{m}_2} + \frac{m_2 C_{pa} T_2}{P} \delta P_h \qquad \textbf{Eq. B-118}$$

where Ph is the term in brackets in eq (17). The deviation δPη can be further evaluated as follows:

$$\delta P_h = Y_T \cdot \delta\left(\frac{\dot{m}_4}{\dot{m}_2}\frac{C_{pg}}{C_{pa}}\frac{T_4}{T_2}\right) + \left[\frac{\dot{m}_4}{\dot{m}_2}\frac{C_{pg}}{C_{pa}}\frac{T_4}{T_2}\delta Y_T - \delta Y_c\right] \qquad \textbf{Eq. B-119}$$

where we have put: $Y_C = \left(\pi_c^{\frac{\gamma_a - 1}{\gamma_a}} - 1\right) / \eta_{cis}$, $Y_T = \eta_{tis}\left(1 - 1/\pi_T^{\frac{\gamma_{g-1}}{\gamma_g}}\right)$ **Eq. B-120**

For evaluation of the first term of the right hand side of eq (18a), when ambient and turbine inlet temperature are constant, we have:

$$\delta\left(\frac{\dot{m}_4}{\dot{m}_2}\frac{C_{pg}}{C_{pa}}\right) = \frac{\dot{m}_4}{\dot{m}_2}\frac{C_{pg}}{C_{pa}}\left(\frac{\delta\left(\frac{\dot{m}_4}{\dot{m}_2}\right)}{\frac{\dot{m}_4}{\dot{m}_2}} + \frac{\delta C_{pg}}{C_{pg}}\right) \qquad \textbf{Eq. B-121}$$

The mass balance for the combustion chamber gives the following relation between the turbine inlet and compressor inlet mass flow rates:

$$\frac{\dot{m}_4}{\dot{m}_2} = \frac{\dot{m}_4}{\dot{m}_3}\frac{\dot{m}_3}{\dot{m}_2} = \left(1 + f'(1+w)\right)\cdot(1-b) \qquad \textbf{Eq. B-122}$$

where b is the fraction of the total air flow bled from the compressor, before entry to the combustion chamber. Application of this equation without and with water injection, gives:

$$\delta\left(\frac{\dot{m}_4}{\dot{m}_2}\right) \Big/ \left(\frac{\dot{m}_4}{\dot{m}_2}\right) = \frac{fw}{1+f} \qquad \textbf{Eq. B-123}$$

Coming to the second term of the right hand side of **Eq. B-119**, it expresses the rate of change of specific power with pressure ratio, for given isentropic efficiencies of compressor and turbine. This term is very small and can be neglected for the following reason: gas turbine designers usually choose the design point of an engine in the 'flat' region of the specific-power versus pressure ratio curve, where derivative over pressure ratio has a value close to zero.

Using now **Eq. B-119, Eq. B-121, Eq. B-123** and **Eq. B-92**, gives:

$$\frac{\delta P}{P} = \frac{\delta \dot{m}_2}{\dot{m}_2} + \frac{P_T}{P}\left(\frac{C_{ps}}{C_{pg}} - \frac{f}{1+f}\right) f' w \qquad \textbf{Eq. B-124}$$

For Cps/Cpg≈2 and f<<1, this relation gives **Eq. B-100** of the main text.

B.8.6.4 Efficiency

The relation for estimating efficiency deviation can be derived from the equation of definition of gas turbine efficiency:

$$\eta_{th} = \frac{P}{\dot{m}_f LHV} = \frac{P}{f\,\dot{m}_3\, LHV} \qquad \textbf{Eq. B-125}$$

Efficiency change can be derived from this relation, by taking logarithms and then differentiating:

$$\frac{\delta(\eta_{th})}{\eta_{tth}} = \frac{\delta P}{P} - \frac{\delta f}{f} - \frac{\delta \dot{m}_3}{\dot{m}_3} \qquad \textbf{Eq. B-126}$$

It is noted here that the gas turbine alone is considered in the definition of efficiency. When steam is injected, the heat of producing it is not accounted for in this expression. This represents the case that steam is produced from the gas turbine exhaust gases and no additional fuel is used.

B.8.6.5 Compressor Pressure Ratio

Pressure ratio can be related to turbine and compressor flow capacities through flow matching relations. Using the definition of turbine and compressor reduced mass flow rates, and **Eq. B-122** that links the inlet mass flow rate to the two components, it is easily deduced that the following relation holds:

$$\pi_C = \frac{q_2}{q_4}\left(1 + f'\left(1+w\right)\right)\left(1-b\right)\left(1-K_b\right)\sqrt{\frac{R_4}{R_2}\frac{\gamma_2}{\gamma_4}}\sqrt{\frac{T_4}{T_2}} \qquad \textbf{Eq. B-127}$$

This relation holds for any operating condition, with or without diluent injection. It is also realistic to assume that the bleed air fraction b and loss factor Kb do not change with diluent injection, namely the term (1-b)(1-Kb) remains constant. It is also noted that the turbine flow function q4 remains constant for a choked turbine, which is the case for the largest part of the operating envelope of modern gas turbines.

Using **Eq. B-99** for gas constant and isentropic exponent deviations we get:

$$\frac{R'_4}{R_4}\frac{\gamma_4}{\gamma'_4} = \frac{(1+\delta R/R)}{(1+\delta\gamma/\gamma)} = \frac{(1+0.61 f' w)}{(1-0.13 f' w)} \approx 1 + 0.74 f' w \quad \Rightarrow \quad \sqrt{\frac{R'_4}{R_4}\frac{\gamma_4}{\gamma'_4}} \cong 1 + 0.37 f' w \qquad \textbf{Eq. B-128}$$

B.8.7 References in Section B.8, Water/Steam Ingestion

[B.89] Lefebvre, A.H., "The Role of Fuel Preparation in Low Emission Combustion", Journal of Engineering for Gas Turbines and Power, October, Vol. 117, pp. 617-654, 1995.

[B.90] Pavri, R. and Moore, G.D., "Gas Turbine Emissions and Control", GE Reference Library, GER-4211, 03/01, 2001.

[B.91] Schetter, B., "Gas Turbine Combustion and Emission Control", Lecture Series 1993-08, Combined Cycles for Power Plants, von Kármán Institute for Fluid Dynamics, 1993.

[B.92] Shaw, H., "The Effects of Water, Pressure, and Equivalence Ratio on Nitric Oxide Production in Gas Turbines", ASME Journal of Engineering for Power, July 1974, pp. 240-246.

[B.93] Digumarthy, R. et al., "Cheng-Cycle Implementation on a Small Gas Turbine Engine", Journal of Engineering for Gas Turbines and Power, Vol. 106, pp. 699-702, 1984.

[B.94] Kolp, D.A. and Moeller, D.J., "World's First Full STIG LM5000 Installed at Simpson Paper Company", ASME Journal of Engineering for Gas Turbines and Power, Vol. 111, pp. 200-210, 1989.

[B.95] Fraize, W.E. and Kinney, C., "Effects of Steam Injection on the Performance of Gas Turbine Power Cycles", ASME Journal of Engineering for Gas Turbines and Power, Vol. 101, pp. 217-227.

[B.96] Burnham, J.B., Giuliani, M.H. and Moeller, D.J., "Development, Installation and Operating Results of a Steam Injection System (STIG) in a General Electric LM5000 Gas Generator", ASME Journal of Engineering for Gas Turbines and Power, Vol. 109, pp. 257-262, pp. 699-702, 1987.

[B.97] Larson, E.D. and Williams, R.H., "Steam-Injected Gas Turbines", ASME Journal of Engineering for Gas Turbines and Power, Vol. 109, pp. 55-63.

[B.98] Tuzson, J., "Status of Steam-Injected Gas Turbines", Journal of Engineering for Gas Turbines and Power, Vol. 114, October 1992, pp. 682-686.

[B.99] Walsh, P.P. and Fletcher, P., "Gas Turbine Performance", Blackwell Science Ltd, ISBN 0-632-04874-3, 1998.

[B.100] Kreitmeier, F., Frutschi, H.U. and Vogel, M., "Economic Evaluation of Methods for Reducing NO_x Emissions of Gas Turbines and Combined Cycle Plants", ABB Review 1/92, pp. 29-36, 1992.

[B.101] Cloyd, S.T. and Harris, A.J., "Gas Turbine Performance – New Application and Test Correction Curves", ASME Paper # 95-GT-167, 1995.

[B.102] Noymer, P.D. and Wilson, D.G., "Thermodynamic Design Considerations for Steam-Injected Gas Turbines", ASME Paper # 93-GT-432, 1993.

[B.103] Mathioudakis, K., "Analysis of the Effects of Water Injection on the Performance of a Gas Turbine", ASME Journal of Engineering for Gas Turbines and Power, July 2002, Vol. 124, pp. 489-495.

[B.104] Stamatis, A., Kamboukos, Ph., Aretakis, N. and Mathioudakis, K., "On Board Adaptive Models: A General Framework and Implementation Aspects", Proceedings of ASME Turbo Expo 2002 June 3-6, 2002, Amsterdam, The Netherlands, ASME Paper # GT-2002-30622.

[B.105] AGARD-AR-332, "Recommended Practices for the Assessment of the Effects of Atmospheric Water Ingestion on the Performance and Operability of Gas Turbines Engines", September 1995, ISBN 92-836-1022-9.

[B.106] Mathioudakis, K., Aretakis, N. and Tsalavoutas, A., "Increasing Diagnostic Effectiveness by Inclusion of Fuel Composition and Water Injection Effects", Proceedings of ASME Turbo Expo June 3-6, 2002, Amsterdam, The Netherlands, ASME Paper # GT-2002-30032.

[B.107] Mathioudakis, K., "Evaluation of Steam and Water Injection Effects on Gas Turbine Operation Using Explicit Analytical Relations", Proceedings of the Institution of Mechanical Engineers, Part A, Journal of Power and Energy, Vol. 216, No. A6, December 2002, pp. 419-431.

[B.108] Tsalavoutas, A., Aretakis, N., Stamatis, A. and Mathioudakis, K., "Combining Advanced Data Analysis Methods for the Constitution of an Integrated Gas Turbine Condition Monitoring and Diagnostic System", ASME Paper # 2000-GT-0034, 2000.

[B.109] Johnston, J.R., "Performance and Reliability Improvements for Heavy-Duty Gas Turbines", GE Reference Library, GER-3571H, 10/00, 2000.

[B.110] Dundas, R., Sullivan, D. and Abegg, F., "Performance Monitoring of Gas Turbines for Failure Prevention", ASME Paper # 92-GT-267, 1992.

[B.111] Cohen, C. and Rogers, G.F.C. and Saravanamutto, H.I.H., "Gas Turbine Theory", 4th Edition, Addison Wisley Longman Ltd, 1996, ISBN 0-321-04346-4.

[B.112] Mathioudakis, K., Stamatis, A., Tsalavoutas, A. and Aretakis, N., "Performance Analysis of Industrial Gas Turbines for Engine Condition Monitoring", Proceedings of Institution of Mechanical Engineers, Part A: Journal of Power and Energy, Vol. 215, March 2000, pp. 173-184.

B.8.8 Additional Bibliography for Section B.8

Hoeft, R. and Gebhardt, E., "Heavy Duty Gas Turbine Operating and Maintenance Considerations", GE Reference Library, GER-3620G, 10/00, 2000.

Turbomachinery International: Handbook 2001-2002, Vol. 42, No. 6, and Handbook/1996, Vol. 37, No. 6.

Horlock, J.H., "The Evaporative Gas Turbine [EGT] Cycle", ASME Paper # 97-GT-408, 1997.

Utamura, M., Takehara, I. and Karasawa, H., "MAT, A NOVEL, Open Cycle Gas Turbine for Power Augmentation", Energy Convers. Mgmt, Vol. 39, No. 16-18, pp. 1631-1642, 1998.

Meher Homji, C.B. and Mee III, T.R., "Inlet Fogging of Gas Turbine Engines Part A: Theory, Psychrometrics and Fog Generation", ASME Paper # 2000-GT-307, 2000.

RTO-TR-044, "Performance Prediction and Simulation of Gas Turbine Engine Operation", RTO Technical Report 44, April 2002, AC/323(AVT-018)TP/29, ISBN 92-837-1083-5.

Mathioudakis, K. and Tsalavoutas, A., "Uncertainty Reduction in Gas Turbine Performance Diagnostics by Accounting for Humidity Effects", Proceedings of ASME Turbo Expo 2001 June 4-7, 2001, New Orleans, Louisiana, ASME Paper # 2001-GT-0010, 2001.

Stamatis, A., Mathioudakis, K. and Papailiou, D.K., "Adaptive Simulation of Gas Turbine Performance", Journal of Engineering for Gas Turbine and Power, April 1990, Vol. 112.

Kurzke, J., "Performance Maps for Gas Turbine Performance Computer Programs", GASTURB Program Manuals, 1996.

Saravanamutto, H.I.H. and McIsaac, B.D., "Thermodynamic Models for Pipeline Gas Turbine Diagnostics", ASME Paper # 83-GT-235, Transaction of the ASME, Vol. 105, Series A, 1983, pp. 875-884.

Kurzke, J. and Riegler, C., "A New Compressor Map Scaling Procedure for Preliminary Conceptional Design of Gas Turbines", ASME Paper # 2000-GT-006, 2000.

Tsalavoutas, A., Stamatis, K. and Mathioudakis, K., "Derivation of Compressor Stage Characteristic, for Accurate Overall Performance Map Prediction", ASME Paper # 94-GT-32, 1994.

Kamboukos, Ph., Oikonomou, P., Stamatis, A. and Mathioudakis, K., "Optimizing Diagnostic Effectiveness of Mixed Turbofans by Means of Adaptive Modeling and Choice of Appropriate Monitoring Parameters", AVT Symposium on "Monitoring and Management of Gas Turbine Fleets for Extended Life and Reduced Costs", Manchester, UK, 8-11 October 2000.

Stamatis, A., Mathioudakis, K., Berios, G. and Papailiou, K., "Jet Engine Fault Detection with Differential Gas Path Analysis at Discrete Operating Points", Journal of Propulsion and Power, Vol. 7, No 6, November-December 1991, pp. 1043-1048.

Burnham, J.B., Giuliani, M.H. and Moeller, D.J., "Development, Installation and Operating Results of a Steam Injection System (STIGTM) in a General Electric LM5000 Gas Generator", Journal of Engineering for Gas Turbine and Power, July 1987, Vol. 109.

Anon., "LM6000 Control Solutions Benefit Operations", Woodward Governor Company, Application Sheet 51178, 1997.

Pavri, R. and Moore, G.D., "Gas Turbine Emissions and Control", GE Reference Library, GER-4211, 03/01, 2001.

Organowski, G., "GE LM6000 Development of the First 40% Thermal Efficiency Gas Turbine", GE Marine & Industrial Engine and Service Division".

Meher Homji, C.B. and Mee III, T.R., "Gas Turbine Power Augmentation by Fogging of Inlet Air", Proceedings of the 28th Turbomachinery Symposium, Texas A&M University, 1999.

Mathioudakis, K., "Gas Turbine Test Parameters Corrections including Operation with Water Injection", ASME Turbo Expo 2002, Paper # GT-2002-30466.

Mathioudakis, K., Stamatis, A., Tsalavoutas, A. and Aretakis, N., "Computer Models for Education on Performance Monitoring and Diagnostics of Gas Turbines", Journal of Mechanical Engineering Education, July 2002, Vol. 30, (3), pp. 204-218.